Совместный выпуск

Октябрь 2020
№3. Часть 1

ВЕСТНИК
Национальной инженерной академии Республики Казахстан

ВЫЧИСЛИТЕЛЬНЫЕ ТЕХНОЛОГИИ
Федеральный исследовательский центр информационных и вычислительных технологий

ВЕСТНИК
Национальной инженерной академии Республики Казахстан

Главный редактор
академик Б. Т. ЖУМАГУЛОВ

ВЫЧИСЛИТЕЛЬНЫЕ ТЕХНОЛОГИИ

Федеральный исследовательский центр информационных и вычислительных технологий

Главный редактор
академик Ю.И. Шокин

по материалам Международной конференции
«Вычислительные и информационные технологии
в науке, технике и образовании»
(**CITech-2020**)

9-10 октября 2020 года

Алматы, 2020

ПРОГРАММНЫЙ КОМИТЕТ

Международной конференции
«Вычислительные и информационные технологии в науке, технике и образовании 2020»

Сопредседатель – Жумагулов Бакытжан Турсынович, академик НАН РК, Национальная инженерная академия РК, Казахстан

Сопредседатель - Шокин Юрий Иванович, академик РАН, Институт вычислительных технологий СО РАН, Россия

Члены:

Абдибеков Уалихан Сейдильдаевич, член-корреспондент НИА РК, Казахский национальный университет им. аль-Фараби, Казахстан

Амиргалиев Едилхан Несипханович, академик НИА РК, Институт информационных технологий, Казахстан

Арипов Мирсаид, профессор, Национальный университет Узбекистана им. М. Улугбека, Узбекистан

Ахмед-Заки Дархан, Astana IT University, Казахстан

Баутин Сергей, профессор, Уральский государственный университет путей сообщения, Россия

Бектемесов Мактагали Абдимажитович, член-корреспондент НИА РК, Казахский национальный педагогический университет им. Абая, Казахстан

Бычков Игорь Вячеславович, член-корреспондент РАН, Институт динамики систем и теории управления СО РАН, Россия

Войцик Вальдемар, профессор, Люблинский технический университет, Польша

Гривенк Андреас, Берлиинский университеет имени Гумбольдта

Есипов Денис, Институт вычислительных технологий СО РАН, Россия

Жайнаков Аманбек Жайнакович, академик НАН КР, Кыргызский государственный технический университет им. И. Раззакова, Кыргызстан

Жакебаев Даурен Бахытбекович, член-корреспондент НИА РК, Казахский национальный университет им. аль-Фараби, Казахстан

Жижимов Олег Львович, Институт вычислительных технологий СО РАН, Россия

Захаров Юрий, профессор, Кемеровский государственный университет, Россия

Иманкулов Тимур Сакенович, Казахский национальный университет им. аль-Фараби, Казахстан

Исахов Алибек Абдиашимович, член-корреспондент НИА РК Казахский национальный университет им. аль-Фараби, Казахстан

Кабанихин Сергей Игоревич, член-корреспондент РАН, Институт вычислительной математики и математической геофизики СО РАН, Россия

Калимолдаев Максат Нурадилович, академик НАН РК, Институт Информационных и Вычислительных Технологий, Казахстан

Калтаев Айдархан Жусупбекович, академик НИА РК, Казахский национальный технический университет им. Сатпаева, Казахстан

Картбаев Тимур Саатдинович, член-корреспондент НИА РК, Алматинский университет энергетики и связи, Казахстан

Краузе Эгон, профессор, Рейнско-Вестфальский технический университет, Ахена, Германия

Маттиас Мейнке, профессор, Рейнско-Вестфальский технический университет Ахена, Германия

Милошевич Хранислав, профессор, Университет Приштины, Сербия

Москвичев Владимир, профессор, Специальное конструкторское бюро «Наука» ИВТ СО РАН, Россия

Пейман Гиви, профессор, Университет Питтсбурга, США

Потапов Вадим, профессор, Институт вычислительных технологий СО РАН, Россия

Потатуркин Олег, профессор, Институт автоматики и электрометрии СО РАН, Россия

Реш Майкл, профессор, высокопроизводительный вычислительный центр в Штутгарте, Германия

Рознер Карл, профессор, Технологический университет Дармштадта, Германия

Рябко Борис, профессор, Институт вычислительных технологий СО РАН, Россия

Садовский Владимир, профессор, Институт вычислительного моделирования СО РАН, Россия

Смагин Сергей, член-корреспондент РАН, Компьютерный центр ДВО РАН, Россия

Сойфер Виктор, академик РАН, Самарский государственный аэрокосмический университет им. Королева, Россия

Стемпковский Александр, член-корреспондент РАН, Институт проблем проектирования в Микроэлектронике РАН, Россия

Томас Бёниш, высокопроизводительный вычислительный центр в Штутгарте, Германия

Турицын Сергей, профессор, Университет Астон, Великобритания

Урмашев Байдаулет Амантаевич, Казахский национальный университет им. аль-Фараби, Казахстан

Федорук Михаил Петрович, член-корреспондент РАН, Новосибирский государственный университет, Россия

Хабаши Вагди Джордж, профессор, Университет Макгилла, Канада

Шайдуров Владимир, член-корреспондент РАН, Институт вычислительного моделирования СО РАН, Россия

Шокина Нина Юрьевна, Университет Фрайбурга, Германия

Шредер Вольфганг, профессор, RTWH Аахенский университет, Германия

Эйнарссон Бо, профессор, Университет Линкопинг, Швеция

Юлдашев Зиявидин Хабибович, профессор, Национальный университет Узбекистана им. Мирзы Улугбека, Узбекистан

Юрченко Андрей, Институт вычислительных технологий СО РАН, Россия

ОРГАНИЗАЦИОННЫЙ КОМИТЕТ

Международной конференции
«Вычислительные и информационные технологии в науке, технике и образовании 2020»

Темирбеков Нурлан Муханович, академик НИА РК, член-корреспондент НАН РК, Национальная инженерная академия Республики Казахстан, Казахстан

Денисова Наталья Федоровна, директор департамента информационных технологий — проректор по информатизации ВКГТУ им. Д.Серикбаева, Казахстан

Есипов Денис Викторович, Институт вычислительных технологий СО РАН, Россия

Гусев Олег Игоревич, Институт вычислительных технологий СО РАН, Россия

Имангалиев Ернар Имангалиевич, Главный Ученый секретарь НИА РК, Казахстан

Мадияров Мураткан Набенович, декан факультета естественных наук и технологий ВКГУ им. С.Аманжолова

Байгереев Досан Ракимгалиевич, доцент кафедры математики ВКГУ им. С. Аманжолова

Numerical Study of Three Dimensional MHD Natural Convection with Hartmann Effects by Hybrid Finite Difference Method

Sultanbek Abdibekov[1 [0000−0002−2540−0508]],
Dauren Zhakebayev[1,2 [0000−0002−0642−327X]],
Askar Khikmetov[1,3 [0000−0002−3045−7592]], and
Oksana Karuna[1,4 [0000−0002−1299−0166]]

[1] Kazakh national university named after al-Farabi,Almaty, Kazakhstan
Abdibekov.sultanbek@gmail.com
[2] Dauren.zhakebayev@gmail.com
[3] Askar.Khikmetov@kaznu.kz
[4] Oksana.Karuna@kaznu.kz

Abstract In the presented work the effect of magnetic field on natural convection flow with a uniformly distributed electron concentration and with a variable electron concentration in three dimensional area have been studied by hybrid finite difference method. The magnetic field is considered vertically and results have been shown at different planes of 3-D enclosure. The two vertical wall are held isothermally at temperature, while the other walls are adiabatic. Numerical results of natural convection were obtained for various values of Grashof and Hartmann numbers and for the Prandtll number $Pr = 0,733$. The results of a detailed study of changes in velocity, temperature and Nusselt number are presented graphically, isothermal surfaces, velocity and temperature contoures, also profiles for different Hartmann numbers are obtained. To verify the accuracy of the presented numerical simulation results, a comparison was made with the literature data of natural convection flow without electron concentration and good agreements were established.

Keywords: Natural convection, Magnetohydrodynamics, Variable electron concentration, Navier Stokes equation, Finite difference method, Spectral method

Natural convection flow with a uniformly distributed electron concentration

Introduction Natural fluid convection resulting from temperature gradients is very important in a number of industrial applications. In addition, buoyancy is very significant in the environment, since the temperature difference between the ground and air can lead to a complex flow structure, and in confined spaces, for example, in ventilated and heated rooms, reactors. Natural convection of the flow is one of the most important problems in fluid mechanics [1],[2]. Owing to the widespread problems in natural processes in three-dimensional natural convection with various boundary conditions, in the last few years it has attracted the attention of many researchers.

The work [3] studied the thermal conductivity of the MHD flow around a heated vertical plate with variable viscosity and temperature. And in [4], free convection was studied along a vertical plate with uniform cut-off, already with low thermal radiation and also with variable viscosity.

Magnetic field convection has been developed and has been studied in recent decades [5],[6]. Two-dimensional mixed convection was solved using the finite volume method in [7]. They investigated the effect of the ratio of velocity amplitudes, phase deviation, Richardson and Hartmann numbers on the heat transfer rate under a sinusoidal boundary condition. As a result of the study, it is shown that the Nusselt number increases in amplitude ratio. [8] presents the results of a finite volume study for a laminar mixed convection flow in the presence of a magnetic field in the upper cavity, controlled by variable values of the Grashof and Hartmann numbers. As a result of modeling, it was obtained, that the transfer rate decreases with increasing Hartmann number.

The influence of an external magnetic field in different directions on natural convection in a three-dimensional cubic region with lateral wall heating at high Rayleigh and Hartmann numbers is considered in [9]. The solution to the problem is based on two numerical methods: a finite second-order volume and a discretization scheme - B on structured Cartesian grids. The used different magnetic field settings have different effects on the thermal conductivity of natural convection. In parallel overlay leads to a temperature drop and a strong suppression of heat transfer and convection flow. With vertical application, the suppression of heat flux is weaker, and in the longitudinal direction it stabilizes the main convection shaft and leads to an increase in kinetic energy and Nusselt number compared to natural convection with the non-magnetic case.

Three-dimensional nanofluidic non-Darsian natural convection is represented in the presence of Lorentz forces by the lattice Boltzmann method (LBM) [10]. The simulation results are presented for various numbers of Darcy, Rayleigh, Hartmann and the volume fraction of Al2O3. The convection dominates at large Darcy and Rayleigh numbers, the velocity of nanofluids increases with increasing volume fraction, Rayleigh and Darcy numbers, but slows down with increasing Hartmann number. The temperature gradient on a hot surface go down with increasing Hartmann number, and growths with increasing Darcy number, Rayleigh number.

In [15], the LBM method was used to solve a two-dimensional MHD flow in an inclined cavity with four heat sources, where the double multiple-relaxation time model simulates the momentum and energy equations and investigates the effect of the Hartman number on fluid flow and heat transfer. As a result, it is shown that the average Nusselt number decreases due to an increase in the Hartmann number for all Rayleigh numbers.

The influence of the Rayleigh and Hartmann numbers, the volume fraction of nanoparticles, and the phase deviation on the heat transfer of natural convection of MHD in a three-dimensional square cavity with a sinusoidal temperature distribution on one side wall using the Boltzmann lattice with a double relaxation time model using nano-liquid copper water is investigated in [12]. As a result of modeling, with an increase in the Hartmann number, convection heat transfer decreases. With an increase in the Hartmann number from 0 to 50, the average Nuselt number decreases by 64% and 70% for the left and right walls, respectively.

The influence of the Hartmann and Grashof numbers on the MHD natural convection flow and heat transfer rates in the three-dimensional cubic region using the Boltzmann lattice with double multi-relaxation time (MRT) is investigated in [13]. As a result of the simulation, it was found that an increase in the Hartmann number leads to a significant decrease in the heat transfer rate, and the flow structure and isotherms in different planes of the shell change sharply due to an increase in the Hartmann and Grashof numbers, since heat transfer rates are suppressed with a strong magnetic field. The average and local Nusselt numbers decrease significantly with increasing Hartmann number.

Numerical study of the natural convection of an electrically conductive fluid in a two-dimensional rectangular region in the presence of a vertical magnetic field that has a direction parallel to gravity is presented in [14]. Two vertical walls are isothermal supported, one of which is heated and the other is cooled, and the horizontal walls have adiabatic conditions. The calculations were performed for the Grashof number in the range from $Gr = 10^4$ to $Gr = 10^6$ and the Hartmann number from 0 to 100. As a result of the study, it was found that with a weak magnetic field and a large Grashof number, convection prevails, and in the central region vertical temperature stratification predominates.

Problem statement In this paper, we consider a mathematical model of the problem of natural convection of flow with an homogeneous electron concentration under the influence of a vertical magnetic field, where the effect of the Hartmann number ($Ha = 50$, $Ha = 100$) is studied. Also, mathematical model of natural convection without affecting magnetic field is considered, when Hartmann number is set to 0.

The applied magnetic field $B = -H_0\bar{k}$ effect in the Navier-Stokes equations is the inclusion of the Lorentz force to the momentum equations $F_l = J \times B$ where $J = \sigma(E + V \times B)-$ is electric current density E - is electric field strength, which we set equal to zero, and σ is electric conductivity, $V = u_1\bar{i} + u_2\bar{j} + u_3\bar{k}$ - velocity of fluid, and all of these in combination we obtain $F_l = \sigma(V \times B)\times$ - Lorentz force, where $F_l = \sigma[(u_1\bar{i} + u_2\bar{j} + u_3\bar{k}) \times (-H_0\bar{k})] \times (-H_0\bar{k})$ is in detail, after using the properties of the multiplication of unit vectors, we obtain $F_l = \sigma(u_1H_0\bar{j} - u_2H_0\bar{i}) \times (-H_0\bar{k})$, or $F_l = \sigma(-u_1H_0^2\bar{i} - u_2H_0^2\bar{j})$, and $F_l = F_1 + F_2 + F_3$, where $F_1 = -\sigma u_1H_0^2\bar{i}$, $F_2 = -\sigma u_2H_0^2\bar{j}$, $F_3 = 0$.

The problem is based on solving non-stationary equations of magnetohydrodynamics with filtration in combination with the continuity equation, equations for temperature in a Cartesian coordinate system in dimensionless form

$$\begin{cases} \frac{\partial(\bar{u}_i)}{\partial t} + \frac{\partial(\bar{u}_i\bar{u}_j)}{\partial x_j} = -\frac{\partial\bar{p}}{\partial x_i} + \frac{1}{Re}\frac{\partial}{\partial x_j}\left(\frac{\partial\bar{u}_i}{\partial x_j}\right) + F_i + \frac{Gr}{Re^2}\bar{\theta}, \\ \frac{\partial(\bar{u}_i)}{\partial x_i} = 0, \\ \frac{\partial(\bar{\theta})}{\partial t} + \frac{\partial(\bar{u}_i\bar{\theta})}{\partial x_j} = \frac{1}{RePr}\frac{\partial}{\partial x_j}\left(\frac{\partial\bar{\theta}}{\partial x_j}\right), \end{cases} \tag{1}$$

where $\bar{u_1}, \bar{u_2}, \bar{u_3}$ - the velocity components, x_1, x_2, x_3 - coordinates, $\bar{F_1} = -\bar{n}N\bar{u}_1$, $\bar{F_2} = -\bar{n}N\bar{u}_2$, $\bar{F_3} = 0$ - non-dimensional Lorentz force [13],

$N = \sigma L H_0^2/\rho V_0 = Ha^2/Re$ is the Stuart number, where $Ha = H_0 L\sqrt{\sigma/\mu}$ - Hartmann number, H - magnetic field strength, σ is the conductivity of the medium, which is determined from plasma physics. $\bar{p}$ is the full pressure, t is the time, $U_0 = \sqrt{g\beta(T_2 - T_1)L}$ - characteristic velocity, $\bar{\theta} = (T - T_0)/(T_2 - T_0)$ - non-dimensional temperature, where $T_0 = (T_1 + T_2)/2$ and T_1 is the cold temperature and T_2 is the hot temperature, $Gr = g\beta(T_2 - T_1)L_3/\nu^2$- is Grahof number, where β is volumetric thermal expansion coefficient, g – acceleration due to gravity, $Re = \sqrt{Gr}$ is the Reynolds number, and to compare numerical simulation results with the work [13]. $Pr = \nu/\alpha$ - Prandtl number, α - thermal diffusivity, $L_1 = L_2 = L_3 = L$ is the typical length of the domain, ν is the kinematic viscosity coefficient, ρ is the density of the flow, t- nondimensional time.

A schematic picture of the computational domain is shown in Figure 1, where the left wall - indicated by the blue color, corresponds to the cold temperature of wall. The right wall layer - highlighted in red, corresponds to hot temperature of the wall.

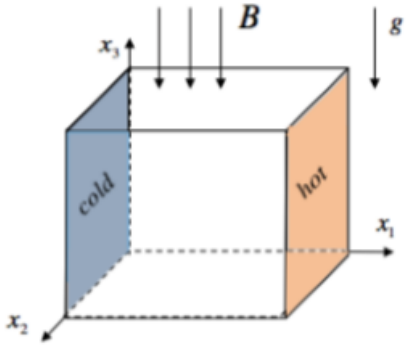

Figure 1. Geometry illustration of the problem statement

Initial conditions for temperature, velocity components are set zero in all directions of the domain. The boundary conditions imposed for temperature is Dirichlet on the right and left boundaries, and Neumann on the other directions of the domain. The velocity components are equal to 0, and electron concentration is set 1 in all directions.

Initial conditions:

$\bar{u}_1 = \bar{u}_2 = \bar{u}_3 = 0, \quad \bar{\theta} = 0, \qquad$ at $t = 0, 0 \le x_1 \le 1, 0 \le x_2 \le 1, 0 \le x_3 \le 1;$

Boundary conditions:

$\bar{u}_1 = \bar{u}_2 = \bar{u}_3 = 0, \quad \bar{\theta} = -1, \quad$ at $x_1 = 0, 0 \le x_2 \le 1, 0 \le x_3 \le 1;$

$\bar{u}_1 = \bar{u}_2 = \bar{u}_3 = 0, \quad \bar{\theta} = 1, \quad$ at $x_1 = 1, 0 \le x_2 \le 1, 0 \le x_3 \le 1;$

$\bar{u}_1 = \bar{u}_2 = \bar{u}_3 = 0, \quad \bar{\theta}/\partial x_2 = 0,$ at $x_2 = 1, x_2 = 0, 0 \le x_1 \le 1, 0 \le x_3 \le 1;$

$\bar{u}_1 = \bar{u}_2 = \bar{u}_3 = 0, \quad \bar{\theta}/\partial x_3 = 0,$ at $x_3 = 1, x_3 = 0, 0 \le x_1 \le 1, 0 \le x_2 \le 1.$

Numerical method To solve the problem of natural convection flow with an homogeneous electron concentration under the influence of a vertical magnetic field, a scheme of splitting by physical parameters is used:

I. $\frac{(\bar{u}^*)^{n+1}-(\bar{u})^n}{\Delta t} - \frac{1}{2Re}\nabla^2(\bar{u}^*)^{n+1} = \frac{1}{2Re}\nabla^2\bar{u}^n + \frac{3}{2}K^n - \frac{1}{2}K^{n-1}$;
II. $\Delta p = \frac{\nabla(\bar{u}^*)^{n+1}}{\tau}$;
III. $\frac{(\bar{u})^{n+1}-(\bar{u}^*)^{n+1}}{\Delta t} = -\nabla p$;
IV. $\frac{\bar{\theta}^{n+1}-\bar{\theta}^n}{\Delta t} - \frac{1}{2Pe}\nabla^2\bar{\theta}^{n+1} = \frac{1}{2Pe}\nabla^2\bar{\theta}^n + (\frac{3}{2}G^n - \frac{1}{2}G^{n-1})$,

where
$K^n = -(\bar{u}^n\nabla)\bar{u}^n + F^n + (Gr/Re^2)\bar{\theta}^n$,
$G^n = -(\bar{u}^n\nabla)\bar{\theta}^n$, where $Pe = RePr$ - Peclet number.

During the first stage, the full magneto hydrodynamic equation system is solved without the pressure consideration. For approximation of the convective and diffusion terms of the intermediate velocity field a finite-difference method in combination with penta-diagonal matrix is used, which allowed to increase the order of accuracy in space. The numerical algorithm for the solution of incompressible MHD turbulence is considered at [15].

At the second step, the pressure Poisson equation is solved, which ensures that the continuity equation is satisfied. The Poisson equation is transformed from the physical space into the spectral space by using a Fourier transform. To solve the three-dimensional Poisson equation, the spectral conversion in combination with matrix sweeping algorithm is developed [16]. The resulting pressure field in the third stage is used to recalculate the final velocity field [15].

At the fourth stage, the equation for temperature is solved by using Adams-Bashforth scheme.

Consider the temperature distribution in the horizontal direction at the point (i, j, k):

$$\frac{\partial\bar{\theta}}{\partial t} + \frac{\partial(\bar{u}_1\bar{\theta})}{\partial x_1} + \frac{\partial(\bar{u}_2\bar{\theta})}{\partial x_2} + \frac{\partial(\bar{u}_3\bar{\theta})}{\partial x_3} = \frac{1}{RePr}\left(\frac{\partial^2\bar{\theta}}{\partial x_1^2} + \frac{\partial^2\bar{\theta}}{\partial x_2^2} + \frac{\partial^2\bar{\theta}}{\partial x_3^2}\right) \tag{2}$$

When using the explicit Adams-Bashfort scheme for convective terms and the implicit Crank-Nicolson scheme for viscous terms, equation (2) takes the form:

$$\begin{aligned}\bar{\theta}^{n+1}_{i,j,k} - \bar{\theta}^n_{i,j,k} = -\frac{3\Delta t}{2}[hr]^n_{i,j,k} + \frac{\Delta t}{2}[hr]^{n-1}_{i,j,k} + \frac{\Delta t}{2}[ar]^n_{i,j,k} + \\ + \frac{\Delta t}{2}\cdot\frac{1}{RePr}\cdot\left[\left(\frac{\partial^2\bar{\theta}}{\partial x_1^2}\right)^{n+1}_{i,j,k} + \left(\frac{\partial^2\bar{\theta}}{\partial x_2^2}\right)^{n+1}_{i,j,k} + \left(\frac{\partial^2\bar{\theta}}{\partial x_3^2}\right)^{n+1}_{i,j,k}\right],\end{aligned} \tag{3}$$

where

$$[hr]^n_{i,j,k} = \left(\frac{\partial(u_1\bar{\theta})}{\partial x_1}\right)^n_{i,j,k} + \left(\frac{\partial(u_2\bar{\theta})}{\partial x_2}\right)^n_{i,j,k} + \left(\frac{\partial(u_3\bar{\theta})}{\partial x_3}\right)^n_{i,j,k},$$

$$[ar]^n_{i+\frac{1}{2},j,k} = \frac{1}{RePr}\left[\left(\frac{\partial^2\bar{\theta}}{\partial x_1^2}\right)^n_{i,j,k} + \left(\frac{\partial^2\bar{\theta}}{\partial x_2^2}\right)^n_{i,j,k} + \left(\frac{\partial^2\bar{\theta}}{\partial x_3^2}\right)^n_{i,j,k}\right].$$

Discretization of convective expressions looks like this:

$$\left(\frac{\partial\bar{u}_1\bar{\theta}}{\partial x_1}\right)|_{i,j,k} = \frac{-(\bar{u}_1\bar{\theta})_{i+2,j,k} + 27(\bar{u}_1\bar{\theta})_{i+1,j,k} - 27(\bar{u}_1\bar{\theta})_{i,j,k}}{24\Delta x_1} + \\ + \frac{(\bar{u}_1\bar{\theta})_{i-1,j,k}}{24\Delta x_1} + O(\Delta x_1^4),$$

$$\left(\frac{\partial\bar{u}_2\bar{\theta}}{\partial x_2}\right)|_{i,j,k} = \frac{(\bar{u}_2\bar{\theta})_{i+1,j-2,k} - 27(\bar{u}_2\bar{\theta})_{i,j-1,k} + 27(\bar{u}_2\bar{\theta})_{i,j,k}}{24\Delta x_2} - \\ - \frac{(\bar{u}_2\bar{\theta})_{i,j+1,k}}{24\Delta x_2} + O(\Delta x_2^4),$$

$$\left(\frac{\partial\bar{u}_3\bar{\theta}}{\partial x_3}\right)|_{i,j,k} = \frac{(\bar{u}_3\bar{\theta})_{i,j,k-2} - 27(\bar{u}_3\bar{\theta})_{i,j,k-1} + 27(\bar{u}_3\bar{\theta})_{i,j,k}}{24\Delta x_3} - \\ - \frac{(\bar{u}_3\bar{\theta})_{i,j,k+1}}{24\Delta x_3} + O(\Delta x_3^4).$$

Discretization of diffusion conditions looks like this:

$$\left(\frac{\partial^2\bar{\theta}}{\partial x_1^2}\right)|_{i,j,k} = \frac{-(\bar{\theta})_{i+2,j,k} + 16\cdot(\bar{\theta})_{i+1,j,k} - 30\cdot(\bar{\theta})_{i,j,k}}{12\Delta x_1^2} + \\ + \frac{16\cdot(\bar{\theta})_{i-1,j,k} - (\bar{\theta})_{i-2,j,k}}{12\Delta x_1^2},$$

$$\left(\frac{\partial^2\bar{\theta}}{\partial x_2^2}\right)|_{i,j+\frac{1}{2},k} = \frac{-(\bar{\theta})_{i,j+2,k} + 16\cdot(\bar{\theta})_{i,j+1,k} - 30\cdot(\bar{\theta})_{i,j,k}}{12\Delta x_2^2} + \\ + \frac{16\cdot(\bar{\theta})_{i,j-1,k} - (\bar{\theta})_{i,j-2,k}}{12\Delta x_2^2},$$

$$\left(\frac{\partial^2\bar{\theta}}{\partial x_3^2}\right)|_{i,j,k+\frac{1}{2}} = \frac{-(\bar{\theta})_{i,j,k+2} + 16\cdot(\bar{\theta})_{i,j,k+1} - 30\cdot(\bar{\theta})_{i,j,k}}{12\Delta x_3^2} + \\ + \frac{16\cdot(\bar{\theta})_{i,j,k-1} - (\bar{\theta})_{i,j,k-2}}{12\Delta x_3^2},$$

where

$$\left(\bar{u}_1\bar{\theta}\right)_{i,j,k} = \left(\frac{-\bar{u}_{1_{i+1,j,k}} + 9\bar{u}_{1i,j,k} + 9\bar{u}_{1_{i-1,j,k}} - \bar{u}_{1_{i-2,j,k}}}{16}\right) \cdot \\ \cdot \left(\frac{-\bar{\theta}_{i+1,j,k} + 9\bar{\theta}_{i,j,k} + 9\bar{\theta}_{i-1,j,k} - \bar{\theta}_{i-2,j,k}}{16}\right),$$

$$\left(u_2\bar{\theta}\right)_{i,j,k} = \left(\frac{-\bar{\theta}_{i,j+2,k} + 9\bar{\theta}_{i,j+1,k} + 9\bar{\theta}_{i,j,k} - \theta_{i-1,j-1,k}}{16}\right) \cdot \\ \cdot \left(\frac{-\bar{u}_{2i+2,j,k} + 9\bar{u}_{2i+1,j,k} + 9\bar{u}_{2_{i,j,k}} - \bar{u}_{2i-1,j,k}}{16}\right),$$

$$\left(u_3\bar{\theta}\right)_{i,j,k} = \left(\frac{-\bar{\theta}_{i,j,k+2} + 9\bar{\theta}_{i,j,k+1} + 9\bar{\theta}_{i,j,k} - \bar{\theta}_{i-1,j,k-1}}{16}\right) \cdot \\ \cdot \left(\frac{-\bar{u}_{3i+2,j,k} + 9\bar{u}_{3i+1,j,k} + 9\bar{u}_{3i,j,k} - \bar{u}_{3i-1,j,k}}{16}\right).$$

Then the left side of equation (3) is denoted by $q_{i,j,k}$

$$q_{i,j,k} \equiv \bar{\theta}^{n+1}_{i+1,j,k} - \bar{\theta}^{n}_{i,j,k} \tag{4}$$

From equation (4) we find $\bar{\theta}^{n+1}_{i,j,k}$

$$\bar{\theta}^{n+1}_{i+1,j,k} = q_{i,j,k} - \bar{\theta}^{n}_{i,j,k}$$

Replacing all $\theta^{n+1}_{i,j,k}$ from the equations (3) , we obtain

$$q_{i,j,k} - \frac{\Delta t}{2}\cdot\frac{1}{RePr}\cdot\left(\frac{\partial^2 q}{\partial x_1^2}\right)_{i,j,k} - \frac{\Delta t}{2}\cdot\frac{1}{RePr}\cdot\left(\frac{\partial^2 q}{\partial x_2^2}\right)_{i,j,k} - \\ - \frac{\Delta t}{2}\cdot\frac{1}{RePr}\cdot\left(\frac{\partial^2 q}{\partial x_3^2}\right)_{i,j,k} = -\frac{3\Delta t}{2}\left[hr\right]^n_{i,j,k} + \frac{\Delta t}{2}\left[hr\right]^{n-1}_{i,j,k} + \Delta t\left[ar\right]^n_{i,j,k}, \tag{5}$$

Equation (5) is converted to

$$\left[1 - \frac{\Delta t}{2}\cdot\frac{1}{RePr}\cdot\frac{\partial^2}{\partial x_1^2} - \frac{\Delta t}{2}\cdot\frac{1}{RePr}\cdot\frac{\partial^2}{\partial x_2^2} - \right. \\ \left. - \frac{\Delta t}{2}\cdot\frac{1}{RePr}\cdot\frac{\partial^2}{\partial x_3^2}\right] q_{i,j,k} = d_{i,j,k} \tag{6}$$

where

$$d_{i,j,k} = -\frac{3\Delta t}{2}\left[hr\right]^n_{i,j,k} + \frac{\Delta t}{2}\left[hr\right]^{n-1}_{i,j,k} + \Delta t\left[ar\right]^n_{i,j,k}$$

Assuming that equation (6) has second-order accuracy in time, we can instead solve the following equation:

$$\left[1-\frac{\Delta t}{2}\cdot\frac{1}{RePr}\cdot\frac{\partial^2}{\partial x_1^2}\right]\cdot\left[1-\frac{\Delta t}{2}\cdot\frac{1}{RePr}\cdot\frac{\partial^2}{\partial x_2^2}\right]\cdot \cdot\left[1-\frac{\Delta t}{2}\cdot\frac{1}{RePr}\cdot\frac{\partial^2}{\partial x_3^2}\right]q^*_{i,j,k}=d_{i,j,k} \quad (7)$$

We can show that equation (7) is an approximation $O\left(\Delta t^4\right)$ to equation (6).Since the difference between $q^*_{i,j,k}$ and $q_{i,j,k}$ has a higher order, we return to the same notation and just use $q_{i,j,k}$. To determine $q_{i+1/2,j,k}$ the equation (7) is solved in 3 stages:

$$\left[1-\frac{\Delta t}{2}\cdot\frac{1}{RePr}\cdot\frac{\partial^2}{\partial x_1^2}\right]A_{i,j,k}=d_{i,j,k} \quad (8)$$

$$\left[1-\frac{\Delta t}{2}\cdot\frac{1}{RePr}\cdot\frac{\partial^2}{\partial x_2^2}\right]B_{i,j,k}=A_{i,j,k} \quad (9)$$

$$\left[1-\frac{\Delta t}{2}\cdot\frac{1}{RePr}\cdot\frac{\partial^2}{\partial x_3^2}\right]q_{i,j,k}=B_{i,j,k} \quad (10)$$

At the first stage, the $A_{i,j,k}$ search is carried out in the direction of the x_1 coordinates:

$$\left[1-\frac{\Delta t}{2}\cdot\frac{1}{RePr}\cdot\frac{\partial^2}{\partial x_1^2}\right]A_{i,j,k}=d_{i,j,k}$$

$$A_{i,j,k}-\tfrac{\Delta t}{2}\cdot\tfrac{1}{RePr}\cdot\left(\tfrac{\partial^2 A}{\partial x_1^2}\right)^{n+1}_{i,j,k}=d_{i,j,k}$$

$$A_{i,j,k}-\frac{\Delta t}{2}\cdot\frac{1}{RePr}\cdot\frac{-A_{i+2,j,k}+16\cdot A_{i+1,j,k}-30\cdot A_{i,j,k}}{12\Delta x_1^2}+ +\frac{16\cdot A_{i-1,j,k}-A_{i-2,j,k}}{12\Delta x_1^2}=d_{i,j,k}$$

$$s_1\cdot A_{i+2,j,k}-16\cdot s_1\cdot A_{i+1,j,k}+(1+30\cdot s_1)\cdot A_{i,j,k}- -16\cdot s_1\cdot A_{i-1,j,k}+s_1\cdot A_{i-2,j,k}=d_{i,j,k} \quad (11)$$

where $s_1=\Delta t/(24\cdot Re\cdot Pr\cdot\Delta x_1^2)$

This equation (8) is solved by the method of the penta-diagonal matrix, which determines $A_{i,j,k}$. The same procedure is repeated further for directions x_2 in the second stage, namely, $B_{i,j,k}$ is determined by solving equation (9) , and the solution from the first stage, as the coefficient on the right, and the s_1 coefficient in the penta-diagonal matrix are replaced by $s_2=\Delta t/(24\cdot Re\cdot Pr\cdot\Delta x_2^2)$. Finally, in the third stage $q_{i,j,k}$ is solved using a similar penta-diagonal system shown in equation (9) . Once we have determined the value $q_{i,j,k}$, we find $\bar{\theta}^{n+1}_{i,j,k}$.

$$\bar{\theta}_{i,j,k}^{n+1} = q_{i,j,k} + \bar{\theta}_{i,j,k}^{n}$$

The other components of temperature $\bar{\theta}_{i,j,k}^{n+1}$ are solved in a similar way.

Simulation results As for the physics of the influence of MHD on the structure of natural convection flow with a homogeneous electron concentration and heat transfer, this is due to the fact that in MHD flows the motion of vortex structures perpendicular to magnetic fields, i.e. horizontally oriented vortex cells, strongly suppressed due to the anisotropic effect of the magnetic field. This is recognized by the universal effect of magnetic fields, which is theoretically interpreted in [17]. Moreover, another important characteristic of the effect of the vertical magnetic field is that when the magnetic fields are stronger, the vortex structures will be more regular and will be shown parallel to each other. Consequently, thermal convection caused by the movement of the vortex cells will decrease due to the amplification of magnetic fields.

The results of modeling three dimensional MHD convection are obtained, where the lateral distribution of the temperature field is considered. Prandtl number is chosen $Pr = 0,733$. Characterestical length is $L = 1m$, characteristical velocity $U_0 = \sqrt{(Gr\nu^2)/L^2}$. To simulate the natural convection of the MHD, the Grashof number, the viscositv (HFDM), the thermal conductivity for different mesh sizes have been shown in Table 2. A comparison of the average Nusselt number for various Grashof

Table 1. Magnitude of the viscosity for different Grashof number.

Gr	$N_1 \times N_2 \times N_3$	Viscosity, ν [13]	Viscosity (HFDM)	α (HFDM)
2×10^3	$60 \times 60 \times 60$	0.077	0,001283	0,00175075
2×10^4	$70 \times 70 \times 70$	0.028	0,0004	0,0005457
2×10^5	$90 \times 90 \times 90$	0.011	0,00012	0,00016371

and Hartmann numbers were made between present work results and with the literature data of works [13], [14] have been shown in Table 2. The rate of heat transfer through the cavity is obtained by estimating the average Nusselt number on the walls of the cavity. It is seen that, Nu decreases with an increase of Hartmann number and the Nusselt number approaches unity for a strong magnetic field. This shows that, the convection in the domain is supressed by the influence of magnetic field, convection proceeds in the diffusion process.

Figure 2 shows the comparison results of present work with authors [13] and [14] the influence of Hartmann number on the average Nusselt number according to the Table 2. The influence of the magnetic field on the Nusselt number is greater in the region of small Grashof numbers. At a high Grashof number, the magnetic field reduces the Nusselt number slightly.

The effect of Grashof number on the local Nusselt number on the cold and hot walls has been investigated for different Grashof numbers and different Hartmann numbers a) $Ha = 0$; b) $Ha = 50$; c) $Ha = 100$. At Figure 3 can be seen, that the local Nusselt number on both the hot and cold walls increases sharply due to an increase in the Grashof

Table 2. Comparison of the average Nusselt number.

Gr	Ha	Present work HFDM	Sajjadi et al. [13]	Rudraiah et al.[14]
$Gr = 2 \times 10^4$	0	2.4325	2.4315	2.5188
	10	2.2520	2.2510	2.2234
	50	1.0875	1.0902	1.0856
	100	1.0210	1.0208	1.0110
$Gr = 2 \times 10^5$	0	5.0025	5.0151	4.9198
	10	4.9013	4.9085	4.8053
	50	2.9877	2.9915	2.8442
	100	1.4335	1.4384	1.4317

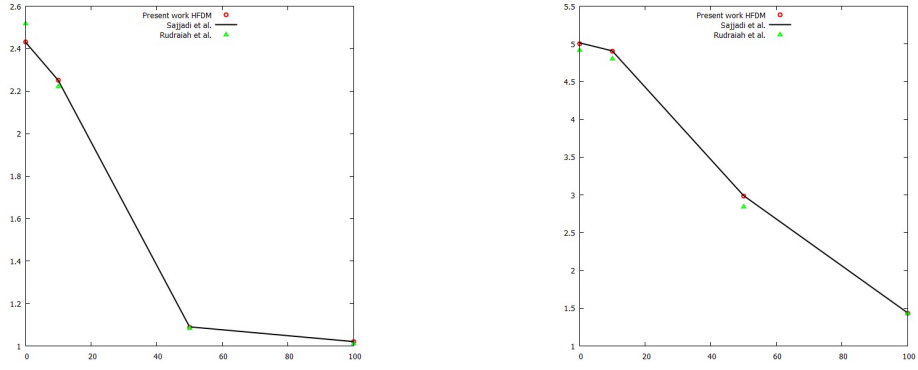

a) b)

Figure 2. Comparison of the average Nusselt number in graphs for (a) $Gr = 2 \times 10^4$, (b)$Gr = 2 \times 10^5$.

number, and the maximum value of the local Nusselt number for $Gr = 2 \times 10^5$ is two times greater, than for $Gr = 2 \times 10^4$ and four times greater, than $Gr = 2 \times 10^3$ at $Ha = 0$. The influence of the Grashof number increases for Hartmann number $Ha = 100$ and for $Ha = 50$, the maximum value of the local Nusselt number for the highest Grashof number $Gr = 2 \times 10^5$ is five times more than the lowest Grashof number $Gr = 2 \times 10^3$.

Figure 4 shows the comparison of the vertical velocity along the section $x_2 = 0.5$ and $x_3 = 0.5$ of the cavity for different Grashof and Hartmann numbers. Obviously, the velocity value increases due to a significant increase of the Hartmann number, which cause an increase in the heat transfer rate, as indicated in Figure 3 and in Table 2.

At Figure 5 illustrates the effect of the Hartmann number on isothermal surfaces at Grashof number $Gr = 2 \times 10^4$. Isothermal surfaces change significantly with a change of the Hartmann number and become parallel to the x_3 direction with an increase in the Hartmann number. In addition, the temperature difference of the cavity decreases, and this means that the heat transfer rate decreases.

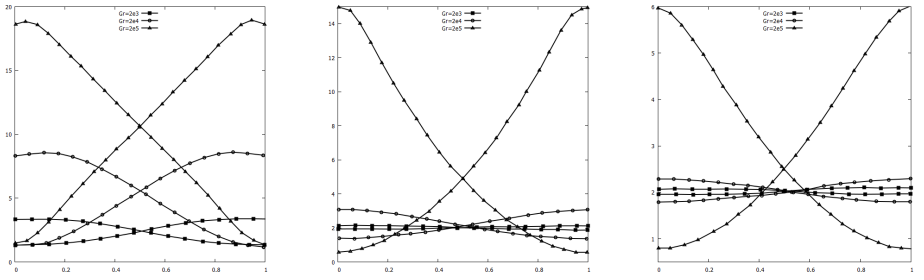

a) b) c)

Figure 3. Local Nusselt number on the hot and cold walls for (a)$Ha = 0$; (b) $Ha = 50$; (c) $Ha = 100$.

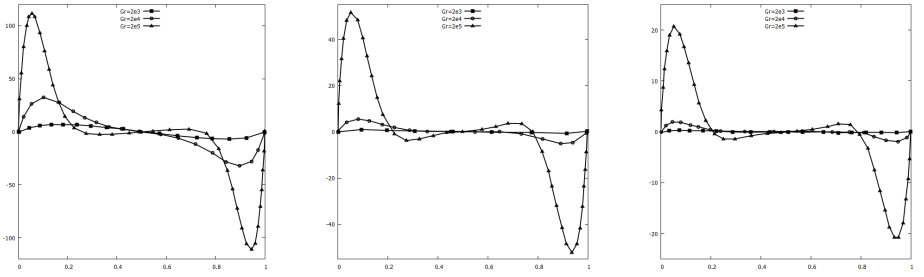

a) b) c)

Figure 4. Vertical velocity on midline $x_2 = 0.5$ and $x_3 = 0.5$ of the cavity (a)$Ha = 0$; (b)$Ha = 50$; (c) $Ha = 100$.

Temperature distributions on the middle of the cavity at different plane $x_1 = 0.5$, $x_2 = 0.5$, $x_3 = 0.5$ of the domain have been shown at Figure 6– Figure 8 for fixed Grashof number $Gr = 2 \times 10^4$ and different Hartmann numbers a) $Ha = 0$; b) $Ha = 50$; c) $Ha = 100$. When a magnetic field B0 is applied in the direction of x_3 , as was mentioned in the equations studied, the electromagnetic force acts on x_1 and x_2 , which means that the field strength in the corresponding directions will be reduced. For the plane $x_3 = 0.5$, it was found in Figure 6, that the temperature contours extended into the center of the domain and distribution becomes uniform by increasing the Hartmann number from 0 to 100.

On the plane $x_1 = 0.5$ of the cavity at Figure 7, the value of the isotherms sharply decreases with incresing the Hartmann number from 0 to 100, and the isotherms gradually become homogeneous and parallel to the x_2 direction. In addition, the flow is suppressed with an increase in the Hartmann number $Ha = 50$ and $Ha = 100$.

It is seen at Figure 8, that the isothermal lines are curved due to the intensification of the convection effect at $Ha = 0$ and with increasing the Hartmann numbers $Ha = 50$ and $Ha = 100$, the isothermal lines change significantly and become almost parallel to the right and left walls, which reduces the rate of heat transfer. The influence of the magnetic field on the vertical velocity can be seen from Figure 9. The vertical velocity U

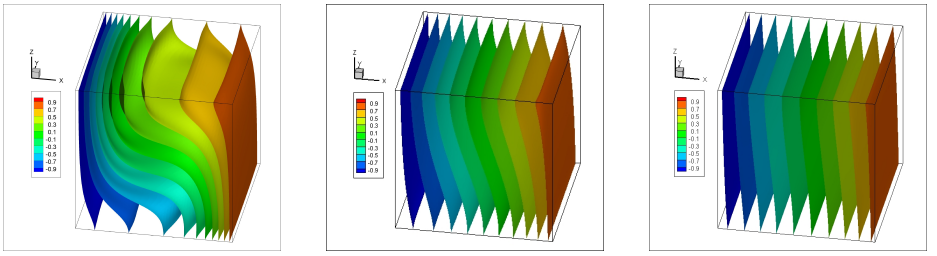

a) b) c)

Figure 5. Isothermal surfaces for (a)$Ha = 0$; (b) $Ha = 50$; (c) $Ha = 100$.

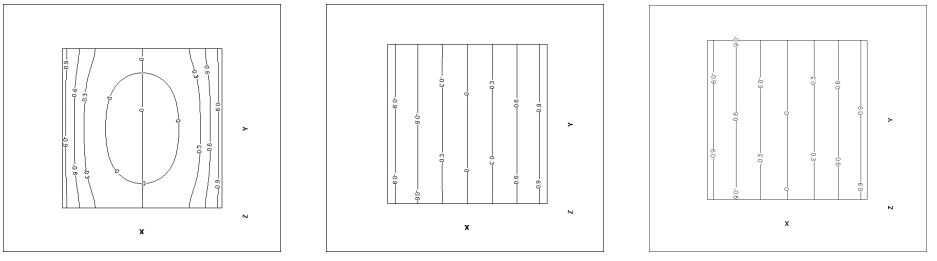

a) b) c)

Figure 6. Isotherms on the $x_3 = 0.5$ plane for $Gr = 2 \times 10^4$ and (a)$Ha = 0$; (b) $Ha = 50$; (c) $Ha = 100$.

aligned to the magnetic field and supressed. The vertical velocity is plotted for various Hartmann numbers $Ha = 0; Ha = 50; Ha = 100$ and for various values Grashof numbers (a) $Gr = 2 \times 10^4$ and (b)$Gr = 2 \times 10^5$. An increase Hartmann number in the magnetic field smoothes the peak of velocity near the wall.

As for the physics of the influence of MHD on the structure of natural convection flows with homogeneous electron concentration and heat transfer, this is due to the fact that in MHD flows the motion of vortex structures perpendicular to magnetic fields, i.e. horizontally oriented vortex cells, strongly suppressed due to the anisotropic effect of the magnetic field. This is recognized by the universal effect of magnetic fields, which is theoretically interpreted in [17]. Moreover, another important characteristic of the effect of the vertical magnetic field is that when the magnetic fields are stronger, the vortex structures will be more regular and will be shown parallel to each other. Consequently, thermal convection caused by the movement of the vortex cells will decrease due to the amplification of magnetic fields.Numerical algorithm results for natural convection flows with homogeneous electron concentration and heat transfer showed good agreements with [13] and [14].

Conclusion

The modeling of MHD natural convection flow with a uniformly distributed electron concentration $\bar{n} = 1$ and for a variable electron concentration in a cubic cavity are

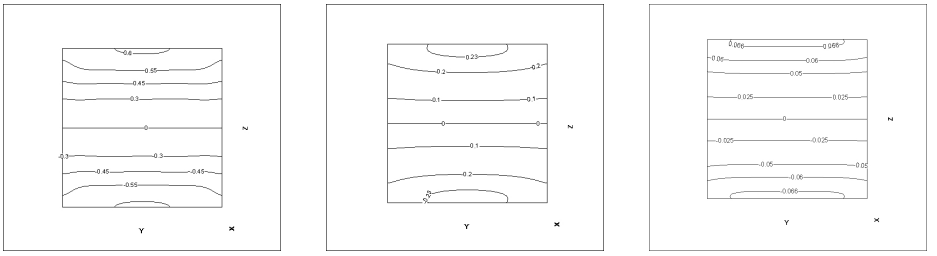

a) b) c)

Figure 7. Isotherms on the $x_1 = 0.5$ plane for $Gr = 2 \times 10^4$ and (a)$Ha = 0$; (b) $Ha = 50$; (c) $Ha = 100$.

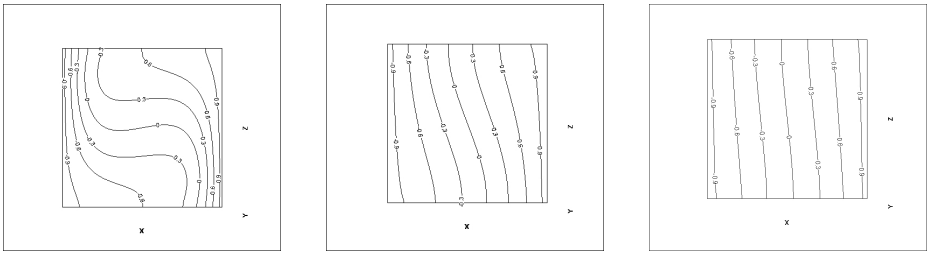

a) b) c)

Figure 8. Isotherms on the $x_2 = 0.5$ plane for $Gr = 2 \times 10^4$ and (a)$Ha = 0$; (b) $Ha = 50$; (c) $Ha = 100$.

studied by HFDM method. Numerical results of natural convection were obtained for various values of Grashof and Hartmann numbers. The effect of Hartmann and Grashof numbers on the projection of heat transfer rate on different surfaces of the concentrated with electron cavity is studied. The results obtained in this study are in qualitative and quantitative agreement with the studyies of work [13] by LBM and two dimensional study [14] by Finite difference methods. The average Nusselt number increases by augmentation of the Grashof number at a fixed Hartmann number. Compared with the available data, results show a good agreement and the average error is less than 1.9%. The structure of the flow and isotherms in different planes of the enclosure change dramatically due to an increase in the Hartmann and Grashof numbers, since the magnetic field is strong, and the velocities with electron concentrated flow are suppressed. The effect of the vertical magnetic field is that, when the magnetic fields are stronger, the vortex structures will be more regular and will be shown parallel to each other. Consequently, thermal convection flow with electron concentration caused by the movement of the vortex cells will decrease due to the amplification of magnetic fields and convection process is transformed to diffusion process.

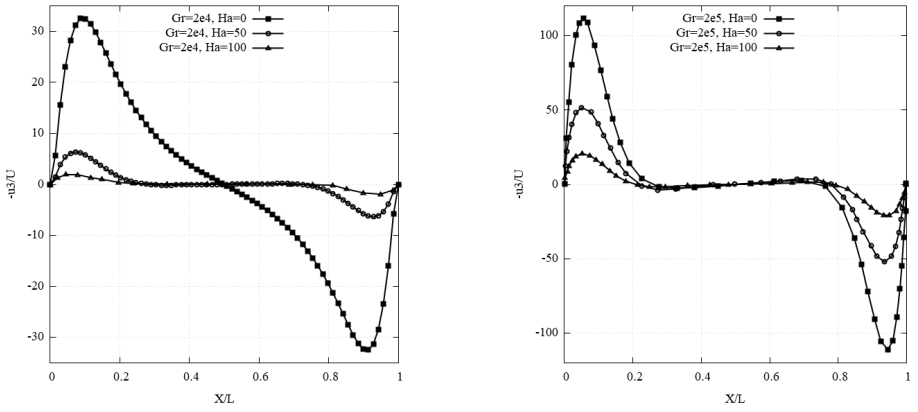

a) b)

Figure 9. Vertical velocity component midheight $x_1 = 0.5$ at $Ha = 0$; $Ha = 50$, $Ha = 100$ for (a)$Gr = 2 \times 10^4$; (b)$Gr = 2 \times 10^5$.

Acknowledgement.

This work was supported by Ministry of Education and Science of the Republic of Kazakhstan [Grant No. AP05133516, 2020]

References

1. Hossain, M.A., and Khanafer, K., and Vafai, K.: The effect of radiation on free convection flow of fluid with variable viscosity from a porous vertical plate.Thermal science **40**, 115–124 (2001).
2. Sajjadi, H., and Hosseinizadeh, S.F., and Gorji, M., and Kefayati, Gh.R.: Numerical analysis of turbulent natural convection flow in a square cavity using Large-Eddy Simulation in Lattice Boltzmann . Transactions of mechanical Engineering**35**, 133–124 (2011).
3. Kefayati, Gh.R., and Sajjadi, H.and Ganji, D., and Gorji, M.: Lattice Boltzmann simulation of MHD mixed convection in a lid-driven square cavity with linearly heated wall .Scientica Iranica **19**, 1053–1065 (2012).
4. Xu,B., and Li,B.Q., and Stock, D.E.: An experimental study of thermally induced convection of molten gallium in magnetic fields .Heat and Mass Transfer **49** 2009–2019 (2006).
5. Ashorynejad, H.R., and Mohamad, A.A., and Sheikholeslami M.: Magnetic field effects on natural convection flow of a nanofluid in a horizontal cylindrical annulus using Lattice Boltzmann method . Thermal Sciences **64**, 240 – 250 (2013).
6. Grosan,T., and Revnic, C., and Pop, I., and Ingham, D.B.: Magnetic field and internal heat generation effects on the free convection in a rectangular cavity filled with a porous medium. Heat and Mass Transfer**104**, 878 – 889 (2017).
7. Sivasankaran, S., andMalleswaran, A., andLee, J., and Sundar,P.: Hydro-magnetic combined convection in a lid-driven cavity with sinusoidal boundary conditions on both sidewalls. Heat and Mass Transfer **54**, 512–525 (2011).
8. Oztop, H.F., and Al-Salem, K., and Pop, I.: MHD mixed convection in a lid-driven cavity with corner heater. Heat and Mass Transfer **54**, 3494-3504 (2011).

9. Gelfgat, A.Yu., and Zikanov, O.: Computational modeling of magnetoconvection: effects of discretization method, grid refinement and grid stretching. Computers and Fluids **175**, 66 – 82 (2018).
10. Sheikholeslami, M.: Lattice Boltzmann method simulation for MHD non-Darcy nanofluid free convection. Physica B: Condensed Matter **516**, 55–71 (2017).
11. Zhang, T., and Che, D.: Double MRT thermal lattice Boltzmann simulation for MHD natural convection of nanofluids in an inclined cavity with four square heat sources. Heat and Mass Transfer**94**, 87–100 (2016).
12. Sajjadi, H.and Atashafrooz, M.: Double MRT thermal lattice Boltzmann simulation for MHD natural convection of nanofluids in an inclined cavity with four square heat sources. Heat and Mass Transfer **126**, 489–503 (2018).
13. Sajjadi, H.and Atashafrooz, M.: Simulation of the dimensional MHD natural convection using double MRT Lattice Boltzmann method. Physica A:Statistical Mechanics and its Applications **515**, 474–496 (2019).
14. Rudraiah, N., and Barron, R., and Venkatachalappa, M., and Subbaraya, C.: Effect of a magnetic field on free convection in a rectangular enclosure. Engineering Science **33**, 1075–1084 (1995).
15. Abdibekova, A., and Zhakebayev, D., and Abdigaliyeva, A., and Zhubat, K.: Modeling of turbulence energy decay based on hybrid methods. Engineering Computations **35**, 1965–1977 (2018).
16. Abdibekova, A., and Zhakebayev, D., and Zhumagulov, B.: The decay of MHD turbulence depending on the conductive properties of the environment. Magnetohydrosynamics **50**, 121–138 (2014).
17. Davidson, P.: Magnetic damping of jets and vortices. Fluid Mechanics **299**, 153–186 (1995).

Movement of Fluid Inside the Sphere

Maksut Abenov[1][0000−0002−9583−5697] and Mars Gabbassov[2][0000−0001−8891−1826]

[1] Al-Farabi Kazakh National University, Almaty, Kazakhstan,
abenov60@gmail.com
[2] "Factor" System Research Company LLP, Nur-Sultan, Kazakhstan,
mars0@mail.ru

Abstract The paper presents an exact analytical solution of the stationary problem of an incompressible ideal fluid flow inside a sphere under the action of an potential gravity mass force.

Keywords: continuity equation, four-dimensional functions, generalized Cauchy - Riemann conditions.

Introduction

Most applied problems in mechanics and theoretical physics lead to the need to define specific four-dimensional vector functions in the form of $\vec{V} = (V_0, V_1, V_2, V_3)$, whose components V_k are real functions of four real variables: time t and spatial variables x, y, z [2-4]. The components of unknown four-dimensional vector are usually appeared in various systems of differential motion equations deduced from the laws of conservation in mechanics and physics. A special interest for practical purposes (engineering calculations) is finding classical solutions of such systems of equations in explicit form, when the components of desired four-dimensional vector are smooth functions in some domain of definition. However, existing mathematical apparatus often leads to the need to study one-dimensional or two-dimensional (simplified) models of these applied problems. In most cases, it is necessary to consider only stationary physical processes. Therefore, searching for a proper mathematical apparatus for finding classical solutions of the basic systems of motion equations in mechanics and theoretical physics is an actual problem. This paper describes an application of a perspective, in our opinion, approach for solving a rather difficult problem of hydrodynamics.

Definition of the Four-Dimensional Functions Space

Definition 1. *Image* $U = [U_0(x_0, x_1, x_2, x_3), U_1(...), U_2(...), U_3(...)]$ *under continuous mapping* $U : X = (x_0, x_1, x_2, x_3) \in G \to U = (U_0, U_1, U_2, U_3) \in R^4$ *is called four-dimensional function.*

It is easy to understand, that each component $U_k(x_0, x_1, x_2, x_3), k = \overline{0,3}$ is a real continuous function of four real variables determined in domain $G \subset R^4$. In what follows, a set of all possible four dimensional functions with continuous components

will be denoted by $C[M(G)]$. Further, any four-dimensional vector of theoretical physics with continuous components $\vec{V} = (V_0, V_1, V_2, V_3)$, can be represented as an element of the $C[M(G)]$ space. Indeed, let the required four-dimensional vector is being sought in some four-dimensional domain $G \subset R^4$ and has continuous components. Then it inevitably follows that $\vec{V} \in C[M(G)]$, since by definition this space contains all possible four-dimensional functions in the given domain.

Next, we study one of the key subspaces of the linear space $C[M(G)]$. It is the elements of this subspace that are directly used in solving applied problems of mechanics and theoretical physics.

Definition 2. *A four-dimensional function $u \in C[M(G)]$ is called regular, if its components everywhere in domain G satisfy generalized Cauchy-Riemann conditions (D'Alembert-Euler) of the form:*

$$\frac{\partial u_0}{\partial x_0} = \frac{\partial u_1}{\partial x_1} = \frac{\partial u_2}{\partial x_2} = \frac{\partial u_3}{\partial x_3},$$

$$\frac{\partial u_0}{\partial x_1} = \frac{\partial u_1}{\partial x_0} = \frac{\partial u_2}{\partial x_3} = \frac{\partial u_3}{\partial x_2},$$

$$\frac{\partial u_0}{\partial x_2} = \frac{\partial u_1}{\partial x_3} = -\frac{\partial u_2}{\partial x_0} = -\frac{\partial u_3}{\partial x_1},$$

$$\frac{\partial u_0}{\partial x_3} = \frac{\partial u_1}{\partial x_2} = -\frac{\partial u_2}{\partial x_1} = -\frac{\partial u_3}{\partial x_0}. \tag{1}$$

The whole set of regular functions in $G \subset R^4$ is denoted by $M_A(G)$. It is obvious that any constant four-dimensional vector, an element of R^4, is certainly a constant regular function in any $G \subset R^4$ domain. It was shown in reference [3], that $M_A(G) \subset C[M(G)]$ is a infinite-dimensional subspace. Further, in [3] an explicit form of the basic elementary functions $u(X) \in M_A(G)$ of the four -dimensional variable $X = (x_0, x_1, x_2, x_3) \in G$. Let us give an explicit form of some elementary functions:

1. $u = X^2 = (u_0, u_1, u_2, u_3)$, where:

$$u_0 = 2(x_0x_1 - x_2x_3); u_1 = x_0^2 + x_1^2 - x_2^2 - x_3^2;$$

$$u_2 = 2(x_0x_3 + x_1x_2); u_3 = 2(x_0x_1 + x_1x_3). \tag{2}$$

2. $u = \sin X = (u_0, u_1, u_2, u_3)$, where:

$$u_0 = \frac{1}{2}[\sin(x_1 + x_0)\cosh(x_2 + x_3) - \sin(x_1 - x_0)\cosh(x_2 - x_3)];$$

$$u_1 = \frac{1}{2}[\sin(x_1 + x_0)\cosh(x_2 + x_3) + \sin(x_1 - x_0)\cosh(x_2 - x_3)];$$

$$u_2 = \frac{1}{2}[\cos(x_1 + x_0)\sinh(x_2 + x_3) + \cos(x_1 - x_0)\sinh(x_2 - x_3)];$$

$$u_3 = \frac{1}{2}[\cos(x_1 + x_0)\sinh(x_2 + x_3) - \cos(x_1 - x_0)\sinh(x_2 - x_3)].$$

It is easy to verify that these components satisfy the regularity conditions (1). The material presented leads to the following conclusions:

1. The linear vector space C[M(G)] of continuous four-dimensional functions is infinite-dimensional;

2. All the elements of its linear subspace $M_A(G) \subset C[M(G)]$ can be considered as four-dimensional generalizations of one dimensional or two-dimensional functions from real or complex analysis. Indeed, setting in the formula of any regular function $x_0 = x_2 = x_3 = 0$, we get a typical function of one real variable x_1. If you set $x_0 = x_3 = 0$ in the formula, you can get a typical function of the complex variable $z = x_1 + ix_2$. More details about this are given in [3].

Valuation and completeness of the $C[M(G)]$ space

Let a domain $G \subset R^4$ is compact. Then for any element of the linear space $U = [U_0(x_0, x_1, x_2, x_3), U_1(...), U_2(...), U_3(...)] \in C[M(G)]$, we can introduce a notion of norm by the following formula:

$$\|U(X)\| = max_{0 \le k \le 3}[sup_{X \in G}|U_k|]. \tag{3}$$

It is easy to verify that, with respect to such a uniform norm, $C[M(G)]$ is a complete normed space, if we mean the componentwise convergence of a sequence of four-dimensional continuous functions. Further, for the application, the most important conclusions following from Stone's well-known theorem [1] are:

1. The subspace $M_A(G)$ is an everywhere dense subset of $C[M(G)]$.

2. Any element $W \in C[M(G)]$ can be approximated with any given accuracy by a finite sum of regular four-dimensional functions.

3. A finite sum of regular functions is also a regular function. Therefore, when solving applied problems of mechanics and theoretical physics, the mathematical apparatus of the theory of four-dimensional regular functions can be used.

All the above-mentioned, we will demonstrate below, based on an actual example of solving one problem of hydrodynamics.

Applications

In this section, we obtain an exact analytic solution of one, rather complicated, problem of hydrodynamics. Let suppose, that an ideal incompressible fluid filled with a spherical vessel of radius R flows with a characteristic velocity c, under the action of a stationary gravity force $\vec{F} = (0, 0, -g)$. Need to find the hydrodynamic characteristics of the fluid moving inside the sphere. Let $\vec{V} = [V_1(x, y, z), V_2(x, y, z), V_3(x, y, z)]$ is required velocity vector of the moving fluid, $P(x, y, z)$ is required pressure function, $\rho > 0$ is known fluid density. Then, as is known from [4], the mathematical setting up the problem is formulated as follows: In the domain $D : x^2 + y^2 + z^2 < R^2$ with boundary $S : x^2 + y^2 + z^2 = R^2$, to find solution of the Euler equations system

$$(\vec{V} \cdot \nabla)\vec{V} + \frac{\nabla P}{\rho} = \vec{F} \tag{4}$$

with contiunity condition:

$$div\vec{V} = 0 \tag{5}$$

and the boundary condition:

$$V_n|_S = 0 \tag{6}$$

Further, in the reference [3] a formula of a general solution of (5) in a class of smooth functions is given in the form:

$$V_1(x,y,z) = cu_1\left(0, \frac{x}{R}, \frac{\beta y}{R}, \frac{\gamma z}{R}\right), \tag{7}$$

$$V_2(x,y,z) = -c\beta_1 u_2\left(0, \frac{x}{R}, \frac{\beta y}{R}, \frac{\gamma z}{R}\right), \tag{8}$$

$$V_3(x,y,z) = -c\gamma_1 u_3\left(0, \frac{x}{R}, \frac{\beta y}{R}, \frac{\gamma z}{R}\right), \tag{9}$$

Here: $\beta, \gamma, \beta_1, \gamma_1$ are arbitrary scalars (real or complex) connected by the condition: $1 - \beta\beta_1 - \gamma\gamma_1 = 0$, c is some speed typical for given flow, R is the characteristic dimension of the flow, $u_k(0, x_1, x_2, x_3), k = \overline{0,3}$ are components of an arbitrary regular function, calculated for $x_0 = 0$.

In this case, from the symmetry considerations (the domain, where the solution is sought, is spherically symmetric) we choose in the formulas (7)–(9) the corresponding components of the four-dimensional function $u = X^2 - 1$ (they are indicated above), i.e:.

$$u_0 = 2(x_0x_1 - x_2x_3); u_1 = x_0^2 + x_1^2 - x_2^2 - x_3^2 - 1;$$
$$u_2 = 2(x_0x_3 + x_1x_2); u_3 = 2(x_0x_1 + x_1x_3). \tag{10}$$

Further, from considerations of symmetry, we can put:

$$\beta = \gamma; \beta_1 = \gamma_1 \to \beta\beta_1 = \gamma\gamma_1 = \frac{1}{2}$$

Then (7)–(9) can be rewritten as:

$$V_1(x,y,z) = \frac{c}{R^2}(x^2 - \beta^2y^2 - \beta^2z^2 - R^2), \tag{11}$$

$$V_2(x,y,z) = \frac{-cxy}{R^2}, \tag{12}$$

$$V_3(x,y,z) = \frac{-cxz}{R^2}, \tag{13}$$

It is easy to check, that (11)–(13) satisfies condition (5) for any β. Now, to determine β, we use the condition (6).

$$V_n = 2xV_1 + 2yV_2 + 2zV_3 = \frac{2cx}{R^2}[x^2 - (\beta^2 + 1)(y^2 + z^2) - R^2]$$

. Thus, condition (6) is satisfied only for $\beta^2 = -2$ and the sought velocity components take the final form:

$$V_1(x,y,z) = \frac{c}{R^2}(x^2 + 2y^2 + 2z^2 - R^2), \tag{14}$$

$$V_2(x,y,z) = \frac{-cxy}{R^2}, \tag{15}$$

$$V_3(x,y,z) = \frac{-cxz}{R^2}, \tag{16}$$

Further, to determine the unknown pressure $P(x,y,z)$, we substitute (14)–(16) into equations (4).Then, we get:

$$\frac{1}{\rho}\frac{\partial P}{\partial x} = -\frac{2c^2x(x^2 - R^2)}{R^4}, \tag{17}$$

$$\frac{1}{\rho}\frac{\partial P}{\partial y} = \frac{c^2y(2y^2 + 2z^2 - R^2)}{R^4}, \tag{18}$$

$$\frac{1}{\rho}\frac{\partial P}{\partial z} = -g + \frac{c^2z(2y^2 + 2z^2 - R^2)}{R^4}. \tag{19}$$

Finally, the unknown pressure $P(x,y,z)$ is written as:

$$P(x,y,z) = C + \frac{\rho c^2}{2R^4}\left[(y^2+z^2)^2 - x^4 + r^2(2x^2 - y^2 - z^2)\right] - \rho g z \tag{20}$$

An arbitrary constant C is determined from the condition

$$\int_D P(x,y,z)dxdydz = 0.$$

By direct substitution it is easy to verify that the functions (14)–(16) and (20) give an exact solution of the original problem (4)–(6).

Conclusion

The exact analytical solution of the problem of fluid flowing inside a sphere with Neumann boundary conditions using the theory of four-dimensional regular functions is obtained. The proposed approach can be applied for solving other similar hydrodynamic problems.The monograph [3] gives some examples of the application of similar methods in quantum mechanics and celestial mechanics. Generally speaking, four-dimensional analysis provides a promising mathematical apparatus for solving applied problems in theoretical physics.

References

1. Stoun M.: Application of the theory of Boolean rings to general topology. Trans.Amer.Math.Soc.,41. (1937)
2. Arfken, George B., and Hans J. Weber.: Mathematical Methods for Physicists, Academic Press, fifth edition, 2001.
3. Abenov M.M. : Four -dimensional mathematics:methods and applications (in Russian). Almaty, Kazakh University Press (2019)
4. Loitzansky L.G. : Fluid Mechanics. 2nd edition. M, Drofa (2003)

Numerical Investigation of Single and Two-phase Flow Through a Fibrous Porous Medium*

Zhibek Akasheva[1 [0000−0001−7668−8911]],
Bakytzhan Assilbekov[1 [0000−0002−0368−0131]],
Aziz Kudaikulov[1 [0000−0002−4389−4097]],
Aidarkhan Kaltayev[1 [0000−0003−2180−2785]], and
Darezhat Bolysbek[1,2 [0000−0001−8936−3921]]

[1] Satbayev University, Almaty, Kazakhstan
http://www.satbayev.university
[2] al-Farabi Kazakh National University, Almaty, Kazakhstan
https://www.kaznu.kz

Abstract Single- and two-phase flow through a fibrous porous medium is numerically simulated, where fibrous porous medium is represented as parallel cylinders with circular cross-section and their centers are located at the same distance from each other. The simulation is based on the numerical solution of incompressible Navier-Stokes equations in irregular domains, where the irregular boundary is represented by its level-set function.

For the case of single-phase flow, the permeability of this medium is calculated and compared with analytical solution. Also, the Reynolds number below which the fluid flow in porous medium obeys linear Darcys law for different kinds of porous medium is determined.

For the case of two-phase flow, the effect of numerical slip length on the distribution of pressure drop and saturation is investigated. Variations of pressure drop and saturation in time are numerically calculated for different values of cylinders radii, surface tension (σ), viscosity ratio (M=μ_{nw}/μ_w), and mesh sizes. The presented results show that variations of saturation and pressure drop in time vary with mesh refinement, so the numerical slip length significantly affects the flow. The results show that the contact line motion significantly depends not only on the microstructure of the porous media, but also on the fluid properties (viscosity ratio, surface tension and etc.).

Numerical calculations are performed using the interFoam solver in OpenFOAM®finite volume library.

Keywords: Pore-scale modeling, Fibrous porous medium, Two-phase flow, Wetting, Permeability.

* Supported by the Science Committee of the Ministry of Education and Science of the Republic of Kazakhstan (Grant No. AP08052055 “Investigation of the influence of the dissolution modes of carbonate core samples on the characteristics of the flow of a two-phase fluid through it in the pore scale”) and project “Stimulation of Productive Innovations” (as part of the sub-project APP-JRG-17/0448F “Development and implementation of an integrated software product for a comprehensive solution of production stimulation problems on hydrocarbon fields”).

Introduction

Pore-scale modeling of multiphase flow is of particular scientific interest. Shams et al. presented a simple and efficient numerical method for modelling two-phase flow in porous media at the micro-scale. Interfacial forces using a sharp surface force model that can efficiently eliminate the problem of spurious currents has been computed. The explicit representation of the interface used to compute interfacial forces leads to an accurate estimation of capillary pressure even for low grid resolutions [1]. Scanzaniani et al. studied two-phase flow invasion patterns in a mixed-wet porous medium, using dynamic high-resolution X-ray synchrotron imaging. They observed that the movement of water in the initially oil-filled medium is limited by interface pinning, responsible for contact angle hysteresis. This prevents interface recession and snap-off during the displacement [2].

Akai et al. performed two-phase direct numerical simulations on complex 3D porous media with three wettability states: uniformly water-wet, uniformly oil-wet, and non-uniform mixed-wet. They computed the thermodynamic contact angle, then compared with the input contact angles. They concluded that the spatial distribution of wettability can be represented by the thermodynamic contact angle computed on a pore-by-pore basis [3]. Foroughi et al. used the results of pore-scale imaging experiments to calibrate and validate simulations, and specifically to find the pore-scale distribution of wettability. Their model predictions for capillary pressure and relative permeability are in good agreement with the experiments [4].

Raeini et al. presented a validation of the generalized network model using micro-CT images of two-phase flow experiments on a pore-by-pore basis. Three experimental secondary imbibition datasets were studied for both sandstone and carbonate rock samples. The results provided a methodology for improving physical models using large experimental datasets which, at the pore scale, can be generated using micro-CT imaging of multiphase flow [5].

Bultreys et al. introduced a methodology to quantitatively compare models to experimental fluid distributions in flow experiments visualized with microcomputed tomography. First, they analyzed five repeated drainage-imbibition experiments on a single sample. Then two fractional flow experiments were used to validate a quasistatic pore network model. The model correctly predicted the fluid present in more than 75% of pores and throats in drainage and imbibition. The presented analysis illustrates the potential of their methodology to systematically and robustly test two-phase flow models to aid in model development and calibration [6].

In this article, numerical calculations were performed for single and two-phase flow in a fibrous porous medium, since they are quite common (filters, catalysts, fuel cells, heat exchangers and etc.).

For the case of a single-phase flow there is a need in only one characteristic absolute permeability, on the basis of which all other characteristics can be calculated. In this work absolute permeability was calculated and compared with analytical solution.

Pore-scale two-phase flow modeling is an important technology to study a rock's relative permeability behavior [6]. For the numerical simulation of a two-phase flow, a clear specification of wettability is necessary, since it significantly affects the nature of the flow. Based on the Young equation, the wettability is defined using contact angle:

the angle that the two-fluid interface forms at the solid surface [3]. Also, the numerical slip length affects the nature of fluid flow in a porous medium. As calculations showed with mesh decreasing, the numerical slip length also decreases.

Single-phase flow

Numerical methodology

Single-phase flow through a fibrous porous medium where porous material is represented as parallel periodic cylinders of equal radius is examined in this section (see Fig. 1). Therefore, the domain with one cylinder in the middle can be considered. Boundary conditions used for this problem are shown on Fig1b (L is the domain size). The flow direction is perpendicular to the axes of cylinders.

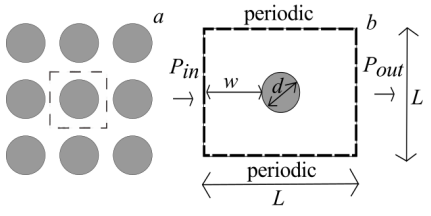

Figure 1. Periodically arranged cylinders

This model is based on numerical solution of the incompressible flow in irregular domains, where irregular boundary is represented by its level-set function [7]. The flow is described using the Navier-Stokes equations:

$$\frac{\partial \vec{u}}{\partial t} + \vec{u} \cdot \nabla \vec{u} = -\nabla P + \frac{1}{Re} \nabla^2 \vec{u}, \tag{1}$$

$$\nabla \cdot \vec{u} = 0, \tag{2}$$

where u is the velocity, m/s; P is the pressure, Pa; and Re is the Reynolds number.

Initial condition for the velocity of fluid flow:

$$\vec{u}(0, x, y) = 0, \tag{3}$$

Boundary conditions on the boundaries of the domain (dashed lines on Fig.1b) are:

$$u(x = 0, y) = u(x = L, y), \tag{4}$$

$$u(x, y = 0) = u(x, y = L), \tag{5}$$

$$P(x = 0, y) = P_{in}, \tag{6}$$

$$P(x = L, y) = P_{out}, \tag{7}$$

$$P(x, y = 0) = P(x, y = L), \tag{8}$$

where P_{in} is the inlet pressure, Pa; P_{out} the outlet pressure, Pa.

No-slip boundary condition is used on the surface of the cylinders:

$$u(t, x, y)|_{d\Omega} = 0. \tag{9}$$

where $d\Omega$ is the surface of the cylinder.

Searching of Reynolds number for linear Darcys law

Reynolds number below which the fluid flow in porous medium obeys linear Darcys law in isotropic and anisotropic porous media is found in this section.

Whitaker examined that the linear Darcys law is valid for Reynolds numbers Re<<1 using the method of volume averaging [8]. To investigate this condition, it is sufficient to calculate the permeability in linear Darcys law, which is written as following for single-phase flow:

$$U = \frac{K}{\mu} \frac{P_{in} - P_{out}}{L}, \tag{10}$$

where K is the absolute permeability, m^2; μ is the dynamic viscosity, Pa*s; and U the is volume-averaged velocity:

$$U = \frac{1}{V} \int_V u dV. \tag{11}$$

where V is the volume, m^3.

In isotropic medium, all cylinders in the model are located at the same distance from each other and the coordinates of one cylinder are x_c=0.5 and y_c=0.5 and have a diameter of d=0.4. In anisotropic medium, cylinder C in the model is shifted relative to other cylinders (y_c has a different values) as shown in Fig. 2. For this case, we move the location of the cylinder (y_c coordinate) and study the relation between the Reynolds number and permeability.

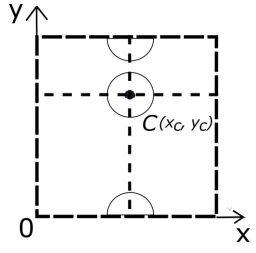

Figure 2. Anisotropic porous medium

Fig. 3 demonstrates the $K - Re$ relationships for the anisotropic porous medium (cylinders with d=0.2 and locations of middle cylinder y_c=0.5, 0.6 and 0.7, respectively).

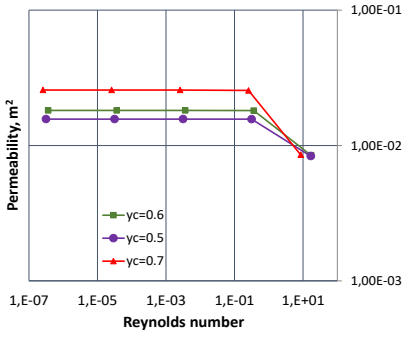

Figure 3. The $K - Re$ for d=0.2 and y_c=0.5, 0.6 and 0.7, respectively

Fig. 4 shows streamlines for the anisotropic porous medium (cylinders with d=0.2 and locations of middle cylinder y_c=0.5, 0.6 and 0.7, respectively) for kinematic viscosities 0.01 m^2/s and 0.1 m^2/s.

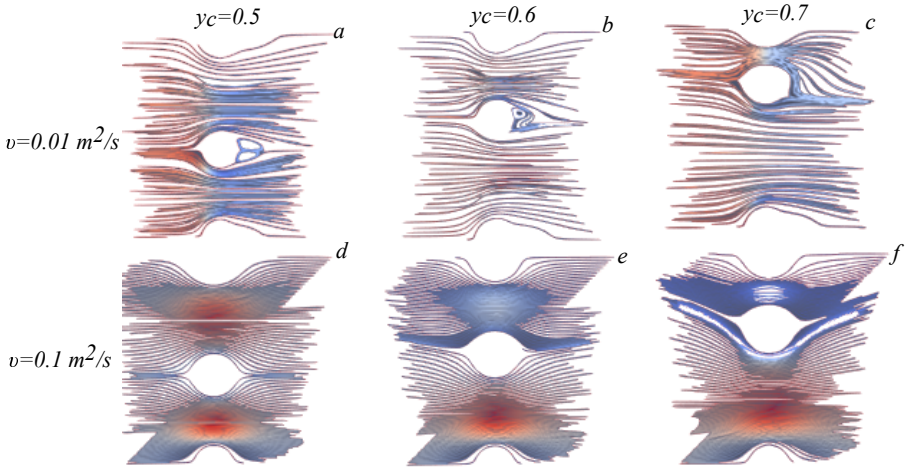

Figure 4. Streamlines for d=0.2 and y_c=0.5, 0.6 and 0.7 for ν=0.01 m^2/s and ν=0.1 m^2/s as indicated

From the numerical results, it can be seen that at lower values of Reynolds number, when vorticity does not occur, the linear Darcys law is fulfilled. It is known that vorticity occurs at high values of Reynolds number [9] and appear inactive zones, therefore the permeability of porous medium depends not only on the geometry of porous medium, but also on the fluid flow properties (see Fig. 4).

Comparison of numerical results with analytical solution

The comparison of numerical results with analytical solution [10] is provided in this section. Tab. 2 and Fig. 5 present numerical results for different radii of the cylinder (R), porosity (ϕ) and numerical predictions of dimensionless permeability (K/R^2) and dimensionless analytic permeability ($K_{analytic}/R^2$). Also, Tab. 2 shows the comparison of relative errors of calculated permeability, which are compared against the analytical values from [10].

Table 1. Numerical results.

mesh	R, m	ϕ	K/R^2	$K_{analytic}/R^2$	RE of K
128x128	0.1261	0.95	$1.02*10^{0}$	$1.01*10^{0}$	$1.17*10^{-2}$
128x128	0.1784	0.90	$3.19*10^{-1}$	$3.32*10^{-1}$	$7.34*10^{-3}$
128x128	0.2523	0.80	$7.73*10^{-2}$	$7.62*10^{-2}$	$1.42*10^{-2}$
128x128	0.3090	0.70	$2.55*10^{-2}$	$2.54*10^{-2}$	$2.69*10^{-3}$
128x128	0.3568	0.60	$8.91*10^{-3}$	$9.01*10^{-3}$	$1.13*10^{-2}$
256x256	0.3989	0.50	$2.95*10^{-3}$	$2.95*10^{-3}$	$1.14*10^{-3}$
256x256	0.4370	0.40	$7.33*10^{-4}$	$7.42*10^{-4}$	$1.32*10^{-2}$
512x512	0.4720	0.30	$8.15*10^{-5}$	$8.30*10^{-5}$	$1.77*10^{-2}$
1024x1024	0.4886	0.25	$8.22*10^{-6}$	$8.29*10^{-5}$	$8.45*10^{-3}$

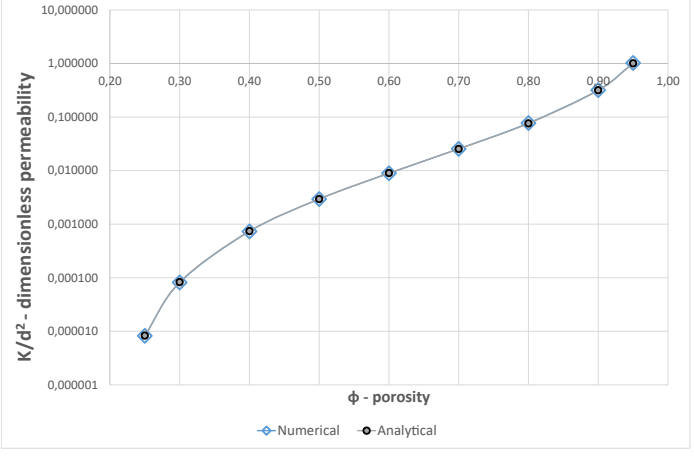

Figure 5. Comparison of numerical and analytical permeabilities

It can be seen that the results are almost the same (relative error between the meshes is less than 1%).

Two-phase flow

Numerical methodology

Two-phase flow of immiscible fluids around a cylinder with radii R in the ranges from 0.1 to 0.4, each fluid has a constant density ρ_i and viscosity μ_i is examined in this section. The flow direction is perpendicular to the axes of cylinder.

Numerical calculations are performed on the staggered grid, so the numerical slip length is introduced [11]. Fig. 6 demonstrates no-slip condition (a) and lenght of numerical slip (b).

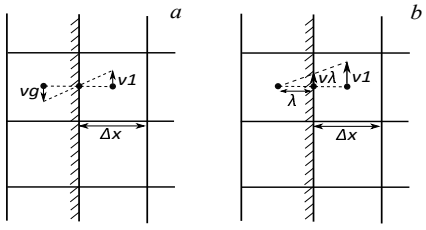

Figure 6. (a) No-slip; (b) Slip length.

This model is based on numerical solution of the incompressible flow in irregular domains, where irregular boundary is represented by its level-set function [12]. The flow is described using the Navier-Stokes equations:

$$\rho_i(\frac{\partial \vec{u}_i}{\partial t}) + \vec{u}_i \cdot \nabla \vec{u}_i = -\nabla P_i + \mu_i \nabla^2 \vec{u}_i, \tag{12}$$

$$\nabla \cdot \vec{u}_i = 0, \tag{13}$$

$$\alpha = \begin{cases} 0, i = nw \\ 1, i = w \end{cases} \tag{14}$$

$$\rho = \alpha\rho_w + (1-\alpha)\rho_{nw} \tag{15}$$

$$\mu = \alpha\mu_w + (1-\alpha)\mu_{nw} \tag{16}$$

$$\frac{\partial \rho}{\partial t} + \nabla \cdot (\rho \vec{u}) = 0, \tag{17}$$

$$\frac{\partial \alpha}{\partial t} + \nabla \cdot (\alpha \vec{u}) = 0, \tag{18}$$

where u is the velocity, m/s; P is the pressure, Pa; ρ is the density, kg/m^3; μ is the visocsity, Pa*s, w is the wetting fluid and nw is the non-wetting fluid.

Equations (1)-(4) are solved using following initial and boundary conditions: Initial condition for the velocity of fluid flow:

$$\vec{u}(0, x, y) = 0, \tag{19}$$

$$\alpha = \begin{cases} 1, \text{ if } x \in [0.05] \\ 0, \text{ otherwise} \end{cases} \tag{20}$$

Boundary conditions on the boundaries of the domain are:

$$u(x = 0, y) = U, \frac{\partial u}{\partial x}(x = L, y) = 0, \tag{21}$$

$$u(x, y = 0) = u(x, y = L), \tag{22}$$

$$\frac{\partial P}{\partial x}(x = 0, y) = 0, \tag{23}$$

$$P(x = L, y) = P_R \tag{24}$$

$$P(x, y = 0) = P(x, y = L). \tag{25}$$

Boundary condition at the interface between wetting and non-wetting fluids - I:

$$[\vec{u}]_i = 0 \tag{26}$$

$$-[-p + 2\mu\vec{n} \cdot E \cdot \vec{n}]_I = \sigma k \tag{27}$$

$$k = -\nabla \cdot \vec{n} \tag{28}$$

$$-[2\mu\vec{t} \cdot E \cdot \vec{n}]_I = 0 \tag{29}$$

where $\vec{n}$ is the normal to the interface I, $\vec{t}$ is the tangent to the interface I, k is the curvature of the interface I and E is the strain rate tensor.

No-slip boundary condition is used on the surface of the cylinder:

$$u(t, x, y)|_{d\Omega} = 0, \tag{30}$$

where $d\Omega$ is the surface of the cylinder.

Calculations are performed using following formulas:

$$\Delta P = P_L - P_R, \tag{31}$$

$$P_L = \int P(x = 0, y) dA \tag{32}$$

$$S = \int_V \alpha dV \tag{33}$$

where V is the flow rate, m^3, A is the area of the left boundary, m^2, S_i is the saturation of the wetting fluid.

Fig. 7 demonstrates the distribution of the saturation of wetting and non-wetting fluids (blue is non-wetting fluid, red is wetting fluid), for cylinder radii R = 0.2 and R = 0.4.

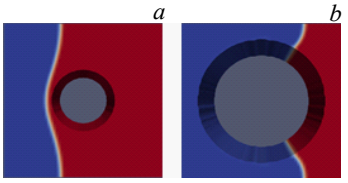

Figure 7. Cylinders Radius (a) $R = 0.2$; (b) $R = 0.4$.

Results and discussion

First, the following parameters were selected: two-phase flow with fluid viscosity ratio $M = 1$ and cylinders radius $R = 0.2$, mesh sizes varies from 8x8 to 256x256. Fig. 8 shows the variation of saturation and pressure drop in time for surface tensions $\sigma = 1$ and $\sigma = 10$. As it can be seen from Fig. 8, the results for the saturation in time for $\sigma = 1$ and $\sigma = 10$ are the same for all mesh sizes. Since the cylinders radius is small, so for this case the effect of the slip length on the flow is negligible. Also, pressure drop (Fig.8c and Fig.8d) is different for different surface tension ($\sigma = 1$ and $\sigma = 10$), so surface tension effect is significant.

Secondly, the following parameters were selected: two-phase flow with fluid viscosity ratio $M = 1$ and cylinders radius $R = 0.4$, mesh sizes varies from 16x16 to 256x256. Fig. 9 shows the variation of saturation and pressure drop in time for surface tensions $\sigma = 1$ and $\sigma = 10$. In comparison with previous results ($R = 0.2$), here, the results for saturation in time are slightly different for time from $t>33$. Since cylinders radius is big enough, so slip length effects to the flow, and for finer meshes (128x128 and 256x256) the residual saturation is observed. As it can be seen from Fig.9c and Fig.9d, the results for variation of pressure drop in time for $R = 0.4$ are same almost for all mesh sizes (except 16x16), because the cylinders radius is big enough and effect of viscous force is more significant than capillary force.

Then, the following parameters were selected: two-phase flow with fluid viscosity ratios $M = 0.01$ and $M = 100$ and cylinders radius R=0.2, mesh sizes varies from 16x16 to 256x256. Fig. 10 shows the variation of saturation and pressure drop in time for surface tension $\sigma = 0.1$. As it can be seen from Fig.10a, the results for variation of saturation in time differ significantly, but the results on the Fig.10b are same for all mesh sizes. Since for viscosity ratio $M = 0.01$ fingering pattern appears and it depends on the slip length, so for coarser mesh the residual saturation is smaller than for finer mesh. As it can be seen from Fig. 10c, the results on pressure drop in time differ significantly, but the results on the Fig. 10d slightly different, because the cylinders radius is small.

Also, the following parameters were considered: two-phase flow with fluid viscosity ratios $M = 0.01$ and $M = 100$ and cylinders radius $R = 0.4$, mesh sizes varies from 16x16 to 256x256. Fig. 11 shows the variation of saturation and pressure drop in time for surface tension $\sigma = 0.1$.

Finally, the following parameters were selected: two-phase flow with fluid viscosity ratios $M = 0.01$ and $M = 100$, surface tension $\sigma = 0.1$ and cylinders radii in the ranges

from 0.1 to 0.4 for mesh 256x256. Fig. 12 shows the variation of saturation and pressure drop in time for cylinders radii from $R = 0.1$ to $R = 0.4$.

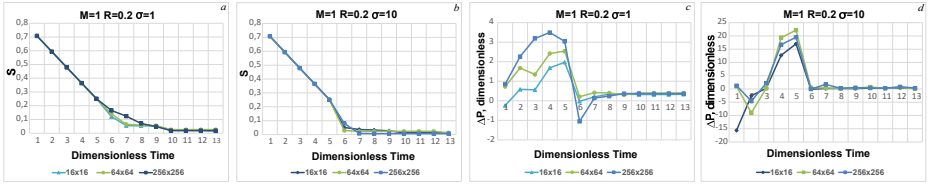

Figure 8. The Variation of Saturation and Pressure Drop in Time for $M = 1$, $R = 0.2$, $\sigma = 1$ (a, c) and $\sigma = 10$ (b, d) for different Meshes, as indicated.

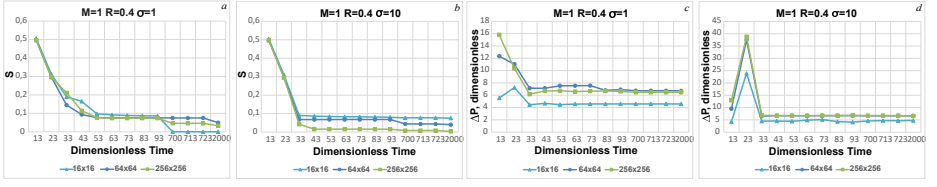

Figure 9. The Variation of Saturation and Pressure Drop in Time for $M = 1$, $R = 0.4$, $\sigma = 1$ (a) and $\sigma = 10$ (b) for different Meshes, as indicated.

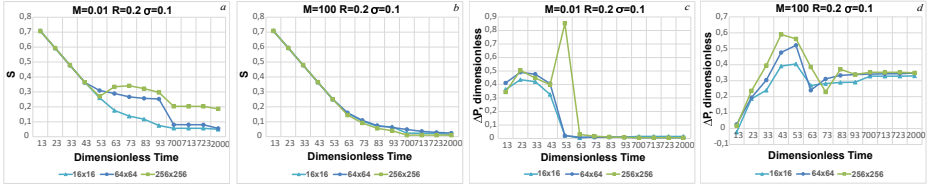

Figure 10. The Variation of Saturation and Pressure Drop in Time for R=0.2, $\sigma = 0.1$, $M = 0.01$ (a) and $M = 100$ (b) for different Meshes, as indicated.

Acknowledgements

This research is funded by the Science Committee of the Ministry of Education and Science of the Republic of Kazakhstan (Grant No. AP08052055 “Investigation of the influence of the dissolution modes of carbonate core samples on the characteristics of

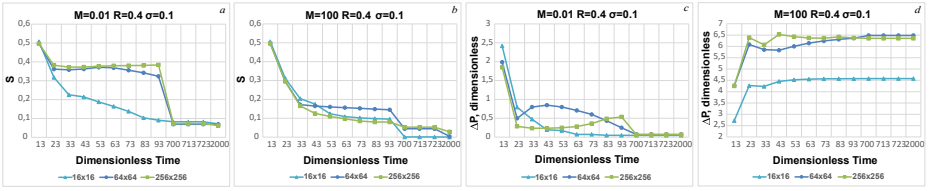

Figure 11. The Variation of Saturation and Pressure Drop in Time for $R = 0.4$, $\sigma = 0.1$, $M = 0.01$ (a, c) and $M = 100$ (b, d) for different Meshes, as indicated.

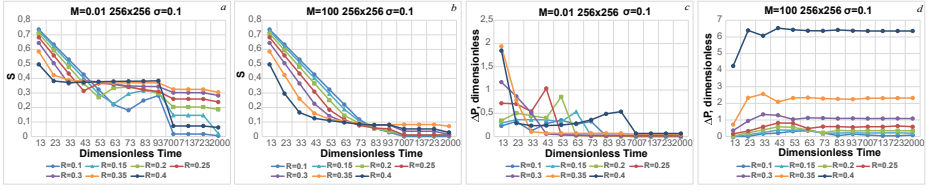

Figure 12. The Variation of Saturation and Pressure Drop in Time for $M = 0.01$ (a, c) and $M = 100$ (b, d), for mesh 256x256 and different cylinders radii, as indicated.

the flow of a two-phase fluid through it in the pore scale") and project "Stimulation of Productive Innovations" (as part of the sub-project APP-JRG-17/0448F "Development and implementation of an integrated software product for a comprehensive solution of production stimulation problems on hydrocarbon fields"), which is gratefully acknowledged by the authors.

Conclusion

Single and two-phase flow through a fibrous porous medium is numerically simulated. The simulation is based on the numerical solution of incompressible Navier-Stokes equations.

For a single-phase flow the permeability of fibrous porous medium is numerically calculated in this paper. Reynolds number below which the flow obeys the linear Darcys law is investigated. Numerical calculation results are in excellent agreement with analytical solution [10] for the flow in porous medium.

For a two-phase flow the sensitivity analysis of slip length is presented in this work. Variations of pressure drop and saturation in time are numerically calculated for different values of surface tension (σ), viscosity ratio ($M = \mu_{nw}/\mu_w$), and mesh sizes. The presented results show that solutions of saturation and pressure drop in time vary with mesh refinement, so the numerical slip length significantly affects the flow. For a coarser mesh the influence of numerical slip length is less than for a finer mesh, also as bigger the value of the viscosity ratio or surface tension as lower the influence of numerical slip length. The results show that the contact line motion significantly depends not only on the microstructure of the porous media, but also on the fluid properties (viscosity ratio, surface tension and etc.).

References

1. Shams, M., Raeini, A.Q., Blunt. M.J. and Bijeljic, B.: *A numerical model of two-phase flow at the micro-scale using the volume-of-fluid method*. J. of Computational Physics, Vol. 357, pp.159–182 (2018). https://doi.org//10.1016/j.jcp.2017.12.027
2. Scanziani, A., Lin, Q., Alhosani, A., Blunt, M.J. and Bijeljic B.: *Dynamics of fluid displacement in mixed-wet porous media*. Proceedings of the Royal Society A. Mathematical, Physical and Engineering Sciences (2020). https://doi.org/10.1098/rspa.2020.0040
3. Akai, T., Lin, Q., Bijeljic, B. and Blunt, M.J.:*Using energy balance to determine pore-scale wettability*. J. of Colloid and Interface Science. vol. 576. pp. 486–495 (2020). https://doi.org/10.1016/j.jcis.2020.03.074
4. Foroughi, S., Bijeljic, B., Lin, Q., Raeini, A.Q., and Blunt, M.J.: *Pore-by-pore modeling, analysis, and prediction of two-phase flow in mixed-wet rocks*. Phys. Rev. E 102, 023302, (2020). https://doi.org/10.1103/PhysRevE.102.023302
5. Raeini, A.Q., Yang, J., Bondino, I., Bultreys, T., Blunt, M.J. and Bijeljic, B.: *Validating the Generalized Pore Network Model Using Micro-CT Images of Two-Phase Flow*. Transport in Porous Media vol. 130, pp. 405-424 (2019). https://doi.org/10.1007/s11242-019-01317-8
6. Bultreys, T., Lin, Q., Gao, Y., Raeini, A.Q., AlRatrout, A., Bijeljic, B., and Blunt, M.J.: *Validation of model predictions of pore-scale fluid distributions during two-phase flow*. Phys. Rev. E 97, 053104 (2018). https://doi.org/10.1103/PhysRevE.97.053104
7. Kudaikulov, A., Josserand, C., A. Kaltayev, A., *Mathematical Modeling of Technological Processes*, Series of Communications in Computer and Information Science, Book Series. - Springer, 549, 85 (2015).
8. Whitaker, S., *Flow in Porous Media I: A theoretical derication of Darcy's Law*, Transp. Porous Media 1, 3 (1986).
9. Batchelor, G.K., *An introduction to fluid dynamics*,Cambridge Univ. Press (2000).
10. Sangani, A.S. and Acrivos, A.: *Slow flow past periodic arrays of cylinders with application to heat transfer*, Int.J.Multiphase flow, 8(3), 193 (1982).
11. Afkhami, S., Zaleski, S., Bussmann, M.: *A mesh-dependent model for applying dynamic contact angles to VOF simulations*, J. Comput. Phys. 228, pp.5370–5389 (2009).
12. Raeini, A.Q., Blunt, M.J., Bejeljic, B.: *Modelling two-phase flow in porous media at the pore scale using the volume-of-fluid method*. J. Comput. Phys. vol. 231, pp. 5653–5668. https://doi.org/10.1016/j.jcp.2012.04.011

High-performance and Intelligent Computational Models for Oil Production Problems*

D. Zh. Akhmed-Zaki[1], D. Lebedev[1], T. S. Imankulov[2], Y. Kenzhebek[2], and N. Kassymbek[2]

[1] Astana IT University, Nur-Sultan, Kazakhstan
[2] Al-Farabi Kazakh National University, Almaty, Kazakhstan
kenzhebekyerzhan@gmail.com

Abstract In recent years, modern information technologies are actively used in various sectors of industry. The oil industry is no exception, since high-performance computing technologies, artificial intelligence algorithms, methods of collecting, processing and storing information are actively used to solve the problems of enhanced oil recovery.
This article discusses the application of modern approaches to solving oil production problems: the fragmented approach technology, the parallel approach technology and machine learning algorithms. The problem of multiphase multicomponent fluid flow in porous medium is solved by the Newton-ILU (0)-GMRES method. To automate the implementation of numerical models on multicomputers, fragmented programming technology and a parallel algorithm on MPI are used. The developed algorithms were tested and analyzed on the MVS-10P supercomputer. Also, the problem of oil displacement is solved using machine learning algorithms. The algorithms are classical supervised learning (linear and polynomial regression) and neural networks.

Keywords: Enhanced oil recovery, MPI, Machine learning, LUNA, Regression methods, Artificial neural network, GMRES, Preconditioner.

Introduction

The development of modern high-performance computing allows humanity to solve important scientific and applied problems in various fields. The accuracy of solving such problems requires the use of a large mesh, which in turn requires large computational resources. Currently, supercomputers are used to solve problems such as weather modeling and climate prediction, acoustic problems, hydrodynamics, economic processes and etc.Actual and at the same time quite a difficult task of hydrodynamic modeling is the simulation of multicomponent multiphase flow of liquid (oil and gas) in porous media (in oil reservoirs). In solving such problems, various methods and schemes [1,2,3] can be used, some of them are iterative methods for solving linear systems [4,5].

Various technologies are used to speed up the execution time of calculations for solving scientific problems, such as MPI [6], OpenMP [7], CUDA [8,9], OpenCL [10], and fragmented programming [11].

* Supported by National Engineering Academy

In this paper, we solve a system of equations using the Newton-Raphson method, at each iteration of which the system of algebraic equations is solved using the generalized minimum residual method (GMRES) with ILU (0) preconditioner. A program for solving this problem using a method called Newton-ILU(0)-GMRES is implemented parallel using MPI and using fragmented programming (FP) technology, which is aimed at automating the construction of parallel programs for supercomputers.

There is a lot of research related to increasing oil production using machine learning methods. In this work [12], the authors found out that the use of machine learning (ML) algorithms may turn out to be more productive in comparison with traditional calculations on a regular grid [13,14].

The work [15] considers machine learning algorithms for estimating the oil production coefficient using a combination of engineering and stratigraphic parameters. For a data set consisting of 30 parameters, linear regression models and the support vector machine (SVM) method were applied. As a result, the data obtained were very close to the results of cross-validation. Thus, the authors of this work suggest that the methods considered by them can be used to predict future production. The authors of [16,17] considered the use of artificial neural network (ANN) for predicting oil production.

The study [18] examined various machine learning methods for predicting downhole pressure, oil production, and forecasting water cut in production tasks. The authors of [19] also examined the use of machine learning methods for interpreting pressure, flow rate, and temperature data from permanent downhole sensors. In this paper, three machine learning methods were applied, such as linear regression (LR), core method, and ridge core regression.

Numerical Simulation of Multicomponent Multiphase Flow in Porous Media using MPI technology

The one-dimensional problem of compositional fluid flow in a porous medium is considered. Compositional flow involves multiple components and three phases, and there is a mass transfer between the vapor and liquid phases

A mathematical model of a multicomponent flow of a three-phase liquid in a porous medium is considered. The law of conservation of mass for each component is written down and a system of nonlinear equations is obtained. Distribution of chemical components in the hydrocarbon phase described by the K-value method [20]. The thermodynamic behaviour of fluids under reservoir conditions are described by the Peng-Robinson equations of state [21].

The system of nonlinear equations is linearized by the Newton-Raphson method. The resulting system of linear equations is reduced to the following form, as shown by [2]:

$$Ax = b, \tag{1}$$

In this work, system (1) was solved by the iterative method GMRES, which is a widely used Krylov subspace method [22].

To reduce the number of iterations in the computation, preconditioning was used as an explicit or implicit modification of the system of linear equations, making it possible to simplify the solution. We choose ILU(0) [23] as a preconditioner for the GMRES algorithm, which was found by decomposing matrix A by a fine-grained ILU factorization algorithm. As a result, for the numerical solution of the given problem for solving a system of linear equations, (1) uses the Newton-ILU0-GMRES algorithm as a fully implicit scheme.

To implement the parallel algorithm of the Newton-ILU0-GMRES, we need to determine the parts of the calculations that can be the basis of parallelization.

For instance, the ILU0-GMRES algorithm consists of the following steps:

1. Initialization. Choose x_0, compute $r = b - Ax_0$, solve $Pw = r$and compute $v_1 = \frac{w}{\|w\|_2}$
2. Arnoldi iteration. Iterate m times: j=1,2,…,m. The specific Arnoldi algorithm is as follows:

for i=1, ...,m
  Pw=Ax$_i$
 for k=1, ...,i
  $h_{k,i} = (w, v_k)$
  $w = w - h_{k,i}v_k$
 endk
 $h_{i+1,i} = \|w\|_2$
 $v_{j+1} = \frac{W}{h_{i+1,i}}$
end i

3. Compute the approximate solution $x^m = x^0$+$Q_{n,m}\ y_m$. Here, y_m minimizes $\|\beta\xi - H_{m,m}\|$; $Q_{n,k}$ is an nxk matrix, the column vector of the matrix is composed of $v_1, v_2, ..., v_k$ orthogonal vectors, and H_{mm} is the Hessenberg matrix.
4. Determination. Compute $r^m = b - x^m$, stop if the condition is met: otherwise let $x^0 = x^m$ and go back to 1) and recalculate. The convergence condition by which the method stops is given by an arbitrary number ε.

In this ILU0-GMRES algorithm, there are common operations such as matrix-matrix multiplication, matrix-vector multiplication, vector-vector multiplication and vector norm calculation in steps of a), b) and c). These operations could be implemented in parallel with data decomposition. In a) and b) steps of the GMRES algorithm, P is used as the ILU(0) preconditioner.

The testing of the program was carried out on matrices corresponding to the cases when the number of grid point schemes varied from 500 to 8000. The size of the matrix being solved is 6 times larger than the number of grid points. The size of the matrix, which corresponds to the case when the number of points in the difference grid is equal to 8000, is 48000 x 48000, since for each point 6 equations are written.

Test runs for the considered problem (1) were made on the MVS-10P supercomputer of the Interdepartmental Supercomputer Center of the Russian Academy of Sciences, which includes nodes with two Xeon X5450 processors and 8 GB of RAM for each node. The test results are shown in Table 1.

Table 1. The runtimes of the parallel program in MPI

Number of processors	Size of Matrix A				
	3000x3000	6000x6000	12000x12000	24000x24000	48000x48000
1	3.74	48.38	334.24	1 688.74	20 219.34
8	1.19	7.57	53.82	394.74	2 942.02
64	2.59	12.03	64.16	389.68	2 565.59
128	2.95	12.66	65.25	395.58	2 569.01
256	4.39	17.29	82.75	450.28	2 798.32
512	11.53	42.56	202.01	866.98	4 185.07

As we can see from the test results, the parallel program running on 8 processors achieved the shortest runtime. As the size of the task increases, the parallel application achieves the shortest calculation time running on 64 processors, but it is not much different from the runtime of a parallel program running on 8, 128 and 256 processors. The reason is because with an increase in the number of processors, the computation time on each processor decreases, and the time spent on communications increases.

It can be seen that the runtimes on 64 and 128 processors are about the same. This finding is explained by the fact that on 64 processors, the communication time is less than the computation time, and on 128 processors, the computation time is less than the communication time, but in total, the time consumed is almost the same. For matrix size 3000x3000 on 256 and 512 processors, the parallel program is slower than the sequential program. With an increase in the size of the matrix, for instance, for matrices 6000x6000 - 48000x48000, the runtime of the parallel program decreases compared to the sequential program. This regularity makes it possible to predict that with an increase in the size of the matrix, in large numbers of processors, acceleration also increases. It can be concluded that it makes sense to run the parallel algorithm of the method on a large number of processors but only with large of matrix that cannot fit in the memory of a single node.

Numerical Simulation of Multicomponent Multiphase Flow in Porous Media on LuNA Fragmented Programming System

To solve the problem presented in the previous chapter, a fragmented version of the ILU(0)-GMRES algorithm for the LuNA system was developed. A fragmented algorithm frees the programmer from parts of parallel program execution, such as data transfer and messaging, and allows him to perform these actions automatically. In the system of fragmented programming LuNA to automate the creation of parallel programs uses the so-called fragmented algorithm (FA), which consists of light processes, computational fragments (CF). The data is represented as an immutable block called data fragments (DF). Accordingly, new data, called output DFs, are computed from input DFs using CF.

In the fragmented version of the Arnoldi orthogonalization algorithm, the vectors w and v_k are divided by n the number of DFs. The resulting matrices $H_{m,m}$ and $Q_{n,k}$ are stored as separate DFs. In each new Arnoldi iteration, the defined CFs calculate the new

output DFs, using the above listed DFs as input parameters. In this case, the input DF, which will no longer be used, can be removed from memory.

You can see that calculating of the residual *r* and finding the approximate solution x^m of the ILU(0)-GMRES algorithm, which was described before, are simple matrix-vector operations, the fragmented algorithms of which can be easily implemented in the LuNA system.

Table 2. The runtimes of the fragmented program in LuNA

Number of processors	Size of Matrix A	
	3000x3000	6000x6000
8	1338,81	8412,66

Table 2 shows the running time of a fragmented program. As you can see from the table, the computation time turns out to be very long, this is due to the fact that the algorithm has a lot of connections between the nodes, it takes a lot of time to organize them, moreover, in the LuNA system, the MPICH library is used to organize parallel computations using the TCP standard / IP. Therefore, a lot of time is spent on data exchange between nodes, in contrast to the MPI program, in which the data exchange was implemented using the faster InfiniBand standard.

Using Machine Learning Methods for Oil Recovery Prediction

In this work, the obtained synthetic data from a mathematical model were divided into a training and test sample. As input parameters, various combinations of parameters of the oil production problem (porosity, viscosity of the oil phase and absolute rock permeability) were taken. And as the output parameter, the value of the oil recovery coefficient was chosen. The data was divided into a training and test set. For training, 8069 sets (80%) of the total data were used, and for the test the remaining 2017 pairs (20%). The total number of sample pairs is 10,086 models. Each sample pair consists of 40 oil recovery factor values. As a result, we have many test pairs, however, in this paper, the results will be shown only for some. Fig. 1 shows the result of one test sample pair for different regression methods. Fig. 2 shows the result of one test sample pair for ANN. The Table 3 shows the average R^2 score for 20% of test sets.

Table 3. Evaluation of R^2 for all pairs of training and test set.

Machine learning algorithms	Test sets (20%) R^2
LR	0.91
Polynomial Regression (PR) degree = 2	0.96
PR degree = 3	0.79
PR degree = 3 with L1	0.92
ANN	0.97

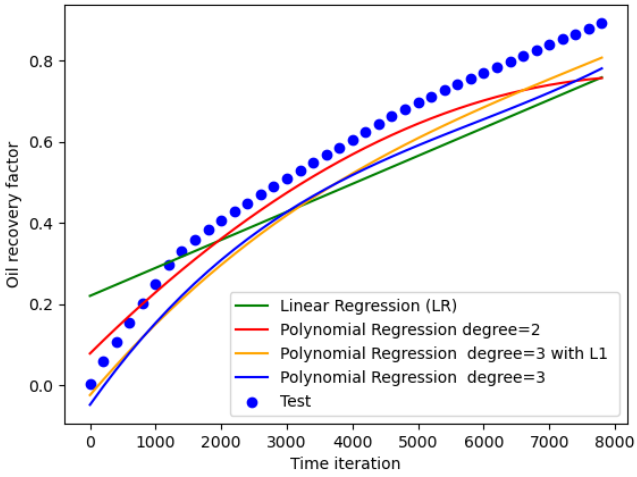

Figure 1. Oil recovery factor on different regression models.

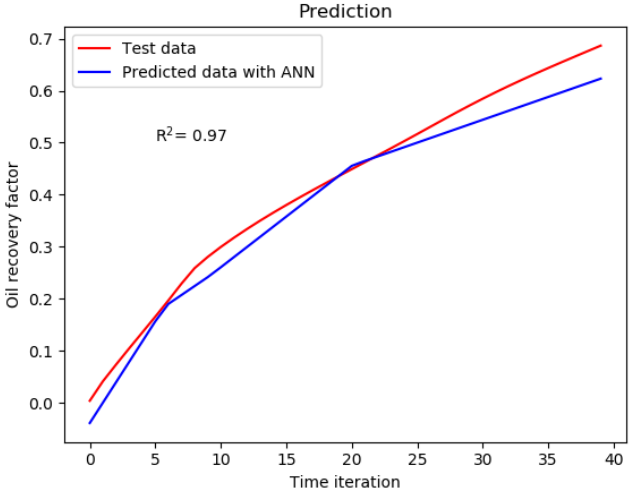

Figure 2. Oil recovery prediction using an artificial neural network.

Conclusion

This research examines the parallel implementation of the Newton-ILU0-GMRES algorithm for a multicomponent three-phase flow problem. Tests were carried out with different node sizes and numbers of processes on supercomputers. The study showed that on a large number of processes, the MPI program runs better in large-scale tasks, in addition the MPI program has higher efficiency and scalability than the LuNA program. In the future we plan to develop a fragmented program to direct control for the considered parallel algorithm, which will increase the effectiveness of the fragmented program.

This article was devoted to the application of machine learning methods for predicting oil production. Different degrees of polynomial regression were tested, and it was also revealed that for our synthetic data, the quadratic polynomial model is quite well trained and predicts the value of the oil recovery coefficient. An artificial neural network with one hidden layer with optimally selected hyperparameters was built. For the constructed neural network, the determination coefficient R^2 was 0.97, which is slightly better than the quadratic model of polynomial regression.Thus, it is assumed that the considered machine learning methods in this article may be useful for predicting oil production.

Acknowledgments

This research was funded by the Science Committee of the Ministry of Education and Science of the Republic of Kazakhstan (Grant No. AP05130366).

References

1. Borisov V. E., Kritskiy B. V., Marchenko N. A., Mitrushkin D. A., & Savenkov E. B. (2013). Non-isothermal compositional flow model with chemical reactions and active solid phase for reservoir simulation. KIAM Preprint, 091.
2. Chen, Z. (2006). Reservoir Simulation: mathematical techniques in oil recovery. Society for Industrial and Applied Mathematics.
3. Akhmed-Zaki, D.Zh., Imankulov, T.S., Matkerim, B., Daribayev, B.S., Aidarov, K.A. and Turar, O.N. (2016) Large-scale simulation of oil recovery by surfactant-polymer flooding. Eurasian Journal of mathematical and computer applications, 4(1), 12-31.
4. Mittal, R.C., & Al-Kurdi, A.H. (2002). LU-decomposition and numerical structure for solving large sparse nonsymmetric linear systems. Computers & Mathematics with Applications, 185(2), 391-403. https://doi.org/10.1016/j.cam.2005.03.018
5. Lacroix, S., Vassilevski, YU., Wheeler, J., & Wheeler, M. (2003). Iterative Solution Methods for Modeling Multiphase Flow in Porous Media Fully Implicitly. SIAM Journal on Scientific Computing, 25(3), 905-926. https://doi.org/10.1137/S106482750240443X
6. Pannala, S., DAzevedo, E., Syamlal, M., & O'Brien, T. (2003). Hybrid (OpenMP and MPI) Parallelization of MFIX: A Multiphase CFD Code for Modeling Fluidized Beds. SAC '03: Proceedings of the 2003 ACM symposium on Applied computing, (pp. 199-206). Association for Computing Machinery. https://doi.org/10.1145/952532.952574

7. Iryanto, I., & Gunawan, P. H. (2017). An OpenMP parallel godunov scheme for 1D two phase oil displacement problem. 5th International Conference on Information and Communication Technology (ICoICT). https://doi.org/10.1109/ICoICT.2017.8074664
8. Zaza, A., Awotunde, A. A., Fairag, F. A., & Al-Mouhamed, M. A. (2016). A CUDA based parallel multi-phase oil reservoir simulator. Computer Physics Communications, 206, 2-16. https://doi.org/10.1016/j.cpc.2016.04.010
9. Akhmed-Zaki, D.Zh., Daribayev, B.S., Imankulov, T.S., & Turar, O.N. (2017). High-performance computing of oil recovery problem on a mobile platform using CUDA technology. Eurasian Journal of mathematical and computer applications, 5(2), 4-13. https://doi.org/10.32523/2306-3172-2017-5-2-4-13
10. Khramchenkov, E., & Khramchenkov, M. (2018). Numerical Model of Two-Phase Flow in Dissolvable Porous Media and Simulation of Reservoir Acidizing. Natural Resources Research, 27(4), 531-537. https://doi.org/10.1007/s11053-018-9371-x
11. Malyshkin, V.E., & Perepelkin, V.A. (2011). LuNA Fragmented Programming System, Main Functions and Peculiarities of Run-Time Subsystem. Proceedings of the 11th International Conference on Parallel Computing Technologies/LNCS, 6873, 53-61. https://doi.org/10.1007/978-3-642-23178-0_5
12. Akhmed-Zaki, D., Danaev, N., Mukhambetzhanov, S., Imankulov, T. [2012]. Analysis and evaluation of heat and mass transfer processes in porous media based on Darcy-Stefan's model. ECMOR 2012 - 13th European Conference on the Mathematics of Oil Recovery. https://doi.org/10.3997/2214-4609.20143274
13. Aliyuda, K., Howell, J. [2019]. Machine Learning Algorithm for Estimating Oil Recovery Factor Using a Combination of Engineering and Stratigraphic Dependent Parameters. Interpretation. 7. 1-34. 10.1190/int-2018-0211.1.
14. Imankulov, T.S., Akhmed-Zaki, D. [2016]. Computer modelling of non-isothermal, multiphase and multicomponent flow by using combined EOR technologies. 15th European Conference on the Mathematics of Oil Recovery, ECMOR 2016. https://doi.org/10.3997/2214-4609.201601765
15. Jreou, G. [2012]. Application of neural network to optimize oil field production. Asian Transactions on Engineering. 3. 1-9.
16. Krasnov, F., Glavnov, N., Sitnikov, A. [2018]. A Machine Learning Approach to Enhanced Oil Recovery Prediction. 10.1007/978-3-319-73013-4_15.
17. Mirzaei-Paiaman, A., Salavati, S. [2012]. The Application of Artificial Neural Networks for the Prediction of Oil Production Flow Rate. Energy Sources. 34. 10.1080/15567036.2010.492386.
18. Ristanto, T., Horne, R. [2018]. Machine Learning Applied to Multiphase Production Problems.
19. Tian, Ch., Horne, R. [2019]. Applying Machine-Learning Techniques To Interpret Flow-Rate, Pressure, and Temperature Data From Permanent Downhole Gauges. SPE Reservoir Evaluation & Engineering. 22. 386-401. 10.2118/174034-PA.
20. Pederson, K.S., & Christensen, P.L. (2008). Phase Behavior of Petroleum Reservoir Fluids. CRC Press.
21. Peng, D.Y., & Robinson, D.B. (1976). A new two-constant equation of state. Industrial and Engineering Chemistry Fundamentals, 15(1), 59-64. https://doi.org/10.1021/i160057a011
22. Saad, Y. (2003). Iterative methods for sparse linear systems. (2nd edn). SIAM.
23. Chow, E., & Saad, Y. (1997). Ilus: An incomplete LU preconditioner in sparse skyline format. International Journal for Numerical Methods in Fluids, 25(7), 739-748.

Finite Element Method for Solving a Fractional Model in Porous Media*

Nurlana Alimbekova[1], Dossan Baigereyev[1], and Yerlan Yergaliyev[1]

S. Amanzholov East Kazakhstan University NJS, Ust-Kamenogorsk, Kazakhstan
ernur09.83@mail.ru, dbaigereyev@gmail.com, ergaliev79@mail.ru

Abstract Currently, there is an increased interest in the problem of numerical implementation of multiphase filtration models due to its huge economic significance in the oil industry, hydrology, and nuclear waste management. In contrast to classical filtration models, filtration models in highly porous fractured formations with fractal well geometry have not been fully studied. The solution of this problem is reduced to solving a system of differential equations with fractional derivatives. In this paper, we consider an initial-boundary value problem for a one-dimensional differential equation with a fractional time derivative in the Caputo sense. The problem under consideration can be classified as a parabolic type, with a fractional derivative in time and a spatial variable. In addition, a single initial condition and a Dirichlet type condition are set. This equation is of great practical importance in the modeling of filtration processes in highly porous fractured reservoirs with fractal geometry wells. For the numerical solution, an approximation is constructed using the finite element method. The results of numerical solution of two model problems are presented, which show the efficiency of the proposed method for modeling flow in fractured porous media.

Keywords: Fractional partial differential equation, Caputo derivative, Finite element method, Numerical method, Approximate solution.

Introduction

The construction of mathematical models and computational algorithms for fluid flow in fractured formations is an urgent and interesting task both from the side of constructing new mathematical models that allow taking into account different-scale processes, and from the side of constructing modern computational methods [1,2,3]. There is also an increased interest in the problem of numerical implementation of multiphase filtration models due to its huge economic significance in the oil industry, hydrology, and nuclear waste management.

A long-term study of filtration flows has shown that their dynamics are significantly affected by memory effects, which are described by the theory of fractional order integro-differentiation. These mathematical models provide a more accurate and realistic description of the processes occurring in such complex environments. This

* This work was supported by the Ministry of education and science of the Republic of Kazakhstan (grant No. AP08053189, 2020-2022)

direction in filtration theory appeared relatively recently [4, 5, 6]. In [7], the classical equations describing the motion of a liquid in a porous medium are rewritten taking into account the memory formalism using a fractional derivative in the Caputo sense. In [8], the phenomenon of longitudinal dispersion in the flow of two mixing liquids through a porous medium is studied using the Caputo-Fabrizio fractional derivative. In [9], fractional derivatives of various orders in the Caputo sense with a variable lower limit are applied in fractured and matrix regions. In [10], a finite-difference scheme is constructed for solving the initial boundary value problem for the convection-diffusion equation with a fractional time derivative in the Caputo sense, which can be used as a model filtration problem.

In this paper, we consider the model problem investigated in [10]. Instead of the finite-difference scheme used in [10], a finite-element scheme is used.

Problem Statement

On the segment $\Omega = [0, L]$, consider the problem

$$\partial_{0,t}^{\alpha} u + q\frac{\partial u}{\partial x} - \frac{\partial}{\partial x}\left(a\frac{\partial u}{\partial x}\right) = f(x,t), \tag{1}$$

$$u(x,0) = \mu(x), \tag{2}$$

$$u(0,t) = u(L,t) = 0. \tag{3}$$

A derivative of fractional order $0 < \alpha < 1$ is defined in the Caputo sense:

$$\partial_{0,t}^{\alpha} u(x,t) = \frac{1}{1-\alpha}\int_0^t \frac{1}{(t-\tau)^{\alpha}}\frac{\partial u}{\partial \tau}(x,\tau)\, d\tau.$$

Approximate solution of the problem

Weak solution of the problem (18)-(19) is the function $u(x,t)$ that satisfies the condition (2) and the integral identity

$$\int_0^L \partial_{0,t}^{\alpha} u\, w\, dx + \int_0^L q\frac{\partial u}{\partial x}\, w\, dx + \int_0^L a\frac{\partial u}{\partial x}\frac{\partial w}{\partial x} dx = \int_0^L f w\, dx, \tag{4}$$

where $w \in C^{\infty}(\Omega)$ is an arbitrary function.

For an approximate solution of the problem (18)-(19) using the finite element method. On the Ω segment, we introduce a set of elements $\Omega_n = [x_{n-1}, x_n]$ with points $0 = x_0 < x_1 < ... < x_N = L$, such that $\bigcup_{n=1}^{N} \Omega_n = \Omega$ и $\Omega_i \cap \Omega_j = \emptyset$ for $i \neq j$. On the time interval $[0,T]$, we introduce the partition $\omega_{\tau} = \left\{t^k = k\tau,\ \ k = 0, 1, ..., M,\ \ M\tau = T\right\}$.

Approximate solution u_h of the problem (18)-(19) on the k-th time layer, we will search in the form

$$u_h\left(x,t^k\right)=\sum_{j=1}^{N}u_j^k\varphi_j\left(x\right),$$

where u_j^k are unknown coefficients, $\varphi_j\left(x\right)$ are basis functions. To approximate the fractional derivative $\partial_{0,t}^{\alpha}u$, we will use the formula

$$\partial_{0,t}^{\alpha}u^{k+1}\approx\Delta_{0,t}^{\alpha}u^{k+1}\equiv\frac{1}{\tau^{\alpha}\Gamma\left(2-\alpha\right)}\sum_{s=0}^{k}b_s^{\alpha}\left(u^{k+1-s}-u^{k-s}\right),\tag{5}$$

where $b_s^{\alpha}=\left(s+1\right)^{1-\alpha}-s^{1-\alpha}$ and the notation $u^k=u\left(\cdot,t^k\right)$ is introduced.

Using(5) and given$b_0^{\alpha}=1$, we rewrite the integral identity (4) as

$$\frac{\tau^{1-\alpha}}{\Gamma\left(2-\alpha\right)}\int_0^L\frac{u^{k+1}-u^k}{\tau}w\,dx+\frac{1}{\tau^{\alpha}\Gamma\left(2-\alpha\right)}\sum_{s=1}^{k}\int_0^L b_s^{\alpha}\left(u^{k+1-s}-u^{k-s}\right)w\,dx+$$

$$+\int_0^L q\frac{\partial u^{k+1}}{\partial x}\,w\,dx+\int_0^L a\frac{\partial u^{k+1}}{\partial x}\frac{\partial w}{\partial x}dx=\int_0^L f w\,dx.$$

Choosing the basis functions so that

$$\varphi_j\left(x_i\right)=\begin{cases}1,\,i=j,\\0,\,i\neq j,\end{cases}$$

we obtain a system of linear algebraic equations for determining the vector$U^k=\left\{u_1^k,u_2^k,...,u_N^k\right\}$ unknown values on the k-th time layer:

$$M\frac{U^{k+1}-U^k}{\tau}+KU^{k+1}=F^{k+1},\tag{6}$$

where M, K are matrices of dimension $N\times N$, and F is a vector of dimension $N\times 1$ with elements

$$M_{ij}=\frac{\tau^{1-\alpha}}{\Gamma\left(2-\alpha\right)}\int_0^L\varphi_i\varphi_j dx,\tag{7}$$

$$K_{ij}=\int_0^L\left(q\frac{\partial\varphi_j}{\partial x}\,\varphi_i+a\frac{\partial\varphi_j}{\partial x}\frac{\partial\varphi_i}{\partial x}\right)dx,\tag{8}$$

$$F_i^{k+1}=-\frac{1}{\tau^{\alpha}\Gamma\left(2-\alpha\right)}\sum_{j=1}^{N}\sum_{s=1}^{k}\int_0^L b_s^{\alpha}\left(u_j^{k+1-s}-u_j^{k-s}\right)\varphi_i\varphi_j dx+\int_0^L f\left(x,t\right)\varphi_i dx.\tag{9}$$

It follows from (6) that the vector U^{k+1} is defined by the formula

$$U^{k+1}=\left(M+\tau K\right)^{-1}\left(MU^k+\tau F^{k+1}\right).\tag{10}$$

For approximate calculation of integrals in (7)-(9), on each element $\Omega_i=[x_{i-1},x_i]$ we introduce the replacement of variables ξ with the relation

$$x = \frac{x_i - x_{i-1}}{2}\xi + \frac{x_{i-1} + x_i}{2}$$

so that the new variable ξ changes from -1 to 1, and we use the quadrature formula for integrating Gauss over five points. As the basis functions, we choose the functions

$$\varphi_1(\xi) = \frac{1}{2}(1-\xi), \quad \varphi_2(\xi) = \frac{1}{2}(1+\xi).$$

Analysis of computational experiments

To test the proposed algorithm, a number of problems are considered.

Example 1. Find an approximate solution to the problem

$$\partial^{\alpha}_{0,t} u - \frac{\partial u}{\partial x} - \frac{\partial^2 u}{\partial x^2} = \frac{2x^2 t^{2-\alpha}(1-x)}{\Gamma(1-\alpha)(\alpha-2)(\alpha-1)} - t^2\left(2-4x-3x^2\right), \quad 0 < x < 1,$$

$$u(x,0) = 0, \quad u(0,t) = u(1,t) = 0.$$

The exact solution to this problem is as follows $u(x,t) = t^2 x^2 (1-x)$.

Example 2. Find an approximate solution to the problem

$$\partial^{\alpha}_{0,t} u - (x+1)\frac{\partial u}{\partial x} - \frac{\partial^2 u}{\partial x^2} = \frac{18e^x x^2 t^{3-\alpha}\left(x^2-1\right)}{\Gamma(1-\alpha)(\alpha-3)(\alpha-2)(\alpha-1)} -$$

$$-3t^3 e^x\left(x^5+6x^4+11x^3+8x^2-6x-2\right), \quad 0 < x < 1,$$

$$u(x,0) = 0, \quad u(0,t) = u(1,t) = 0.$$

The exact solution to this problem is as follows $u(x,t) = 3e^x t^3 x^2\left(1-x^2\right)$.

Tables 1 and 2 show error values for various values of the x and t.

x	t	$error$
0.097	0.05	$7.4 \cdot 10^{-7}$
0.498	0.05	$2.1 \cdot 10^{-5}$
0.949	0.05	$9.9 \cdot 10^{-6}$
0.097	0.25	$7.8 \cdot 10^{-6}$
0.498	0.25	$1.4 \cdot 10^{-4}$
0.949	0.25	$5.4 \cdot 10^{-5}$
0.097	0.75	$2.9 \cdot 10^{-5}$
0.498	0.75	$4.5 \cdot 10^{-4}$
0.949	0.75	$1.6 \cdot 10^{-4}$

Table 1. Error analysis for the Example 1

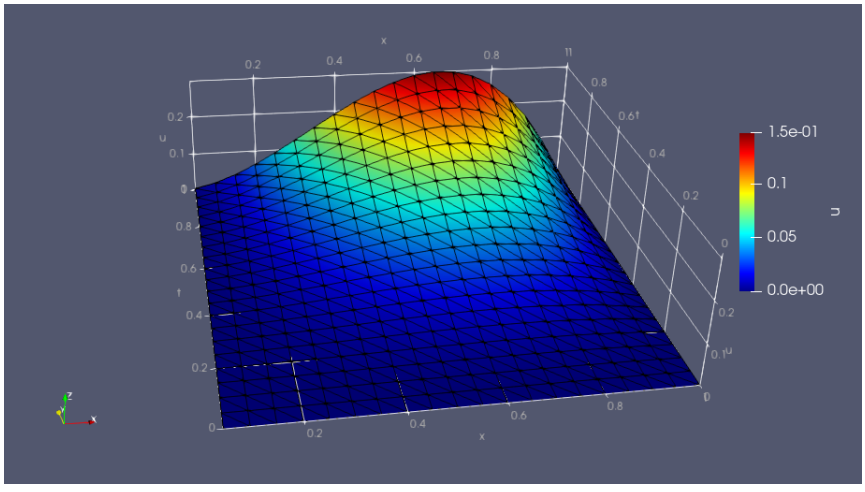

Figure 1. Approximate solution of Example 1

x	t	$error$
0.097	0.05	$2.1 \cdot 10^{-5}$
0.498	0.05	$5.1 \cdot 10^{-5}$
0.949	0.05	$2.0 \cdot 10^{-5}$
0.097	0.25	$2.9 \cdot 10^{-3}$
0.498	0.25	$2.4 \cdot 10^{-3}$
0.949	0.25	$7.2 \cdot 10^{-3}$
0.097	0.75	$3.9 \cdot 10^{-2}$
0.498	0.75	$2.7 \cdot 10^{-2}$
0.949	0.75	$2.4 \cdot 10^{-2}$

Table 2. Error analysis for the Example 2

Conclusion

Thus, a finite element scheme is constructed for a fractional differential equation with variable coefficients containing a fractional time derivative in the Caputo sense. The results obtained can be applied to the numerical solution of other equations containing a fractional time derivative.

Acknowledgments

This work was supported by the Ministry of education and Science of the Republic of Kazakhstan (grant No. AP08053189, 2020-2022).

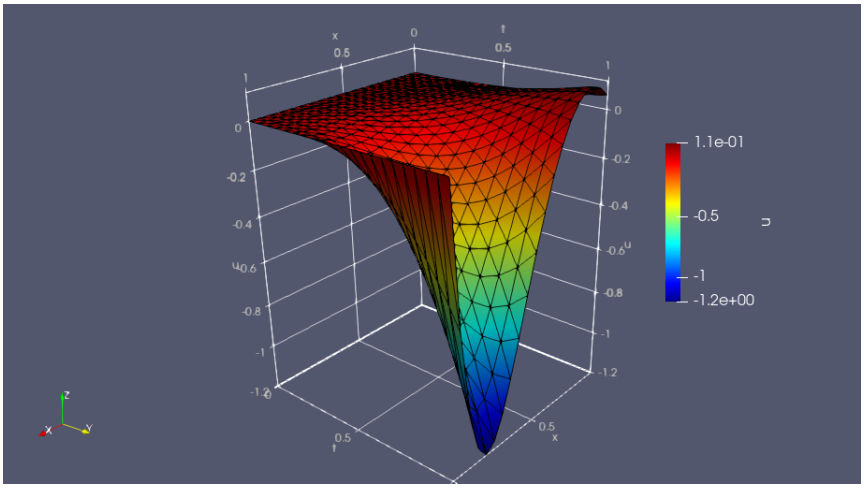

Figure 2. Approximate solution of Example 2

References

1. Akkutlu I. Y., Efendiev Y., Vasilyeva M., Wang Y.Multiscale model reduction for shale gastransport in poroelastic fractured media // J. Comput. Phys. 2018. V. 353. P. 356–376.
2. Vabishchevich P., Vasil'eva M.Iterative solution of the pressure problem for the multiphasefiltration // Math. Model. Anal. 2012. V. 17, N 4. P. 532–548.
3. Vasilieva M. B., Vasiliev V. I., Timofeyeva T. S. Numerical solution of diffusive and convective transport problems in highly heterogeneous porous media by the finite element method // Scientific notes of Kazan University. Series Physical and mathematical Sciences. - 2016. - Vol. 158, No 2. - P. 243–261 (in Russian).
4. Di Giuseppe E., Moroni M., Caputo M. Flux in porous media with memory: models and experiments // Transport in Porous Media. - 2010. - Vol. 83(3). - P. 479–500.
5. Gazizov R. K., Lukaschuk S. Yu. Fractional-differential approach to modeling filtration processes in complex inhomogeneous porous media // Bulletin of UGATU. - 2017. - Vol. 21, No. 4. - P. 104–112.
6. Abiola O. D., Enamul H. M., Kaseem M., Sidqi A. A. A modified memorybased mathematical model describing fluid flow in porous me-dia // Computers and Mathematics with Applications. - 2017. - Vol. 73(6). - P. 1385–1402.
7. Caputo M. Models of flux in porous media with memory // Water Resources Research. - 2000. - Vol. 36(3). - P. 693–705.
8. Agarwal R., Yadav M. P., Baleanu D., Purohit S. D. Existence and uniqueness of miscible flow equation through porous media with a non singular fractional derivative // AIMS Mathematics. - 2020. - Vol. 5(2). - P. 1062–1073.
9. Zhong W., Li C., Kou J. Numerical fractionalcalculus model for twophase flow in fractured media // Advances in Mathematical Phys-ics. - 2013. - Vol. 2013, No. 429835. - P. 1–7.
10. Alimbekova N.B., Baigereyev D.R., Madiyarov M.N. Mathematical Problems of Solving a Boundary Value Problem for a Differential Equation with a Fractional Time Derivative in the Sense of Caputo // News of Altai State University. - 2020. - No. 4 (114). - P. 64-69.

An Academic Assistant Based on a Pre-trained Model for Contextual Answering Questions

Yermek Alimzhanov[0000−0002−8758−2220]

University of International Business, Almaty, Kazakhstan
aermek81@gmail.com

Abstract The aim of this work is to develop a sufficiently effective system for question answering which should perform as academic assistant in Russian or Kazakh. For this purpose Google's pre-trained multilingual language representation model BERT (Bidirectional Encoder Representations from Transformers) is used. BERT is a transformer-based technique for pre-training contextual word representations that enables state-of-the-art results across a wide array of natural language processing tasks.
Using a pre-trained model with 12 layers for 104 languages and zero-shot transfer learning, it turned out to build a prototype of a question&answer system (academic assistant), the answers to which need to be found from the presented text (context). The built system showed good performance for Russian texts and fair results for Kazakh. To improve the quality of the system we specially created academic question and answer dataset in Kazakh, and it is managed by fine-tuning the pre-trained BERT with this dataset obtain an acceptable performance for Kazakh language.

Keywords: Natural Language Processing, Deep Learning, Transformer Architecture, Question Answering.

Introduction

Due to the pandemic and the emergency transition to distance learning, in addition to the educational process, universities need to establish feedback with students and quickly respond to their requests. The number of student appeals during assessment periods and examinations grows exponentially, and so does the beginning of the academic year. For example, in the automated dialogue system of the University of International Business (UIB), on the first day of the academic year, more than 890 student requests were recorded. Dealing with such a large flow of requests is difficult without automating the business processes of the call center and other departments of university. Therefore, the purpose of this work is to develop a sufficiently effective system of question answering for academic organizations.

Question answering is a computer science subject within the fields of information retrieval and natural language processing (NLP), which is concerned with building systems that automatically answer questions posed by humans. Though automatic question answering has a significant advance in the state-of-art information retrieval technology in recent years but still there are many challenging issues that are yet to

be resolved. One of the challenging tasks for existing QA systems is to understand the natural language questions correctly and deduce the precise meaning to retrieve exact responses. Improvement in mechanized understanding of questions faces issues like question classification, formulation of right queries, ambiguity resolution, semantic symmetry detection, identification of temporal relationship in complex questions. In the similar way identification of a perfect answer requires proper validation mechanism.

Question Answering with *context* is a task to find an answer on question in a given passage of text, where the answer to each question is a segment of the passage. A question answering system can automate many processes in academia and business. For example, it can help students get answers based on the external or internal regulatory and reference documents of the higher education institution. In addition, it helps you to check the reading comprehension ability of your students in tutoring.

In order to develop an automated academic assistant, various natural language processing technologies have been tested using machine learning methods. In recent years, significant progress has been made in this direction, primarily related to the use of computer technologies and techniques of artificial intelligence. Recent advances in deep learning for NLP have made explosive progress in the past two years. The combination of multiple techniques - including transfer learning and the invention of the Transformer neural architecture - have led to dramatic improvements in several NLP tasks including sentiment analysis, document classification, question answering, and more. In 2018, Google employees [1] published a work in which they created a new language representation model BERT (Bidirectional Encoder Representations from Transformers). BERT performed the best in 11 natural language processing tasks, beating all previous developments in this area.

The use of a bidirectional attention mechanism in a deep neural network with the Transformer architecture [2] allows one to build context-based natural language representation models. This approach allows to improve the accuracy of text interpretation by a computer, eliminating the ambiguity of words, and also to learn from unlabeled text. Pre-trained BERT models for different languages with a different number of encoder layers have been published on the hosting service for IT projects GitHub (https://github.com/google-research/bert).

Methods

Recently, the context-based question answering task attracted a lot of attention in academy. One of the major milestones in this field was the release of Stanford Question Answering Dataset (SQuAD). SQuAD a new reading comprehension dataset, consisting of questions posed by crowdworkers on a set of Wikipedia articles, where the answer to every question is a segment of text, or span, from the corresponding reading passage. With 100,000 question-answer pairs on more than 500 articles, SQuAD is significantly larger than previous reading comprehension datasets [3].

Extractive reading comprehension systems can often locate the correct answer to a question in a context document, but they also tend to make unreliable guesses on questions for which the correct answer is not stated in the context. Existing datasets either focused exclusively on answerable questions, or used automatically generated

unanswerable questions that are easy to identify. To address these weaknesses the latest version of the Stanford Question Answering Dataset (SQuAD) presented in [4]. SQuAD 2.0 combines the 100,000 questions in SQuAD1.1 with over 50,000 unanswerable questions written adversarially by crowdworkers to look similar to answerable ones. To do well on SQuAD 2.0, systems must not only answer questions when possible, but also determine when no answer is supported by the paragraph and abstain from answering.

BERT model was originally trained only for English language, but lately multilingual model trained on 104 was released. It gives ability to train models on language and use them for 104 other language. This technique is called zero-shot transfer as we don't use any training data for target language. Multilingual BERT models allow to perform zero-shot transfer from one language to another.

Zero-shot learning could provide extremely interesting applications, especially when there is a lack of proper datasets. Zero-shot learning relies on the existence of a labeled training set of seen classes and unseen class. Both seen and unseen classes are related in a high dimensional vector space, called semantic space, where the knowledge from seen classes can be transferred to unseen classes [5]. As you see in the figure 1, multilingual BERT performs well on answering questions in the Kazakh language in a given context.

```
model(['Жалпы білім беретін пәндер циклінің көлемі 56 академиялық кредитті құрайды.\
      Олардың 51 академиялық кредиті міндетті компонент пәндеріне тиесілі: Қазақстанның қазіргі заман тарихы,\
      Философия, Қазақ (орыс) тілі, Шетел тілі, Ақпараттық-коммуникациялық технологиялар (ағылшын тілінде),\
      Дене шынықтыру, Әлеуметтік-саяси білім модулі (саясаттану, әлеуметтану, мәдениеттану, психология).\
      Бұл ретте бакалавриат деңгейіндегі барлық мамандықтар және (немесе) кадрлар даярлау бағыттары бойынша\
      ЖОО білім алушылары "Қазақстанның қазіргі заман тарихы" пәнінен оны оқып аяқтағаннан кейін сол\
      академиялық кезеңде мемлекеттік емтихан тапсырады.'],
      ['Жалпы білім беретін пәндер циклінің көлемі нешеге тең?'])
```

```
[['56 академиялық кредитті'], [43], [1.4836091995239258]]
```

```
model(['Жалпы білім беретін пәндер циклінің көлемі 56 академиялық кредитті құрайды.\
      Олардың 51 академиялық кредиті міндетті компонент пәндеріне тиесілі: Қазақстанның қазіргі заман тарихы,\
      Философия, Қазақ (орыс) тілі, Шетел тілі, Ақпараттық-коммуникациялық технологиялар (ағылшын тілінде),\
      Дене шынықтыру, Әлеуметтік-саяси білім модулі (саясаттану, әлеуметтану, мәдениеттану, психология).\
      Бұл ретте бакалавриат деңгейіндегі барлық мамандықтар және (немесе) кадрлар даярлау бағыттары бойынша\
      ЖОО білім алушылары "Қазақстанның қазіргі заман тарихы" пәнінен оны оқып аяқтағаннан кейін сол\
      академиялық кезеңде мемлекеттік емтихан тапсырады.'],
      ['Міндетті компонент пәндер циклінің көлемі нешеге тең?'])
```

```
[['51 академиялық кредиті'], [84], [0.04279876500368118]]
```

Figure 1. Example of answering questions in Kazakh by Zero-shot learning.

The Kazakh is low-resource language, but in Wikipedia it is not the last in terms of the number of articles [6]. There are several developments for natural language processing tasks in Kazakh, which are maintained by various groups of scientists. But there is no consolidated resource and open access for researchers, which complicates progress in the development of new tools for NLP. For example, so-called Almaty Corpus of the Kazakh Language contains more than 40 million word tokens from the written and oral texts of different genres [7]. Also there is a Kazakh Language Corpus containing over 135 million words and conveying five stylistic genres: literary, publicistic, official, scientific and informal [8]. However, even this volume is not enough

to train and get a high-quality language model based on BERT when compared with the volume of the corpus, which used for pre-training BERT in English [1].

Fine-tuning BERT on Question Answering Tasks

To feed a question answering task into BERT, we pack both the question and the reference text into the input. The first token of every sequence is always a special classification token [CLS]. The two pieces of text are separated by the special [SEP] token. BERT also uses ”Segment Embeddings”to differentiate the question from the reference text. These are simply two embeddings that BERT learned, and which it adds to the token embeddings before feeding them into the input layer. In addition, for a given token, its input representation is constructed by summing the corresponding token, segment, and position embeddings [1].

Pre-trained BERT can be used for question answering over the text just by applying two linear transformations to the BERT outputs for each subtoken. The first/second linear transformation is used for predicting the probability that the current subtoken is the start/end position of the answer (fig. 2).

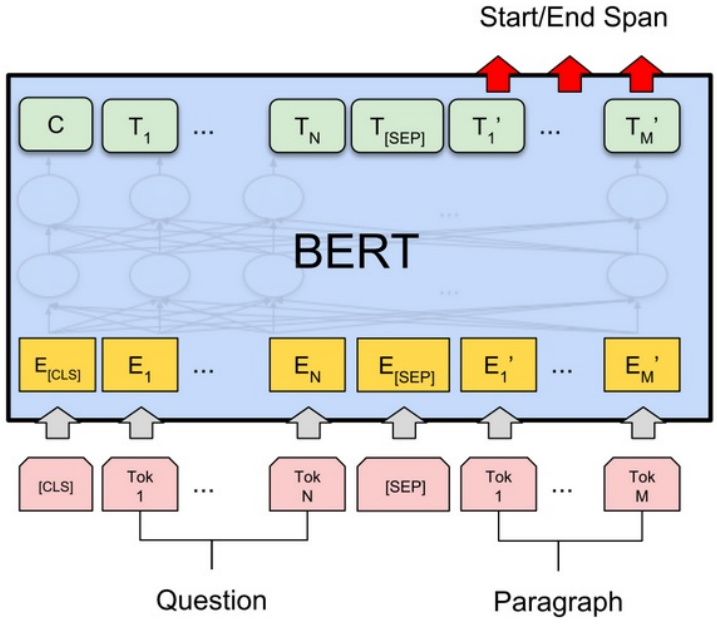

Figure 2. Illustration of Fine-tuning BERT on Question Answering Tasks [1]

For additional fine-tuning of pre-trained BERT, we collected a special dataset with questions and answers from the main regulatory documents of the Ministry of Education and Science of the Republic of Kazakhstan (see, i.e. [9]), as well as internal documents

regulating the academic policy of the university and containing answers to the most frequently asked questions. We used these documents only for a dataset in Kazakh, since BERT works quite well in Russian and there are trained models with open access [10]. Our dataset currently contains about 350 questions and will be supplemented in the future.

Fine-tuning of BERT was performed in the Google Colab environment with GPU (https://colab.research.google.com) and 12 GB RAM and it took about 2 hours, since BERT in base size contains of 110 millions parameters. We fine-tuned for 2 epochs with a learning rate of 3e-5 and a batch size of 12, as it recommended in the GitHub project webpage of BERT (https://github.com/google-research/bert).

Results

The built system showed good performance for Russian texts and fair results for Kazakh. To improve the quality of the system we specially created academic question and answer dataset in Kazakh, and it is managed by fine-tuning the pre-trained BERT with this dataset obtain an acceptable performance for Kazakh language.

Performance results are given in the table 1 where the metrics are exact matching (EM) and F1. There RuBERT QA is a fine-tuned BERT question answering model from the DeepPavlov project [10]. It is interesting fact that model can work even if context and question languages are different (fig. 3).

Table 1. Results for Zero-Shot QA from English to Russian and Kazakh.

Model in Kazakh	EM	F1	Model in Russian	EM	F1
Fine-Tuned BERT QA	72	74.3	RuBERT QA	82	84.6
Zero-shot Multilingual BERT QA	65	68.4	Zero-shot ML BERT QA	73	76.5

Such a fine-tuned model can be used for building a modern automated question answering system on top of a large collection of unstructured text documents such as Wikipedia – but we could imagine other use cases, such as a system built atop a newsfeed or a set of internal- or external-facing corporate documents.

Discussion

Recent advances in deep learning for NLP have made explosive progress in the past two years. The combination of multiple techniques - including transfer learning and the invention of the Transformer neural architecture - have led to dramatic improvements in several NLP tasks including sentiment analysis, document classification, question answering, and more. Models like BERT, XLNet [11], and Googles new T5 [12] work by processing a document and identifying a passage within that best answers the question.

Many authors note the slowness of the BERT model when working on production. Therefore, many works have been devoted to optimizing and improving performance

```
[ ] model(['Su área de distribución comprende casi toda Sudamérica al este de los Andes en las \
       cuencas del río Orinoco, del Amazonas y del Río de la Plata; cubriendo desde el este \
       de Venezuela y la Guyana hasta Uruguay y el norte y centro de Argentina. Pueden vivir \
       en diferentes tipos de hábitat, pero muestran preferencia por algunos en concreto. \
       Suelen encontrarse cerca de lagos, ríos, marismas o manglares.'],
      ['What countries do capybara live in?'])

[['Venezuela y la Guyana hasta Uruguay y el norte y centro de Argentina'],
 [185],
 [1155.131591796875]]
```

Figure 3. Example of answering questions in English from Spanish context by Zero-shot Multilingual BERT QA model.

(see, i.e. [13] and [14], [15]), and also obtained state-of-the-art results using ensembles of several models with the BERT [16].

However, since training of large models occurs mainly with the help of languages with large resources, which represent more developed countries and parts of the world, in the future there may be problems in interpreting the meaning of texts in low-resource languages. It can also lead to even greater inequality between rich and poor countries in the introduction of artificial intelligence into the industry.

Conclusion

In order to react in time to the requests of citizens and not aggravate social tension among the population, all institutions of social importance, as well as universities, need to digitalize the processes of relationships with their customers. Dialogue systems based on chatbots can automate requests from stakeholders and help to respond to their requests in time.

As far as the author knows, there are very few works on automatic answering questions in the Kazakh language, so this work is very relevant. In the future, these aproach can be used to develop full-fledged dialogue systems and conversational AI deploying speech pipeline of automatic speech recognition and text to speech technologies with NLP unit as demonstrated in [17].

Acknowledgment

This research is funded by the Science Committee of the Ministry of Education and Science of the Republic of Kazakhstan (Grant No. BR05236340) as a part of the project ”Creation of high-performance intelligent analysis and decision making technologies for the ”logistics-agglomeration” system within formation of the Republic of Kazakhstan digital economics”.

References

1. Devlin, J. and Chang, M. and Lee, K. and Toutanova, K. *Bert: Pre-training of deep bidirectional transformers for language understanding*, arXiv preprint arXiv:1810.04805, (2018).

2. Vaswani, A. and Shazeer, N. and Parmar, N. and et al.: *Attention is all you need*, In Advances in Neural Information Processing Systems, 60006010 (2017).
3. Rajpurkar, P., Zhang, J., Lopyrev, K., and Liang, P.: *SQUAD: 100,000+ questions for machine comprehension of text*. In Proceedings of the 2016 Conference on Empirical Methods in Natural Language Processing, pages 23832392. (2016).
4. Rajpurkar, P., Jia, R., Liang, P.: Know what you dont know: Unanswerable questions for SQuAD. In Proceedings of the 56th Annual Meeting of the Association for Computational Linguistics (Volume 2: Short Papers), pp. 784-789, Melbourne, Australia, July 2018. Association for Computational Linguistics. https://doi.org/10.18653/v1/P18-2124.
5. Howard, J., Ruder, S.: Universal language model fine-tuning for text classification. In ACL. Association for Computational Linguistics. (2018)
6. List of Wikipedias, `https://meta.wikimedia.org/wiki/List\_of\_Wikipedias`. Last accessed 14 Aug 2020
7. *Almaty corpus of the Kazakh language*, `http://web-corpora.net/KazakhCorpus/search`. Last accessed 14 Sep 2020.
8. Olzhas Makhambetov, Aibek Makazhanov, Zhandos Yessenbayev, Bakhyt Matkarimov, Islam Sabyrgaliyev, Anuar Sharafudinov: Assembling the Kazakh Language Corpus, Proceedings of the 2013 Conference on Empirical Methods in Natural Language Processing, pages 1022-1031, Seattle, Washington, USA, (2013). https://doi.org/10.13140/2.1.5127.4882
9. State Compulsory Educational Standards for all levels of education (SCES), The Rules for Organizing the Educational Process on Credit Technology of Education (CTE). `http://adilet.zan.kz/eng/docs/V1800017669`. `http://adilet.zan.kz/kaz/docs/V1100006976`. Last accessed 14 Sep 2020.
10. The Neural Networks and Deep Learning Laboratory at Moscow Institute Physics and Technology. `https://deeppavlov.ai/about-us`. Last accessed 15 Sep 2020.
11. Zhilin Yang, Zihang Dai, Yiming Yang, Jaime Carbonell, Ruslan Salakhutdinov, Quoc V. Lee: XLNet: Generalized Autoregressive Pretraining for Language Understanding, 33rd Conference on Neural Information Processing Systems (NeurIPS 2019), Vancouver, Canada.
12. Colin Raffel, Noam Shazeer, Adam Roberts, Katherine Lee, Sharan Narang, Michael Matena, Yanqi Zhou, Wei Li, Peter J. Liu: Exploring the Limits of Transfer Learning with a Unified Text-to-Text Transformer, Journal of Machine Learning Research 21, pages 1-67, (2020).
13. Lan, Zh., Chen, M., Goodman, S., Gimpel, K., Sharma, P., Soricut, R.: ALBERT: A lite bert for self-supervised learning of language representations. Published as a conference paper at ICLR 2020. arXiv preprint arXiv:1909.11942, (2019).
14. Yinhan Liu, Myle Ott, Naman Goyal, Jingfei Du, Mandar Joshi, Danqi Chen, Omer Levy, MikeLewis, Luke Zettlemoyer, and Veselin Stoyanov. Roberta: A robustly optimized bert pretraining approach. arXiv preprint arXiv:1907.11692, (2019).
15. Yang You, Jing Li, Sashank Reddi, Jonathan Hseu, Sanjiv Kumar, Srinadh Bhojanapalli, Xiaodan Song, James Demmel, Kurt Keutzer, Cho-Jui Hsieh: Large Batch Optimization for Deep Learning: Training BERT in 76 Minutes, Published as a conference paper at ICLR 2020, arXiv preprint arXiv:1904.00962v5, (2020).
16. `https://rajpurkar.github.io/SQuAD-explorer`. Last accessed 14 Sep 2020.
17. Conversational AI Inference Deployment using TensorRT Inference Server. `https://developer.nvidia.com/gtc-dc/2019/video/DC91249-vid` Last accessed 1 Sep 2020.

On the Conditional Stability of Finite-difference Analogue of a Two-dimensional Problem of Integral Geometry with a Weight Function

Galitdin Bakanov[0000−0003−1262−7874]

Khoja Akhmet Yassawi International Kazakh-Turkish University,
B.Sattarkhanov avenue 29, Turkestan, 161200, Kazakhstan
galitdin.bakanov@ayu.edu.kz

Abstract The problems of integral geometry are to find the functions, which are determined on certain variety, through its integrals on certain set of subvarities with lower dimension.
Additionally, the problems of integral geometry are correlated with various solutions (data interpretation objectives of exploration seismology, electro-exploration, acoustics, and inverse problems of kinetic equations, widely used in plasma physics and astrophysics). In recent years, the studies on problems of integral geometry have critical significance for tomography, which is intensively developing scientific - technic pillar that has several applications in medicine and industry. Therefore, development of various solution methods for the integral geometry problems is actual issue.
In this paper, we get estimate the conditional stability of the finite-difference analogue of the two-dimensional problem of an integral problem with a weight function

Keywords: Finite-difference problem, Solution, Stability.

Introduction and problem statement

The problems of integral geometry are to find the functions, which are determined on certain variety, through its integrals on certain set of subvarities with lower dimension.

One of the stimuli for studying such problems is their connection with multidimensional inverse problems for differential equations [1]. In some inverse problems for hyperbolic equations were shown to reduce to integral geometry problems and, in particular, a problem of integral geometry was considered in the case of shift-invariant curves. Mukhometov [2] showed the uniqueness and estimated the stability of the solution of a two-dimensional integral geometry on the whole. His results were mainly based on the reduction of the two-dimensional integral geometry problem

$$V(\gamma, z) = \int\limits_{K(\gamma,z)} U(x,y)\,\rho(x,y,z)\,ds, \quad \gamma \in [0,l], \quad z \in [0,l] \tag{1}$$

where $U \in C^2\left(\overline{D}\right)$, $\rho(x,y,z)$ is a known function to the boundary value problem

$$\frac{\partial}{\partial z}\left(\frac{\partial W}{\partial x}\frac{\cos\theta}{\rho} + \frac{\partial W}{\partial y}\frac{\sin\theta}{\rho}\right) = 0, \ (x,y,z) \in \Omega_1, \tag{2}$$

$$W(\xi(\gamma),\eta(\gamma),z)=V(\gamma,z),V(z,z)=0,\gamma,z\in[0,l]. \tag{3}$$

Here D is a plane bounded by a simply connected domain with a smooth boundary Γ :

$$x=\xi(z),\ y=\eta(z),\ z\in[0,l],\ \xi(0)=\xi(l),\ \eta(0)=\eta(l),$$

where a parameter z is the length of the curve Γ :

$$\Omega_1=\Omega/\{(\xi(\gamma),\ \eta(\gamma),z):z\in[0,l]\},\ \Omega=\bar{D}\times[0,l];$$

$K(x,y,z)$ is the part of the curve $K(\gamma,z)$ included between the points $(x,y)\in\overline{D}$ and $(\xi(z),\eta(z)),\ z\in[0,l]$;

$$W(x,y,z)=\int\limits_{K(x,y,z)}U(x,y)\,\rho(x,y,z)\,ds,$$

$\theta(x,y,z)$ is an angle between the tangent to $K(x,y,z)$ at the point (x,y) and the x -axis and the variable parameter s is the curve length.

Suppose that the requirements on the family of curves $K(\gamma,z)$and the domain D the are necessary for the problem (1) to reduce to problem (2), (3) are met [2], [3]. Assume also that every line parallel to either the $x-$ or the $y-$ axis intersects boundary of D at no more than two points. Let

$$a_1=\inf_{(x,y)\in D}\{x\},\ b_1=\sup_{(x,y)\in D}\{x\},\ a_2=\inf_{(x,y)\in D}\{y\},\ b_2=\sup_{(x,y)\in D}\{y\},$$

$$h_j=(b_j-a_j)/N_j,\ j=1,2;\ h_3=l/N_3,$$

and the $N_j,j=1,2,3$, are natural number. Suppose that

$$0<\varepsilon<\min\{(b_1-a_1)/3,\ (b_2-a_2)/3\},$$

$$D^{\varepsilon}=\left\{(x,y)\in D:\min_{(\alpha,\beta)\in\Gamma}\rho((x,y),(\alpha,\beta))>\varepsilon\right\},$$

$$R_h=\{(x_i,y_j):x_i=a_1+ih_1,y_j=a_2+jh_2,\ \ i=1,...,N_1,j=1,...,N_2\}.$$

A neighborhood $B(ih_1,jh_2)$ of the point (a_1+ih_1,a_2+jh_2) is defined as the five-point set

$$\{(a_1+ih_1,a_2+jh_2),(a_1+(i\pm1)h_1,a_2+(j\pm1)h_2)\}.$$

A set D_h^{ε} consists of all points (a_1+ih_1,a_2+jh_2) such that their neighborhoods $B(ih_1,jh_2)$ are contained in $D^{\varepsilon}\cap R_h$. A set Γ_h^{ε} is made of all points $(a_1+ih_1,a_2+jh_2)\in D_h^{\varepsilon}$ such that $B(ih_1,jh_2)\cap(D^{\varepsilon}\cap R_h)\setminus D_h^{\varepsilon}\neq0$. Finally,

$$\Delta_h^{\varepsilon}=\bigcup_{\Gamma_h^{\varepsilon}}B(ih_1,jh_2),D_h=R_h\cap D,$$

$$\Omega_h^{\varepsilon}=(a_1+ih_1,a_2+jh_2,kh_3):(a_1+ih_1,a_2+jh_2)\in D_h^{\varepsilon},k=0,1,...,N_3-1.$$

From here on we suppose that the coefficients and the solution of problem (2), (3) have the following properties:

$$W(x,y,z) \in C^3(\Omega^\varepsilon), \theta(x,y,z) \in C^2(\Omega^\varepsilon), \Omega^\varepsilon = \overline{D^\varepsilon} \times [0,l], \tag{4}$$

$$\rho(x,y,z) \in C^2(\Omega), \rho(x,y,z) > c_1 > 0, \frac{\partial\theta}{\partial z} > \left|\frac{\partial\rho}{\partial z}\frac{1}{\rho}\right|. \tag{5}$$

We consider the finite-difference problem of finding the functions $\Phi^k_{i,j}$, which satisfy the equation

$$\left[\Phi_{\overset{\circ}{x}}\frac{\mathrm{A}}{C} + \Phi_{\overset{\circ}{y}}\frac{B}{C}\right]_z = 0, \quad (a_1+ih_1, a_2+jh_2, kh_3) \in \Omega^\varepsilon_h, \tag{6}$$

and the boundary condition

$$\Phi^k_{i,j} = F^k_{i,j}, (a_1+ih_1, a_2+jh_2) \in \Delta^\varepsilon_h, k = 1, ..., N_3 - 1 \tag{7}$$

$$\Phi^0_{i,j} = \Phi^{N_3}_{i,j}, \quad (a_1+ih_1, a_2+jh_2) \in D^\varepsilon_h, \tag{8}$$

where

$$\Phi^k_{i,j} = \Phi(x_i, y_j, z_k) = \Phi(a_1+ih_1, a_2+jh_2, kh_3),$$

$$\Phi_{\overset{\circ}{x}} = (\Phi_{i+1,j} - \Phi_{i-1,j})/2h_1,$$

$$\Phi_{\overset{\circ}{y}} = (\Phi_{i,j+1} - \Phi_{i,j-1})/2h_2,$$

$$f_z = \frac{\left(f^{k+1}_{i,j} - f^k_{i,j}\right)}{h_3},\ A = \cos\theta^k_{i,j},\ B = \sin\theta^k_{i,j},$$

$$\theta^k_{i,j} = \theta(a_1+ih_1, a_2+jh_2, kh_3),\ C = \rho^k_{i,j} = \rho(a_1+ih_1, a_2+jh_2, kh_3).$$

We note that in the finite-difference formulation information on the solution is given not only on the boundary Γ but also in its $\varepsilon-$ neighborhood, because the partial derivatives $\theta_z, W_{xz}, W_{yz}, W_{xy}$ have singularities of the type

$$\left[(x-\xi(z))^2 + (y-\eta(z))^2\right]^{-\frac{1}{2}}$$

in a neighborhood of an arbitrary point $(\xi(z), \eta(z), z)$ (see [2]).

Stability estimation of the solution of the finite - difference problem

It is not difficult to verify the following assertion.

Lemma 1. *If u and ν are mesh functions, then*

$$\left(\frac{u}{\nu}\right)_z = \frac{u_z\nu^k - u^k\nu_z}{\nu^k\nu^{k+1}} \tag{9}$$

$$(u\nu)_z = u^k\nu_z + u_z\nu^k + h_3u_z\nu_z \tag{10}$$

$$(u\nu)_{\overset{\circ}{x}} = u_{\overset{\circ}{x}}\nu_i + u_i\nu_{\overset{\circ}{x}} + \frac{h_1^2}{2}[u_x\nu_x]_{\bar{x}} \tag{11}$$

Theorem 1. *Suppose that the solution of problem (6) - (8) exists on* Ω_h^ε *and* $\left|\Phi_{\overset{\circ}{xz}}\right| \leq c_2$, $\left|\Phi_{\overset{\circ}{yz}}\right| \leq c_2$, *where* c_2 *is constant, and that*

$$(AB_z - A_z B) - \left|\frac{C_z}{C}\right| \geq \alpha > 0$$

for all N_j, $j = 1, 2, 3$. *Then there exists a positive constant* N^{**} *such that, for all* $N_j > N^{**}, j = 1, 2, 3,$

$$\begin{gathered} \sum_{\Omega_h^\varepsilon} \left(\Phi_{\overset{\circ}{x}}^2 + \Phi_{\overset{\circ}{y}}^2\right) h_1\, h_2\, h_3 \leq \\ \leq c_3 \sum_{\Delta_h^\varepsilon} \left(F_{\overset{\circ}{x}}^2 h_1 h_3 + F_{\overset{\circ}{y}}^2 h_2 h_3 + F_z^2 (h_2 + h_1) h_3\right) + c_2 h_3^2. \end{gathered} \tag{12}$$

Here c_3 *is a constant dependent on the function* $\rho(x, y, z)$ *and on the family of curves* $K(\gamma, z)$.

Доказательство. Multiplying both sides of (6) by $2C\left(-B\Phi_{\overset{\circ}{x}} + A\Phi_{\overset{\circ}{y}}\right)$ (see [3], [4], [5], [6]), we get $J_1 + J_2 = 0$, where

$$J_1 = J_2 = C\left[-\Phi_{\overset{\circ}{x}} B + \Phi_{\overset{\circ}{y}} A\right]\left[\Phi_{\overset{\circ}{x}} \frac{A}{C} + \Phi_{\overset{\circ}{y}} \frac{B}{C}\right]_z.$$

Using the product differentiation formula (10) we obtain

$$\begin{gathered} J_1 = \left[C\left(-\Phi_{\overset{\circ}{x}} B + \Phi_{\overset{\circ}{y}} A\right)\left(\Phi_{\overset{\circ}{x}} \frac{A}{C} + \Phi_{\overset{\circ}{y}} \frac{B}{C}\right)\right]_z - \\ -\left[C\left(-\Phi_{\overset{\circ}{x}} B + \Phi_{\overset{\circ}{y}} A\right)\right]_z \left(\Phi_{\overset{\circ}{x}} \frac{A}{C} + \Phi_{\overset{\circ}{y}} \frac{B}{C}\right) - \\ -h_3\left[C\left(-\Phi_{\overset{\circ}{x}} B + \Phi_{\overset{\circ}{y}} A\right)\right]_z \left[\Phi_{\overset{\circ}{x}} \frac{A}{C} + \Phi_{\overset{\circ}{y}} \frac{B}{C}\right]_z = 0 \end{gathered}$$

Exposing brackets in expression J_1 and J_2 taking into account formulas (9), (10) and equality (6), taking into account that

$$\left(1 - \frac{C^k}{C^{k+1}}\right) \approx o(h_3), \left(\frac{1}{C^{k+1}} - \frac{1}{C^k}\right) \approx o(h_3), \left(\frac{1}{C^{k+1}} + \frac{1}{C^k}\right) \approx \frac{2}{C^k} + o(h_3),$$

$$D = 2AB = 2\cos\theta \sin\theta = \sin 2\theta,\ \mathrm{E} = A^2 - B^2 = \cos^2\theta - \sin^2\theta = \cos 2\theta,$$

using the formulas

$$\Phi_{\overset{\circ}{x}} \Phi_{\overset{\circ}{xz}} = \frac{1}{2}\left(\Phi_{\overset{\circ}{x}}^2\right)_z - \frac{h_3}{2}\Phi_{\overset{\circ}{xz}}^2,\ \Phi_{\overset{\circ}{y}} \Phi_{\overset{\circ}{yz}} = \frac{1}{2}\left(\Phi_{\overset{\circ}{y}}^2\right)_z - \frac{h_3}{2}\Phi_{\overset{\circ}{yz}}^2$$

we get

$$J_3 + J_4 + J_5 + J_6 + J_7 + J_8 = 0, \tag{13}$$

where

$$J_3 = \frac{1}{2}\cdot\left\{\Phi^2_{\underset{x}{\circ}}\cdot\left[(AB_z - A_zB) + D\cdot\frac{C_z}{C}\right] - 2\cdot\Phi^{k+1}_{\underset{y}{\circ}}\cdot \mathrm{E}\cdot\frac{C_z}{C} + \right.$$

$$\left. + \left(\Phi^{k+1}_{\underset{y}{\circ}}\right)^2\cdot\left[(AB_z - A_zB) - D\cdot\frac{C_z}{C}\right]\right\},$$

$$J_4 = \frac{1}{2}\cdot\left\{\left(\Phi^{k+1}_{\underset{y}{\circ}}\right)^2\cdot\left[(AB_z - A_zB) + D\cdot\frac{C_z}{C}\right] - 2\Phi^{k+1}_{\underset{x}{\circ}}\cdot\Phi_{\underset{y}{\circ}}\cdot\mathrm{E}\cdot\frac{C_z}{C} + \right.$$

$$\left. + \Phi^2_{\underset{y}{\circ}}\cdot\left[(AB_z - A_zB) - D\cdot\frac{C_z}{C}\right]\right\},$$

$$J_5 = -\frac{h_3^2}{2}\cdot\Phi^2_{\underset{xz}{\circ}}\cdot\left[(\mathrm{AB}_z - \mathrm{A}_z\mathrm{B}) + D\cdot\frac{C_z}{C}\right] -$$

$$\frac{h_3^2}{2}\cdot\Phi^2_{\underset{yz}{\circ}}\cdot\left[(\mathrm{AB}_z - \mathrm{A}_z\mathrm{B}) - D\cdot\frac{C_z}{C}\right] +$$

$$+\Phi^2_{\underset{x}{\circ}}\cdot(\mathrm{A}_z\mathrm{B} + \mathrm{AB}\cdot C_z)\cdot o(h_3) + \Phi^2_{\underset{y}{\circ}}\cdot(\mathrm{AB}_z - \mathrm{AB}\cdot C_z)\cdot o(h_3) +$$

$$+\Phi_{\underset{x}{\circ}}\Phi^{k+1}_{\underset{y}{\circ}}B^2C_z o(h_3) - \Phi_{\underset{y}{\circ}}\Phi^{k+1}_{\underset{x}{\circ}}A^2C_z o(h_3).$$

$$J_6 = \Phi_{\underset{x}{\circ}}\Phi_{\underset{y}{\circ}}BB_z\left(1 - \frac{C^k}{C^{k+1}}\right) + \Phi_{\underset{x}{\circ}}\Phi_{\underset{y}{\circ}}AA_z\left(\frac{C^k}{C^{k+1}} - 1\right) -$$

$$-h_3\Phi_{\underset{x}{\circ}}\Phi_{\underset{yz}{\circ}}\left(AA_z + BB_z\frac{C^k}{C^{k+1}}\right) + h_3\Phi_{\underset{y}{\circ}}\Phi_{\underset{xz}{\circ}}\left(AA_z\frac{C^k}{C^{k+1}} + BB_z\right),$$

$$J_7 = \left[\left(-\Phi_{\underset{x}{\circ}}B + \Phi_{\underset{y}{\circ}}A\right)\left(\Phi_{\underset{x}{\circ}}A + \Phi_{\underset{y}{\circ}}B\right)\right]_z - \Phi_{\underset{x}{\circ}}\Phi_{\underset{yz}{\circ}} + \Phi_{\underset{y}{\circ}}\Phi_{\underset{xz}{\circ}},$$

$$J_8 = h_3\Phi^2_{\underset{x}{\circ}}AB_z\frac{C_z}{C} + h_3^2\Phi_{\underset{x}{\circ}}\Phi_{\underset{xz}{\circ}}AB_z\frac{C_z}{C} +$$

$$+h_3\Phi_{\underset{x}{\circ}}\Phi_{\underset{y}{\circ}}AA_z\frac{C_z}{C} + h_3\Phi_{\underset{x}{\circ}}\Phi_{\underset{y}{\circ}}BB_z\frac{C_z}{C} - h_3^2\Phi_{\underset{x}{\circ}}\Phi_{\underset{yz}{\circ}}AA_z\frac{C_z}{C} +$$

$$+h_3^2\Phi_{\underset{y}{\circ}}\Phi_{\underset{xz}{\circ}}BB_z\frac{C_z}{C} - h_3\Phi^2_{\underset{y}{\circ}}A_zB\frac{C_z}{C} - h_3^2\Phi_{\underset{y}{\circ}}\Phi_{\underset{yz}{\circ}}A_zB\frac{C_z}{C}.$$

Now we will transform and we estimate each of these elements.

The expression for J_3 and J_4 is a quadratic form with respect to $\Phi_{\underset{x}{\circ}}$ and $\Phi^{k+1}_{\underset{y}{\circ}}$, to $\Phi^{k+1}_{\underset{x}{\circ}}$ and $\Phi_{\underset{y}{\circ}}$, whose determinant

$$\begin{vmatrix} (AB_z - A_zB) + D\frac{C_z}{C} & -\mathrm{E}\frac{C_z}{C} \\ -\mathrm{E}\frac{C_z}{C} & (AB_z - A_zB) - D\frac{C_z}{C} \end{vmatrix} =$$

$$= (AB_z - A_zB)^2 - D^2\left|\frac{C_z}{C}\right|^2 - \mathrm{E}^2\left|\frac{C_z}{C}\right|^2 =$$

$$(AB_z - A_zB)^2 - \left|\frac{C_z}{C}\right|^2,$$

because $\mathrm{E}^2 + D^2 = 1$, where $\mathrm{E} = \cos 2\theta$, $D = sin2\theta$. Then, from the condition $(AB_z - A_zB) - \left|\frac{C_z}{C}\right| \geq \alpha > 0$ the positive definiteness of the quadratic form J_3 and J_4 follows. Using the inequality

$$ax^2 + 2bxy + cy^2 \geq \frac{2\left(ac - b^2\right)}{a + c + \sqrt{(a-c)^2 + 4b^2}}\left(x^2 + y^2\right)$$

for a positively definite quadratic form $ax^2 + 2bxy + cy^2$, we obtain

$$J_3 \geq \frac{1}{2}\left[(AB_z - A_zB) - \left|\frac{C_z}{C}\right|\right]\left[\left(\Phi^k_{\circ x}\right)^2 + \left(\Phi^{k+1}_{\circ y}\right)^2\right], \tag{14}$$

$$J_4 \geq \frac{1}{2}\left[AB_z - A_zB - \left|\frac{C_z}{C}\right|\right]\left[\left(\Phi^{k+1}_{\circ x}\right)^2 + \left(\Phi^k_{\circ y}\right)^2\right] \tag{15}$$

Taking into account that $\left(1 - \frac{C^k}{C^{k+1}}\right) \approx o\left(h_3\right)$, we have

$$J_6 = \Phi_{\circ x}\Phi_{\circ y}BB_z o\left(h_3\right) + \Phi_{\circ x}\Phi_{\circ y}AA_z o\left(h_3\right) - h_3\Phi_{\circ x}\Phi_{\circ yz}\left(AA_z + \frac{BB_zC^k}{C^{k+1}}\right) +$$

$$+h_3\Phi_{\circ y}\Phi_{\circ xz}\left(\frac{AA_zC^k}{C^{k+1}} + BB_z\right) =$$

$$= \Phi_{\circ x}\Phi_{\circ y}BB_z o\left(h_3\right) + \Phi_{\circ x}\Phi_{\circ y}AA_z o\left(h_3\right)\left(AA_z + BB_z\right) \times$$

$$\times\left(\Phi_{\circ y}\Phi_{\circ xz} - \Phi_{\circ x}\Phi_{\circ yz}\right) - h_3\Phi_{\circ x}\Phi_{\circ yz}BB_z o\left(h_3\right) + h_3\Phi_{\circ y}\Phi_{\circ xz}AA_z o\left(h_3\right) =$$

$$= \Phi_{\circ x}\Phi_{\circ y}\left(AA_z + BB_z\right) o\left(h_3\right) + \left(AA_z + BB_z\right)\left(\Phi^k_{\circ y}\Phi^{k+1}_{\circ x} - \Phi^k_{\circ x}\Phi^{k+1}_{\circ y}\right) -$$

$$-\left(\Phi^k_{\circ x}\Phi^{k+1}_{\circ y} + \Phi^k_{\circ x}\Phi^k_{\circ y}\right)BB_z o\left(h_3\right) + \left(\Phi^k_{\circ y}\Phi^{k+1}_{\circ x} - \Phi^k_{\circ y}\Phi^k_{\circ x}\right)AA_z o\left(h_3\right)$$

Using the inequality $|ab| \leq (a^2 + b^2)/2$, we get

$$\begin{aligned} J_6 \leq \tfrac{1}{2}\Bigg\{ & \left[\left(\Phi^k_{\circ x}\right)^2 + \left(\Phi^k_{\circ y}\right)^2\right]\left(AA_z + BB_z\right) o\left(h_3\right) + \\ & + \left[\left(\Phi^k_{\circ x}\right)^2 + \left(\Phi^{k+1}_{\circ y}\right)^2\right]\left(AA_z + BB_z\right) + \\ & + \left[\left(\Phi^k_{\circ x}\right)^2 + \left(\Phi^{k+1}_{\circ y}\right)^2 + \left(\Phi^k_{\circ x}\right)^2 + \left(\Phi^k_{\circ y}\right)^2\right] BB_z o\left(h_3\right) + \\ & + \left[\left(\Phi^k_{\circ y}\right)^2 + \left(\Phi^{k+1}_{\circ x}\right)^2 + \left(\Phi^k_{\circ y}\right)^2 + \left(\Phi^k_{\circ x}\right)^2\right] AA_z o\left(h_3\right)\Bigg\}. \end{aligned} \tag{16}$$

Then, into account that $(AB_z - A_zB) - \left|\frac{C_z}{C}\right| \geq \alpha > 0$, conditions $\left|\Phi_{\underset{xz}{\circ}}\right| \leq c_2$, $\left|\Phi_{\underset{yz}{\circ}}\right| \leq c_2$ and the inequality
$|ab| \leq (a^2+b^2)/2$, we obtain

$$\begin{aligned} J_5 \leq \Phi_{\underset{x}{\circ}}^2 (A_zB + ABC_z)\, o(h_3) + \Phi_{\underset{y}{\circ}}^2 (AB_z - ABC_z)\, o(h_3) + \\ + \tfrac{1}{2}\left\{\left[\left(\Phi_{\underset{x}{\circ}}^k\right)^2 + \left(\Phi_{\underset{x}{\circ}}^{k+1}\right)^2\right](A_zB + ABC_z)\; o(h_3) + \right. \\ + \left[\left(\Phi_{\underset{y}{\circ}}^k\right)^2 + \left(\Phi_{\underset{y}{\circ}}^{k+1}\right)^2\right] \times (AB_z + ABC_z)\; o(h_3) + \\ + \left[\left(\Phi_{\underset{x}{\circ}}^k\right)^2 + \left(\Phi_{\underset{y}{\circ}}^{k+1}\right)^2\right] B^2C_z o(h_3) + \\ \left. + \left[\left(\Phi_{\underset{y}{\circ}}^k\right)^2 + \left(\Phi_{\underset{x}{\circ}}^{k+1}\right)^2\right] A^2C_z o(h_3)\right\} + c_2h_3^2. \end{aligned} \tag{17}$$

Due to formula (11) we have

$$\begin{aligned} \Phi_{\underset{y}{\circ}}\Phi_{\underset{xz}{\circ}} &= \left[\Phi_{\underset{y}{\circ}}\Phi_z\right]_{\underset{x}{\circ}} - \Phi_{\underset{xy}{\circ\circ}}\Phi_z - \frac{h_1^2}{2}\left[\Phi_{\underset{yx}{\circ}}\Phi_{zx}\right]_{\bar{x}}, \\ -\Phi_{\underset{x}{\circ}}\Phi_{\underset{y}{\circ}z} &= -\left[\Phi_{\underset{x}{\circ}}\Phi_z\right]_{\underset{y}{\circ}} + \Phi_{\underset{xy}{\circ\circ}}\Phi_z + \frac{h_2^2}{2}\left[\Phi_{\underset{xy}{\circ}}\Phi_{zy}\right]_{\bar{y}}. \end{aligned}$$

Consequently,

$$\begin{aligned} J_7 &= \left[(-\Phi_{\underset{x}{\circ}}B + \Phi_{\underset{y}{\circ}}A)(\Phi_{\underset{x}{\circ}}A + \Phi_{\underset{y}{\circ}}B)\right]_z - \Phi_{\underset{x}{\circ}}\Phi_{\underset{y}{\circ}z} + \Phi_{\underset{y}{\circ}}\Phi_{\underset{x}{\circ}z} = \\ &= \left[\left(-\Phi_{\underset{x}{\circ}}B + \Phi_{\underset{y}{\circ}}A\right)\left(\Phi_{\underset{x}{\circ}}A + \Phi_{\underset{y}{\circ}}B\right)\right]_{\bar{z}} + \left[\Phi_{\underset{y}{\circ}}\Phi_z\right]_{\underset{x}{\circ}} - \\ &\quad - \left[\Phi_{\underset{x}{\circ}}\Phi_z\right]_{\underset{y}{\circ}} - \frac{h_1^2}{2}\left[\Phi_{\underset{yx}{\circ}}\Phi_{zx}\right]_{\bar{x}} + \frac{h_2^2}{2}\left[\Phi_{\underset{xy}{\circ}}\Phi_{zy}\right]_{\bar{y}}. \end{aligned} \tag{18}$$

Now we will transform and estimate J_8:

$$\begin{aligned} J_8 = h_3\Phi_{\underset{x}{\circ}}^2AB_z\frac{C_z}{C} + h_3\Phi_{\underset{x}{\circ}}^k\Phi_{\underset{x}{\circ}}^{k+1}AB_z\frac{C_z}{C} - h_3\Phi_{\underset{x}{\circ}}^2AB_z\frac{C_z}{C} - h_3\Phi_{\underset{x}{\circ}}\Phi_{\underset{y}{\circ}}AA_z\frac{C_z}{C} + \\ + h_3\Phi_{\underset{x}{\circ}}\Phi_{\underset{y}{\circ}}BB_z\frac{C_z}{C} - h_3\Phi_{\underset{x}{\circ}}^k\Phi_{\underset{y}{\circ}}^{k+1}AA_z\frac{C_z}{C} + h_3\Phi_{\underset{x}{\circ}}\Phi_{\underset{y}{\circ}}AA_z\frac{C_z}{C} + h_3\Phi_{\underset{y}{\circ}}^k\Phi_{\underset{x}{\circ}}^{k+1}BB_z\frac{C_z}{C} - \\ - h_3\Phi_{\underset{y}{\circ}}\Phi_{\underset{x}{\circ}}BB_z\frac{C_z}{C} - h_3\Phi_{\underset{y}{\circ}}^2A_zB\frac{C_z}{C} - h_3\Phi_{\underset{y}{\circ}}^k\Phi_{\underset{y}{\circ}}^{k+1}A_zB\frac{C_z}{C} + h_3\Phi_{\underset{y}{\circ}}^2A_zB\frac{C_z}{C}. \end{aligned}$$

Using the inequality $|ab| \leq (a^2+b^2)/2$, we obtain

$$\begin{aligned} J_8 \leq \tfrac{h_3}{2}\left\{\left[\left(\Phi_{\underset{x}{\circ}}^k\right)^2 + \left(\Phi_{\underset{x}{\circ}}^{k+1}\right)^2\right]AB_z\tfrac{C_z}{C} + \left[\left(\Phi_{\underset{x}{\circ}}^k\right)^2 + \left(\Phi_{\underset{y}{\circ}}^{k+1}\right)^2\right]AA_z\tfrac{C_z}{C} + \right. \\ \left. + \left[\left(\Phi_{\underset{y}{\circ}}^k\right)^2 + \left(\Phi_{\underset{x}{\circ}}^{k+1}\right)^2\right]BB_z\tfrac{C_z}{C} + \left[\left(\Phi_{\underset{y}{\circ}}^k\right)^2 + \left(\Phi_{\underset{y}{\circ}}^{k+1}\right)^2\right]A_zB\tfrac{C_z}{C}\right\}. \end{aligned} \tag{19}$$

Supposing that A, B, C enough smooth limit functions and taking into account the expressions (14) -(19), from (13) we get

$$\begin{aligned} \tfrac{1}{2}\left[(AB_z - A_zB) - \left|\tfrac{C_z}{C}\right|\right] \times \left[\left(\Phi_{\underset{x}{\circ}}^k\right)^2 + \left(\Phi_{\underset{x}{\circ}}^{k+1}\right)^2 + \left(\Phi_{\underset{y}{\circ}}^k\right)^2 + \left(\Phi_{\underset{y}{\circ}}^{k+1}\right)^2\right] \leq \\ \leq \tfrac{h_3}{2}K\left[\left(\Phi_{\underset{x}{\circ}}^k\right)^2 + \left(\Phi_{\underset{x}{\circ}}^{k+1}\right)^2 + \left(\Phi_{\underset{y}{\circ}}^k\right)^2 + \left(\Phi_{\underset{y}{\circ}}^{k+1}\right)^2\right] + R_{i,j}^k + c_2h_3^2 \end{aligned} \tag{20}$$

where

$$R^k_{i,j} = \left[\Phi_{\overset{\circ}{x}}\Phi_z\right]_{\overset{\circ}{y}} - \left[\Phi_{\overset{\circ}{y}}\Phi_z\right]_{\overset{\circ}{x}} - \left[\left(\Phi_{\overset{\circ}{x}}A + \Phi_{\overset{\circ}{y}}B\right)\left(-\Phi_{\overset{\circ}{x}}B + \Phi_{\overset{\circ}{y}}A\right)\right]_z +$$

$$+\frac{h_1^2}{2}\left[\Phi_{zx}\Phi_{\overset{\circ}{yx}}\right]_{\bar{x}} - \frac{h_2^2}{2}\left[\Phi_{zy}\Phi_{\overset{\circ}{xy}}\right]_{\bar{y}}.$$

Let

$$\left[(AB_z - A_zB) - \left|\frac{C_z}{C}\right|\right] \geq \alpha > 0, \;\; N_j > 9, \;\; j = 1,2, \quad \mathrm{K}h_3 < \frac{\alpha}{2},$$

i.e. $N_3 > \frac{2\mathrm{K}l}{\alpha}$, because $h_3 = \frac{l}{N_3}$, where α and K is a constant. Then from (20) we have

$$\sum_{\Omega^\varepsilon_h}\left(\Phi^2_{\overset{\circ}{x}} + \Phi^2_{\overset{\circ}{y}}\right)h_1\, h_2\, h_3 \leq \frac{2}{\alpha}\sum_{\Omega^\varepsilon_h} R^k_{i,j} + c_2 h_3^2 \tag{21}$$

Using conditions (7), (8) and inequality $|ab| \leq (a^2 + b^2)/2$, we can transform (21) so as to obtain the desired estimate (12). Thus, the proof of Theorem is completed.

References

1. Romanov, V.: Integral Geometry and Inverse Problems for Hyperbolic Equations. Springer, Verlag (1974)
2. Mukhometov, R.G.: On a problem of integral geometry. Mathematical Problems of Geophysics. **6**, 212–242 (1975) (in Russian)
3. Kabanikhin, S.I., Bakanov, G.B.: On the stability of a finite-difference analogue of a two dimensional problem of integral geometry. Soviet Math.Dokl. **35**, 16–19 (1987)
4. Kabanikhin, S.I., Bakanov, G.B.: Discret analogy of Gel'fand-Levitan metod. Doklady Akademii Nauk. **356**, 157–160 (1997)
5. Bakanov, G.B.: On the stability estimation of differential- difference analogue of the integral geometry problem with a weight function. AIP Conference Proceedings. **1759**, 020067 (2016)
6. Bakanov, G.: On the stability of a differential- difference analogue of a two-dimensional problem of integral geometry. *Filomat 32:3 (2018), 933–938*. doi: 10.2298/FIL1803933B.

Optimization of SQL-queries of the Search Module of the Software System of the Text Document Corpus Processing*

Vladimir Barakhnin[1,2] [0000-0003-3299-0507],
Olga Kozhemyakina[1] [0000-0003-3619-1120], and
Yulia Borzilova[1] [0000-0002-8265-9356]

[1] Federal Research Center for Information and Computational Technologies, 6 Academician Lavrentiev Ave., Novosibirsk, 630090, Russia
[2] Novosibirsk State University, 1 Pirogov Str., Novosibirsk, 630090, Russia
bar@ict.nsc.ru

Abstract The optimization of user's SQL-queries is the important problem that occurs when the software systems of the text document corpus processing are created, and these systems are accessed by external users using the web interface. In the systems discussed in this article, the search module is a separate interface component that interacts with the storage (database) by generating and processing of SQL-queries. The user can perform the complex search queries to the information system, which increase the database load. The optimization of the search module with the implementation of indexes in the database is applied. The experiment which included the iterations on forming the queries to the database of Russian poetic texts with a measurement of the query runtime — with indexes and without ones — is conducted; when the query time decreased, the added indexes were saved and the iteration was repeated. The conclusions about the effectiveness of the usage of indexes in the database are made, within the database the structure of literary texts is organized.

Keywords: Automation of the Analysis of Literary Texts, SQL Queries Optimization, Search Module Design.

Introduction

One of the most difficult tasks is to develop a universal tool for the analysis of texts of literary and business style. As stated in [1], "when the words in a business text are recognized, the most important factor is the knowing of the text (its theme, structure, and most frequent words), the keywords and topic elements are recognized relatively well, and the end of the text is predictable and well recognized. For a literary text, a large "support" falls on the initial (preamble) and middle (plot development) compositional fragments and relates differently to the components of the communicative and semantic

* The work was funded by grant BR05236839 of the Ministry of education and science of the Republic of Kazakhstan; by RFBR, project number 19-37-90019; and in the framework of the topic of state task No. AAAA17-117120670141-7 (No. 0316-2018-0009).

division: with the theme for the preamble, with the dialogue (especially the keywords or a rhyme) for the middle fragment. Thus, we are talking about text structures and analysis procedures, we must take into account the various types of context, in particular, the functional style, compositional structure and rhetorical coherence of the text".

Currently, the text information processing is an actively developing branch of information technologies. The overview of works in this area is available, for example, in [2,3,4,5].

The authors of this article are the part of the Russian-Kazakh team engaged in the design and subsequent development of systems for processing text document corpus: both business (the news) and literary. The concept of these systems is described in detail in [6]. Their design takes into account the requirements for large-scale systems: the modularity, the ability to scale the components and their conditional independence. The designed systems are the set of the components, each of which is formed and used as Docker-containers. The systems's levels: the data processing, the data storage, the visualization, and the management of data processing results. At the data processing level, the text documents (such as the news events) are collected (scrapped) and further processed using an ensemble of machine learning methods, each of which is implemented in the system as a separate Airflow-task. The results are stored in a relational database, and the ElasticSearch tool is used to increase the speed of data search (more than 1 million units). The visualization of statistics, which is obtained as a result of algorithms, is performed using the Plotly plugin. The administration and viewing of processed texts are available via the web interface using the Django framework. The General scheme of interaction of components is organized according to the ETL (extract, transform, load) principle [7].

Currently, the systems that are used for the analysis of news text corpus in order to compare the parameters of texts and mass media in general [6], as well as for analysis of poetic texts [8], have been created.

The end-user works with the system through a web interface, in which the results of text analysis are presented in a convenient way for perception and search. To perform the search, the separate module has been developed that allows to create complex user queries. It should be noted that during the work with a database, that a single user can perform several search queries at the same time; this, in turn, inevitably increases the database load.

The purpose of this work is to find the variants of optimization of the search module to reduce the database load. It should be noted that this study does not solve the problem of reducing the load on the database from the other modules of the system — many module tasks are performed once and do not require special optimization. We will consider the work of the other modules (in terms of accessing the database) to be constant and we will not take it into account in the future.

Review of the experimental researches on the topic

Since the analysis of literary texts is more difficult than the analysis of business texts, we will consider some systems of the analysis of linguistic research that are typical for literary texts in Russian and other languages. The systems of the analysis of literary texts

from the point of view of their functional purpose, the variants for aggregating results, and the availability of a publicly accessible user interface, are presented. We should note that the current review does not take into account the accuracy of determining of the characteristics of literary texts.

The Aoidos system [9] is a tool for the complete analysis of literary texts in Portuguese. At the input, the system receives the works in TEI format and performs the analysis for each work, regardless of other exemplars of the analyzed corpus. The author published a corpus of literary texts in TEI format [10], but there is no mention of public usage of the system itself.

Metricalizer web application [11] which is developed by K. Bobenhausen and B. Americom, allows to perform the automatic analysis of the metric characteristics of literary texts by German authors. The system includes the following components [12]:

1. The subsystem of metric analysis. Displays the fragments in the analyzed poem that are used to determine the poem's metric. Calculates statistics.
2. The subsystem of the analysis of text corpus. Includes the analysis of texts by accentuation and rhyming. The statistics are maintained for individual metric forms. The "Freiburger Anthologie" and "Textgrid" text corpus are used.
3. The advanced features of the system for registered users: the storage of the individual works and the creation of XML documents based on the results of the analysis.
4. The phonetic analysis of words. Allows the parse a single word in German in X-SAMPA and IPA formats [13].

The SPARSAR system described in R. Delmonte's work [14] assumes an automatic complex analysis of literary texts in order to study their style; SPARSAR [15] analyzes each poem at different levels. Then all this data is used to create a marked-up version of a poem that can be read by the machine with appropriate expressiveness. As for the search module, it is implemented using standard tools of the Wordpress platform [16], which allows to search for standard articles in the system without the possibility of the creation of the unique queries.

As for Russian literary texts corpus analysis, the project "Automated linguistic and psychological analysis of Russian poetic texts" or "The tower of Babel" can be marked. "The tower of Babel" is the name of an international Internet project which is dedicated to comparative historical linguistics. The information system includes the following components [17]:

1. The databases of etymologies (origin of words): global, Nostratic, Indo-European, Altaic, Uralic, etc. Each database is available for viewing, searching (for all users), and editing (for authorized users).
2. The database "Thematic classification and distribution of folklore and mythological motifs by area" by Yu. E. Berezkin.
3. The database "The quantitative-implementation grammatical dictionary of the modern Mongolian language" by S. A. Krylov.
4. The dictionaries of Russian language (Ozhegov, Zaliznyak, The etymological dictionary of Fasmer, Reference book on the metalanguage of Russian grammarians of the first half of the XX century by S. A. Krylov).

5. The STARLING database management tool, which is used to work with existing databases (composing and executing the complex search queries, adding new records, organizing links). The support for hieroglyphs and various text encodings is provided.
6. The morphological analyzer. It provides an opportunity to analyze any Russian word and to get its full accentuated paradigm.

A team of other authors [18] developed an open network resource [19], which is represented by the components: a problem-oriented "Thesaurus on poetology" and a "Block of analysis and specification" of text objects; the system is used to perform the metrorhythmic marking and the identification of a verse meter. In the section "analysis and specification" there are two sets of tasks: the specification of terminological articles of thesaurus and the specification of a literary text. The complex structure includes the groups of problem solutions:

– the metrorhythmic markup of a text;
– the filling of the specification fields of a work;
– the identification of the meter.

A summary of the considered systems is shown in table 1. A public resource is the user interface that allows to use the system in question for its intended purpose.

Table 1. A summary of the reviewed systems

The name of the system	Multilevel analysis of literary texts	User interface	Aggregation of the results	Search by characteristics
Aoidos	+	–	–	–
Metricalizer	+	+	+	–
SPARSAR	+	+	+	+
"The tower of Babel"	+	+	+	+
Resource wikipoetics.ru	+	+	–	–

The "results aggregation" column shows whether there is a visible subsystem for displaying the results of the considered system for several exemplars, in other words, whether the system saves the results of the previous iteration (in the form of metadata or in another form). "The search by characteristics" implies the presence of the user interface for compiling the search queries by characteristics in the considered system.

Search module in the system of complex analysis of literary texts

One of the user interface components of the system for complex analysis of literary texts is the search module, whose task is to extract the existing characteristics in the

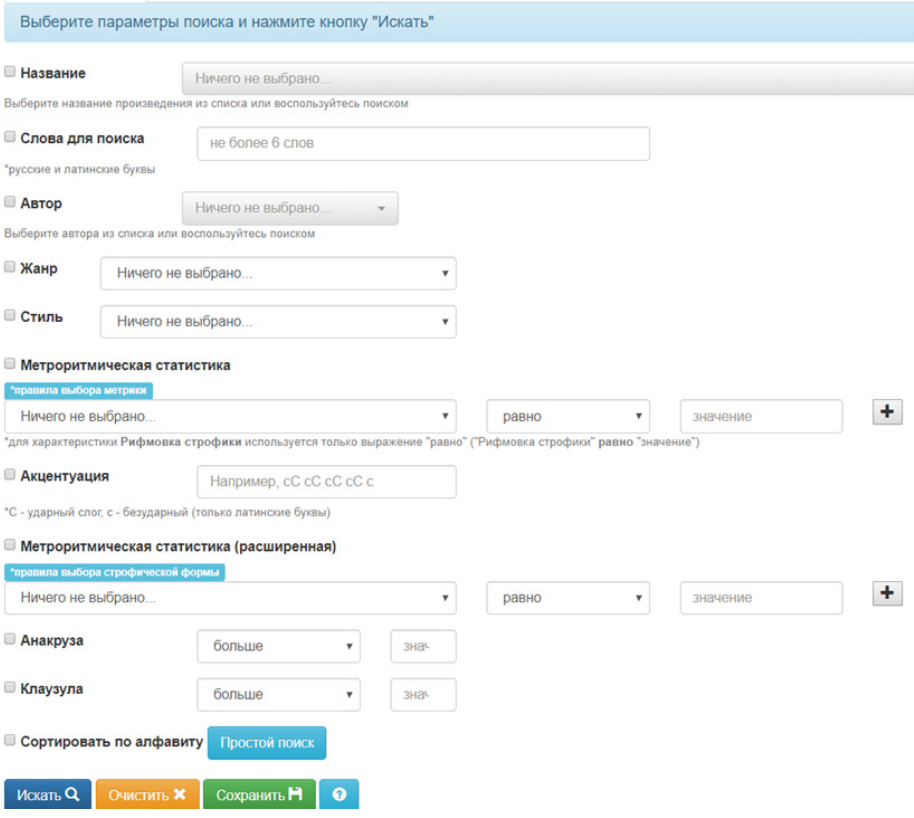

Figure 1. Search module interface in the information system

information system and to present them in a user-friendly form. The interface fragment is shown in fig. 1.

The search process includes the following steps (fig. 2):

1. The filling of the search form by the system user. The search is divided into simple, which includes the search for authors, their works, the main metrorhythmic characteristics, and advanced search, which involves the search on those parts of the work, as anacrusa (the initial part of the verse) and clause (the final part of the verse); the characteristics are obtained at the stage of structural analysis.
2. SQL query generation and sending it to the database. The system uses a PostgreSQL database (version 9.4 at the moment of development of the information system).
3. SQL query processing with a selection of data that match the specified search criteria; the forming of an array of results that are sent to the clientside.
4. Displaying results using the web interface (fig. 3).

The script is used to export the result that converts data from the web interface to a CSV format that can be processed with a separator (commas).

The search is performed according to a number of characteristics:

– words from the text or from title of the work;
– metrorhythmic statistics;
– genre;
– accentuation mask;
– anacruz;
– clause.

These characteristics are conditionally divided into statistical and informative ones.

The informative characteristics include the words and phrases from the text, and genre. In other words, these are text characteristics that take up more resources (time and database server capacity) than statistical characteristics.

Statistical characteristics are determined within the metrorhythmic analysis module. It is assumed that the search for them will take up a significant part of the general queries generated within the system of complex analysis of literary texts.

At the user interface level, there are no significant restrictions on combinations of search characteristics, what allows the user to form the complex composite queries that consume server resources; the optimization of such queries will increase the database productivity (a productivity in this context means the number of operations which are performed per unit of time).

The structure of the database

Within the framework of the developed information system, it is assumed that more than one work is used simultaneously — the objects of the subject area are represented as the entities and the relationships in accordance with the laws:

1. One author can write several works. In this case, a situation is allowed when one work can have more than one author.

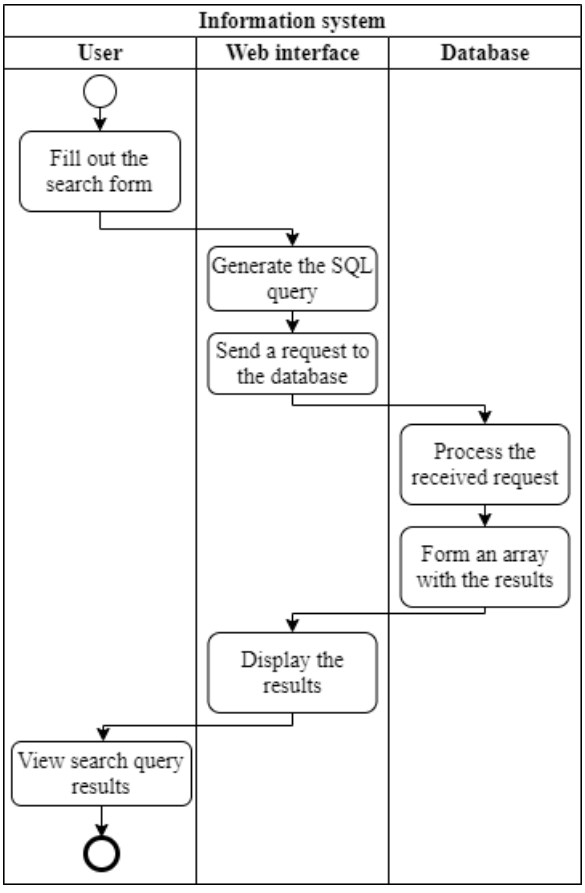

Figure 2. Search module working process at workflow diagram

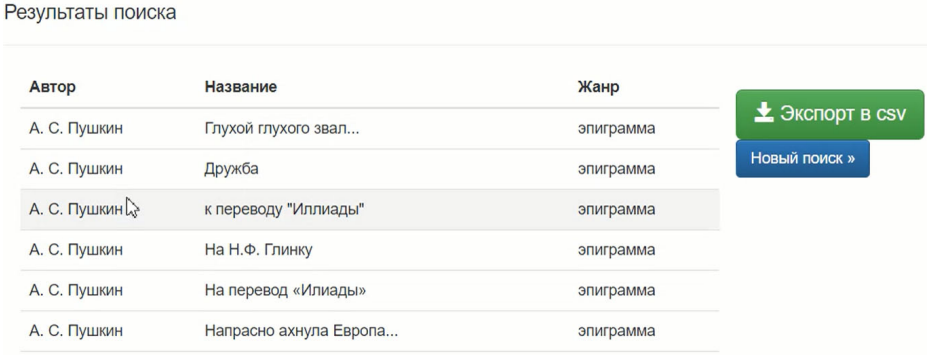

Figure 3. Table with search results in the user interface

2. The work can be produced under several editions, which may be the same by year of publication.
3. The work belongs to only one genre.
4. The work can have a number of words and phrases, however, their repetition is allowed in different works.
5. The work has a number of defined metrorhythmic characteristics (meter, rhyme, stanzas).

The database schema was constructed on the base of the selected patterns and subject area, the tables and key fields of which are shown in fig. 4.

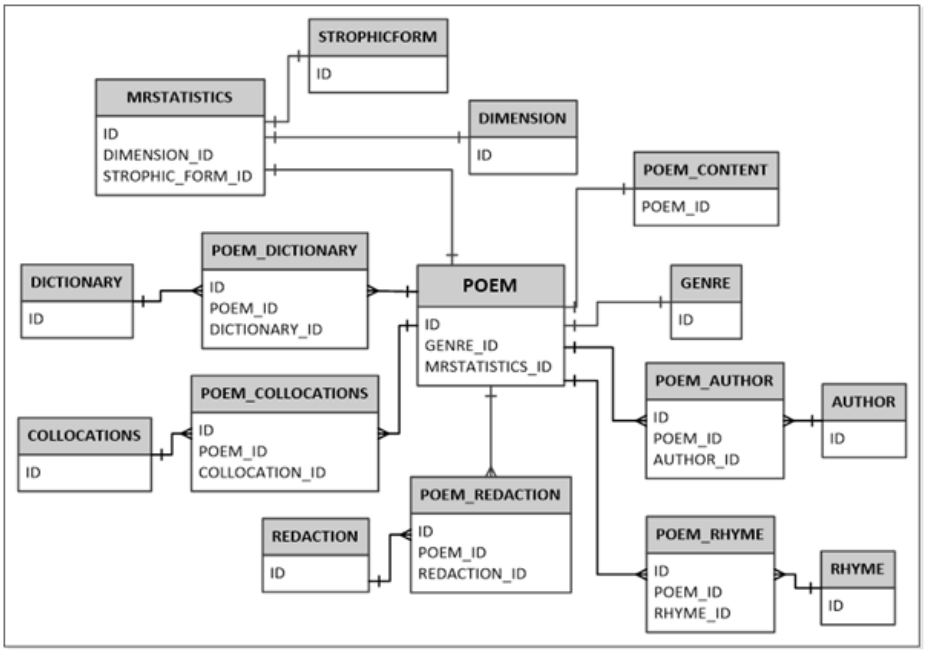

Figure 4. Database schema

We should note that the table `POEM` aggregates all works and authors that are used for the system of complex analysis of literary texts. The tables `POEM_CONTENT`, `POEM_DICTIONARY`, `POEM_COLLOCATIONS` are divided by the authors, for example, the table `POEM_CONTENT_1` contains the text of the author's works only with the *ID*=1.

The following is an example of an SQL-query that displays the author's full name and the titles of all his works.

```
SELECT
  a."ID" as AUTHOR_ID, a."LASTNAME", a."FIRSTNAME",
  a."MIDDLENAME", p."NAME"
```

```
  as POEM_NAME,
  p."ADDITIONAL_NAME" as AD_NAME
FROM
  "AUTHOR" a
LEFT JOIN
  "POEM" p ON p."AUTHOR_ID" = a."ID"
ORDER BY p."ID" ASC;
```

The variants of the optimization of work with the database

Let's list the standard variants of the optimization of work with the database [20]:

- the elimination of data redundancy with the help of the normalization of database tables;
- the definition of the data type of fields based on the appropriate data type, i.e. the setting of smallest data type for the field;
- the definition of primary and secondary keys only on numeric fields, or on datetime fields;
- the periodic compression of the database.

One of the additional methods of speeding up the execution of SQL queries is also the adding indexes to the database; the indexes are recommended to be used for sort and merge fields. The system uses a PostgreSQL database, which allows us to use the following types of indexes:

- B-tree — can handle equality and range queries on data that can be sorted into some ordering.
- Hash — can only handle simple equality comparisons; hash indexes might need to be rebuilt with *REINDEX* after a database crash if there were unwritten changes. Also, changes to hash indexes are not replicated over streaming or file-based replication after the initial base backup, so they give wrong answers to queries that subsequently use them. For these reasons, hash index use is presently discouraged.
- GiST — infrastructure within which many different indexing strategies can be implemented; can be used vary depending on the indexing strategy (the opera-tor class).
- SP-GiST — permits implementation of a wide range of different non-balanced disk-based data structures, such as quadtrees, k-d trees, and radix trees (tries).
- GIN — inverted indexes which can handle values that contain more than one key, for example, arrays.

Experiments

The experiment consisted of a series of iterative queries to the database, each of which uses a new version of indexes; the time that was spent on the generated SQL query was measured. During the initial iteration, the time spent on processing SQL queries without using indexes was measured.

The indexes were added according to the following principles:

– for integer fields, the b-tree and hash indexes were used alternately; an index was selected where the processing time was less when executing an SQL query;
– for text fields (with varchar, text data types), GIST, SP-GiST, and GIN indexes were used with a class of trigram search operators.

The corpus of A. S. Pushkin's and A. K. Tolstoy's works was loaded to the DB; the main tables with the texts of works and their metadata contain data with a volume of more than 900 rows; at maximum occupancy, the number of records (characteristics of each individual work) can increase by more than 5 times.

The experiment was performed for the next search queries:

– "Select all authors and their works (only titles)"; the request is made with the initialization of the search module — the list of authors and works is loaded every time when the browser page is loaded.
– "Select authors with a specific genre and a minimum number of rows"; the query includes a search for both statistical characteristics (number of lines) and genre-style characteristics; we assume that the results of the experiment for the selected query type are applicable to the rest of the queries in the form "select authors with a specific genre-style and structural characteristic".
– "Search by accentuation mask"; the query is separated into a separate category, since the search by accentuation mask is used in a number of text analysis tasks and can be performed quite often.
– "Search by words from a work"; this type of query includes a search for both the words from the text of the work and its title.

  The results are presented in Tables 2–5. The rows are sorted in descending order of query execution time (the "Total query runtime" column). We do not take into account the error that may occur when the database is running, for example, due to an extraneous load on the server when the experiment was conducted.

Table 2. Query "Select all authors and titles of their poems"

Index name	Total query runtime, msec	Rows affected count
without indexes	437	948
GIN	360	
GIST	350	
Hash	323	
SP-GIST	323	
B-tree	314	

The usage of the indexes that only apply to integer characteristics in the query "Works of a certain genre with a limit on the number of lines" is due to the structure of tables in the database: the search doesn't use the genre name (*varchar* data type), but its ID in an external table (*smallint* data type).

Table 3. Query “Select authors with a specific genre and a minimum number of rows”

Index name	Total query runtime, msec	Rows affected count
without indexes	197	1
B-tree	140	
Hash	99	
GIST, GIN, SP-GIST	don’t used	

Table 4. Query “Search by accentuation mask”

Index name	Total query runtime, msec	Rows affected count
without indexes	198	0
Hash	132	
GIN	111	
GIST	107	
B-tree	100	
SP-GIST	94	

Table 5. Query “Search by words from the name and text”

Index name	Total query runtime, msec	Rows affected count
without indexes	228	95
Hash	201	
GIST	193	
GIN	172	
SP-GIST	164	
B-tree	160/215	

The runtime of the query "Search by words from the name and text" differs due to the used operator classes: the result of 139 msec was obtained using the `varchar_ops` class; the result of 184 msec was obtained using the `text_pattern_ops` class.

The results of the experiment showed a noticeable acceleration of processing SQL queries when adding indexes — in some cases, the processing time was reduced by half. If only integer variables were used in the search query, the adding of hash and b-tree indexes in all cases reduced the query execution time; it should be noted that the usage of hash indexes is not recommended due to their relative unreliability. On the other hand, the adding indexes to *varchar* variables did not always improve results: the reason could be either the used operator classes (as in the case of the b-tree index in the "Search by words from name and text" query), or the specifics of the indexes used for *varchar* variables.

Conclusions

The adding of indexes has proved to be a successful method for acceleration of the processing of user queries to the search module. The results of the experiment showed the acceleration of SQL query processing from 15 to 50% (depending on the class of the search query). In addition to the standard optimization variants mentioned in this article, the following recommendations for construction of indexes can be identified as part of a relational database to reduce the time for processing queries:

- use indexes for integer fields; it is not recommended to use hash indexes; however, it's better to consider the structure of the constructed database — in cases where it is possible to use the integer identifiers.
- do not add indexes for fields in tables that have a relatively small number of records (and will not increase in the future) — in this case, the adding of indexes may, on the contrary, increase the query processing.
- use a class of operators to work with text values when the non-numeric indexes are used, such as trigram search operators for GIST and GIN indexes.
- take into account the capabilities of the database itself: some older versions do not support the modern index types.

In the future, we can make a number of modifications, such as the creation of stored procedures for SQL queries or views for them, the results of which are displayed in the interface independently of the user's actions.

The query optimization will reduce the database load on the one hand, and reduce the system response time for the end-user on the other.

References

1. Bolshakova E.I., Klishinskii E.S., Lande D.V., Noskov A.A., Peskova O.V., Yagunova E.V.: Automatic natural language text processing and computer linguistics. Moscow: MIEM (2011). [In Russian]

2. Pang B., Lee L., Vaithyanathan S.: Thumbs up? Sentiment classification using machine learning techniques. In: Proceedings of the 2002 Conference on Empirical Methods in Natural Language Processing 2002, EMNLP, pp. 79–86. ArXiv preprint cs/0205070, Philadelphia (2002). https://doi.org/10.3115/1118693.1118704
3. Choi Y., Cardie Cl., Riloff E., Patwardhan S.: Identifying sources of opinions with conditional random fields and extraction patterns. In: Proceedings of the Conference on Human Language Technology and Empirical Methods in Natural Language Processing 2005, HLT, pp. 355–362. Association for Computational Linguistics, Vancouver (2005).
4. Manning C.D.: Part-of-speech tagging from 97% to 100%: Is it time for some linguistics? In: Proceedings of the 12th International conference on intelligent text processing and computational linguistics 2011, CICLing, pp. 171–189. Springer, Berlin, Heidelberg (2011).
5. Mukhamedyev R.I., Kuchin Y., Kosyakov D., Murzakhmetov S., Symagulov A., Yakunin K.: Assessment of the Dynamics of Publication Activity in the Field of Natural Language Processing and Deep Learning. In: Alexandrov D., Boukhanovsky A., Chugunov A., Kabanov Y., Koltsova O., Musabirov I. (eds.) Digital Transformation and Global Society 2019, DTGS, vol 1038, pp. 744–753. Springer, Cham (2019). `https://doi.org/10.1007/978-3-030-37858-5_63`
6. Barakhnin V.B., Kozhemyakina O.Yu., Mukhamediev R.I., Borzilova Yu.S., Yakunin K.O.: The design of the structure of the software system for processing text document corpus. Business Informatics, **13**(4), 60–72 (2019). https://doi.org/10.17323/1998-0663.2019.4.60.72
7. Loshin, D.: ETL (Extract, Transform, Load). Business Intelligence, 2nd edn., Morgan Kaufmann (2012).
8. Barakhnin, V., Kozhemyakina, O., Kuznetsova I.: Development and Implementation of the Algorithm for Automatic Analysis of Metrorhythmic Characteristics of Russian Poetic Texts. CEUR Workshop Proceedings, **2523**, 290–298 (2019).
9. Mittmann A.: Automatic spanning of verses in Portuguese. Federal University of Santa Catarina, Technological Center, Florianópolis (2016). [In Portugese]
10. Adiel-mittmann GitHub, `https://github.com/adiel-mittmann/poemas`. Last accessed 10 Jun 2020.
11. The project Metricalizer, `https://metricalizer.de`. Last accessed 10 Jun 2020. [In German]
12. Bobenhausen K., Hammerich B.: Literature metrics, linguistic metrics and German algorithmic metrics brought into play in the Metricalizer program. Languages, **199**, 67–87 (2015). https://doi.org/10.3917/lang.199.0067 [In French]
13. SAMPA — computer readable phonetic alphabet, `https://www.phon.ucl.ac.uk/home/sampa`. Last accessed 10 Jun 2020.
14. Delmonte R.: Computing poetry style. CEUR Workshop Proceedings, **1096**, 148–155 (2013).
15. The project SPARSAR: An Expressive Poetry Reader, `sparsar.wordpress.com`. Last accessed 10 Jun 2020.
16. The project WordPress, `https://wordpress.com/`. Last accessed 10 Jun 2020.
17. The project "The Tower of Babel", `http://starling.rinet.ru`. Last accessed 10 Jun 2020.
18. Boikov B. N., Karyaev M. S., Sokolov V. A., Pilschikov A. I.: On an Automatic Procedure for the Specification of a Poetic Text for an Open Information-Analytical System. CEUR Workshop Proceedings, **1536**, 144–151 (2015). [In Russian]
19. The project Wikipoetic, `http://wikipoetics.ru/`. Last accessed 10 Jun 2020. [In Russian]
20. Shustova L., Tarakanov O.: Databases. INFRA-M Publishing House, Moscow (2016). [In Russian]

Two Models of Surface Waves Propagation Generated by an Underwater Landslide Movement

Sofya Beizel[1] [0000−0002−0406−1631],
Yuri Zakharov[1,2] [0000−0002−2895−1428], and
Anton Zimin[2] [0000−0002−6949−5107]

[1] Federal Research Center for Information and Computational Technologies, Novosibirsk, Russia
[2] Kemerovo State University, Kemerovo, Russia

Abstract The goal of the paper is to determine possible differences in generation and advance of surface waves created by the motion of solid and liquid landslides on the shelving. The goals are researched by means of numerical computations of shallow water nonlinear equations and Navier–Stokes equations. The computations for two models of different landslide configurations have been performed. The principal wave according to its characteristic properties (amplitude, length) is quantitatively resembling in both models as well as wave propagation velocity. It was demonstrated that a definite configuration of liquid and solid landslides create waves which can be very different at shallow water due to decay process of a liquid landslide under the action of gravity.

Keywords: Submarine landslide, Numerical modelling, Nonlinear shallow water equations, Three-component model.

Introduction

A submarine landslide is a large mass of soil and sedimentary rock which moves on the shelving by gravity. Such movement creates waves on the water surface which can be of serious hazard to population and facilities on the coastal area.

Laboratory researches are often performed in order to study generation and advance of long surface waves created by landslide movement [1,2,3,4,5]. However, such studies demand significant financial investments and preparation time. Thus, the application of mathematical simulation of the surface wave generation due to submarine landslide movement proves its relevance.

There are several techniques of modeling of submarine landslide movement and surface wave generation. It is conventional to represent a landslide as a solid body moving on the flat slope [6,7]. It is worthy to note that in laboratory experiment a landslide is often rather a solid body than a loose granular mass in order to make a test and its preparation simpler. Also, in this case it is possible to determine and describe the movement of a solid body on the sloping bottom during the test. That is, such experiment can provide very accurate data on changes of bottom bathymetry that significantly increases the convenience of checking the results of computational models. In case of a solid landslide, different versions of shallow water models and

models based on Boussinesq equationas [8,9,10,11] or a complete system of Navier–Stokes equations are applied in order to perform modeling of surface wave generation and advance [12,13,14,15].

The representation of a landslide as a solid body is often a simplification of a physical phenomenon. In order to perform modeling of real environment, it is necessary to take into consideration the irregularities of the bottom slope and the possibility of a landslide deformation. For example, in papers [16,17], the deformability of a modelled landslide while moving on the uneven surface was obtained by its representation by way of several solid units connected one by one with flexible links. Simulation models take this effect into account by either applying the model of a quasi-deformed landslide when its surface shape changes as a deformed body but motion dynamics corresponds to a solid body or by representation of a landslide as a fluid flow different from water. In case of a liquid landslide it usually refers to multiphase or multicomponent models where one constituent models liquid landslide motion, and others model motion of water and air. The differences of such models consist in the chosen rheological model for specifying landslide movement. For example, there are viscous model [12,13] and different versions of non-Newtonian fluids [14,15,18]. A detailed review of existing numerical studies of this phenomenon is presented in the paper [19].

This paper considers two significantly different models of a submarine landslide. In the first model, a landslide is considered as a quasi-deformed solid body, where generation and advance of surface waves are calculated based on a classical non-linear model of shallow water. In the second model a landslide is considered as deformed and liquid, and its motion and wave processes are described by the system of differential equations of ternary viscous incompressible fluid, meanwhile a landslide is regarded as much more dense and viscous component. As the existent landslides are mostly either solid (consisting of massive rocks moving as one unit) or liquid (sediments and silt on the shelving), the goal of the present paper is to distinguish differences in surface wave generation by different types of landslides.

Mathematical models

Here we will consider two models of submarine landslide motion and the dynamics of surface waves generated by it.

In the first model, a landslide is considered as a quasi-deformed body [20,21], where derivation equations of its motion demands breaking up its volume into infinite number of units; and the force causing its motion on the slope is equal to the sum of gravity, buoyancy, friction and resistance of water affecting infinitely small elementary volumes. In this model, the configuration of landslide surface changes due to bottom irregularities on its way (as in a deformed body), but momentary horizontal components are similar at any point of a landslide (as in a solid body).

The motion of a quasi-deformed submarine landslide is determined by the following system of four ordinary differential equations:

$$\frac{dv_\alpha}{dt} = \frac{R_\alpha}{2} + \frac{\sqrt{g_{\alpha\alpha}}}{(\gamma + C_w)\, V} \times \Big[(\gamma - 1)\, g\, (I_{1,\alpha} - \sigma_\alpha C_{fr} I_2) - \\ -\sigma_\alpha \left(\gamma C_{fr} \left(u^2 I_{3,11} + 2uv I_{3,12} + v^2 I_{3,22}\right) + \frac{C_d}{2} \Pi v_c^2\right)\Big], \tag{1}$$

$$\frac{dx_c}{dt} = u, \qquad \frac{dy_c}{dt} = v, \tag{2}$$

where $\alpha = 1, 2$, g – free fall acceleration, $\gamma = \rho_{sl}/\rho_w > 1$, ρ_w – water density, ρ_{sl} – landslide density, C_w, C_{fr}, C_d – coefficients of added-mass, sliding friction and hydrodynamic water resistance, respectively, $C_{fr} = tg\theta_*$, θ_* – friction angle, $V = const$ – landslide volume,

$$\sigma_\alpha = \frac{v_\alpha}{\sqrt{g_{\alpha\alpha}} v_c}, \qquad R_\alpha = \frac{\partial g_{11}}{\partial x^\alpha} u^2 + 2\frac{\partial g_{12}}{\partial x^\alpha} uv + \frac{\partial g_{22}}{\partial x^\alpha} v^2,$$

$$I_{1,\alpha} = -\iint_{\Omega_t} \frac{h_{sl}(x,y,t)}{\sqrt{g_{\alpha\alpha}(x,y)}} \frac{\partial h_{bt}}{\partial x^\alpha}(x,y) dxdy, \qquad I_2 = \iint_{\Omega_t} \frac{h_{sl}(x,y,t)}{\sqrt{G(x,y)}} dxdy > 0,$$

$$I_{3,\alpha\beta} = \iint_{\Omega_t} \frac{h_{sl}(x,y,t)}{\sqrt{G(x,y)}} \frac{\partial^2 h_{bt}}{\partial x^\alpha \partial x^\beta}(x,y) dxdy, \quad \alpha, \beta = 1, 2, \;\; G = g_{11} g_{22} - g_{12}^2 \geq 1,$$

Ω_t – orthogonal projection of three dimensional area occupied by a landslide mass onto the subspace $z = 0$, and in order to reduce the note we use new nomenclature $x^1 = x, x^2 = y$ for rectangular coordinates of the frame of reference O_{xyz}, axis O_z is directed upward vertically, and the coordinate subspace O_{xy} coincides with still water surface.

It is assumed that a landslide limited from the top by the surface $z = h_{bt}(x, y) + h_{sl}(x, y, t)$ where $h_{sl}(x, y, t) > 0$ begins its motion from the state of rest and it slides without disconnecting from the specified curved surface of the submarine slope $z = h_{bt}(x, y) < 0$ which geometrical properties are determined by the components of metric tensor:

$$g_{11} = 1 + \left(\frac{\partial h_{bt}}{\partial x}\right)^2, g_{12} = g_{21} = \frac{\partial h_{bt}}{\partial x}\frac{\partial h_{bt}}{\partial y}, g_{22} = 1 + \left(\frac{\partial h_{bt}}{\partial y}\right)^2.$$

The equations of quasi-deformed landslide motion (1), (2) are based on the premise that at any specific time its position is determined by the point $\mathbf{x_c}(t) = (x_c(t), y_c(t), z_c(t))$ sliding on the bottom, herein $(x_c(t), y_c(t)) \epsilon \Omega_t, z_c(t) = h_{bt}(x_c(t), y_c(t))$. In the moving coordinate system the beginning of which coincides with the point $\mathbf{x_c}(t)$ the first two covariant components v_α of velocity vector $\mathbf{v_c}$ of this point are determined by the solution of nonlinear equations (1). Cartesian components u, v of the vector $\mathbf{v_c}$, and its value is determined from the correlations:

$$u = \frac{g_{22}v_1 - g_{12}v_2}{G}, v = \frac{-g_{21}v_1 + g_{11}v_2}{G}, v_c = |\mathbf{v_c}| = \sqrt{g_{11}u^2 + 2g_{12}uv + g_{22}v^2}.$$

The processes of generation and advance of surface waves are calculated by means of classical nonlinear model of shallow water.

In the second model, a landslide is considered as deformed and it proceeds as some liquid with density and viscosity different from water (a liquid landslide). Thus, we observe a flow stream of three-component viscous incompressible fluid where each component (a liquid landslide, water, air) is viscous incompressible fluid with its own values of viscosity and density [22,23]. Mass diffusion between these components is possible. The motion of such medium is described by nonstationary system of Navier-stokes equations with variable density and viscosity, and the shift of medium components – by equations of convective diffusion. The equations depending upon the component concentration are applied to determine viscosity and density. In all. The system is as follows as:

$$\begin{cases} \dfrac{d\left(\rho\overline{U}\right)}{dt} = -\nabla p + div(\mu\mathbf{D}) + \rho\overline{F}, \\ div\overline{U} = 0, \\ \dfrac{dC_1}{dt} = D_{12}\Delta C_1, \\ \dfrac{dC_3}{dt} = D_{23}\Delta C_3, \\ C_2 = 1 - C_1 - C_3, \\ \mu = \dfrac{\mu_1\mu_2\mu_3}{\mu_2\mu_3C_1 + \mu_1\mu_3C_2 + \mu_1\mu_2C_3}, \\ \rho = \rho_1C_1 + \rho_2C_2 + \rho_3C_3. \end{cases} \tag{3}$$

where $\overline{U} = (u_1, u_2, u_3)$ – velocity vector of the mix in the point $\overline{x} = (x_1, x_2, x_3)$ and time point t, $\mu(\overline{x}, t)$ – dynamic viscosity, $\rho(\overline{x}, t)$ – density, $C_1(\overline{x}, t)$, $C_2(\overline{x}, t)$, $C_3(\overline{x}, t)$ – volumetric concentrations of components with constant densities ρ_1, ρ_2, ρ_3 and viscosities μ_1, μ_2, μ_3, $\overline{f} = (f_1, f_2, f_3)$ – volume force vector, p – pressure, $\mathbf{D}$ – tensor of strain rate which components are equal to $\tau_{ij} = \frac{du_i}{dx_j} + \frac{du_j}{dx_i}$, $D_{12} = const$ – coefficient of diffusion between first and second components, $D_{23} = const$ – coefficient of diffusion between second and third components.

Solution methods

The finite-difference two-stage MacCormack scheme on the uniform grid is applied for computational solutions of nonlinear equations of shallow water [20]. The ordinary differential equations describing solid landslide motion are approximated by application of Euler method.

The method of finite differences without selecting specifications for determination of the interface of components is applied for implementation of the three-component

model. A rectangular staggered mesh is applied for digitalization. The Navier-Stokes equations system (3) is approximated by splitting scheme by physical factors taking into account variable density. Predictor-corrector methods are applied for solution of equations of convective diffusion. The detailed description of this numerical algorithm is represented in the article [22].

Wave generation by landslide motion on the shelving

In order to analyze the differences between two models we consider the model problem of landslide motion on the slope bottom which generates waves on the water surface. The landslide configuration at the start time is determined by the following formula [20]:

$$h_{sl}(x,t) = T\frac{[1+tanh\left(2\left(x-x_1(t)\right)\right)/p]\,[1-tanh\left(2\left(x-x_2(t)\right)\right)/p]}{[1+tanh(1)]\,[1-tanh(-1)]} \tag{4}$$

where $x_1(t) = x_c(t) - p/2, x_2(t) = x_c(t) + p/2, x_c(0) = 10,000, T = 500, p = 2,500$.

Hence, the length of a landslide is $2,500$ m, the height is 500 m, the initial longitudinal center of a landslide is $10,000$. A quasi-deformed landslide also has the following parameters: friction angle – 2 degrees, relative density of a landslide is 1.95.

The scheme and dimensions of the solution region and the initial position of a landslide are represented at Fig. 1.

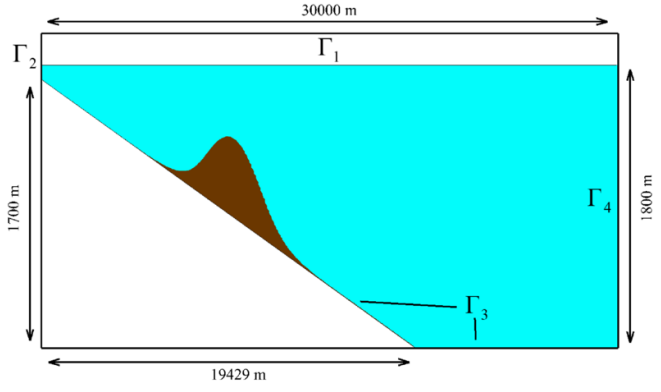

Figure 1. Geometry of the region and the initial position of a landslide, in meters

The medium component in three-component model applies the following values of densities and viscosities:

$$\rho_1 = 1\ \frac{kg}{m^3}, \rho_2 = 1,000\ \frac{kg}{m^3}, \rho_3 = 1,950\ \frac{kg}{m^3},$$
$$\mu_1 = 10^{-5}\ \frac{kg}{m\cdot s}, \mu_2 = 10^{-3}\ \frac{kg}{m\cdot s}, \mu_3 = 10\ \frac{kg}{m\cdot s}.$$

Boundary conditions at the edge of the solution region (Fig. 1) for the system (3) are defined as follows as:

Γ_1 – boundary of free discharge where atmospheric pressure has impact

$$\left.\frac{\partial u_1}{\partial y}\right|_{\Gamma_1} = 0,\ \left.\frac{\partial u_2}{\partial y}\right|_{\Gamma_1} = 0,\ \left.p\right|_{\Gamma_1} = 101,325,\ \left.\frac{\partial C_1}{\partial y}\right|_{\Gamma_1} = 0,\ \left.\frac{\partial C_3}{\partial y}\right|_{\Gamma_1} = 0.$$

Γ_2 – solid boundary where there is adhesion condition

$$\left.u_1\right|_{\Gamma_2} = 0,\ \left.u_2\right|_{\Gamma_2} = 0,\ \left.\frac{\partial p}{\partial \bar{n}}\right|_{\Gamma_2} = 0,\ \left.\frac{\partial C_1}{\partial \bar{n}}\right|_{\Gamma_2} = 0,\ \left.\frac{\partial C_3}{\partial \bar{n}}\right|_{\Gamma_2} = 0.$$

Γ_3 – solid boundary where slipping condition is possible

$$\left.\frac{\partial \bar{U}}{\partial \bar{n}}\right|_{\Gamma_3} = 0,\ \left.\frac{\partial \bar{U}}{\partial \bar{\tau}}\right|_{\Gamma_3} = \alpha \bar{U},\ \left.\frac{\partial p}{\partial \bar{n}}\right|_{\Gamma_3} = 0,\ \left.\frac{\partial C_1}{\partial \bar{n}}\right|_{\Gamma_3} = 0,\ \left.\frac{\partial C_3}{\partial \bar{n}}\right|_{\Gamma_3} = 0.$$

Γ_4 – boundary of free discharge

$$\left.\frac{\partial u_1}{\partial x}\right|_{\Gamma_4} = 0,\ \left.\frac{\partial u_2}{\partial x}\right|_{\Gamma_4} = 0,\ \left.\frac{\partial p}{\partial x}\right|_{\Gamma_4} = 0,\ \left.\frac{\partial C_1}{\partial x}\right|_{\Gamma_4} = 0,\ \left.\frac{\partial C_3}{\partial x}\right|_{\Gamma_4} = 0.$$

For nonlinear model of shallow water we set the condition of return at the left boundary and the condition of clear passage of waves – at the right boundary.

The tide gauges were set at every $5,000$ meters from point 0 to point $30,000$ meters in order to evaluate the level of fluid surface.

Fig. 2 represents the change of configuration of liquid and solid landslides and surface waves induced by them at time points 100, 200 and 300 seconds.

Fig. 3 shows marigrams of fluid surface at different points of the region for aforesaid calculations for two models.

Correspondence of wave generation to the landslide configuration

As it is observed at Fig. 2, a landslide splits into two parts at the start of motion. On part of a landslide advances upward the slope and can reach the coast, the other part moves down ward the slope. That is why, it is important to define the impact of the initial landslide configuration on properties and motion velocity of the wave. Let us consider three initial configurations of a landslide.

We label the landslide which initial configuration (4) was described above with "O1", and with "O2" we label the landslide which configuration is described by the transformation of formula (4):

$$h_{sl}(x,t) = T\frac{\left[1 + tanh\left(2\left(x - x_1(t)\right)\right)/p_1\right]\left[1 - tanh\left(2\left(x - x_2(t)\right)\right)/p_2\right]}{\left[1 + tanh(1)\right]\left[1 - tanh(-1)\right]} \qquad (5)$$

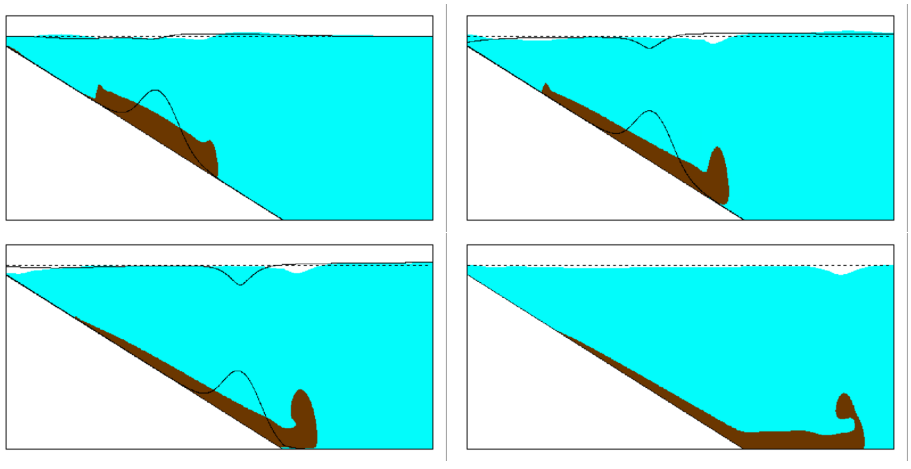

Figure 2. Landslide configurations at time points 100, 200 and 300 seconds

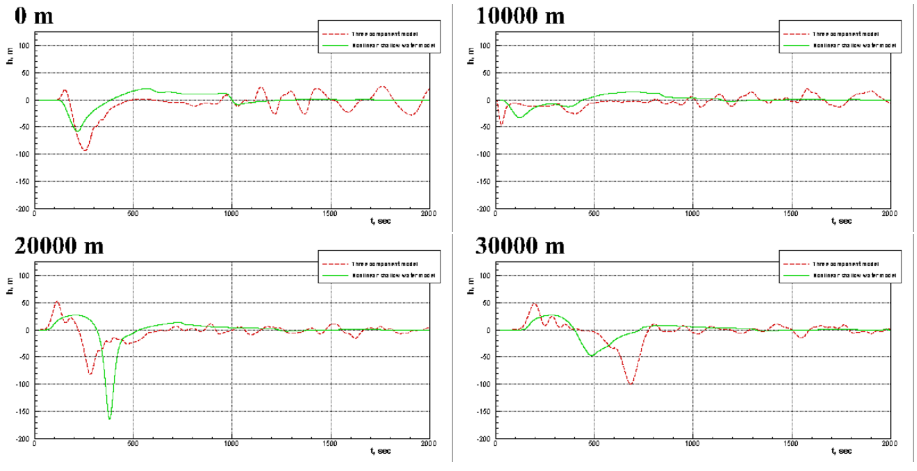

Figure 3. Marigrams

where $x_1(t) = x_c(t) - p/2, x_2(t) = x_c(t) + p/2, x_c(0) = 10,000, T = 300, p = 3,000$, $p_1 = 4,500$, $p_2 = 1,000$ (Fig. 4).

A third landslide "O3" is described by formula (4), where $T = 325$, $p = 5,500$ (Fig. 4).

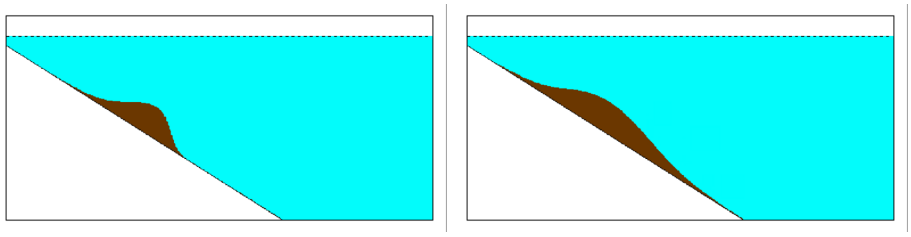

Figure 4. Landslide configuration O2 and O3

Fig. 5, 6 show the transformation of landslide configurations O1 –O3 at time points 100, 300 and 500 seconds for each configuration for two models where crosshatched region is a liquid landslide and unbroken line is a solid landslide.

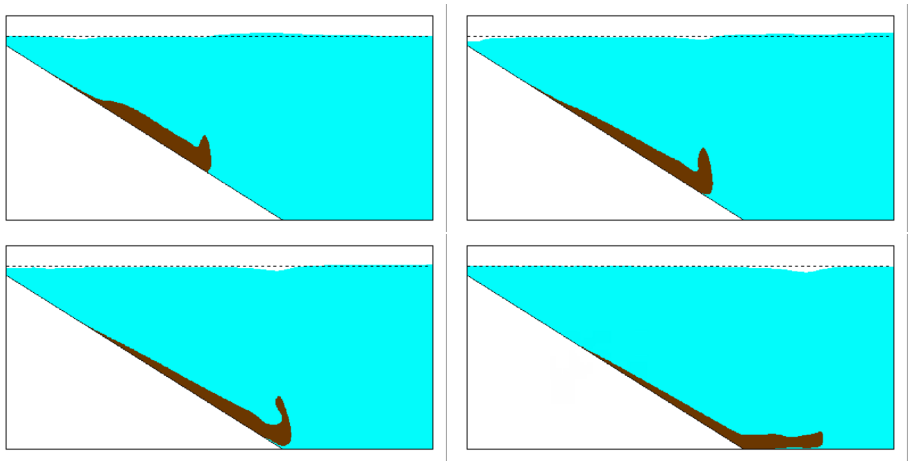

Figure 5. Landslide configuration O2 and O3

Fig. 7, 8 represent marigrams for all landslide configurations for two models.

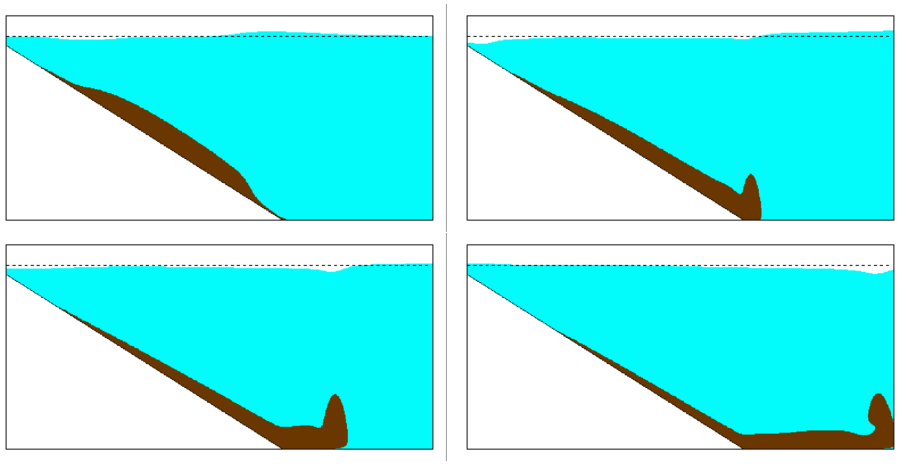

Figure 6. Landslide configuration O2 and O3

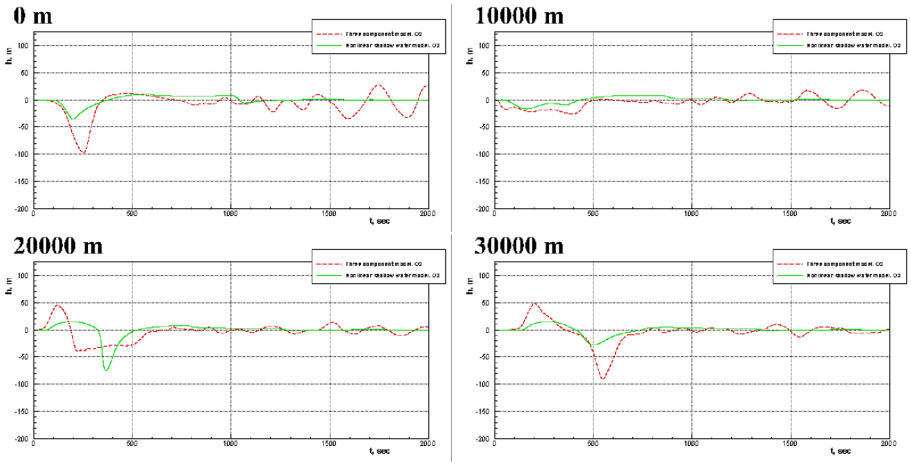

Figure 7. Marigrams

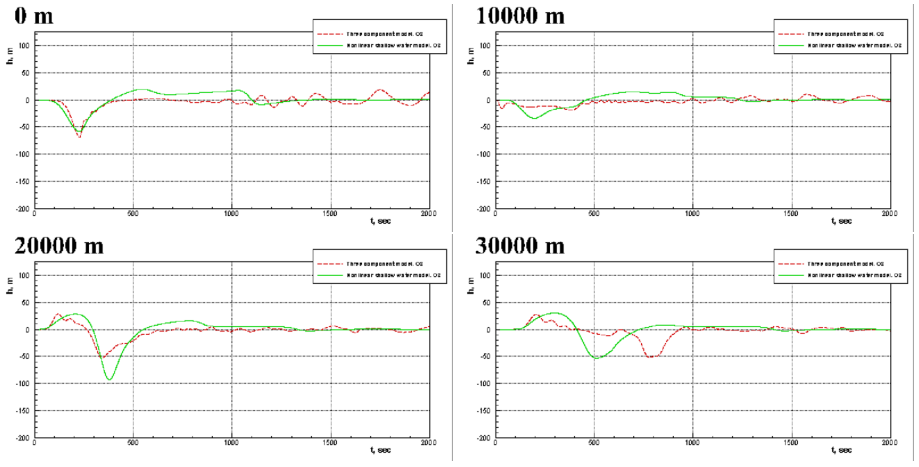

Figure 8. Marigrams

Argument

Waves generated by liquid and solid landslides

First, it can be noted that solid and liquid landslides generate different surface waves. A ”solid“ landslide retains its configuration while moving on the slope, and its motion generates mostly a negative wave advancing towards shallow water against the motion of a landslide, and a positive wave advancing towards deep-water area.

Contrary to a solid landslide, a liquid one splits under gravity in such a way that one part advances downward and the other part – upward the slope. That results in generating an additional positive wave running to the left wall (Figure 4 shows data of wave meters located at points 0 m and 5,000 m) as well as to spreading of a landslide on the slope.

As it is observed at the diagrams (Figure 4 shows data of wave meters located at point 15,000 m and further), the surface wave from both landslides advances with the similar velocity, though it has different configuration. In particular, positive and negative peaks are more expressed for a liquid landslide. It may have effect on the force and character of the wave impact upon coastal facilities.

In due course of time, a solid landslide stops and the waves generated on the surface leave the solution region, and after the water surface becomes still. A liquid landslide does not stop, it spreads and generates subsiding oscillatory motions of the surface.

As for the quantitative specifications of the generated waves, positive wave amplitudes advancing towards the shallow water are very similar in both models. Negative wave amplitudes in the quasi-deformed landslide model are one third of the value of a many-component model. Waves generated by a ‘solid’ landslide and advancing towards deep-water area are one third or two times less.

The impact of the original landslide configuration

We have performed the numerical experiments with three configurations of a submarine landslide (O1, O2 and O3) for two models (a quasi-deformed solid landslide in nonlinear model of shallow water and a liquid landslide in three-component model of viscous incompressible fluid).

A liquid landslide of O1 configuration on the slope splits up under action of gravity, and some part of its mass spreads up the slope. This motion generates the positive wave on the surface running to the left boundary (Figure 4, mark 0 m). The choice of configurations O2 and O3 was stipulated by the desire to eliminate the splitting effect of a liquid landslide on the slope in three-component model, thus eliminating the differences in wave generation near the left boundary. Figure 6 shows that at the start time of the motion of landslides of configurations O2 and O3 there is no splitting on the slope, the return wave is not generated. This is confirmed by marigram data at the mark 0 m (Figure 10) where a negative wave running to the left wall is observed for both configurations.

Thus, a landslide configuration does not only have impact on the performance of surface wave motion but also in some cases it can cause additional effects such as positive wave motion towards shallow water for a O1 configuration liquid landslide.

Conclusion

The preformed research makes it possible to estimate the motion state of an induced wave and the level of hazard for coastal facilities depending upon the landslide type and configuration.

References

1. Enet, F., Grilli, S. T.: Experimental study of tsunami generation by three-dimensional rigid underwater landslides. Journal of waterway, port, coastal, and ocean engineering **133**(6), 442–454 (2007)
2. Rzadkiewicz, S. A., Mariotti, C., Heinrich, P.: Numerical simulation of submarine landslides and their hydraulic effects. Journal of Waterway, Port, Coastal, and Ocean Engineering **123**(4), 149–157 (1997)
3. Sue, L. P., Nokes, R. I., Davidson, M. J.: Tsunami generation by submarine landslides: comparison of physical and numerical models. Environmental fluid mechanics **11**(2), 133–165 (2011)
4. Ataie-Ashtiani, B., Najafi-Jilani, A.: Laboratory investigations on impulsive waves caused by underwater landslide. Coastal Engineering **55**(12), 989–1004 (2008)
5. McFall, B. C., Mohammed, F., Fritz, H. M., Liu, Y.: Laboratory experiments on three-dimensional deformable granular landslides on planar and conical slopes. Landslides **15**(9), 1713–1730 (2018)
6. Watts, P., Imamura, F., Grilli, S. T.: Comparing model simulations of three benchmark tsunami generation cases. Sci. Tsunami Hazards **18**(2), 107–124 (2000)
7. Eletskii, S. V., Maiorov, Yu. B., Maksimov, V. V., Nudner, I. S., Fedotova, Z. I., Khazhoyan, M. G., Khakimzyanov, G. S., Chubarov, L. B.: Simulation of surface waves generation by a moving part of the bottom down the coastal slope. Comp. Tech. **9**, Special issue, Part 2, 194–-206 (2004) (in Russian).

8. Pelinovsky, E., Poplavsky, A.: Simplified model of tsunami generation by submarine landslides. Physics and Chemistry of the Earth **21**(1-2), 13–17 (1996)
9. Lynett, P., Liu, P. L. F.: A numerical study of submarine–landslide–generated waves and run–up. Proceedings of the Royal Society of London. Series A: Mathematical, Physical and Engineering Sciences **458**(2028), 2885–2910 (2002)
10. Fuhrman, D. R., Madsen, P. A.: Tsunami generation, propagation, and run-up with a high-order Boussinesq model. Coastal Engineering **56**(7), 747–758 (2009)
11. Zhou, H., Teng, M. H.: Extended fourth-order depth-integrated model for water waves and currents generated by submarine landslides. Journal of engineering mechanics **136**(4), 506–516 (2010)
12. Smith, R. C., Hill, J., Collins, G. S., Piggott, M. D., Kramer, S. C., Parkinson, S. D., Wilson, C.: Comparing approaches for numerical modelling of tsunami generation by deformable submarine slides. Ocean Modelling **100**, 125–140 (2016)
13. Ma, G., Kirby, J. T., Shi, F.: Numerical simulation of tsunami waves generated by deformable submarine landslides. Ocean Modelling **69**, 146–165 (2013)
14. Salazar, F., Irazabal, J., Larese, A., Oñate, E.: Numerical modelling of landslide-generated waves with the particle finite element method (PFEM) and a non-Newtonian flow model. International Journal for Numerical and Analytical Methods in Geomechanics **40**(6), 809–826 (2016)
15. Zhang, X., Oñate, E., Torres, S. A. G., Bleyer, J., Krabbenhoft, K.: A unified Lagrangian formulation for solid and fluid dynamics and its possibility for modelling submarine landslides and their consequences. Computer Methods in Applied Mechanics and Engineering **343**, 314–338 (2019)
16. Tinti, S., Bortolucci, E., Vannini, C.: A block-based theoretical model suited to gravitational sliding. Natural Hazards **16**(1), 1–28 (1997)
17. Lindstrom, E. K., Pedersen, G. K., Jensen, A., Glimsdal, S.: Experiments on slide generated waves in a 1: 500 scale fjord model. Coastal engineering **92**, 12–23 (2014)
18. Fernandez-Nieto, E. D., Bouchut, F., Bresch, D., Diaz, M. C., Mangeney, A.: A new Savage–Hutter type model for submarine avalanches and generated tsunami. Journal of Computational Physics **227**(16), 7720–7754 (2008)
19. Yavari-Ramshe, S., Ataie-Ashtiani, B.: Numerical modeling of subaerial and submarine landslide-generated tsunami waves—recent advances and future challenges. Landslides **13**(6), 1325–1368 (2016)
20. Beizel, S. A., Chubarov, L. B., Khakimzyanov, G. S.: Simulation of surface waves generated by an underwater landslide moving over an uneven slope. Russian Journal of Numerical Analysis and Mathematical Modelling **26**(1), 17–38 (2011)
21. Beizel, S. A., Chubarov, L. B., Dutykh, D., Khakimzyanov, G. S., Shokina, N. Y.: Simulation of surface waves generated by an underwater landslide in a bounded reservoir. Russian Journal of Numerical Analysis and Mathematical Modelling **27**(6), 539–558 (2012)
22. Zakharov, Y., Zimin, A., Ragulin, V.: Two-component incompressible fluid model for simulating surface wave propagation. Communications in Computer and Information Science **549**, 201–210 (2015)
23. Zakharov, Y., Zimin, A.: Numerical simulation of surface waves arising from underwater landslide movement. In CEUR Workshop Proceedings **1839**, 535–546 (2017)

Calculating Distance to Tomato Using Stereo Vision for Automatic Harvesting

Z. Buribayev[1,2][0000−0002−3486−227X],
T. Merembayev[2,3][0000−0001−8185−235X],
Y. Amirgaliyev[1,2][0000−0002−6528−0619],
T. Miyachi[4], and
A. Yeleussinov[1,2][0000−0002−0425−6527]

[1] Al-Farabi Kazakh National University, Almaty, Kazakhstan
[2] Institute of Information and Computational Technologies, Almaty, Kazakhstan
[3] International IT University, Almaty, Kazakhstan
[4] School of Information Science and Technology, Tokai University, Hiratsuka, Japan

Abstract An accurate estimate of the distance between the robot and equipment is essential for the application of robots. Sensors such as laser and sonar are mainly used to calculate distances. The research considers a pair of Web cameras for distance measurements To solve this problem, the stereo vision method was proposed. A comparison of the accuracy of the calculations was done for 3 zones: left, right and center. This separation allows us to identify possible distortion or camera failure at the edge of the image. As a result of research, the accuracy of 71.939% was achieved. Also defined parameters which can help to improve the precision of object coordinates in 3D.

Keywords: Stereo vision, Robots, Pattern recognition, Disparity map, Depth map;

INTRODUCTION

Using computer vision technology is widely implemented in various fields and also has commercial success. Due to the success of the technology, scientific research in this area is of great interest to scientists. In the direction of computer vision, there are two large areas of research: image processing and pattern recognition. This paper discussed the problems of image processing, this is the first step for future research in the area of pattern recognition.

Computer vision devices can be divided into two categories:

- 2D - obtaining an image with no image depth.
- 3D - image acquisition with which you can calculate Z values.

2D images.

Image data is obtained from a mono camera and the result is a 'flat' image. Often, these cameras are installed on devices that perform dynamic movements and decompose 2D images in time.

3D images.

Image data is achieved by using a stereo pair of images. The device that takes photographs consists of two identical cameras.

RELATED WORK

Normal monocular visuals suffer from scale bias. Pioneering researchers [1,2,6,7] show that this problem can be mitigated by learning from 2D flow functions. Inspired by RGBD-SLAM, relative conversion can be estimated directly from the solution to the PnP problem when depth is specified.

To solve this problem, the authors used deep learning algorithms. CNN-SLAM [8] is a precursor for learning depth prediction training with monocular SLAM to create an accurate dense 3D map.

The research [6] considers the solution to the problem of calculating three-dimensional (3D) coordinates for a material point. For this purpose, two flat images (stereo pair) are used, which correspond to the left and right view points of the 3D scene. A stereo pair is obtained using two cameras with parallel optical axes. A series of experimental studies were conducted to verify theoretical results. During these experiments, aminor discrepancy was caused by the spatial distortion of the camera (distortion) in the optical system and its discrepancy. When using a high-quality stereoscopic system, the existing discrepancy calculation allows applying this method to a wide range of practical problems.

In [7], the errors of calculating the distance to an object using a stereoscopic system are analyzed. It was found that the percentage error in calculating the distance is inversely proportional to the number of pixels used when shifting between two images, and is directly proportional to the distance to the object.

The application of stereo image processing is used for geology interpretation based on the image log (image of downhole). It helps to save time for core sample interpretation [8].

Based on the review of the work, we highlight the following conclusions:

- Determination of distance using a mono camera does not have widespread use and research. Although the use of monocamera should reduce the cost of production of technical devices.
- Reducing the error of distance determination, research in the field of stereo vision is not sufficiently studied and has prospects for a more detailed study.

In this research, we attempted to solve the problems obtained from the literature reviews. This research describes an experiment with a stereo camera, calculating the error and identifying the parameters that affected this error.

METHODS

The paper describes a method of training artificial intelligence to recognize the distance to an object using the modern computer vision detector YOLO, using triangulation.

When shooting objects, a monocamera was used, and to calculate the distance between the camera and the object, the image is transmitted from the camera to the object classifier, based on the modern computer vision object detector YOLO (You Only Look Once). YOLO is a fast and accurate object detector based on the Convolution Neural Network (CNN) [9]. The output is the bounding borders of the detected objects in the image and the class labels of the detected objects. First of all, objects are classified by certain parameters, in our case by color. After classification, parameters are processed to calculate the coordinates of the bounding frames. Based on the coordinates of the bounding frame, the distance from the object to the camera is calculated. The block diagram of the proposed system is illustrated in Figure 1, an example of estimating tomato distances. To make research work realistics and apply the results in any conditions, we used the Tomato DataSet, obtained when shooting objects in a greenhouse complex without the participation of professional shooting mechanisms (prof. photographer, special lighting, etc.). Tomato DataSet was collected in the greenhouse complex ”BRB APK”located in Almaty city, Kazakhstan.

The measurement of the distance between the robot and the object is necessary to control the actions of the robot, such as capturing the object or even avoiding obstacles [10,11]. There are many methods for estimating distance, such as ultrasound, laser, and (video, photo) cameras. A technique based on a video camera has the advantage of its low cost, so in this paper, we will describe a method for measuring the distance between a stereo camera and an object (tomato).

The process of calculating the distance includes five steps: calibrating a stereo camera, calculating a disparity map, calculating a depth map, calculating 3D coordinates of an object in the real world, calculating the distance between a stereo camera and an object.

The stage of calibrating a stereo camera includes the processes of straightening the image and filtering the received image. Calibration of a stereo camera is the process of obtaining internal parameters and external parameters. The internal parameters are the result of the distortion of the lens, while the external parameters depend on the modeling of geometric relationships between the two cameras. For this process, we simultaneously shot a chessboard from two webcams. To increase the quality of the calibration, we took 65 photos Figure 2.

During the calibration process, a checkerboard corners are searched for in all images shot by the left and right cameras simultaneously. The position of the corners for each image is then stored in the image vector, and the object points for the 3d scene are saved in another vector. The image correction process is then carried out using these values. To successfully calibrate the stereo camera, 65 pairs of chessboard images were used. After the completion of the process, we got such data as: camera matrix, distortion coefficients, rotation and displacement vectors

To calculate the stereo camera mismatch map, we used the OpenCV libraries Stereo SGBM algorithm. The Stereo SGBM algorithm is based on the idea of pixel-by-pixel matching and the subsequent application of global twodimensional constraints [13]. The task of calculating parallax in SGBM is formulated as the problem of minimizing the similarity criterion:

$$S(p,d) = \sum_{r} L_r(p,d) \tag{1}$$

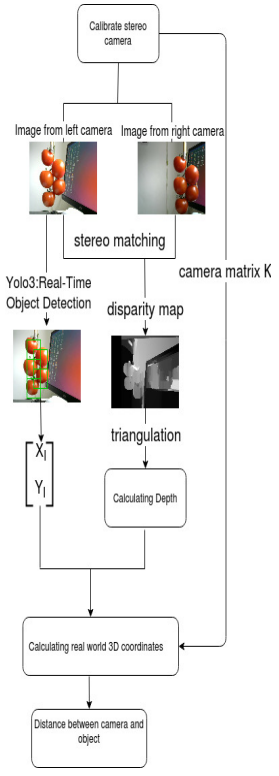

Figure 1. The block diagram of the proposed system.

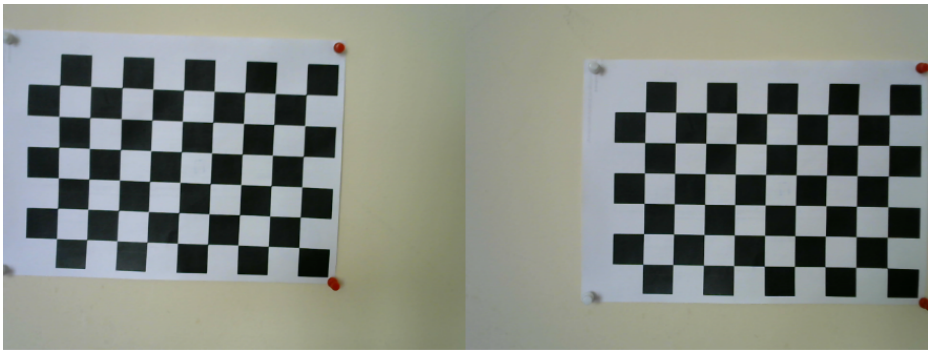

Figure 2. Example of calibrating a stereo camera.

where is the p-pixel of the first image, d is the horizontal parallax of this pixel, and L is a quantity characterizing the path that has been traveled in the r direction. The mismatch map for the base image is calculated, as in the usual methods of local matching, by choosing for each pixel p such an offset d that meets the least similarity criterion, i.e. $min_S(p, d)$.

The pixel disparity value is often interpreted as the inverse distance to the observed objects. In other words, the mismatch is inversely proportional to depth. Therefore, detecting non-conformities is important for building a depth map.

$$Depth = \frac{f * b}{Disparity} \tag{2}$$

where f is the focal length of the camera, b is the distance between the cameras, Disparity is the value of the mismatch map. 3D coordinates of the object in the real world are calculated according to formula 3.

$$\begin{aligned} X &= \frac{Depth * (x_{pixel} - c_x)}{f_x} \\ Y &= \frac{Depth * (y_{pixel} - c_y)}{f_y} \\ Z &= Depth \end{aligned} \tag{3}$$

where $Depth$ is the pixel depth value, fx, fy are the focal lengths expressed in pixel units, cx, cy is the main point that is usually located in the center of the image, X pixel, Y pixel are 2D coordinates in pixels.

After completing the above steps, to calculate the distance between the stereo camera and the object, we used the Euclidean distance according to 4.

$$D = \sqrt{(x_2 - x_1)^2 + (y_2 - y_1)^2 + (z_2 - z_1)^2} \tag{4}$$

where, $x1$, $y1$, $z1$ are the coordinates of the stereo camera, $x2$, $y2$, $z2$ are the coordinates of the object.

In this study, we used a Logitech HD Webcam C270 webcam with the following Table 2 specifications.

Table 1. CAMERA SPECIFICATION.

N	Type	Description
1	The matrix	Resolution: 1280 x 720 pixels
2	Camera resolution	Up to 3 megapixels with software processing
3	Max Resolution	720p/30fps
4	FoV(°)	60
5	Focus type	fixed focus

RESULTS AND FUTURE WORK

The purpose of the experiment is to calculate the distance from the stereo camera to the desired object (tomato). A detected object is tracked using the bounding box shown in Fig 3. When testing the average detection in the frame takes 69 ms, it is 15-16 FPS (frames per second).

Table **??** displays the experimental results. As you can see, the calculated distance data does not quite correspond to the real data. This problem is related to the calculation of the disparity value and it depends on four factors such as:

1. Pulsed lighting
2. Short exposure
3. Uncoordinated shutters
4. Large low contrast areas in the scene

Figure 3. An example of detecting a tomato.

Based on the data obtained, errors between the real distance and that calculated using the camera were calculated. The following metrics were used for this calculation: R2 and Mean squared Table 2.

A comparison of the accuracy of distance calculation is divided into 3 zones, left, right, center. This separation allows us to identify possible distortion or camera failure at the edge of the image. Based on the results of Table 2, metric accuracy was obtained. The general accuracy of the distance was also calculated for all measurements - General.

In Fig. 4 shows the tabular results of TABLE 3 in graphical form.

Based on the developed algorithm, it is possible to improve the accuracy and speed of distance calculation by using parallel computing algorithms. Also, given the results, it is possible to apply this method to the TakoBot robot [13].

Table 2. Actual vs measured distance.

Real distance (cm)	Estimate distance Right (cm)	Estimate distance Left (cm)	Estimate distance center (cm)
10			8.19
15			10.48
20	12.01		14.33
25	14.49	13.68	13.47
30	15.6	16.88	16.67
35	17.78	18.85	18.91
40	19.83	21	21.68
45	22.51	22.22	24.81
50	24.81	23.71	28.37
55	29.47	25.16	29.63
60	29.47	29.31	33.34
65	29.97	32.33	35.8
70	31.3		37.04
75			39.22
80			

Table 3. DISTANCE ACCURACY METRIC.

Zone of measurement	R2 metrics	MSE metrics
Center	0.869	98.314
Left	0.946	32.437
Right	0.879	81.404
General	0.894	71.939

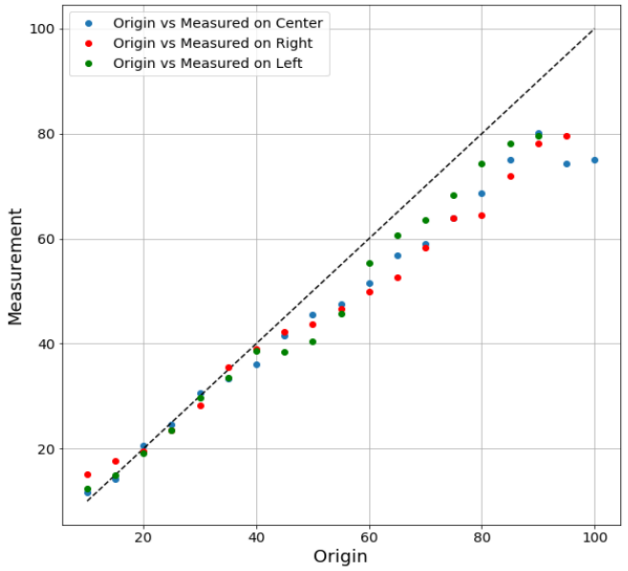

Figure 4. Graphical display comparing the results of known distances and measured.

CONCLUSION

This experiment is conducted with a low-resolution camera to verify whether the proposed algorithm is and the measurement accuracy can be improved using a highresolution camera. Image noise is the main unavoidable cause of errors during the image acquisition phase. Such errors can occur when finding the exact point of contact with the object on the ground. Another potential cause of the error is image change.

Also, the accuracy of the measurement is illuminated, whether it is natural or artificial lighting. Testing this hypothesis requires additional research.

The study conducted an experiment to identify parameters that would improve the accuracy of calculating the distance to the object using one fixed camera, even if the surface of the object is not parallel to the camera and the object is not limited by the vertical movement of the optical axis.

ACKNOWLEDGMENT

This work is supported by a grant from the Ministry of Education and Science of the Republic of Kazakhstan within the framework of the Project ”AP05132648 - Creating verbal and interactive robots based on advanced voice and mobile technologies“. Conflicts of Interest: The authors declare no conflict of interest.

References

1. Costante, Gabriele, and Thomas Alessandro Ciarfuglia.: LS-VO: Learning dense optical subspace for robust visual odometry estimation. IEEE Robotics and Automation Letters **3**(3), 1735–1742 (2018)
2. Clark, Ronald, et al.: Vinet: Visual-inertial odometry as a sequence-to-sequence learning problem. Thirty-First AAAI Conference on Artificial Intelligence. 2017.
3. Muller, Peter, and Andreas Savakis.: Flowdometry: An optical flow and deep learning based approach to visual odometry. In: IEEE Winter Conference on Applications of Computer Vision (WACV). IEEE, (2017)
4. Wang, Sen, et al.: Deepvo: Towards end-to-end visual odometry with deep recurrent convolutional neural networks. IEEE International Conference on Robotics and Automation (ICRA). IEEE, 2017.
5. Tateno, Keisuke, et al.: Cnn-slam: Real-time dense monocular slam with learned depth prediction. Proceedings of the IEEE Conference on Computer Vision and Pattern Recognition. (2017).
6. Mussabayev, R. R., Kalimoldayev, M. N., Amirgaliyev, Y. N., Tairova, A. T., Mussabayev, T. R.: Calculation of 3D Coordinates of a Point on the Basis of a Stereoscopic System. Open Engineering. **8**(1), 109–117 (2018)
7. Marengoni, Mauricio, and Denise Stringhini.: High level computer vision using opencv."In: 24th SIBGRAPI Conference on Graphics, Patterns, and Images Tutorials. IEEE, (2011).
8. Merembayev T., Yunussov R. and Amirgaliyev Y.: Machine Learning Algorithms for Classification Geology Data from Well Logging. 14th International Conference on Electronics Computer and Computation (ICECCO) pp. 206–212, IEEE, (2018)
9. Joseph Redmon, Santosh Divvala, Ross Girshick, Ali Farhadi.: You Only Look Once:Unified, Real-Time Object Detection. Computer Vision and Pattern Recognition, (2016)
10. A. Yeshmukhametov, Z. Buribayev, Y. Amirgaliyev, B. Amirgaliyev, K. Latuta.: Bio-inspired a novel continuum robot arm with variable backbone design: Modelling and validation. Journal of Theoretical and Applied Information Technology. **97**(19), 5036-5047 (2019)
11. Yeleussinov, T. Islamgozhayev, M. Satymbekov and A. Kozhagul.: CVCER: Robot to Learn Basics of Computer Vision and Cryptography. IOP Conference Series: Materials Science and Engineering, **417**(1), (2018)
12. StereoSGBM, `http://docs.opencv.org`. Last accessed 11 Sep 2020
13. A.Yeshmukhametov, K.Koganezawa, A.Seidakhmet, Y. Yamamoto.: A Novel Passive Pretension Mechanism for WireDriven Discrete Continuum Manipulators. Proceedings of the 2020 IEEE/SICE International Symposium on System Integration Honolulu, Hawaii, USA, (2020)

Processing of Images Using Orthogonal Matrixes

Elmira Daiyrbayeva[2 [0000−0002−4255−5456]], Feodor Murzin[3 [0000−0002−4644−5406]], Aigerim Yerimbetova[1,2 [0000−0002−2013−1513]], and Marina Lipskaya[2 [0000−0001−8173−4505]]

[1] Institute of Information and Computational Technologies CS MES RK,
[2] Kazakh Academy of Transport and Communications named after M. Tynyshpayev, Almaty, Kazakhstan
[3] A.P. Ershov Institute of Informatics Systems SB RAS, Novosibirsk, Russia
nurbekkyzy_e@mail.ru

Abstract This article presents methods for using orthogonal matrices in image processing. Features and rational aspects of orthogonal matrices are described. The results obtained by processing specific images were shown. Currently, much attention is paid to image processing using the Hadamard transform. In certain tasks of information processing and transformation, matrices with orthogonal columns (rows) are often used. For developers of image processing systems, it is necessary to be able to easily select the optimal type of structured two-level orthogonal matrices. The main transformations of images are reduced to compression, protection in the channel from unauthorized acquaintance, from interference of natural and artificial origin, which are based on orthogonal matrix transformations. One of the goals of this work is to study the so-called strip method as applied to the restoration of signals and images that have been subjected to influences that have led to a large loss of information. Various variants of the Hadamard matrix used in the strip method are considered. Software experiments were carried out in the Matlab system.

Keywords: orthogonal matrices, images, Hadamard matrix, image compression.

Currently, much attention is paid to image processing using the Hadamard transform.

In certain tasks of information processing and transformation, matrices with orthogonal columns (rows) are often used. For developers of image processing systems, it is necessary to be able to easily select the optimal type of structured two-level orthogonal matrices.

1.1. Matrix is a mathematical object that is a collection of rows and columns, at the intersection of which its elements are located. The number of rows and columns determines the size of the matrix. The numbers of rows and columns of the matrix are called the indices of the elements of the matrix [1]. Indexes are written starting from the line number

$$A = \begin{bmatrix} a_{11} & a_{12} & \dots & a_{1m} \\ a_{21} & a_{22} & \dots & a_{2m} \\ \vdots & \vdots & \ddots & \vdots \\ a_{n1} & a_{n2} & \dots & a_{nm} \end{bmatrix} \quad (1)$$

An n x m matrix is called rectangular, it is called square when the number of its rows and columns is equal n = m. The size n of a square matrix is called the order.

A square matrix of the form $I = diag(1, 1, \ldots, 1)$ with unit entries along the main diagonal (other zeros) is called the identity matrix.

1.2. The inverse of the matrix A is the matrix A^{-1}, for which

$$A \wedge (-1)A = I \tag{2}$$

If the result of the transformation, which consists in multiplying a matrix P of order n by an orthogonal matrix A of the same order, is a matrix P*, then multiplying P* by an inverse matrix A^{-1} leads to obtaining (restoring) a matrix P with an accuracy of calculation errors. The main condition is that the matrix A^{-1} is not ill-conditioned [1,2].

1.3. The operation of replacing all rows of the matrix A with its columns is called transposition; the result of its action is denoted as A^T. The operation of transposing square matrices is reduced to a pairwise permutation of elements located symmetrically about the main diagonal.

1.4. Matrix A is orthogonal if it satisfies

$$A^{-1}A = A^T A = I \tag{3}$$

If most of the elements of an orthogonal matrix are equal to each other, its form can be simplified by scaling - dividing by the most common element in the matrix. Scaled matrices do not lose the pairwise orthogonality of their rows and columns, since scaling does not change the diagonal appearance of the right side.

Obviously, the orthogonality allows replacing the matrix A^{-1} with AT when reconstructing P from the matrix P*. Such a replacement guarantees a higher accuracy of calculations, in which there is no accumulating error from an inaccurate calculation of A^{-1}. This feature of orthogonal matrices ensures a simple inverse transformation, making the transformation with orthogonal matrices symmetric in general. Among orthogonal matrices, the Hadamard matrices are distinguished by the simplicity of the elements.

1.5. An nxn Hadamard matrix H is a square matrix with elements 1, -1 that satisfies the equation $H^T H = nI$ [3]. All columns (rows) of such a matrix are pairwise orthogonal to each other - their scalar product is 0, and the square of the norm is n.

For greater rigor of reasoning and conclusions, such matrices will be called quasi-orthogonal, meaning that they are not orthogonal in the strict sense of the word, but are close to orthogonal up to the scaling factor. It is believed that such matrices were first identified by Sylvester in 1867 [4], although they were also known to his other contemporaries.

1.6. The values of the elements of orthogonal (quasi-orthogonal) matrices will be called levels [3,4]. The attractiveness of Hadamard matrices lies in the fact that they have only two integer levels 1 and -1 and the algorithms for computing with them, therefore, are very simple to implement. It is customary to depict Hadamard matrices not only in mathematical representation as matrices, but also graphically - in the form of ”portraits”of matrices [4, 5] for the convenience of assessing the features of their structure, the presence of symmetries, cyclicities, etc. For the first time, the

representation of a matrix in the form of a portrait was used by Golomb (Golomb, Baumert and Hall).

1.7. A portrait of a two-level matrix is a graphic image in the form of a set of squares, where a black square corresponds to an element with a minus sign, and a white square corresponds to a positive element [4].

1.8. The Kronecker product [8, 9] of two matrices A and B is an operation (x) of the form

$$Ax\mathbf{B} = \begin{bmatrix} a_{11}\mathbf{B} & a_{12}\mathbf{B} & \dots & a_{1m}\mathbf{B} \\ a_{21}\mathbf{B} & a_{22}\mathbf{B} & \dots & a_{2m}\mathbf{B} \\ \vdots & \vdots & \ddots & \vdots \\ a_{n1}\mathbf{B} & a_{n2}\mathbf{B} & \dots & a_{nm}\mathbf{B} \end{bmatrix} \tag{4}$$

Since orthogonality is an invariant of the Kronecker product, the result of the multiplication of two Hadamard matrices of orders n and m is a Hadamard matrix of order nm. This is also a property of quasi-orthogonal (scaled orthogonal) matrices. Variations of Hadamard matrices associated with their block structures have recently been of great interest.

1.9. Block matrices will be called the type matrix

$$\begin{bmatrix} A & B \\ C & D \end{bmatrix}^T = \begin{bmatrix} A^T & C^T \\ B^T & D^T \end{bmatrix} \tag{5}$$

consisting of blocks (matrices) of the same order n. The transposition of block matrices is reduced to the transposition of all its blocks with pairwise permutation of blocks located symmetrically with respect to the main diagonal.

Many applied problems of distributed systems for collecting, storing and transmitting information include the processes of compressing it, converting formats, maintaining confidentiality, protecting against distortions and separating the transmitted information against the background of interference in the channel [6,7]. Digital visual information is the most time consuming to process in such distributed systems based on IP networks, implemented on a combined basis - wired and wireless.

Image compression - the use of data compression algorithms for images stored in digital form. Compression reduces the size of the image, which reduces the time it takes to transfer the image over the network and conserves storage space.

Image compression is classified into lossy compression and lossless compression. Lossless compression is often preferred for artificially constructed images, such as graphics, program icons, or for special cases, such as when images are intended for post-processing by image recognition algorithms. Lossy compression algorithms with increasing compression ratio usually generate artifacts that are clearly visible to the human eye [8].

Anti-jamming coding - when we transmit a message from a source to a receiver, an error may occur during data transmission (interference, equipment malfunction, etc.). To detect and correct the error, noise-immune coding is used, i.e. encode the message so that the receiving party knows whether an error has occurred or not, and can correct errors if they occur.

In fact, coding is the addition of additional, verification information to the original information. For encoding, the transmitting side uses an encoder, and the receiving side uses a decoder to get the original message.

Other transformations of images (frames) are also based on the principle of symmetry of transformations using orthogonal matrices, in particular, their noise-immune coding and protection from unauthorized acquaintance during their transmission in communication channels. One of the methods of error-correcting coding is strip-transformation of images [7], which was originally developed for coding signals and images transmitted in channels with impulse noise. Its basis is ”cutting”of the image P on the transmitting side of the distributed system into fragments X of equal length - strips, two-sided multiplication by a low-order orthogonal matrix, forming their linear combinations and inverse orthogonal transformation with subsequent ”gluing”on the receiving side.

There are two best known strip transform modifications: with two-sided matrix Kronecker multiplication [7-9] and simple two-sided matrix multiplication [17, 18] using orthogonal matrices. Figure: 1.4 demonstrates the sequence of transformations. In both modifications, the two-sided matrix transformation with Kronecker (x) multiplication of X by the orthogonal matrix on the left and right of the ”stripes”of the image (obtained by the operator S) provides better mixing of image fragments and, ultimately, weakening the amplitude of the impulse noise imposed in the channel on a specific place on the converted image.

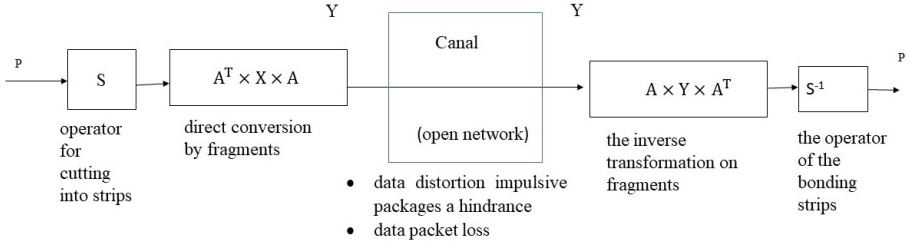

Figure 1. Scheme of a two-way strip transform

Image fragments are converted according to the formula

Reconstruction on the receiving side of the image formed from fragments Y and transmitted over the communication network is performed through an inverse two-way transformation in the form

The resulting image P is the result of defragmentation from fragments of the X type of the received image. Two-sided (two-dimensional) strip transformation of images is shown in Fig. 2. Here a is the original image, b is a strip-transformed image, c is a reconstructed image after transmission in a channel with impulse noise using a strip transform, e is a reconstructed image after transmission in a channel with interference without using a strip-transform. The above example of a strip transform is implemented using a 4x4 Hadamard matrix, and a single noise corresponds to a 30x30 pixel rectangle.

The weakening of the influence of impulse noise is realized by the fact that during inverse transformations performed on the receiving side with a transposed orthogonal matrix, the noise is evenly distributed over the entire reconstructed image. For maximum attenuation of the noise amplitude in the strip transform, as a rule, extreme orthogonal Hadamard matrices [9] of orders 4 and 8 are used. Hadamard matrices exist on orders 4t, where t is a natural number. There are more than two such matrices on each order. However, the existing algorithms for calculating Hadamard matrices ensure the legacy of only the structures of the matrices corresponding to these methods. There is no their structural and quantitative diversity in the orders of existence.

Masking. Masking is a computational procedure for transforming a digital image, destroying it to a form perceived visually as noise.

The task of masking is to keep the image inaccessible to a third party during the time of the relevance of this image.

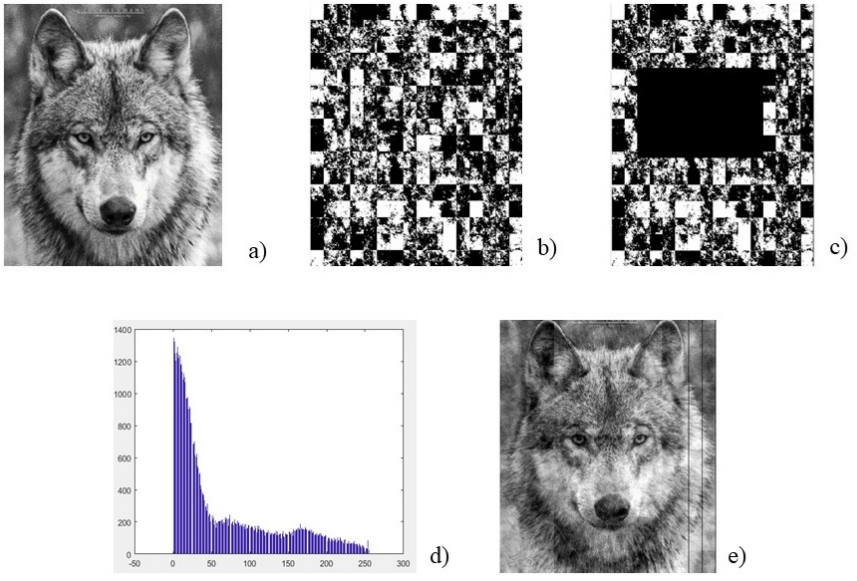

Figure 2. Image at the stages of a two-way strip conversion cycle: a) original image, b) fragmented image, c) fragmented image with noise, d) histogram of the error, e) the result of the strip-transformation

The result of the inverse transformation coincides with the original image, up to the transposition of the masking matrix: there is no need to separately store not only the inverse matrix itself, but also its half due to its symmetry. This saves memory when directly implementing the method on the system. It is the presented simplified version of the strip transformation (without the use of Kronecker multiplication and cutting the image into strips), but implemented with unique matrices, that is called masking [3].

Discrete cosine transform is most often used as orthogonal transformations in digital marking algorithms, as well as in compression, due to its use in JPEG and JPEG 2000 formats. However, in a number of works [10, 11] and others for digital marking of still images (frames), discrete Haar and Hadamard transforms are used, the kernel of which is the Hadamard matrix of order n = 2k, where k is a natural number. It should be noted that matrix methods for converting information are very practical, since they imply effective structural implementation in both PLM and software implementation in all modern microprocessor structures focused on digital signal processing.

After analyzing, we can say that in the field of processing images and video frames, the requirements for their quality and resolution are constantly increasing - this is a modern trend implemented by both manufacturers of video matrices and manufacturers of display matrices for video control devices, monitors, televisions.

Currently, the UHD (Ultra High Definition) digital format, becoming the most widespread, requires processing of 3840x2160 (4K) and 7680x4320 (8K) frames, and the Quality Box technology requires processing frames of generally arbitrary size.

These circumstances give rise to the need for compression, masking, marking, noise-immune image coding and others to have a wide family of orthogonal matrices, including matrices of not only large orders, unknown until now, but also matrices of odd orders [11], preferably symmetric structures. Hadamard matrices exist on orders of 4t and this significantly limits the possibilities of their application for images of arbitrary resolution. In addition, there is no universal algorithm for their computation, and the known methods do not allow one to find Hadamard matrices of all orders 4t.

Thus, we can briefly formulate the general requirements for the family of matrices in the following form:

-the orders of the matrices should correspond to the largest possible number of natural numbers to be able to choose the best matrices (or multiple use of them) for images of various sizes;

-more than one quasi-orthogonal matrix must exist for each order to provide an alternative choice;

-in order to optimize the amount of memory when storing matrices and to simplify computational procedures, the number of possible values of elements (levels) of matrices should be minimal, and their structures should have symmetries.

Additional requirements for two-sided matrix masking matrices are the need to ensure:

- resistance of masked information to interference and losses in the communication channel;

- Invariance of matrices to two-sided matrix transformation.

Despite the fact that the strip transform is not the basis of the masking method, the image masked by the proposed method remains resistant to possible distortions and information loss in communication channels. As an example for two test images (”Lena”and ”Book”) with a resolution of 512x512 pixels, shown in Fig. 3, we present the results of some experiments.

Conclusion: The main transformations of images are reduced to compression, protection in the channel from unauthorized acquaintance, from interference of natural and artificial origin, which are based on orthogonal matrix transformations.

Figure 3. Test images for the experiment

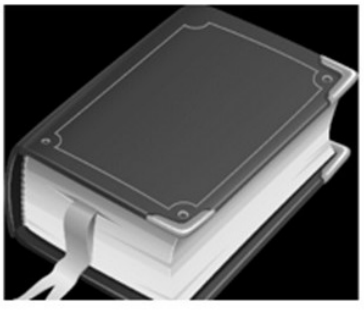

Figure 4. a) original image

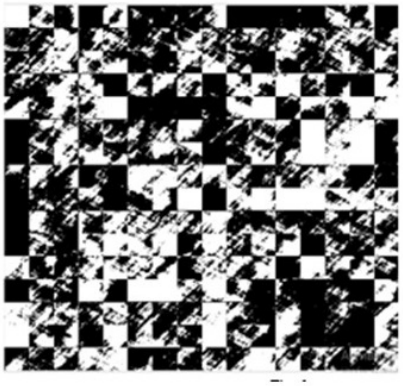

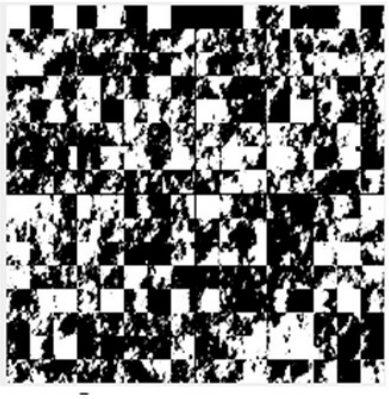

Figure 5. b) fragmented image

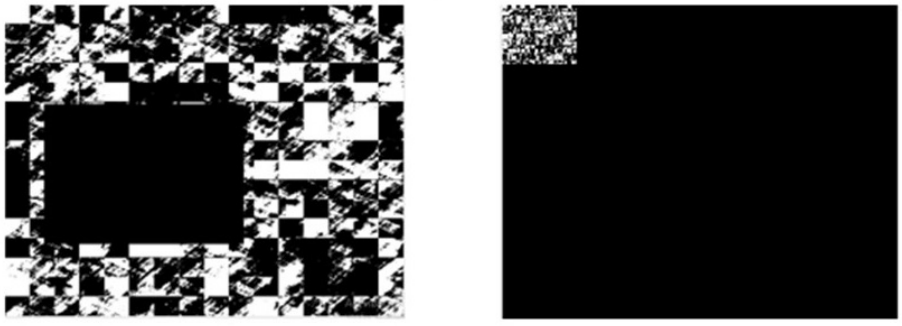

Figure 6. c) fragmented image with noise

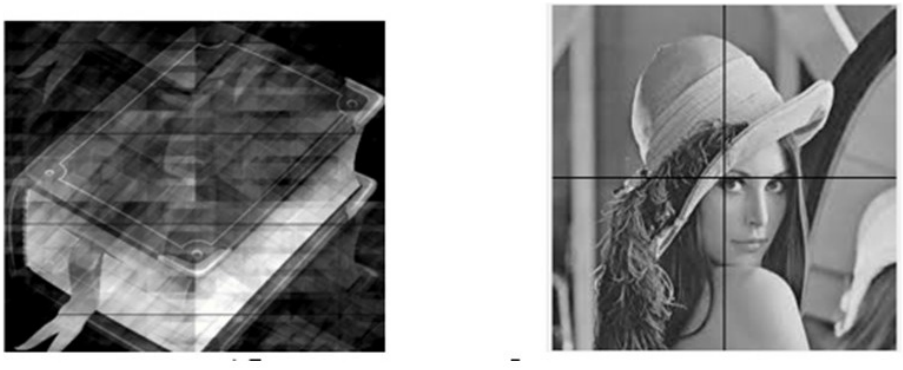

Figure 7. d) The result of the strip conversion

One of the goals of this work is to study the so-called strip method as applied to the restoration of signals and images that were subjected to influences that led to a large loss of information.

This method is poorly studied, it is not clear which matrices are better to use in it, what kind of error arises after restoring damaged signals or images in certain situations. Various variants of matrices used in the strip method are considered: Hadamard, Haar.

The essence of the strip method is to transform a signal or image at the transmitting end by ”dividing”it into fragments of equal length or area, respectively, forming their linear combinations and back ”gluing”.

In the work, mainly, orthogonal matrices, two-dimensional strip transform, i.e. the method is applied to images, the strip transform matrices are selected based on the fact that it is necessary to achieve the most uniform distribution of the interference over the image as a result of inverse decoding at the receiving end of the communication channel. This allows you to recover information about distorted or lost fragments. Software experiments were carried out in the Matlab system.

References

1. Akhmed, N., Rao, K.R.: Orthogonal Transforms for Digital Signal Processing. Springer-Verlag Berlin Heidelberg **1**, 130-132, (1980)
2. Sergeyev, A.M., Blaunshtein, N. Sh.: Orthogonal matrices of symmetric structures for image processing tasks Ortogonal’nyye matritsy simmetrichnykh struktur dlya zadach obrabotki izobrazheniy. Information management systemsInformatsionno-upravlyayushchiye sistemy **6** (91), 2-8 (2017).
3. Sergeyev, A.M.: Methods for transforming images and coding signals in channels of distributed systems based on the use of special quasi-orthogonal matrices Metody preobrazovaniya izobrazheniy i kodirovaniya signalov v kanalakh raspredelennykh sistem na osnove ispol’zovaniya spetsial’nykh kvaziortogonal’nykh matrits, dis ... candidate of technical sciences: 05.12.13. - St. Petersburg,**153**, (2020).
4. Balonin, N.A., Sergeyev N.B.: Norms of generalized Hadamard matrices Normy obobshchennykh matrits Adamara, Bulletin of St. Petersburg University Vestnik Sankt-Peterburgskogo universiteta, Ser. 10: Applied mathematics. Informatics. Management processes, **2**, 5-12 (2014).
5. Balonin, N.A., Dokovic, D.Z.: Symmetric Hadamard Matrices of Orders 268, 412, 436 and 604. Information management systems Informatsionno-upravlyayushchiye sistemy **4**, 2-8, (2018).
6. Paley, R.E.A.C.: On orthogonal matrices. Journal of mathematics and physics. Vol. 12., 311-320, (1933)
7. Mironovskii, L.A., Slayev V.A.: Strip method for transforming images and signals Strip-metod preobrazovaniya izobrazheniy i signalov,SPb.: Polytechnic, 163 p, (2006).
8. Vatolin, D., Ratushnyak, A., Smirnov, M., Yukin, V.: Data compression methods Metody szhatiya dannykh. The device of archivers, compression of images and video Ustroystvo arkhivatorov, szhatiye izobrazheniy i video. M.:DialogMIFI, 384 p. (2002).
9. Goethals, J.M., Seidel, J.J., Orthogonal matrices with zero diagonal. Canadian Journal of Mathematics, vol. 19, 1001-1010, (1967)
10. Rassokhina, A.A.: Study of the strip method for signal and image processing Issledovaniye strip-metoda obrabotki signalov i izobrazheniy. Materials of the 50th International Scientific Student Conference ”Student and Scientific and Technical Progress”: Information Technology, Novosibirsk NSU, p. 19, (2012).

11. Murzin, F.A., Ryaskina, N.A.: Analysis of noise stability of strip-transformation. Bull. Nov. Comp. Center, Comp. Science, **41** 41-54, (2017)
12. Mahafza, B.R.:Radar Systems Analysis and Design using MATLAB. Chapman&Hall/CRC, 532 p. (2000).

Real-Time Human Emotions Recognition on Mobile Devices using Machine Learning Algorithms

Beimbet Daribayev[1,2] [0000−0003−1313−9004] and Nurkhan Zhaksylyk[2]

[1] University of International Business, Almaty, Kazakhstan
[2] Al-Farabi Kazakh National University, Almaty, Kazakhstan
beimbet.daribayev@gmail.com

Abstract Modern methods of deep learning of neural networks are to find the minimum of some continuous error function. Currently, various optimization algorithms are known that use different approaches to update model parameters. This article is devoted to the analysis of convolutional neural networks with a teacher, as well as the most common optimization methods for learning deep networks in order to recognize the human emotion in the picture. Learning with a teacher is one of the ways of machine learning, during which the test system is forcibly trained with the help of " stimulus-reaction "examples. During the analysis, activation functions such as ReLU, softmax were used. And also, categorical crossentropy was chosen to find errors in the network. And they minimized the error by updating weights to correctly output the response using the Adam optimizer. Corrected a network error using the Dropout regulator. To test the performance of the above algorithms, a mobile application was created for the android platform. And also, we accelerated image processing in the video stream by dividing processes into different threads.

Keywords: Multilayer Perceptron, Neural Network, Activation Function, Weighting Factors, Tensors, Convolutional Neural Network, Gradient Descent.

Introduction

People communicating with each other constantly analyze any human manifestations. It is no secret that one of the important aspects of the analysis is human emotions. Therefore, the creation of modern technology of machine systems is relevant application of methods for automatic recognition of emotions.

One of the common ways of recognizing human emotions by another person is the analysis of visual information. Based on this, it can be understood that the automation of this process should be obvious based on the use of computer vision methods, which is implemented using modern technology of neural networks.

Computer vision is a branch of science where theory and methods are studied, as well as algorithms for analyzing images of objects [1]. This technology is the creation of machines that can detect, track and classify objects. As a scientific discipline, computer vision refers to the theory and technology of creating artificial systems that receive information from images.

Automatic recognition of emotions is quite widespread. For example, recently, Kia

Motors introduced [2] a system that can assess the mood of a person in a car and adjust the atmosphere in the cabin for him.
Such artificial systems are well-implemented using convolutional neural networks. At present, the use of convolutional neural networks allows one to recognize human emotion with various methods of data analysis. For example, one can recognize a person's emotion with the help of an audio recording implemented by Reza Chu [3]. Using this technology, we implemented a network that can recognize the emotion in the picture.
In order to recognize human emotion, a convolutional neural network (CNN) [4] was used, which was trained based on Kaggle [5] data, where gray images with 1 channel are stored in 48x48 pixels format. For 2 reasons, we used this particular method and not a simple multilayer perceptron [6]:
– The percentage of accuracy on the verification data is greater. Due to this, the computer determines the emotion of a person in our case better in our cases
– The concept of total weights. Let´s look at it better to understand the above-mentioned pluses of the CNN. First, let's see how version 2 of the usual multilayer perceptron works. A multilayer perceptron consists of an input, hidden (there may be several of them, depending on the task), output layer (Fig. 1).
As you can see, each node (neuron) in each layer is interconnected. The binding strands of neurons are called synapses, which have their own weights (weighting factors). In machine learning, weights are usually marked with the letter "w", and "X" is the input data that is transmitted to the first layer. To get a response from the output layer, in each layer, all neurons must perform several operations and transfer data to the last layer.
Accordingly, each neuron is 1 pixel of the picture. If we multiply the width of 48px by the height of 48px, then we get the value 2304. Our input layer would have 2304 neurons and since each neuron in each layer is interconnected, we would have many weighting factors. And this is not beneficial for us since it would require a large amount of resources. Conversely, convolutional neural networks are limited by the number of weights. And this has become the main reason for the success of the CNN in the recognition of large objects such as pictures, audio, video, etc. Since our emotions are tensors (48x48 matrix), we used this method to train our model.

To date, the best results in image recognition are obtained with their help. On average, the recognition accuracy of such networks exceeds conventional perceptrons by 10-15%. CNN is the core technology of Deep Learning.
The main difference between a fully connected layer and a convolutional layer is the following: multilayer perceptron layers study global patterns in the space of input features (in the case of emotions from the Kaggle set, these patterns involve all pixels), while convolutional layers study local patterns (Fig. 2).

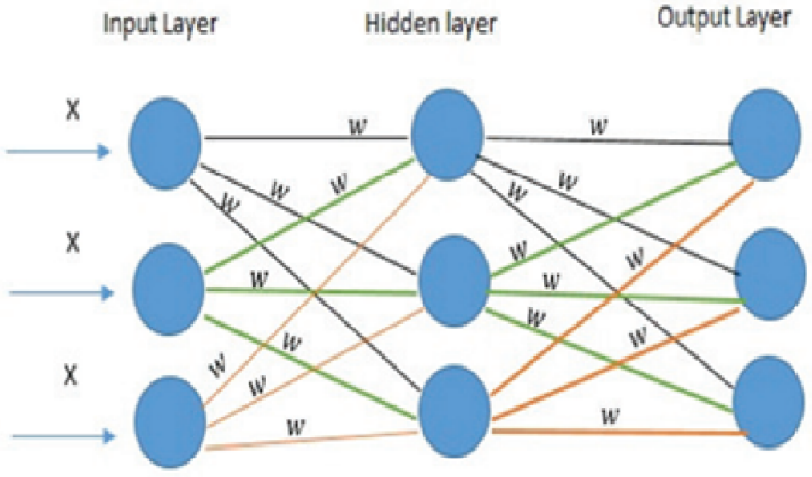

Figure 1. The structure of neural networks.

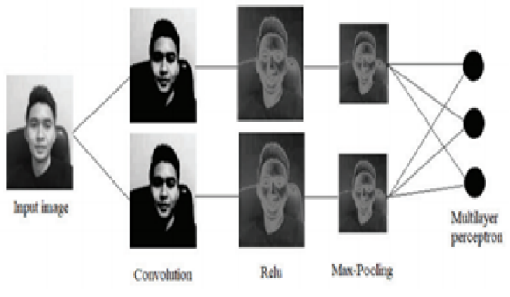

Figure 2. Convolution operation.

Input layer

The input data are gray images of the type JPEG, size 48x48 pixels. If the size is too large, the computational complexity will increase, respectively, the restrictions on the response speed will be violated, the determination of the size in this problem is solved by the selection method. If you select a size too small, then the network will not be able to identify key signs of faces.
The picture with human emotions has only 1 channel (48x48x1). The input layer takes into account the two-dimensional topology of the images and consists of one map (matrices), the map can be one, if the image is presented in shades of gray, otherwise there are 3, where each map corresponds to an image with a specific channel (red, blue and green).
The input data of each specific pixel value is normalized to a range from 0 to 1, according to the formula:

$$f\left(p, min, max\right) = \frac{p - min}{max - min} \tag{1}$$

where,
f = normalization function.
p = specific color value in pixels from 0 to 255.
min = minimum pixel value-0.
max = maximum pixel value-255.

Convolutional layer

Convolution is connected to three-dimensional tensors, called feature maps, with two spatial axes (height and width), as well as with the profundity hub (or the hub of the channels). For black and white pictures, as within the Kaggle dataset, the profundity pivot incorporates a measurement of 1 (shades of gray). The collapse operation extricates patterns from its input include outline and applies the same changes to all patterns, producing an output feature map. The measure of the output card can be calculated utilizing this equation:

$$\left(w, h\right) = mW - kW + 1, mH - kH + 1 \tag{2}$$

where,

(w,h)-calculatedconvolutioncardsize.
mW-width of previous map.
hW-height of previous map.
kW-core width.
kH-core height.

The core is a filter or a window that slides over the complete range of the past map and finds certain signs of objects. Since we trained the network on numerous faces in arrange to recognize human emotion, one of the cores could give the most noteworthy signal in the process of training in the mouth, eyebrow, eye and nose (Fig. 3).

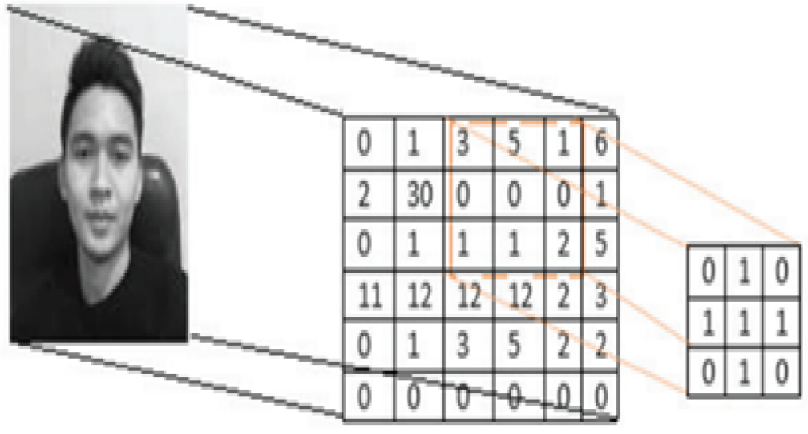

Figure 3. The convolution operation and obtaining the value of the convolution card.

The kernel glides over the past map and performs the convolution operation and transfers the values to the activation function, at that point, the characteristic maps are made (new matrix), the equation:

$$(f * g)[m,n] = \sum_{k,l} f[m-k, n-l] * g[k,l] \tag{3}$$

where,

f-source image matrix,
g-convolution core.

Relu was chosen as the activation function, since it does not lead to problems with attenuation or increasing gradients. And also, for the hidden layers of the perceptron, we used Relu, and the output was Sigmoid.

$$f(s) = max(0, s) - activationfunctionReLU$$

The operation of this function is simple, as you can see this, the function displays 0 if the value passed to the function is s < 0, and if $s \geq 0$ returns the same value.

Having performed the activation function, we transfer the resulting matrix to the subsample layer (Fig. 4).
The reason of the layer is to diminish the measurement of the maps of the past layer. In case a few signs were as of now recognized within the past convolution operation, at that point such a detailed picture is not required for advance preparing, and it is compressed to a less detailed one. In addition, filtering already unnecessary parts helps not to retrain. During filtering by the center of the subsample layer (channel) of the map of the past layer, the checking center does not intersect, unlike the convolutional layer. Ordinarily, each card includes a 2x2 center, which permits you to diminish the past card convolution layer by 2 times. In our task, there will be 3 convolutional layers of 1 subsample layer

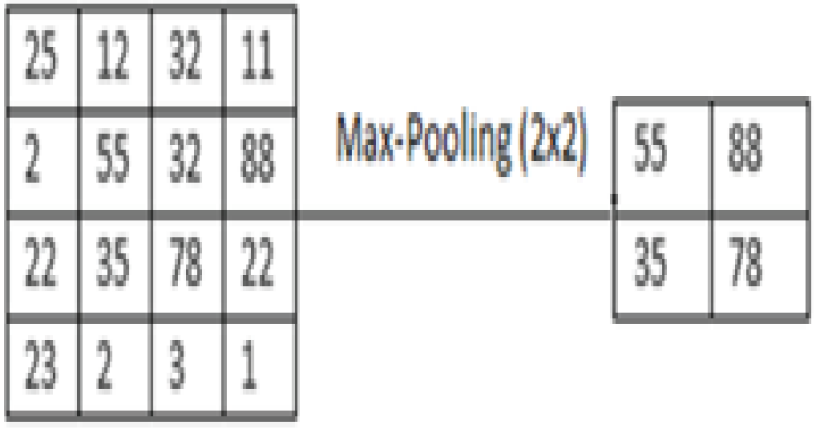

Figure 4. Layer subsampling.

for each and a multilayer perceptron with 1 hidden layer. As you can see after reducing the size, we transfer the reduced image size to the input of the multilayer perceptron without losing important information.
After receiving the vector data, we carry out the training. The essence of training is to reduce the function of loss. Typically executed utilizing the backpropagation strategy. To discover the mistake, we'll utilize los function categorical crossentropy. This work will figure it out by the formula:

$$E = -\sum_{i=1}^{n} D_i * log_2(Y_i) \tag{4}$$

where,

D-expected result, Y-output.

The output is calculated using the softmax activation function. Softmax is a logistic function for the multidimensional case. This means that the function is not applied to a single value, but to a vector. For example, it can be used when the task of multiclass classification is.
The softmax is expressed by the formula:

$$Softmax(x) = \frac{e^{S_i}}{\sum_j e^{S_j}} \tag{5}$$

where,

$$S = \sum_{i=1}^{n} x_i * \omega_i$$

n-number of neurons.

As we said above, in order for the network to work correctly, we must reduce losses. This is implemented using the gradient descent method [7]. For this we will use the Adam optimizer [8].
During the first experiment, we obtained results of loss and network accuracy (Fig. 5a, Fig. 5b):

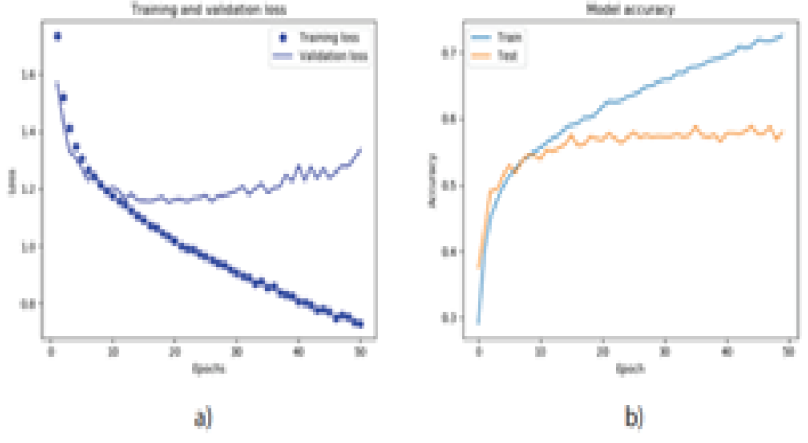

Figure 5. a) Losses on training and validation data in the 50th epochs. b). Accuracy on training and validation data in the 50th epochs.

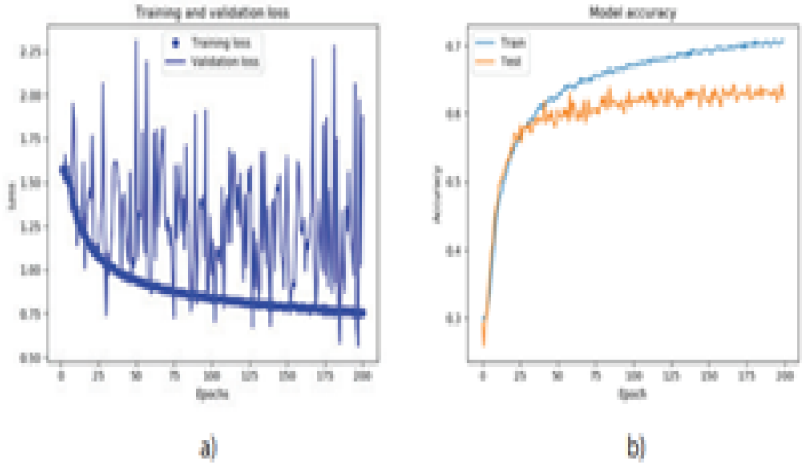

Figure 6. a) Losses on training and validation data in the 200th epochs. b). Accuracy on training and validation data in the 200th epochs.

Increasing the number of epochs from 50 to 200, we got the following results (Fig. 6a, Fig. 6b):

Entrance training model we are confronted with retraining. This term implies that our network recognizes emotion on the training data well, in any case, the precision on the validation data did not rise. Due to this, the strategy of diminishing (Dropout) was used. Retraining could be a issue for numerous neural systems. Due to truth that the network starts to memorize training data, our network will start to memorize excessively. Any methods that we utilize to anticipate retraining is called the regularization method.

One of these regularization methods is loss (thinning), which is utilized in profound systems by counting drop-down layers. This layer does not contain neurons; appropriately, it does not calculate anything. Instead, it incidentallydisengages a few neural from the past layer. Such a layer will be temporarily active in the learning process. When we use the network for prediction, the drop-down layer does not work. The trained model can now be used to implement software. Using this model, a mobile application for recognizing human emotions in real time was implemented on the android platform.

For the implementation, we used the Android Studio development environment, the OpenCV library for image processing. We chose Java as the programming language, and also used our trained model in the tflite format, since the mobile application does not support the h5 file.

The program consists of 5 classes: MainActivity, MultiThread, Classifier and Result. In the first class, we connect the library we need, in our cases it is openCV.

We also initialize files such as Emoji.tflite (our trained model), haarcascade frontalface atl2.xml for high speed face recognition. Our class implements the interfaces: CameraBridgeViewBase.CvCameraViewListener2 for working with the camera, View.OnClickListener for listening to buttons to change the camera. We initialized global variables with the following types: JavaCameraView, File, CascadeClassifier, Mat, Interpreter, int, ImageButton. In the onCreate () method, which sets the initial setting of the initialization parameters, we connect our layout for display, create a JavaCameraView object, load the openCV 3.4.0 version using the OpenCVLoader.initAsync method. On successful loading, we call the onManagerConnected () callback function. In this method, we initialize our cascading face recognition file. After that, we go back to the onCreate () method and start installing our models. The android lifecycle is not only about onCreate (), so we need to implement other methods, in particular onDestroy (). After completing the work or when rolling, we must turn off the camera, for this we use this method. Also, the camera itself has a certain analogue, similar to the life cycle of an android application: onCameraViewStarted (), onCameraViewStopped (), onCameraFrame (). In the first method, we create a Mat object. This object stores images in a two-dimensional array. In the next method, when the camera is turned off, we delete the object, since we need to free memory. In the last method, we load our images that we receive in the video stream. After assigning the image to the Mat, we start the thread to make the program work faster and in this thread we pass 4 parameters to the MultiThread class: Mat, CascadeClasifier, Interpreter, absoluteFaceSize. The parameters passed to the stream are needed in order to recognize the face and draw the recognition result in it. But the work of the first class did not end there. Then we worked to ensure that during installation it was possible to configure access to the camera without going into the settings. For this, built-in methods have been redefined, such as: checkPermission (), onRequestPermissionsResult ().

After completing all the necessary tasks, we switched to the third grade in which we will recognize a person's emotion. In this class, we have created variables with the types Mat, CascadeClassifier, Interpreter, int, ByteBuffer. We assigned the received data from the first class to the variables we needed that we created. The thread that we started in the first class is implemented in the second class. This thread creates a MatofRect object in which we will store our rendered faces in a three-dimensional array. That is, a set of two-dimensional arrays can be stored in MatofRect, which are the faces of the decoded people. This is implemented using the detectMultiScale () method of the CascadeClassifier object. In this method, we pass our Mat, CascadeClssifier, specify scaleFactor, minNeighbors, flags and create a new Size object with the absoluteFaceSize attributes we took from the first class. Next, we create a list for our emotions that we will decode. For the list, ArrayList () was used (Fig. 7).

Next, we create a new Mat object for faces. Each time a face is recognized, a new Mat object will be created. Next, we will draw a rectangle on the found faces. It was implemented using the rectangle () method of the Imgproc object. In this metot, we passed Mat, specified the coordinates using Point () and the color of the square using Scaler (). Further from the picture, we cropped the faces and transferred them

```
ArrayList<String> outputString = new ArrayList<>();
outputString.add("Angry");
outputString.add("Happy");
outputString.add("Neutral");
outputString.add("Sad");
outputString.add("Surprise");
```

Figure 7. List of emotions.

to the newly created Mat object. Then we reduced the cropped image by 48x48 since our model was trained with 48x48 images. Then we created a new class Classifier and passed the Interpreter to its constructor, which we got from the first class, so we create an object of the third class. The putText () method of the ImgProc object was used to draw the label of the resolved emotion. This is where we pass Mat and coordinates to Point (), as well as our text that we got using the classify (matFace) method of the Classifier object. As you can see, we are passing our thumbnails into the classify method.

In the class where we will perform the classification, we created variables:

DIM_ BATCH_ SIZE=1,
DIM_ PIXEL_ SIZE=3,
DIM_ HEIGHT=48,
DIM_ WIDTH=48,
BYTES=4.

We need these variables in order to create a buffer for storing the image in order to use them in the Interpreter. We need an Interpreter to recognize an emotion. The buffer was created using the ByteBuffer.allocateDirect () method. The 1x5 array was used to store the recognition result. The classify method that does the classification converts the resulting Mat into a byte buffer. For this, the convertMatToBteBuffer (Mat) method was created. In this method, if the buffer is empty, we stop the method, if there is data, then we convert Mat to byte and add it to the buffer. We pass the resulting buffer and the array for the result that was created above to the run method of the Interpreter object to get the result of the classification. After that, we create the Result class and pass our result to its constructor. In this class, using the maximum index, we recognize a person's emotion. The result is drawn in the second class.

The developed application can recognize 5 emotions: 1. Angry (Fig. 8a), 2. Happy (Fig. 8b), 3. Neutral (Fig. 9a), 4. Sad (Fig. 9b), 5. Surprise (Fig. 10).

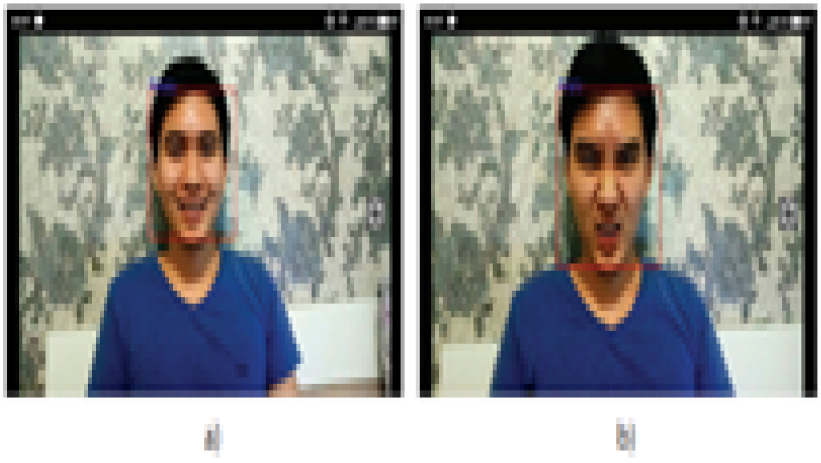

Figure 8. a) Happy. b). Angry

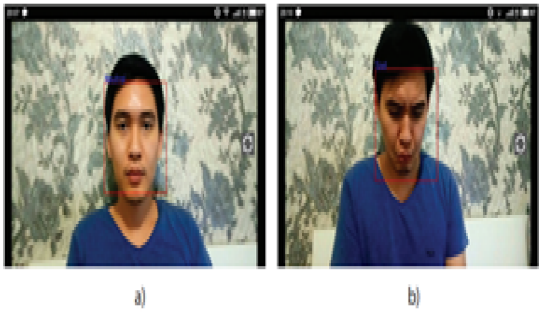

Figure 9. a) Neutral. b). Sad.

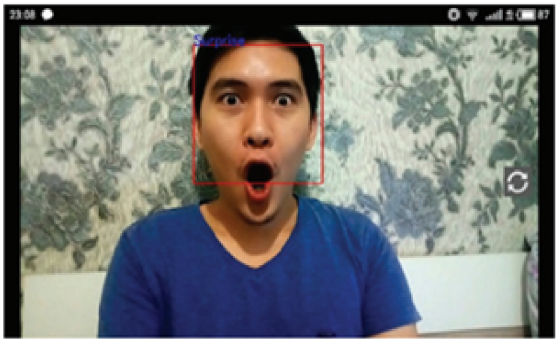

Figure 10. Surprise.

Figure 11. Surprise.

Conclusion

During the study, we achieved 70validating data. This is not a bad result for not more data. By further increasing our data, we will improve prediction accuracy.
The given approach to automatic recognition of emotions can be effectively applied in various intelligent human-machine systems. The mobile application of emotion recognition using by machine learning algorithms was developed and image processing in the video stream was accelerated.

References

1. Klette, R.: Concise Computer Vision. An Introduction into Theory and Algorithms. Springer, UK(2014).
2. Emotion Recognition Adjusts the Self-driving Car Interior to the Passenger's Mood, https://nplus1.ru/news/2019/01/07/kia-read. Last accessed 13 June 2019
3. Speech Emotion Recognition with Convolutional Neural Network, https://towardsdatascience.com/speech-emotion-recognition-with-convolutionneural-network-1e6bb7130ce3. Last accessed 19 Sept 2019
4. Chollet, F.: Deep Learning with Python. Manning Publications Co., USA(2018)
5. Data sources, https://www.kaggle.com/deadskull7/fer2013. Last accessed 11 May 2019
6. Rashid, T.: Make your own neural network. CreateSpace Independent Publishing Platform (2018)
7. Glassner, A.: Deep Learning, Vol. 1: From Basics to Practice. Kindle Edition(2018)
8. Neural network optimization methods, https://habr.com/ru/post/318970/. Last accessed 04 Jan 2017

Teaching Computer Science to Students with Disabilities*

Aibek Ibraimkulov[1,3] [0000−0002−9337−9595],
Aigerim Yerimbetova[1,2] [0000−0002−2013−1513], and
Bulat Kubekov[1] [0000−0001−8658−3742]

[1] Institute of Information and Computational Technologies CS MES RK,
[2] Kazakh Academy of Transport and Communications named after M. Tynyshpayev,
[3] Al-Farabi Kazakh National University, Almaty, Kazakhstan
{aibek_ibraimkulov,aigerian,b.kubekov}@mail.ru

Abstract The article is devoted to the analysis of the current state of the problem of integrating inclusive education into the practice of mass educational organizations. The implementation of inclusive practice in a comprehensive school is one of the pressing pedagogical problems. The adaptation of children with special needs in general education schools is better than in specialized institutions, since children also gain social experience there. In addition, it is believed that healthy children, learning together with children with special needs, develop tolerance and responsibility, and become more independent. It is important to emphasize that effective inclusive education is feasible only when the teacher knows the psychological and pedagogical features of teaching children with disabilities, is able to apply this knowledge in practice, and is aimed at success in the implementation of inclusion. The article discusses the main problems of teaching students with disabilities in the aspect of creating special conditions for the implementation of inclusion. The article also discusses teaching informatics for children with disabilities in Kazakhstan. The essence of inclusive education in the conditions of a modern school has been studied. The possibilities of using active teaching methods in computer science lessons are considered.

Keywords: education, inclusive education, children with spacial educational needs, computer science, active competences, active teaching methods, accessible environment.

Introduction

The relevance of the topic of this work is that students with disabilities should have equal potential with healthy children in getting an education. There is a need to introduce such forms of education as inclusive education, which provide the best conditions for children with disabilities. Inclusive education involves the creation of a flexible adaptive educational environment that can meet the educational needs of all students. One of the most important trends in the informatization of education is the search for

* The researches presented in this paper are supported by Grant funding for scientific and scientific and technical research for 2018-2020 MES RK (No. AP05133550)

methods, forms and training tools that provide favourable conditions for the formation and realization of the potential of the individual.

The term ”inclusive education adopted in international practice, characterizes deeper processes: the child is given not only the right to attend regular school, but for this the necessary adapted educational environment is created and support services are provided. Full inclusion means that all students, regardless of the type, severity and nature of developmental disabilities, are enrolled in the general education class, receiving, if necessary, additional services, using coeducation with healthy peers. Inclusive education is a strategic and affects the entire education system, rather than the individual elements at the level of institutions, which introduced inclusion. The main difference between an inclusive approach and an integrative one is that in ordinary schools the attitude towards children with disabilities and their parents is changing [1]. The ideology of education is shifting towards the humanization of the educational process and the strengthening of the educational orientation of the training of all its participants.

For the effective implementation of the true integration of children with disabilities in the general educational environment, it is necessary to have some prerequisites for the introduction of inclusive education, which include:

- ability to choose educational and correctional services provided by the system of general and special education;
- presence of a wide range of special educational services and special living conditions for children with disabilities in the structure of a comprehensive school, kindergarten.

The main conditions for the implementation of successful inclusive education in secondary schools are:

1. Acceptance of all principles of inclusive education and readiness for its implementation.
2. The inclusion of children in the general educational process, and not the creation of special classes.
3. Adapted curriculum, adapted grading system, adapted teaching.
4. Recognition of the right of children with special educational needs to education by all participants in the educational process (classmates, teachers, parents).
5. Comprehensive support from all specialists (defectologist, speech therapist, psychologist).
6. Provision of special technical equipment for children with special educational needs.

The international experience of inclusive education also makes it possible to talk about the possibility of expanding the educational field for people with disabilities of health of all ages. For this, lifelong education, focused on the holistic and expanded reproduction of human life, is called upon to unite various spheres of human activity around itself: from health-improving and psychological-pedagogical to communal and everyday life. This requires a fundamental review of the established ideas about the main subjects of the educational process, as well as the need to recognize changes that require new strategies in the field of education, upbringing and personality development [2].

The implementation of inclusive practice in a comprehensive school is one of the most pressing pedagogical problems. The key issue in solving this problem is the preparation of future teachers for the organization of the educational process in an inclusive learning environment. It is important to emphasize that effective inclusive education is feasible only when the teacher knows the psychological and pedagogical features of teaching children with disabilities, knows how to put this knowledge into practice, and is aimed at success in implementing inclusion. So, let's clarify the meaning of Inclusive Education.

According to the World Health Organization, "Inclusive education is based on the right of all students to receive a quality education that meets basic educational needs"[3].

The concept of "inclusive education"was formed from the belief that education is a fundamental human right and that it forms the basis for a more just society. All students have the right to education, regardless of their individual qualities or problems [4].

The world community, guided by the principle of the equal rights of all people, regardless of their racial, ethnic, gender, physical, mental and other differences, has fixed the basic principles of inclusive education in UN international legal acts.

"Inclusive education is an ongoing process of development of general education, aimed at providing quality education for all, taking into account the diversity, different needs and abilities, characteristics and expectations in teaching students and communities, eliminating all forms of discrimination"(UNESCO 2008).

In world practice, inclusive education is recognized as the most effective mechanism for ensuring equal access to education. In Kazakhstan, as in most countries of the world, they also recognize the idea that an educational institution with an inclusive orientation is the most acceptable mechanism for providing secondary education for all, while contributing to the building and development of an inclusive society in the country.

Inclusive Education in Kazakhstan

Providing all citizens with equal access to high-quality education is one of the key foundations of the educational policies of the world community.

The policy of Kazakhstan is aimed at prioritizing the rights of all citizens, regardless of their social, economic, cultural status, for quality education. In particular, in the Address of the First President of Kazakhstan Nursultan Nazarbayev to the people of Kazakhstan "Kazakhstan's Way - 2050: A Single Goal, Common Interests, Common Future"instructed "to strengthen attention to our citizens with disabilities. For them, Kazakhstan should become a barrier-free zone. It's our duty to ourselves and society to take care of these people, who are many".

The Law of the Republic of Kazakhstan "On Education"guarantees the equal rights of all to receive quality education, the availability of education at all levels for the population, taking into account the intellectual development, psychophysiological and individual characteristics of each person [5]. According to the State Education Development Program for 2011-2020. by 2020, the proportion of schools that created conditions for inclusive education will increase from a total of 70% . The share of schools in which "barrier-free access"for children with disabilities will be created will

be 20%. The percentage of children enrolled in inclusive education, of the total number of children with developmental disabilities (RIA) will be 50%[6].

Throughout the civilized world, society has come to understand that, in accordance with universal morality and the requirement of social justice, discrimination against children in education is unacceptable.

The legislation of the Republic of Kazakhstan, in accordance with international documents in the field of protecting the rights of children, introduced the concept of persons (children) with special educational needs and the principle of equal rights to receive high-quality education for all students, taking into account individual opportunities.

In accordance with the State Program for the Development of Education in our country, since 2011, inclusive education has been gradually introduced. The strategic development plan of the Republic of Kazakhstan until 2025, according to paragraph 1.1 ”Ensuring the accessibility and inclusiveness of education involves achieving the following goals:

1. Providing psychological and pedagogical support for inclusive education, creating special rooms for psychological and pedagogical support, developing curricula for secondary, technical and vocational, post-secondary education in demanding working qualifications, advanced training of teachers.

2. For people with special educational needs, work to ensure access to all levels of education, within the framework of per capita financing, an increased funding standard is provided, the state order for their training is increased [7].

The development of inclusive education requires serious psychological, methodological and methodological training of teachers.

According to the Ministry of Education and Science of the Republic of Kazakhstan: annually more than 320 special teachers take advanced training courses for working with children with special educational needs at the National Scientific and Practical Center for Corrective Pedagogy. In 2015, refresher courses on inclusive education for school teachers began on the basis of JSC NCPK ”Orleu”. Over three years, more than 3,000 people have completed courses.

Throughout the civilized world, society has come to understand that, in accordance with universal morality and the requirement of social justice, discrimination against children in education is unacceptable.

Educational methods and material and technical conditions for inclusive education

Educational methods and material and technical conditions for inclusive education. Currently, more and more Kazakhstan schools practice the inclusion of children with special educational needs in the mass classes. More and more parents of children with special educational needs want their child to attend a regular school.

According to the ”Model Rules for the Activities of Educational Institutions of Education children with special educational needs are taught in ordinary classes of comprehensive schools (no more than 2 children with special educational needs) and in special classes (by type of violation) of comprehensive schools[8].

Special classes for types of disorders in the development of children are differentiated as follows: with hearing impairment (inaudible, hard of hearing, late deaf); with visual impairment (blind, visually impaired, late blind); with impaired function of the musculoskeletal system; with speech impairment; with mental retardation; with a delay in mental development; with a disorder of the emotional-volitional sphere and behavior; with complex disorders, including deaf-blindness [9].

According to paragraph 5 of Article 8 of the Law of the Republic of Kazakhstan "On Education"for citizens who, due to health reasons, for a long time cannot attend organizations of primary, basic secondary, general secondary education, individual free education at home or in medical organizations is organized.

If a child with special educational needs appears in the classroom, then the school with the Department of Education equips its study place with the necessary furniture and equipment, provides textbooks and psychological and pedagogical support.

In order of the Minister of Education and Science of the Republic of Kazakhstan dated January 22, 2016 No. 70: "On approving the standards for equipping pre-school, secondary education, and special education organizations with equipment and furniture"a list of what schools and kindergartens should be equipped with is attached. For example, tactile tracks, classes with embossed braille (books and posters) and special lights for visually impaired children, sanitary rooms and call buttons [10].

Nowadays, in Kazakhstan has developed more than 300 training programs for children with special educational needs for families with types of violations:

1) with the hearing impaired (deaf)
2) hearing impaired (hard of hearing)
3) with visual impairment
4) with a violation of the musculoskeletal system
5) with severe speech impairment
6) with impaired intelligence
7) with impaired intelligence

As an example in our research we consider the problems of teaching computer science to children with visual impairment. Violation of the function of vision reduces visual sensations, slowing down perception. In visually impaired children, the speed of perception is halved, the recognition of objects slows down, which leads to a deterioration in memory processes, blurred perception, fragmentation, schematism, a low level of generalization and verbalism, insufficient understanding of the material being studied, and defects in speech activity. As computer technologies evolve, the electronic form of presenting information for people with visual impairment becomes more accessible, thus increasing the importance of computer typhlotechnology. Children with visual problems are divided into two groups: blind and visually impaired. In medicine, blind children are considered to be those who have completely lost the ability to visually perceive the world around them, that is, they have no light perception and light discrimination. A case with complete loss of vision is considered total or absolute blindness. Children with practical blindness are partially seeing children, because they have no impaired light perception or residual vision, which allows them to partially distinguish contours, color, light, allows them to navigate in space and is a way of acquiring information about the outside world [11].

The purpose of studying the subject ”Informatics/(or)computer science”in school is to provide students with visual impairments with basic knowledge, skills, working with a personal computer, the sound program JawsforWindows, and typhlotechnical devices for their effective use in everyday life.

JAWS, Job Access With Speech, is the world’s most popular screen reader, developed for computer users whose vision loss prevents them from seeing screen content or navigating with a mouse [12]. JAWS provides speech and braille output for the most popular computer applications on PC:

- Read documents, emails, websites and apps
- Easily navigate with your mouse
- Scan and read all of your documents, including PDF
- Fill out web forms with ease
- Easy to use with Daisy formatted basic training
- Save time with Skim Reading and Text Analyzer
- Surf the net with web browsing keystrokes.

Computer science lessons for students with visual impairments are carried out in compliance with the time interval when working at the computer for each student, taking into account the diseases of the eye analyzer and age characteristics, in the middle of the lesson, a physical education minute is held, aimed at relieving visual, muscle and tactile tension.

Exercises aimed at relieving visual stress are carried out taking into account the state of vision of students (clinical forms of visual disease, existing contraindications), the continuous duration of work at the computer should not exceed:

1) for students of grades 5-7, no more than 15 minutes with a break for a physical education minute;

2) for students of grades 8-10, no more than 20 minutes with a break for a physical training minute.

Teaching computer science is carried out in 2 stages: 1) the first stage (grades 5-7) - acquaintance with the computer and the world around it through the computer;

2) the second stage (grades 8-10) - the use of a computer by students with visual impairments as a ”white cane the formation and development of electronic communication skills and information retrieval while mastering the principles of operation of the technical equipment.

The specifics of teaching the subject ”Computer Science”for students with visual impairments is manifested in the following:

1) taking into account the general laws and specific features of the development of children with visual impairments;

2) modification of curricula and programs, increasing the duration of training, redistributing and changing educational material, while maintaining its basic content, changing the pace of its passage;

3) the use of special forms and methods of work;

4) in the special design of classrooms and classrooms, the creation of sanitary conditions, the organization of medical rehabilitation work.

A major role in inclusive education is played by computer science lessons. Schools are equipped with computer classes, educational and methodological support is being

improved, and practical work is focused on, as skills in students with limited health abilities in most cases develop more slowly than in healthy ones.

Some important requirements for an informatics lesson in schools with inclusive education can be highlighted:

• the teacher must not only know the subject matter, but also be proficient in various forms and methods of organizing the lesson, be ready to present information to children;

• it is necessary to adjust the structure of knowledge, abilities and skills in accordance with the mental and physical capabilities of both an individual student and the entire class;

• at each lesson, an individually-differentiated approach should be implemented in accordance with the capabilities of the students. For example, programming, site building, and for deaf-mute children, logic and algorithmization are difficult;

• didactic materials should correspond to the level of development of the child, the lesson should be technically equipped;

• if you are working with a computer, then the teacher needs to clearly show students the algorithm of actions;

• tasks for independent work should be given after analysis of similar examples;

• a lesson should always be started by repeating the information obtained in previous lessons;

• during training, it is necessary to focus on the practical experience of the student and on the most developed abilities, since children with disabilities have less developed logic and a less formed conceptual apparatus.

In order to provide comfortable access to education for a blind student, it is necessary to use:

1) a personal computer equipped with the Jaws for Windows sound software;

2) programs that allow you to enlarge the image (screen magnifier), background, create a contrasting image;

3) interactive whiteboard;

4) a high-quality network of open access to the Internet to ensure the exchange of data between devices and communications between participants in the educational process;

5) peripheral devices: braille printers, scanners, braille monitors, reading talking books, multimedia presentations, electronic teaching aids, subject learning systems, computer educational games, videos; 6) special textbooks with enlarged and relief-point type, containing illustrative-graphic material made in relief on a plane, phonic materials;

7) special educational supplies: braille instruments, flat writing instruments, pencils, notebooks made of thick (braille) paper; text didactic manuals, made in relief-point type; illustrative-graphic aids made in relief on a plane designed for tactile-tactile perception (for the totally blind); illustrative-graphic aids made in relief on a plane, but with a color scheme, designed for visual-tactile perception (for students with residual vision) [13].

If children with visual impairment are studying at the school, the school administration must create an adaptive educational environment, apply adapted programs, and use additional didactic material for children with visual impairment. We show the technical infrastructure for teaching computer science to children with visual impairments in the form of a table. (See Table 1).

Table 1. Technical solutions for people with visual impairments

No	Types	Kinds	Description
1	Computer complex for visually impaired	Personal Computer, Screen readers, Video enlarger, Speech synthesizer, Reading devices	Allows you to work with graphic, text and printed information. The use of the complex helps students to view teaching aids in a convenient form and participate in the workflow on an equal basis with others
2	Electronic video enlarger	Stationary, Manual, Portable	Allows you to read literature, view illustrations and graphics
3	Study guides and writing materials		Help to organize the educational process in accordance with the standard school curriculum. All text information is duplicated in Braille. Convenient for use, both in class and at home to consolidate the knowledge gained
4	A device for listening to educational audio aids	Portable tiflo player	Helps students to better memorize educational material. Large memory capacity and an intuitive interface make using the device convenient and comfortable

Using active teaching methods in computer science lessons

Active teaching methods are methods that encourage students to actively think and practice in the process of mastering the educational material. Active learning involves the use of such a system of methods, which is aimed at mastering students' knowledge and skills in the process of active thinking and practical activity. Each method is made active by the one who uses it. Currently, the following active teaching methods are most common:

• practical experiment;

• method of projects - a form of organization of the educational process, focused on the creative self-realization of the student's personality, the development of his intellectual and physical abilities, volitional qualities and creative abilities in the process of creating new products that have objective or subjective novelty and have practical significance;

• group discussions - group discussions on a specific issue in relatively small groups of students (from 6 to 15 people);

• brainstorming is a specialized method of group work aimed at generating new ideas, stimulating the creative thinking of each participant;

• business games - a method of organizing the active work of students, aimed at developing certain recipes for effective educational and professional activities;

• role-playing games - a method used to assimilate new knowledge and practice certain skills in the field of communication. A role-playing game involves the participation of at least two "players each of whom is invited to conduct targeted communication with each other in accordance with a given role;

• basketball method - a teaching method based on simulating situations. For example, the trainee is offered to act as a tour guide in a museum of computer technology. In the materials for the preparation, he receives all the necessary information about the exhibits presented in the hall;

• trainings - training, in which, in the course of living or modeling specially assigned situations, students have the opportunity to develop and consolidate the necessary knowledge and skills, to change their attitude to their own experience and approaches used in work;

• training using computer training programs;

• analysis of practical situations (case-study) - a method of teaching skills) - a method of teaching decision-making skills; its goal is to teach students to analyze information, identify key problems, generate alternative solutions, evaluate them, choose the best solution and form action programs.

Basic methodological principles of active learning:

- careful selection of working terms, educational, professional vocabulary, conventions;

- a comprehensive analysis of specific practical examples of some activities in which students perform different role functions;

- support by all students of continuous visual contact with each other;

- performing at each lesson by one of the students the function of a leader (leader), who initiates and orients the discussion of the educational problem

- active use of technical teaching aids, in particular tables, slides, films, videos, video clips, video equipment, with the help of which educational material is illustrated;

- constant support by the teacher of active intragroup interaction, relieving tension in relations between participants;

- prompt intervention of the teacher in the course of the discussion in case of unforeseen difficulties, as well as in order to explain the new provisions of the curriculum;

- intensive use of individual lessons (self-diagnostic or creative homework) and individual abilities in group lessons;

- organization of the spatial environment - ”playing field which should contribute to the psychological comfort of the student (for example, discussion within teams or intergroup discussion)

Currently, many educational games have been created that are used in working with students with disabilities, which allow you to select exercises depending on the level of development of the student, and not his age. Special exercises develop visual memory, attention, thinking. Computer games increase interest in the content of educational material, thereby increasing interest in the learning process, contribute to the development of self-control skills and independent work.

The peculiarity of interactive methods is that you can use various methods and forms, regardless of the type of lesson and the stage of the lesson. At the same time, individual, pair and group work is organized, project work, role-playing games are used, work is carried out with documents and various sources of information. In addition, such innovative technologies are used as electronic multimedia textbooks and study guides, electronic educational resources: interactive presentations, tests, etc.

The lesson of computer science, unlike many other school disciplines, should be conducted not only with an orientation towards the assimilation of theoretical knowledge by students, but also the development of practical skills and abilities. Therefore, the practical part is an important stage of the lesson. It is organized in such a way that students independently perform work, conduct research by highlighting the elements of action that are essential for the performance of a specific task, which contributes to further generalization and implementation of the transition from student assessment to self-assessment and reflection. At this stage of the lesson, you can use discussion, work in pairs, in groups. This approach to the organization of educational activities makes it possible to form students’ skills to carry out a targeted search for information and use for this various information and analytical sources; the ability to use ICT tools to organize interaction; ability to identify stages and operations in problem solving technology.

The systematic use of active teaching methods in computer science lessons entails constant activity of students, the emotional response of students to the learning process, motivation of educational activities, interest in mastering new knowledge, skills and their practical application in comparison with traditional teaching methods increases.

Conclusion

The use of information technologies in working with children with disabilities contributes to the development of existing capabilities, is aimed at reducing deficiencies in cognitive activity and the formation of personal qualities. The computer helps the child acquire such knowledge, skills and abilities, with the help of which he can socially adapt. Ensuring a good result in mastering the subject and facilitating the lesson is facilitated by the availability of universal technical means in classrooms where children with various types of disabilities are trained:

1. Special keyboards (differ from standard keyboards in size, more contrasting color of characters, distance between keys). Various modifications are adapted for different physical characteristics.

2. Interactive computer board with a projector. Multifunctional work surface for joint education of children with different health conditions. Used for writing, drawing, doing exercises, making presentations, watching movies.

For the teacher, the main problem in the lesson is to correlate the individual capabilities of children with disabilities with the need to meet the educational standard. When developing informatics lessons in an inclusive class, both general educational tasks (meeting educational needs within the framework of the state standard) and correctional and developmental tasks should be taken into account. There are many active forms and methods of teaching. It is necessary to select such methods taking into account the age category of the group, class, their life experience and knowledge, remembering that children like non-standard approaches. And if you add ”the most necessary thing”to the lesson, that is, activate students to learning, arouse interest - then the result will be much better. So at the end of this article, let’s summarize the results of principles of inclusive education. Inclusive education includes a number of important values:

• recognition for society of the equal value of all students and teachers;

• increasing the degree of participation of all students in the school in all aspects of school life and at the same time reducing the level of isolation of some groups of students;

• changing the teaching methods of the school so that the school can fully meet the diverse needs of all students living near the school;

• analysis, study and overcoming barriers to knowledge and full participation in school life for all students of the school, and not just for those with disabilities or special educational needs;

• implementation of reforms and changes aimed at the benefit of all students of the school as a whole, and not just any one group;

• differences between students are resources that contribute to the pedagogical process, not obstacles to be overcome;

• recognizing the role of schools not only in improving the academic performance of students, but also in the development of social values of local communities;

• recognition that inclusion in education is one of the aspects of inclusion in society.

References

1. Nazarova, N.M.: Modern Vector of Development of Continuous Inclusive Education. Bulletin of the Perm State Humanitarian and Pedagogical University. **1**, 104–109 (2017)
2. Yuryeva, A.A.: The use of interactive technologies in inclusive education. Young scientist. **16**, 322–323 (2018)
3. World Disability Report 2011
4. Open dossier on inclusive education. UNESCO 2003
5. The Law of the Republic of Kazakhstan "On Education"http://online.zakon.kz/Document/?doc_id=30118747 Last accessed 19 Sep 2020
6. The state program for the development of education in the Republic of Kazakhstan for 2011-2020. http://adilet.zan.kz/rus/docs/U1000. Last accessed 19 Sep 2020
7. Strategic Plan for the Development of the Republic of Kazakhstan until 2025 (Decree of the First President of the Republic of Kazakhstan dated February 15, 2018, No. 636)
8. Demkina, T.O.: Integration of children with disabilities into mainstream schools Integratsiya detey s ogranichennymi vozmozhnostyami zdorov'ya v obshcheobrazovatel'nuyu shkolu. School pedagogy Shkol'naya pedagogika. **4**(7), 26–28 (2016) https://moluch.ru/th/2/archive/42/1177/. Last accessed 20 Sep 2020
9. Law "On social and medical-pedagogical correctional support for children with disabilities". http://adilet.zan.kz/rus/docs/Z020000343. Last accessed 21 Sep 2020
10. On approval of standards for equipping equipment and furniture for organizations of preschool, secondary education, as well as special educational organizations. Order of the Minister of Education and Science of the Republic of Kazakhstan dated January 22, 2016 No.70. http://adilet.zan.kz/rus/docs/V1600013272. Last accessed 19 Sep 2020
11. Vartapetova, G.M.: Features of teaching children with visual impairment. MyDox.ru. https://mydocx.ru/3-77679.html. Last accessed 19 Sep 2020
12. From official site of Freedom Scientific https://www.freedomscientific.com/
13. A typical curriculum for the academic subject "Informatics"for students with visual impairments (blind and visually impaired) 5-10 grades of the level of basic secondary education according to the updated content. https://special-edu.kz/oop.html. Last accessed 20 Sep 2020

High Performance 3D Simulator of Turbulent Reacting Flows*

Medet Inkarbekov[1 [0000−0001−8646−2916]] and
Aidarkhan Kaltayev[1 [0000−0003−2180−2785]]

Satbayev University, Almaty, Kazakhstan
info@satbayev.university

Abstract A new GPU-accelerated computational methodology is developed for large eddy simulation (LES) of turbulent reacting flows. The effect of chemical reactions is modelled via the filtered density function (FDF) sub-grid scale model. The base filtered flow equations are solved by a discontinuous Galerkin (DG) method. The FDF transport equation is solved numerically by a particle based Lagrangian Monte Carlo (MC) method. The computational methodology is developed in a manner suitable for GPU computing. The parallel algorithm is implemented by the means of CUDA technology. The consistency and the accuracy of the methodology are demonstrated by simulations of a temporally developing mixing layer, under both non-reacting and reacting conditions.

Keywords: GPU computing, Large eddy simulation, Filtered density function, Monte Carlo, Discontinuous Galerkin.

Introduction

Since the time of Osborne Reynolds (over a century ago), there was a need to develop accurate methods for predicting the behavior of chemically passive and reactive turbulent flows [1]. Large eddy simulation (LES), as it is now widely believed, is the optimal means of capturing the detailed, unsteady physics of such flows [2]. The successful implementation of LES depends on two factors: first, how accurately the subgrid scale (SGS) quantities are modeled; second, and how accurately these models are solved using numerical methods. In the former, we use the filtered density function (FDF) methodology [3] that has proven to be most effective for closing the system of equations of LES. The main advantage of FDF is that after its application, the source of chemical reactions in the transfer equation of scalar variables is obtained in a closed form. In the latter, we use the discontinuous Galerkin (DG) method in combination with the Monte Carlo (MC) method. The DG combines versatility of the finite volume (FV) discretization with the accuracy of spectral approximations. The MC is free of numerical diffusion; thus it is especially suitable for turbulent flow calculations.

Such a combination of mathematical and numerical modeling provides reliable prediction of turbulent flows. However, this approach is computationally demanding,

* This work is sponsored by the Ministry of Education and Science of Republic of Kazakhstan under [grant numbers AP05135365 and BR05236316]

especially when finite-rate kinetics are to be captured [4]. The reason for this is the huge number of particles in the MC method, which is on the order of millions to billions of particles. Even so, the computational requirements for the proposed LES, in its most sophisticated form, and utilizing the highest resolution will be several orders of magnitude less than required for direct numerical simulations.

The simulation time for applied problems using the proposed LES / FDF model using sequential code reaches order of months, sometimes might reach order of several years [4]. Therefore, the use of parallel technology is required [5]. Parallel code can be adapted on computing systems based on a CPU (central processing unit) and / or on a GPU (graphics processing unit). It is known that the GPU has a number of advantages over the CPU. The main one is its cost.

In our work, we develop a new highly efficient large eddy simulator of complex turbulent flows. To achieve high efficiency, the hybrid DG-MC scheme and the FDF model will be coupled in a computational package which facilitates massively parallel large scale simulations using GPUs. The success of the simulator as demonstrated in this work ensures its further extension and applications for LES of complex turbulent combustion problems.

Modeling

We consider an incompressible, isothermal, turbulent reacting flow involving N_s species [6]. The transport parameters are denoted by: the velocity vector components $u_i(\mathbf{x},t)$, where $\mathbf{x}$ and t denote space and time, respectively; the pressure $P(\mathbf{x},t)$, and the species mass fractions $\phi_\alpha(\mathbf{x},t)$ ($\alpha = 1,2,\ldots,N_s$). The chemical reaction source terms $S_\alpha \equiv S_\alpha(\boldsymbol{\phi}(\mathbf{x},t))$ are functions of compositional scalars ($\boldsymbol{\phi} \equiv [\phi_1,\phi_2,\ldots,\phi_{N_s}]$). Implementation of LES involves the use of the spatial filtering operation [7] $\langle Q(\mathbf{x},t)\rangle_L = \int_{-\infty}^{+\infty} Q(\mathbf{x}',t)G(\mathbf{x}',\mathbf{x})d\mathbf{x}'$, where $G(\mathbf{x}',\mathbf{x}) \equiv G(\mathbf{x}'-\mathbf{x})$ denotes a filter function of width Δ_G, and $\langle Q(\mathbf{x},t)\rangle_L$ is the filtered value of the transport variable $Q(\mathbf{x},t)$. After applying the filter function to the basic transport equations, we get $\Sigma_{ij} = \langle u_i u_j\rangle_L - \langle u_i\rangle_L \langle u_j\rangle_L$ and $M_j^\alpha = \langle u_j\phi_\alpha\rangle_L - \langle u_j\rangle_L \langle\phi_\alpha\rangle_L$, the subgrid scale (SGS) stresses and the mass fluxes, respectively. Hydrodynamic closure associated with the subgrid stresses and the subgrid mass fluxes are modelled by the standard Smagorinsky [8] model. The subgrid stress is modelled via $\Sigma_{ij} - (\delta_{ij}/3)\Sigma_{kk} = -\nu_t\left(\frac{\partial\langle u_i\rangle_L}{\partial x_j} + \frac{\partial\langle u_j\rangle_L}{\partial x_i}\right)$, while the subgrid mass flux is modelled via $M_j^\alpha = -\Gamma_t\frac{\partial\langle\phi_\alpha\rangle_L}{\partial x_j}$. Here, ν_t is the subgrid kinematic viscosity, $\Gamma_t = \frac{\nu_t}{Sc_t}$ is the subgrid diffusion coefficient, where Sc_t is the subgrid Schmidt number. Accordingly, the subgrid kinematic viscosity is $\nu_t = C_s\Delta_G^2\sqrt{\langle S_{ij}\rangle_L \langle S_{ij}\rangle_L}$, where $\langle S_{ij}\rangle_L$ is resolved strain rate tensor and C_s is a model constant. In reacting flows, an additional model is required for the filtered chemical reaction term. For closing that, we use the modelled FDF transport equation [3]:

$$\frac{\partial F_L}{\partial t} + \frac{\partial[\langle u_j\rangle_L F_L]}{\partial x_j} = \frac{\partial}{\partial x_j}\left[(\Gamma+\Gamma_t)\frac{\partial F_L}{\partial x_j}\right] + \frac{\partial}{\partial\psi_\alpha}\left[\Omega_m(\psi_\alpha - \langle\phi_\alpha\rangle_L)F_L\right] - \frac{\partial[S_\alpha F_L]}{\partial\psi_\alpha} \tag{1}$$

where F_L is the FDF and ψ_α represents the scalar array in the sample space. In this model, $\Omega_m = C_\phi (\Gamma + \Gamma_t)/\Delta_G^2$ is the SGS mixing frequency and C_ϕ is a model constant.

Numerics

The system of filtered flow equations are solved via a hybrid DG-MC scheme. In this scheme, the computational domain is discretized into structured rectangular elements. All hydrodynamic variables are determined by the DG method on the elements, while the set of SDEs is solved by the MC.

For the spatial discretization, for a given conservation law

$$\frac{\partial q_h^k(\mathbf{x},t)}{\partial t} + \nabla \cdot \mathbf{f}_h^k(q_h) = 0, \tag{2}$$

it is assumed that the local solution q_h^k and local flux $\mathbf{f}_i^k$ in the element with volume D^k are expressed in the modal form as

$$\mathbf{x} \in D^k : q_h^k(\mathbf{x},t) = \sum_{i=1}^{Nm} \overset{\square^k}{\mathrm{q}}_i(t)\varphi_i(\mathbf{x}),\ \mathbf{f}_h^k(q_h(\mathbf{x},t)) = \sum_{i=1}^{Nm} \overset{\square^k}{\mathbf{f}}_i(t)\varphi_i(\mathbf{x}). \tag{3}$$

Here, k is the element number, $\overset{\square^k}{\mathrm{q}}_i$ and $\overset{\square^k}{\mathbf{f}}_i$ are the modes and $\{\varphi_i(\mathbf{x})\}_{n=1}^{Nm}$ are the polynomial basis of the order p. Nm denotes the number of the modes in the local expansion and can be calculated as a function of polynomial of order p:

$$Nm = \frac{(p+1)(p+2)}{2}.$$

Equation (2) is multiplied by a smooth test function, $v_h \in V_h$, where V_h is the space of all piece-wise polynomial functions. This results in the following DG scheme in weak form:

$$\int_{D_k} \left(\frac{\partial q_h^k}{\partial t} v_h - \mathbf{f}_h^k(q_h) \cdot \nabla v_h \right) d\mathbf{x} = -\int_{\partial D_k} \overset{\square}{\mathbf{n}} \cdot \mathbf{f}^* v_h d\mathbf{x}. \tag{4}$$

Here, $\overset{\square}{\mathbf{n}}$ denotes the normal and $\mathbf{f}^*$ is the numerical flux that is calculated using a Riemann solver. As a set of basis and test functions, Legendre polynomials are chosen and employed in conjunction with Gaussian quadrature points:

$$M_{ij}^k \frac{\mathrm{d}\overset{\square^k}{\mathrm{q}}_i(\mathrm{t})}{\mathrm{d}t} - \mathbf{S}_{ij}^k \cdot \overset{\square^k}{\mathbf{f}}_i(t) = -\int_{\partial D_k} \overset{\square}{\mathbf{n}} \cdot \mathbf{f}^* \varphi_i(\mathbf{x}) d\mathbf{x}, \tag{5}$$

where M_{ij}^k are elements of the mass matrix and $\mathbf{S}_{ij}^k$ are elements of the stiffness matrices:

$$M_{ij}^k = \int_{D_k} \varphi_i(\mathbf{x})\varphi_j(\mathbf{x}) d\mathbf{x}, \quad \mathbf{S}_{ij}^k = \int_{D_k} \varphi_i(\mathbf{x}) \nabla \varphi_j(\mathbf{x}) d\mathbf{x}. \tag{6}$$

Equation (1) can be solved effectively via Lagrangian Monte Carlo (MC) scheme, where FDF is represented by an ensemble of computational particles, each with a set of scalars $\phi_\alpha^+(t) = \phi_\alpha^+(X_i(t), t)$ and Lagrangian position vector X_i^+. This information is updated via temporal integration of the stochastic differential equations (SDEs) [7]:

$$dX_i^+(t) = \left[\langle u_i \rangle_L + \frac{\partial(\Gamma + \Gamma_t)}{\partial x_i}\right] dt + \sqrt{2(\Gamma + \Gamma_t)}\, dW_i(t), \tag{7}$$

$$d\phi_\alpha^+ = -\Omega_m \left(\phi_\alpha^+ - \langle \phi_\alpha \rangle_L\right) dt + S_\alpha(\boldsymbol{\phi}^+)\, dt, \tag{8}$$

where W_i denotes the Wiener-Lévy process [10]. By doing so, the position of the MC particles are updated due to drift and diffusion (random walk) and their compositions are modified due to mixing and chemical reaction. Eqs. (7)-(8) are integrated by the Euler-Maruyamma scheme. The filtered quantities are constructed on LES quadrature points by averaging over the particles within the ensemble domain as

$$\langle g \rangle_E \equiv \frac{1}{N_E} \sum_{n \in \triangle_E} g^{(n)}, \tag{9}$$

where N_E denotes the number of MC particles residing within an ensemble domain of characteristic length $\triangle_E$ centered around each DG quadrature point. The particle variable $g^{(n)}$ denotes the information carried by nth MC particle pertaining to transport variable g.

Parallel Implementation

The parallel algorithm of the DG-MC solver is implemented using the PGI CUDA Fortran Compiler, and the calculations were carried out using an NVIDIA GTX 1080Ti video card. This graphics processing unit (GPU) is equipped with 3584 CUDA cores with a clock speed of 1582 MHz each. And also the device has 11 GB of memory with a bandwidth of 484 Gbps and a memory bus bandwidth of 352 bits.

In CUDA programming, the most important aspect is memory handling. The GPU device is equipped with five types of memory. First, global memory, as its name suggests, is available to all threads running on the device. It is the most voluminous, and the data stored here exists throughout the application. The second is shared memory available to all threads belonging to the same thread block. The device erases all data stored in shared memory after the kernel finishes executing. The latter is much faster than global memory due to its on-chip location, so its latency is about 10-15 times lower than the latency of uncached global memory. Shared memory capacity can be configured up to 48KB per streaming multiprocessor to avoid inefficient global memory access. The third type of memory is persistent memory, which offers one alternative to global memory when high bandwidth global access is required. Persistent memory is very limited, 64KB, and as the name implies, it is used for data that remains unchanged throughout the run. The other two memory types, register memory and texture memory, were not used in this project. When dealing with global memory, grouping accesses can

greatly improve computational efficiency. There is a term called warping, which is a collection of threads that execute according to the SIMT (single instruction, multiple-thread) principle. Every instruction on a device is part of a thread framework, and all threads belonging to that framework execute this instruction synchronously. Grouping in deformation is important not only from a computational point of view, but also from a global memory access point of view. Maximum performance is achieved when the threads belonging to the warp access the data using the minimum number of transactions.

To optimize memory allocation, reading and writing data from / to global memory must be implemented in a concatenated manner. The CUDA language was designed to work with data structures of predictable size. Therefore, arrays of data structures of constant size are used in the calculations. Because a perfect union requires access to data within 32 contiguous elements in global memory for each load, the data is stored in arrays that are a factor of 32. When all threads need to access the same constant variable, persistent memory is used. If variables are reused, they are cached in shared memory.

The detailed strategy of the implementation of the parallel DG and MC via CUDA is given in our previous work [5].

Simulations

Flow configuration

The effectiveness of the developed numerical methodology demonstrated via LES of a temporally developing mixing layer. Initially, this layer consists of two parallel streams flowing in opposite directions at the same absolute speed. In notation, x corresponds to the fluid flow in the longitudinal direction, y and z - to the transverse directions. The velocity components in these directions are designated as u and v, w, respectively.

The flow variables are normalized with respect to the half initial vorticity thickness, $L_r = [\delta_v (t = 0)/2]; \delta_v = \Delta U/|\partial\overline{\langle u\rangle}/\partial y|_{max}$, where $\overline{\langle u\rangle}$ is the Reynolds averaged value of the filtered stream-wise velocity and ΔU is the velocity difference across the layer. The reference velocity is $U_r = \Delta U/2$. The Reynolds number based on the reference velocity and length scales is $Re = 200$. Both non-reacting and reacting temporally developing mixing layer problems are considered. In the former, the trace of a passive scalar ϕ is considered. This is again initialized as a hyperbolic tangent profile with $\langle\phi\rangle_L = 1$ and 0 on the top and bottom streams, respectively. In the reacting case, an irreversible, second-order reaction scheme of type $\mathcal{A} + \nu\mathcal{B} \rightarrow (\nu + 1)\mathcal{P}$ is considered. The reactant conversion is governed by $S_A = -k_r AB$, where k_r is the reaction rate constant; and A, B denote the mass fractions of the two reactants, so the set of scalars takes form ($\boldsymbol{\phi} \equiv [\phi_1, \phi_2] = [A, B]$). In this case, the reactants are initialized such that $A \equiv \phi$ (as described above), and $B = 1 - A$. The stoichiometric coefficient is unity. The rate of reactant conversion is parameterized by the Damköhler number, $Da = k_r L_r/U_r$. Simulations are conducted with relatively slow ($Da = 10^{-2}$), moderate ($Da = 1$) and relatively fast ($Da = 10^2$) reactions.

Flow Physics

This section presents the results of simulations that reflect the consistency, convergence and predictive capabilities of the developed numerical methodology. The overall

consistency of the DG-MC hybrid scheme is best achieved by comparing the first two moments of the scalar functions obtained by the FDF with those obtained directly through the DG on the same grid. The chemical source values are calculated purely using MC and then used in the DG solution of the filtered scalar equations.

Numerical implementations of DNS and LES calculations are carried out. The main flow parameters are the Reynolds number and the Damköhler number. All DG calculations were performed on a structured grid with a constant integration step over all spatial coordinates ($\triangle x = \triangle y = \triangle z$). DNS calculations were carried out with Re = 200 and on a $128 \times 128 \times 128$ grid and with an approximation order of p = 2. FDF and LES-DG calculations are carried out on a coarser mesh with the resolution $32 \times 32 \times 32$ with different values of the order of the polynomial p. Figures 1 and 2 show comparisons of the contours and iso-surfaces of the scalar $\langle \phi_\alpha \rangle_L$ obtained using MC with the results obtained using DG. These figures clearly demonstrate the consistency of the FDF simulations as the MC results agree with the DG results. It can also be seen here, as we stated earlier, compared to DG, the MC results have no numerical diffusion.

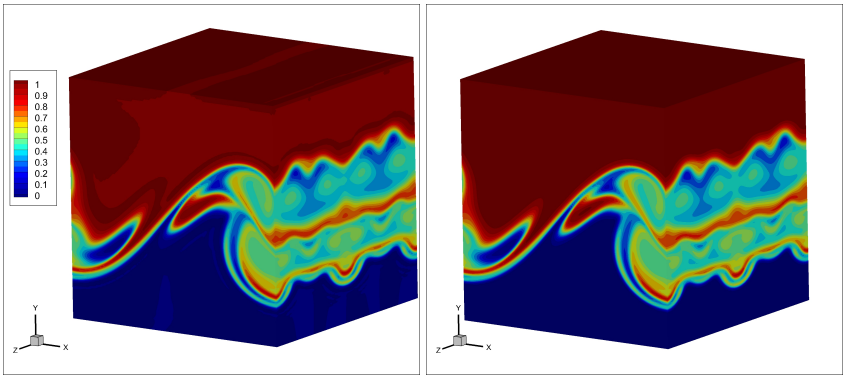

(a) (b)

Figure 1. Contour plots of the filtered scalar field for $p = 2$ at $t = 60$. (a) DG, (b) MC.

A quantitative comparison of the first two moments obtained with DG and MC is presented in Figure 3 by the means of correlation diagrams. For both moments, the correlation coefficient is very close to unity, which indicates a high consistency of FDF and LES-DG calculations.

Calculations of Reynolds-averaged subgrid variance, resolved variance and total variance are shown in Figure 4. Analysis of the results leads to the conclusion that about 78% of the total energy is resolved directly, and the rest is modelled. The total flow energy is determined with high accuracy even at a value of the order of the approximation polynomial $p = 2$. This is evidenced by the third figure, which compares the results obtained with the FDF-MC and LES-DG with the DNS results.

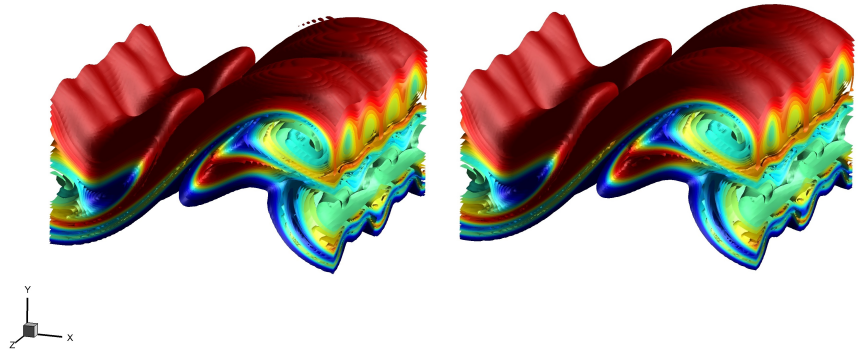

(a) (b)

Figure 2. Iso-surfaces of the filtered scalar field for $p = 2$ at $t = 60$. (a) DG, (b) MC.

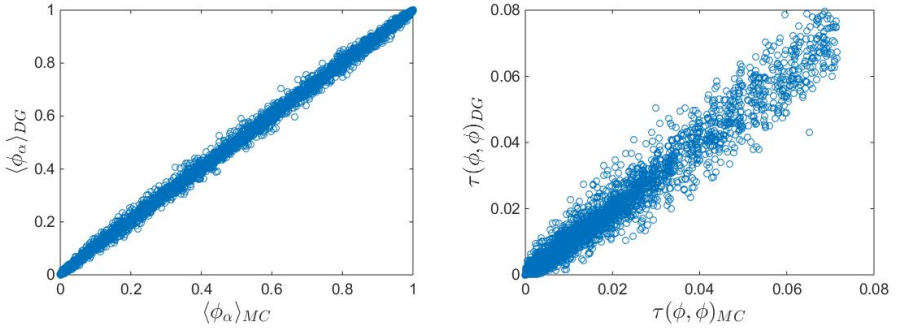

(a) (b)

Figure 3. Scatter plot of the filtered values as obtained by MC vs. those obtained by DG. (a) filtered scalar, the correlation coefficient is 0.99967. (b) second-order SGS moment, the correlation coefficient is 0.99302.

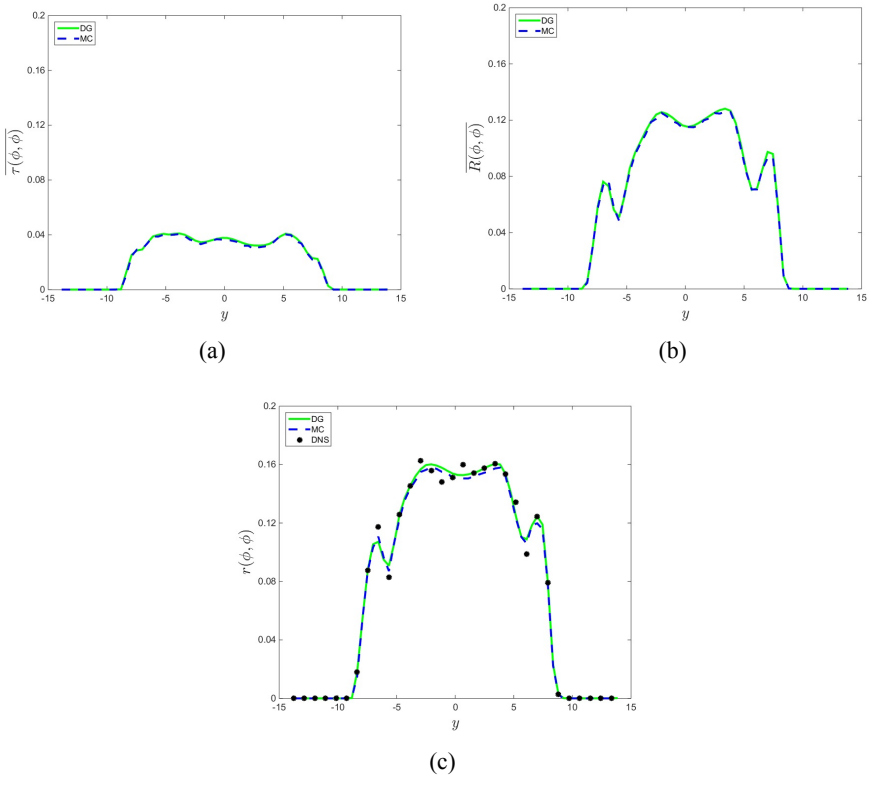

Figure 4. Cross-stream variation of the Reynolds averaged values. (a) SGS scalar variance, (b) resolved scalar variance, (c) total variance.

Computational Capabilities

This subsection demonstrates the computational capabilities of the DG-MC parallel solver.The performance of a parallel algorithm is estimated by calculating the average number of floating point operations per second (FLOPS). Figure 5 shows the results of tests where the grid size Ne and the number of particles at each quadrature point NPQ are fixed, and the value of the polynomial order p varies from 1 to 4. It is observed that when the value of p is higher, the performance of the algorithm increases monotonically. The average number of GFLOPs performed is heterogeneous for both DG and MC. The maximum value of GFLOPs for DG takes place at $p = 3$ and is 203; at the same time, for MC, the maximum is taken at $p = 4$ and is 255. You can also notice that the overall performance plateau is reached after $p = 3$.

Figure 6 shows the results of tests where the polynomial order p and the number of particles at each quadrature point NPQ are fixed, and the mesh resolution changes from 32^3 to 160^3. It is observed that the scalability increases monotonically as Ne value gets higher. In this case the maximum value of GFLOPs for DG takes place at 128^3 and is 211; at the same time, for MC, the maximum is also taken at 32^3 and is 248. The theoretical peak compute bandwidth of the GPU device is 354 GFLOPs in double precision. As it is shown, for the given computational parameters, the solver may achieve nearly 70% of the overall device arithmetic throughput.

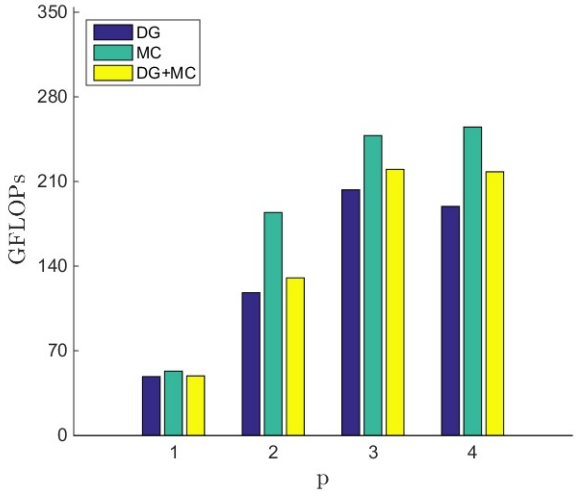

Figure 5. Effect of the polynomial degree p on the Speedup Factor at fixed $32 \times 32 \times 32$ and $NPQ = 32$.

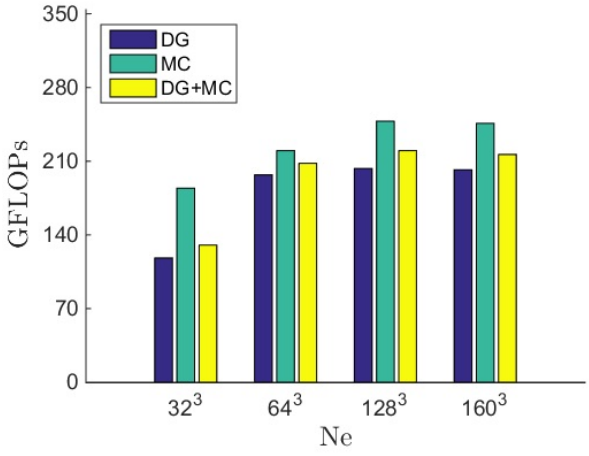

Figure 6. Effect of the mesh resolution Ne on the Speedup Factor at fixed $p = 2$ and $NPQ = 32$.

Conclusion

In this paper, a new high-performance computational methodology is developed for large eddy simulation of reacting turbulent flows. The effects of chemical reactions are modelled via the filtered density function (FDF) methodology. For the numerical solution of the base filtered flow equations the discontinuous Galerkin method (DG) is used. The FDF transport equation is solved numerically using the Lagrangian Monte Carlo (MC) method. The hybrid DG-MC algorithm is designed in such a way that it can be implemented using parallel computations. The parallel version of the code is implemented using the CUDA technology. This significantly expands the range of reacting turbulent flow problems available for numerical study for researchers.

The overall performance of the methodology is estimated by large eddy simulation (LES) of two- and three-dimensional temporally mixing layer under both chemically passive and reactive turbulent flows. The predictive ability is demonstrated by comparison of the Reynolds-averaged statistics with experimental data and show excellent agreements. This illustrates the capability of the gpu-accelerated solver, based on the DG and MC methods, for LES of complex flows, and warrants future applications of the methodology for LES of practical problems.

References

1. Reynolds, O.: An experimental investigation of the circumstances which determine whether the motion of water shall be direct or sinuous, and of the law of resistance in parallel channels. Philosophical Transactions of the Royal Society of London **174**, 935 –- 982 (1883)
2. Ansari, N., Jaberi, F. A., Sheikhi, M. R. H. and Givi P.: Filtered density function as a modern cfd tool. Engineering Applications of Computational Fluid Dynamics **1**, 1 –- 22 (2011)

3. Givi, P. Filtered density function for subgrid scale modeling of turbulent combustion. AIAA J. **44** (1),16-–23 (2006)
4. Pisciuneri, P. H., Yilmaz, S. L., Strakey, P. A. and Givi, P.: An irregularly portioned FDF simulator. SIAM J. Sci. Comput.**35**, 438 -– 452 (2013)
5. Inkarbekov, M., Aitzhan, A., Kaltayev, A. and Sammak, S.: A GPU-Accelerated Filtered Density Function Simulator of Turbulent Reacting Flows. International Journal of Computational Fluid Dynamics **34**(6), 381–396 (2020)
6. Colucci, P. J., Jaberi, F. A., Givi, P. and Pope, S.: Filtered density function for large eddy simulation of turbulent reacting flows. Physics of Fluids **10** (2), 499–-515 (1998)
7. Pope, S. B.: Turbulent Flows. Cambridge University Press, Cambridge, U.K. (2000)
8. Smagorinsky, J.: General circulation experiments with the primitive equations. I. The Basic Experiment. Monthly Weather Review **91**, 99 -– 164 (1963)
9. Author, A.-B.: Contribution title. In: 9th International Proceedings on Proceedings, pp. 1–2. Publisher, Location (2010)
10. Karlin, S. and Taylor, H. M.: A second course in stochastic processes. Academic Press., New, York (1981)

Spatial Analysis of the Earthquakes Distribution in Kazakhstan for Risk Mapping

Makhaba Karmenova[1][0000−0002−3028−9461],
Aizhan Tlebaldinova[2][0000−0003−1271−0352],
Muratkan Madiyarov[2][0000−0002−9890−0589], and
Zheniskul Zhantassova[2][0000−0001−5550−7587]

[1] D. Serikbayev East Kazakhstan Technical University, Kazakhstan
[2] S. Amanzholov East Kazakhstan University, Kazakhstan
kense@vkgu.kz
http://www.vkgu.kz

Abstract The article presents the results of a study on data analysis of recorded seismic events, earthquakes using data mining tools. The research was carried out in two stages. At the initial stage, statistical processing of the data of recorded seismic events was carried out. The quantitative results of the distribution of earthquakes over time intervals are obtained, and graphs of the earthquake density by magnitude classes are also constructed. At the next stage, a visual analysis of the geospatial points of earthquakes by magnitude classes was carried out and the sources belonging to the territory of the Republic of Kazakhstan were determined. This kind of research will be useful when updating seismic zoning maps when designing modern construction, as well as for conducting a more in-depth and comparative analysis of data with accumulated historical data on earthquakes. Besides, the obtained research results will be used in further data analysis to build earthquake clusters using machine learning methods.

Keywords: Data mining, Statistical data analysis, Spatial analysis, Visualization.

Introduction

The issues of modern construction in conditions of seismic risk remain relevant to this day. In this kind of research, the initial and most important necessary information for the study is the data on the earthquakes themselves. A detailed study of earthquake data is of great interest not only for seismologists but also for specialists in the field of earthquake-resistant construction. Earthquakes are earth-shaking events due to the sudden release of energy in the earth that is marked by the breaking of rock layers in the earth's crust. The accumulation of earthquake energy is generated from the movement of tectonic plates [1]. As you know, the territory of the Republic of Kazakhstan is subject to seismic impacts with an intensity of 9 or more points (on the MSK-64 scale). Besides, in the past, there were facts about several strong and catastrophic earthquakes. To prevent large losses from earthquakes, the accumulated historical data about them are investigated and seismic risk maps are updated. In this regard, there is a need for a thorough study and analysis of the spatial data on earthquakes recorded in the Republic

of Kazakhstan. The structure of the article consists of the main sections, which present important aspects of the research.

Related works

Intelligent analysis of recorded seismic events plays an important role especially in those countries where earthquakes are most common [1,3,4]. There is a large number of works in which the methods of spatial data mining are used for the analysis of seismic events. In this context, the application of the geostatistical approach will make it possible to carry out spatial and statistical correlation between various factors [2]. In [6], using the methods of space-time clustering and using the algorithms of associative links, a new system for the analysis of causal relationships in the distribution of earthquake data was developed for mapping the risks of the regions of Indonesia. The system extracts earthquake data and transforms it into transaction data, performs mining association rule using A-Priori algorithm and finds interesting patterns, then visualizes into risk mapping. A similar application of spatial analysis to data on earthquake points can be seen in [7]. In [8], a spatial analysis of the earthquake epicentres in the northwest of Ankara is carried out. The research was carried out in two stages. At the first stage, the spatial distribution of earthquake epicentres of the last decade is analyzed. At the second stage, the relationship between earthquake epicentres and faults in the region under study is analyzed using GIS methods to predict segments of probable faults in which earthquakes may occur. Spatial statistical analysis to the epicentres of earthquakes in Kyrgyzstan and its environs was carried out by the authors of [3]. The researchers also identified clusters by magnitude using the mid-centre and directional distribution methods. This paper [4] present geostatistical earthquake analysis, an innovative approach in this field of research based on GIS spatial statistical tools to evaluate the importance of the different variables after an earthquake that may have caused damage in a city. According to the authors, the results obtained will allow one to hierarchize the importance of the different detected phenomena to prepare the city better against future earthquakes and to elaborate an improved seismic mitigation strategy.

Data Set

In the study, an open-source of the data provision is LLP ”SOME”JSC ”National Center for Seismological Observations and Research”. An earthquake dataset consists of several attributes, such as the date (day/month/year) of the event, the exact time in GMT (hour/minute/second), latitude, longitude, depth, energy class, and magnitude. The total number of records in the dataset is 1742 records (between 2012 and 2020 September of the month). Table I. presents a fragment of the dataset. At the initial stage of the analysis of the spatial data of earthquake propagation, preliminary data processing was carried out. Factor variables such as date and time have been converted to the corresponding date and POSIXct formats. Also, the variables latitude, longitude, depth, energy class, magnitude are converted to numerical formats.

Table 1. Fragment of data set

Date	GMT	Latitude,N.	Longitude,E.	Depth,km	Energy class,K	Magnitude,MPVA
14.10.2012	16:30:00	40.88	74.17	15	10.8	4.7
12.10.2012	18:08:00	40.82	76.97	0	9.8	4.2
12.10.2012	7:18:00	43.05	78.22	20	9	4.4
11.10.2012	10:58:00	44.13	78.95	20	8.1	3.6

Brief Description of the Concept of Magnitude

Earthquake magnitude (M, from Latin magnitudo - magnitude) is a quantitative characteristic of the magnitude of the earthquake focus. ”In the ISC-GEM catalogue, in the catalogue of Central Asia, as well as in the catalogue of Kazakhstan, you can see a whole set of energy and magnitude characteristics of earthquakes, which are determined using different scales” [5]. MPVA is the regional body wave magnitude determined from the P-wave recorded by short-period instruments. Determined from the values of the amplitude and period of displacements using the regional calibration curve for the Northern Tien Shan [6] for distances up to 1000 km. It is used in the practice of SOME Ministry of Education and Science of the Republic of Kazakhstan and the IGI Data Center.

Results

As we already know, data mining is about processing information and identifying patterns and trends in it, which in turn help make decisions. The principles of data mining have been known for many years, but with the advent of big data, they have become even more widespread. The field of spatial data mining is still evolving and at a very early stage. ”Spatial data mining has deep roots in both traditional spatial analysis fields (such as spatial statistics, analytical cartography, exploratory data analysis) and various data mining fields in statistics and computer science (such as clustering, classification, association rule mining, information visualization, and visual analytics). Its goal is to integrate and further develop methods in various fields for the analysis of large and complex spatial data. Not surprisingly, spatial data mining research efforts are often placed under different umbrellas, such as spatial statistics, geocomputation, geovisualization, and spatial data mining, depending on the type of methods that a research focuses on” [7]. In spatial data mining, input data has a more complex structure than normal data. ”The data inputs of spatial Data Mining have two distinct types of attributes: non-spatial attribute and spatial attribute. Non-spatial attributes are used to characterize non-spatial features of objects, such as name, population, and unemployment rate for a city. They are the same as the attributes used in the data inputs of classical Data Mining. Spatial attributes are used to define the spatial location and extent of spatial objects (Bolstad, 2002). The spatial attributes of a spatial object most often include information related to spatial locations, e.g., longitude, latitude and elevation, as well as shape [1]”. Intellectual analysis of data on the quantitative characteristics of the magnitude of the earthquake source revealed the

following classes of magnitudes [15] and their numerical indicators. These magnitude classes with numerical indicators are shown in Table 2. Based on this, the data analysis results show the largest number of registered seismic events have magnitudes 4-5, also 3-4 and 5-6. As a continuation of the study on the analysis of data from recorded seismic

Table 2. Magnitude classes

Magnitude class	n
2-3	1
3-4	311
4-5	1089
5-6	303
6-7	35
7-8	3

events, the distribution of the data over the time interval was studied. The resulting density plot in Figure 1 visualizes the distribution of data over a continuous interval from 2012 to 2020.

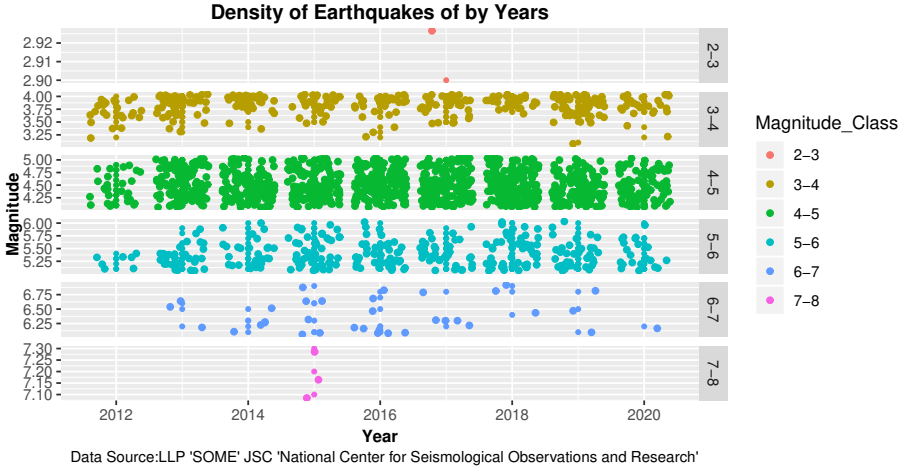

Figure 1. Visualizations and graphs of density distribution of earthquake data.

A more detailed interpretation of the graphs of the density of the distribution of earthquakes by year is also presented in Table 3. From the graphs and tabular information, it was determined that > 100 seismic events with a magnitude class 4-5 were recorded in 2013-2019. 3 earthquakes with magnitude class 7-8 in 2015. Magnitude

class with seismic events of 6-7 from 1 to 9, except for 2012. Earthquakes with magnitudes 3-4 and 5-6 were also recorded in all time intervals of the dataset.

Table 3. Distribution of magnitude class by year

Year	2-3	3-4	4-5	5-6	6-7	7-8
2012		25	27	7		
2013		44	121	32	3	
2014		36	121	27	5	
2015		29	134	48	6	3
2016		30	167	43	9	
2017	1	37	149	37	5	
2018		26	165	52	3	
2019		59	112	36	3	
2020		25	93	21	1	

Also, using the data mining tool, a more in-depth and detailed analysis of the recorded seismic event data was carried out, which is presented in Figure 2.

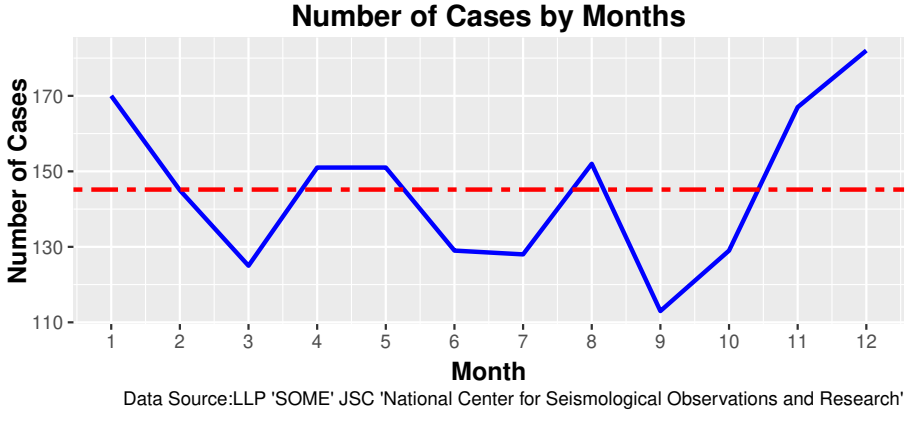

Figure 2. Visualization of recorded seismic events by month.

Therefore, this analysis shows that the occurrence of seismic events occurred in every month and with the corresponding class of magnitudes, which is also presented in Fig. 3. The number of seismic events by month is shown in Table 4, where the conditional breakdown of> 150 events falls on months 1,4,5,8,11,12, among which the

largest recorded earthquakes occur in the months of the winter period, as well as the number in the interval <150 events for the rest of the months.

Table 4. Number of seismic events by month

Month	n
1	170
2	145
3	125
4	151
5	151
6	129
7	128
8	152
9	113
10	129
11	167
12	182

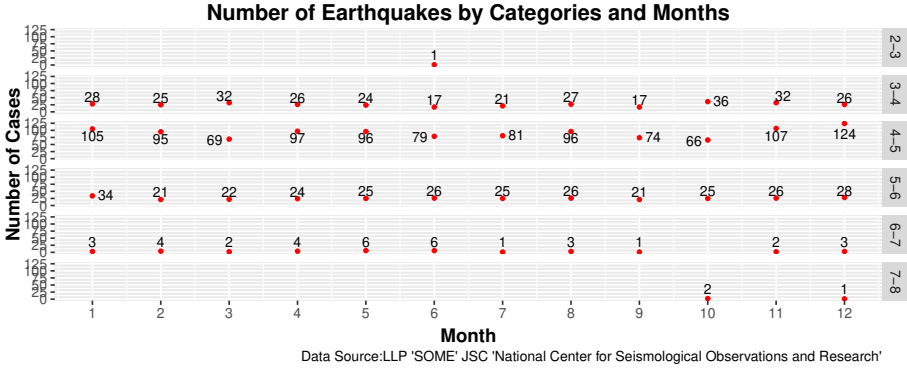

Figure 3. Diagram of the distribution of recorded seismic events by months and magnitude class.

A similar study of data analysis was carried out based on the time of occurrence of recorded seismic events per day. Benchmarking and data visualization is shown in Figure 4-5. At the initial stage of the study, the results of statistical analysis of seismic event data were obtained regarding the class of earthquake magnitudes, their distribution by years, months and time of day. Since, among the first information about the occurred seismic event, namely about the earthquake, its magnitude becomes known.

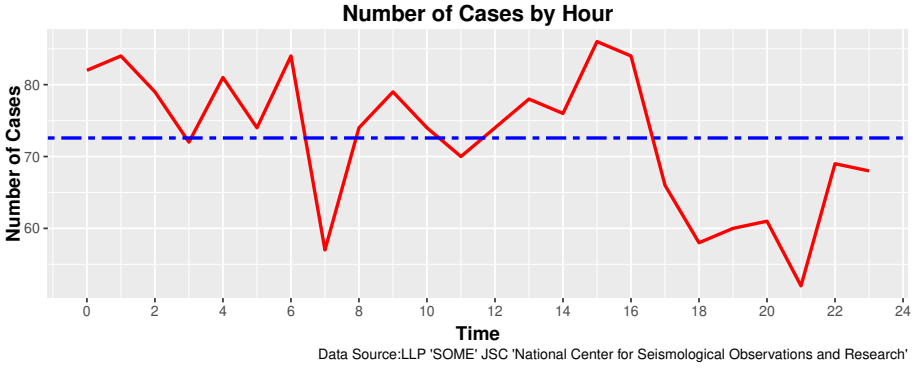

Figure 4. Visualization of the number of recorded seismic events by time per day.

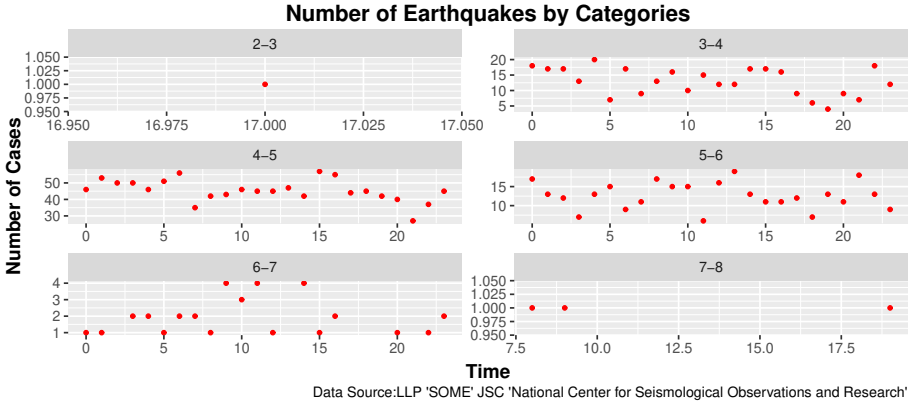

Figure 5. Diagram of the distribution of recorded seismic events in time and magnitude class.

The magnitude of an earthquake is not a measure of the intensity of an earthquake felt at a particular point on the earth's surface. The intensity of the manifestation of an earthquake in a specific area on the surface depends on the magnitude of the earthquake, the depth of the hypocenter, the type of rocks and the distance to the source.

In the next stage of the research work, the locations of the geographic coordinates are analyzed, i.e. visual analysis was carried out and regions were identified. Visual analysis of the propagation of earthquakes by magnitude class 7-8 did not reveal their belonging to the regions of the Republic of Kazakhstan. An analysis of the spatial data on the spread of earthquakes by magnitude class 6-7 on the map shows that the number of earthquake epicentres belonging to the territory of the Republic of Kazakhstan is 3 points and 2 points on the border with the Republic of Kyrgyzstan. The geographic area of belonging of these epicentres in the East Kazakhstan region, Almaty region and Almaty city. The location of the spatial points of earthquake epicentres is shown in Figure 6, which are indicated by ellipses.

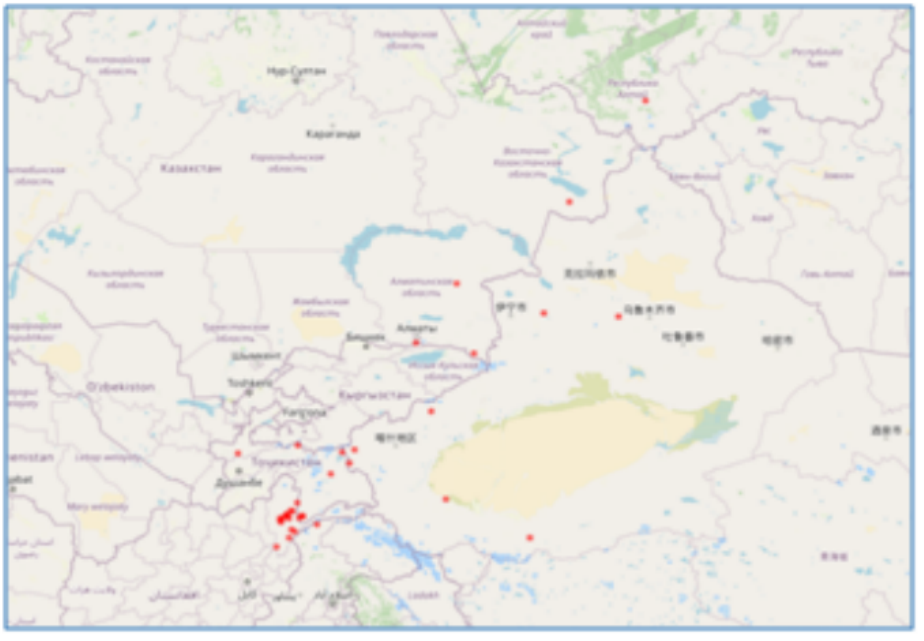

Figure 6. Magnitude Class = 6-7.

Visual analysis of the propagation of earthquakes according to the magnitude class of 5-6, also shows the epicentres of the adjacent territories of the Republic of Kazakhstan on the map. Such regions are the East Kazakhstan region, Almaty region, Almaty city and Zhambyl region. The location of the spatial points of earthquake epicentres is shown in Figure 7.

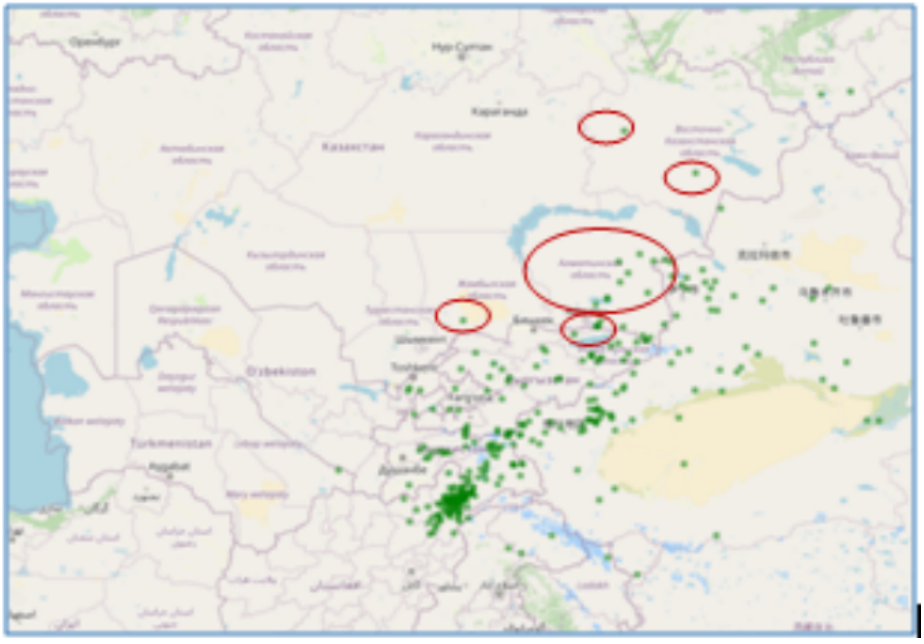

Figure 7. Magnitude Class = 5-6.

Conclusion

Today, data mining and a variety of data processing tools provide the researcher with many opportunities for qualitative analysis of various data. Thus, the constructed computational algorithms make it possible to extract knowledge from experimental data, as well as transform and model data to extract useful information and make decisions. So, using the data mining toolkit, this article analyzed the data of recorded seismic events, earthquakes. The research stages were carried out in two stages. In the first stage of the study, statistical data processing was carried out. In the second stage, visual data analysis using the constructed map. The obtained results of the statistical analysis of these seismic events were carried out on the attributes of earthquakes as magnitude, date and time. Visualization of the data on the distribution of earthquake epicentres on the map also helped to identify the geographical affiliation of the points. In further works, research will be carried out and methods of cluster analysis will be applied to identify the dependences of characteristics and obtain clusters of earthquakes.

References

1. Gempa Bumi. (n.d.). Retrieved July 8, 2015, from Baand Meteorologi, Klimatologi, and Geofisika, `https://www.bmkg.go.id/`. Last accessed 15 July 2020
2. Liu, M., Grana, D.: Accelerating geostatistical seismic inversion using TensorFlow: A heterogeneous distributed deep learning framework. Comput. Geosci. **2**(124), 37–45 (2019)

3. Zhou, Y., Gao L.: An Apriori Based Algorithm Associated Point Line Pattern Applied in Seismic Spatial Data. In: International Conference on Artificial Intelligence: Technologies and Applications. on Proceedings. Atlantis Press(2016)
4. Karmenova, M., Nugumanova A., Tlebaldinova A., Beldeubaev A., Popova G., Sedchenko A.: Seismic Assessment of Urban Buildings Using Data Mining Methods. In: 96th International Conference on Computer and Technology Applications, pp. 154–159., Turkey (2020)
5. García-Ayllón, S., Tomás, A., Ródenas J.: Accelerating geostatistical seismic inversion using TensorFlow: A heterogeneous distributed deep learning framework. Appl. Sci., **2**9(15), 3182 (2019)
6. Edelani, R., Barakbah A., Harsono T., Sudarsono A.: Association Analysis Of Earthquake Distribution in Indonesia For Spatial Risk Mapping. In: International Electronics Symposium on Knowledge Creation and Intelligent Computing, pp. 231–238., Indonesia (2017)
7. Shodiq, M., Barakbah A., Harsono T.: Spatial analysis of earthquake distribution with Automatic Clustering for prediction of earthquake seismicity in Indonesia. In: The Fourth Indonesian-Japanese Conference on Knowledge Creation dan Intelligent Computing, pp. 47–55., Indonesia (2015)
8. Sarp, G., Düzgün S., Toprak V.: Spatial Analysis of Earthquake Epicenters in North-West of Ankara. In: The Fourth Indonesian-Japanese Conference on Knowledge Creation dan Intelligent Comp International Conference on Environment: Survival and Sustainability, pp. 4619-4633., Nicosia-Northern Cyprus (2007)
9. Djenaliev, A., Kada, M., Chymyrov A., Helwich O., Muraliev A.: Spatial statistical analysis of earthquakes in Kyrgyzstan. International Journal of Geoinformatics, **2**14(1), 11-20 (2018)
10. Aslam, B., Naseer F.: A statistical analysis of the spatial existence of earthquakes in Balochistan: clusters of seismicity. Environmental Earth Sciences, **2**79(1), 41 (2020)
11. Mukambayev, A., Mikhaylova N.: Resheniye problemy neodnorodnosti magnitud v rabotakh po seysmicheskomu zonirovaniyu territorii Respubliki Kazakhstan. Vestnik NYATS RK, **2**4, 86-92 (2014)
12. Mikhailova, N., Neverova N.: Calibration function s (d) for determining the MPVA of the Northern Tien Shan earthquakes. Comprehensive research at the Alma-Ata prognostic site, , 41-47 (1986)
13. Mennis, J., Diansheng G.: Calibration function s (d) for determining the MPVA of the Northern Tien Shan earthquakes Data Mining and Geographic Knowledge Discovery – An Introduction. Computers Environment and Urban Systems, **2**33(6), 403-408 (2009)
14. Shekhar, S., Zhang, P., Huang, Y.: Spatial Data Mining. Data Mining and Knowledge Discovery Handbook. Springer, Boston, MA, USA (1999)
15. Bulut T. Exploratory Data Analysis of Turkey Earthquages II, , `https://tevfikbulut.com/2020/02/02/exploratory-data-analysis-of-turkey-earthquakes-ii/`. Last accessed 20 July 2020

Modeling of calibration characteristic estimation of AES – ICP

Muratkan Madiyarov, Roza Aubakirova, Batima Tantybaeva, Zukhra Dautova

S. Amanzholov East Kazakhstan University
madiyarov_mur@mail.ru

In this paper, we used modeling of the processes of constructing the calibration characteristic of atomic emission spectral analysis with inductively coupled plasma (AES-ICP) and evaluating it from the standpoint of error and uncertainty.

Monitoring compliance with the standards for maximum permissible arsenic discharges into wastewater and natural waters is a prerequisite for environmental protection measures of each industrial enterprise. The regulatory framework of the Republic of Kazakhstan regulates colorimetric [1], photometric [2] and atomic emission with inductively coupled plasma [3] methods for determining the arsenic content in various types of water (table 1).

Table 1. Methods of analytical control of arsenic content

The method of analytical control	The range of the designated contents	Object of analysis	Name of the regulatory document	Reference to the literature
Colorimetric	5*10-4 – 6*10-3 mg	Mineral waters: drinking, medicinal, medicinal-table and natural table	State Industry Standard 23268.14-78	1
Photometric	0,050 – 0,8 mg/l	Natural and waste water	Federal environmental regulation documents 14.1:2.49-96	2
AES-ICP	0,005 – 5,00 mg/l	Surface, underground, and waste water	Measurement methods 30884350-02-28-14	3

The availability of modern instrumentation in most of the factory laboratories makes it possible to fully implement such features of physical and chemical methods as expressiveness, low detection and detection limits. These methods include inductively coupled plasma atomic emission spectroscopy (AES-ICP). The limit for the

determination of arsenic in the certified measurement method 30884350-02-28-14 is 0.005 mg/l. Methods for controlling lower arsenic levels in waters are not regulated. To determine the arsenic content in wastewater in the range of analyte concentrations from 0.002 mg/l to 0.020 mg/l, studies were conducted to reduce the limit of determination to 0.002 mg/l and to build a calibration model of the AES-ICP for the determination of analyte. In this case, the overall error of the calibration characteristic is due not only to instrumental errors in measuring the intensity of the analytical signal, but also to errors in the preparation of calibration solutions. Therefore, the statistical processing of the constructed calibration dependence is carried out from the standpoint of the concepts of error and uncertainty.

The purpose of this work is to evaluate the calibration characteristics of the AES-ICP for arsenic determination from the point of view of the concepts of error and uncertainty.

Experimental part

For research, a standard solution of arsenic (III) with a concentration of the main component of 1 mg/dm3 was used, which was prepared from the State Standard Sample 7264-96 composition of the ions of the arsenic (III) solution. Working solutions of arsenic (III) in the concentration range from 0.002 to 0.020 mg/dm3 were prepared by successive dilution of the standard solution. Only freshly prepared solutions were used for research. The arsenic (III) content in solutions was determined using an Optima 8000 atomic emission spectrometer (PerkinElmer, USA) with inductively coupled plasma at a wavelength of 188.979 nm. To establish the calibration characteristic (CC), 5 calibration solutions with a known arsenic content in the concentration range of 0.002 - 0.020 mg/dm3 were used. For statistical processing of CC, 6 solutions of each concentration were prepared. For each solution, the intensity of the analytical signal was measured 1 time. The data required for constructing the CC are shown in table 2.

Table 2 –The results of AES-ICP determination of arsenic in the calibration solutions

Table 2. Methods of analytical control of arsenic content

N	1	2	3	4	5
$C_{A_s}, mg/dm^3$	0,002	0,005	0,010	0,015	0,020
I_N, counts/sec	80	185	370	550	729
Remarks: N – calibration solution number; C_{A_s} – arsenic content in N-th calibration solution, mg/dm^3 I_N – average intensity of the arsenic analytical signal, counts/sec					

Based on the obtained data, we plotted the dependence of the intensity of the arsenic (III) analytical signal on the analyte content in the calibration solution (mg/dm^3). A

statistical regression model (1) was used to construct the linear grading function.

$$I_N = a + bC_{A_s} \quad (1)$$

where I_N – arithmetic mean value of the intensity of the analytical signal of the AES-ICP definition, counts/sec;

a, b –parameters of the regression model;

C_{A_s} –arsenic content in N-th calibration solution, mg/dm^3.

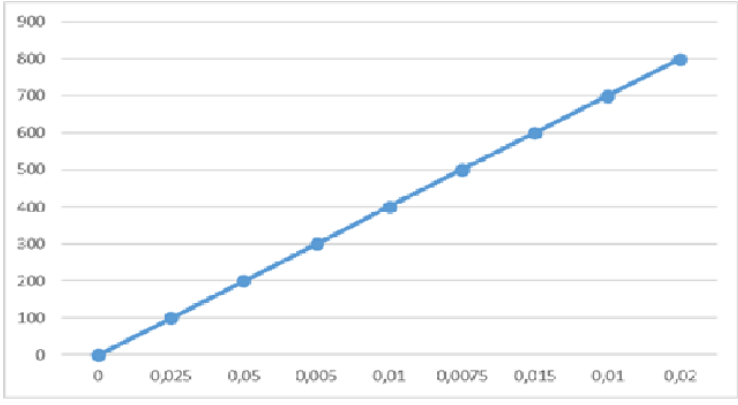

Picture1 –Dependence of the intensity of the analytical signal of arsenic (III) on the analyte content.

The value of the correlation coefficient of the calibration characteristic (picture1) is 0.9999, which indicates a strong correlation between the values of the arsenic (III) content (mg/dm^3) and the signal intensity. Statistical processing of the calibration characteristic from the standpoint of the error concept was carried out in accordance with Recommendations for Interstate Standardization 54-2002[4]. The results are presented in table 2. The arithmetic mean of the relative standard deviations $\gamma \leq 0.4$, so the statistical processing of the calibration characteristic from the standpoint of the concept of error was carried out using the least squares method (table 2). The calculated value of V_y (table 3) was compared with the table value of the quantile of the F-distribution with degrees of freedom V_1 = N-2 and V_2 = N (J-1). Since V_y < F (V_1,V_2), the calibration characteristic can be considered linear with a confidence probability of 0.95 in the concentration range of 0.002-0.020 mg/dm^3.

To determine the lower limit of the arsenic content, 6 solutions with analyte concentrations of 0.0006-0.002 mg/l were prepared. For each sample population, the relative standard deviation of the Sr(C) concentration from the analyte content was calculated (table 4). Table 3 –Results of statistical processing of the calibration characteristics of ASE-ICP for arsenic determination (III)

Table 3. Methods of analytical control of arsenic content

$\overline{\gamma}$	a	S_a	b	S_b	V_γ	$F(V_1, V_2)$
0,008	6,73	1,66	36160,41	135,33	2,50	2,69
Remarks: $\overline{\gamma}$– arithmetic mean of relative standard deviations a and b – coefficients in the equation $y = a + bx$ S_a and S_b - standard deviations of coefficients a and b V_γ - ratio of average squares of deviations F – quantile of the distribution						

Table 4. Estimation of the limit of arsenic determination by ASE-ICP method

$C_{A_s}, mg/dm^3$	0,0006	0,0008	0,0001	0,0002
S(I)	1,40	1,45	1,46	1,35
S (c)	0,0221	0,0210	0,0191	0,0187

The determination limit of 0.002 mg/dm^3 corresponds to the minimum arsenic concentration that can be determined with a relative standard deviation of no more than 33%.

The procedure for statistical processing of the calibration characteristic from the perspective of the uncertainty concept included several stages: construction of the ”cause-effect”diagram, identification and quantification of sources of uncertainty, calculation of standard uncertainty and extended uncertainty. The uncertainty of the calibration schedule for determining the arsenic (III) content by the AES - ICP method was carried out in accordance with the requirements set out in Recommendations for Interstate Standardization 43-2001.

The ”cause-effect ”diagram of the calibration characteristic is shown in Picture 2. It is established that the value of the extended uncertainty of each calibration solution contains the following sources of uncertainty: the uncertainty of the preparation of calibration solutions and the uncertainties that arise during the operation of the AES - ICP spectrometer. The standard uncertainty values for each identified source are shown

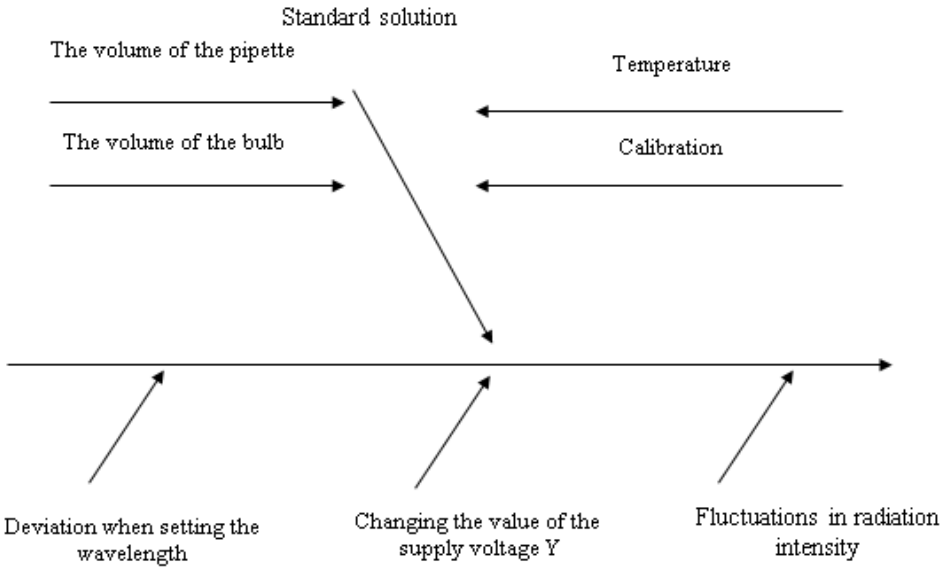

in table 5.

Deviation in determining the wavelength based on the values of the relative standard uncertainty of all sources, the total standard uncertainty us(CAs) of calibration solutions was estimated using the formula (2).

Table 5. Results of estimation of uncertainties in the construction of the calibration schedule.

Designation of the source of uncertainty	Name of the source of uncertainty	Standard uncertainty u (x)	Relative standard uncertainty $\frac{u(x)}{x}$
$U(p_A, i)$	Dilution coefficient of the intermediate solution A	0,080	1.60*10_{-4}
$U(p_B, i)$	Dilution coefficient of the intermediate solution B	0,110	2.21*10_{-4}
$U(v_\pi, i)$	The volume of the pipette	0,004	1.604.13
$U(v_k, i)$	The volume of the bulb	0.052	$1.05 * 10_{-4}$
$U(t, i)$	Temperature deviation from standard relative to calibration	0,002	2.10*10_{-3}
$U(r, i)$	Fluctuations in radiation intensity	0,003	1.51*10_{-3}
$U(Y, i)$	Changing the value of the supply voltage Y	0,002	1.23*10_{-3}
$U(\lambda, i)$	Deviation when setting the wavelength	0,003	1.45*10_{-3}

$u_s(C_{A_s}) = \sqrt{U(p_A,i)^2 + U(p_B,i)^2 + U(v_\pi,i)^2 + U(v_k,i)^2 + U(t,i)^2 U(r,i)^2 + U(Y,i)^2 + U(\lambda,i)^2}$ (2)

During the calculations, it was found that the total standard uncertainty of calibration solutions is 0.001 mg/dm^3.

The value of the extended uncertainty of U$u_s(C_{A_s})$ calibration Solutions was estimated using the formula (3). $u_s(C_{A_s}) = k * u(C_{A_s})$ (3)

It was found that the extended uncertainty of calibration solutions is 0.002 mg/dm^3.

Conclusions

To assess the calibration characteristics of the AES-ICP for arsenic determination from the point of view of the concepts of error and uncertainty, a calibration graph was constructed using a standard sample of arsenic. The results obtained during statistical processing of the calibration graph and uncertainty estimation show that the use of modeling of this process makes it possible to determine the concentration of arsenic in wastewater and natural waters with a confidence probability of 95%.

References

1. State Industry Standart 23268.14-78. Mineral waters: drinking, medicinal, medicinal-table and natural table. Methods for determining arsenic ions. Introduction.01.01.80. – Moscow.: Publishing and Printing Complex of standards, 2003. – 7 pages.
2. Federal Environment Regulation Djcuments 14.1:2.49-96 Method for measuring the mass concentration of arsenic ions in natural and wastewater by photometric method with silver diethyldithiocarbamate.. Introduction.30.05.2001. –Moscow: Ministry of environment and natural resources RF, 2001. – 15 pages.
3. Measurement Methods 30884350 – 02 – 28 – 14 Measurement procedure. Surface, underground, and waste water. Atomic emission method with inductively coupled plasma for determining the mass concentrations of copper, lead, zinc, iron, and arsenic.
4. Recommendations for Interstate Standardization 54-2002. Recommendations for interstate standardization. State system for ensuring the uniformity of measurements. Calibration characteristics of measuring instruments for the composition and properties of substances and materials. Method of performing measurements using standard samples. – Introduction. 01.07.2004. – M.: Standards publishing house, 2004. – 9 pages.
5. Kadis R. L. Quantitative description of uncertainty in analytical measurements. 2nd edition, 2000. – S-Pt.: All-Russian scientific research Institute of Metrology named after D. I. Mendeleev, 2002. – 149 pages.
6. Recommendations for Interstate Standardization 43-2001. Recommendations for interstate standardization. State system for ensuring the uniformity of measurements. Application of ”Guide to the expression of uncertainty in measurement» Introduction. 01.07.2003. – M.: Standards publishing house, 2003. – 26 pages.

Predicting Academic Performance using a Machine Learning Algorithm

Timur Merembayev[1,2] [0000−0001−8185−235X] and
Saltanat Amirgaliyeva[2] [0000−0002−6528−0619]

[1] Institute Information and Computational Technologies CS MES RK, Almaty,Kazakhstan
timur.merembayev@gmail.com
[2] Suleyman Demirel University, Kaskelen, Kazakhstan
saltanat_amirgal@mail.ru

Abstract Educational data mining is more focused on processing large amounts of data, as learning analytics studies on the relationship between students and the learning environment. Objectives of research in learning analytics and educational data mining are: modeling student behavior, predicting academic performance, increasing reflection and awareness, improving grades and feedback, improving social interaction in the learning environment, understanding student influence, and recommending resources. These goals are achieved using various algorithms such as clustering, regression, text mining, social media analysis, statistics, and various visualization techniques.
The experiments were carried out with a group of 115 first-year undergraduate students from a university in Kazakhstan. The dataset contains time series of students' results over six sessions of the course lab. There are 6 folders containing student data per session. Each file contains 13 features. To compare models also applied on dataset from Diagnostic Questions: The NeurIPS 2020 Education Challenge. It is challenging to write good diagnostic questions, where each of the incorrect answers is a plausible distractor. In this competition, the organizer challenge participants to develop novel methodologies to understand and improve students learning and measure the quality of diagnostic questions.
Three methods of machine learning were compared: logistic regression, XGBoost, LightGBM. LithtGBM performed best on three recall, precision, f1 metrics. This method can be used for adaptive learning systems that will allow students to choose the correct and fastest direction in learning subjects. The results for the metrics show high accuracy and give good results of applying machine learning algorithms for this task. For a deep analysis of the educational mining task, big data is necessary but it is time-consuming to mining data.

Keywords: Item Response Theory, gradient boosting tree, computerized adaptive testing

Introduction

IRT is an area of research; the goal is to provide personalized instruction for students. Early works date back to the late 1970s. It was studied a wide range of artificial intelligence and knowledge representation methods, we can mention Bayesian

representations of student knowledge and delusions, modeling with logistic regression in subject theory, reinforcement learning and, deep training [1, 2]. It can even be argued that most of the basic methods used in artificial intelligence and data mining have found their application in the field of IRT. In particular, in the problem of tracking knowledge, the purpose of which is to simulate the student's possession of conceptual or procedural knowledge from observed assignments [3].

Deep knowledge tracing (DKT), the recent introduction of neural networks such as RNN in the field of educational data mining, has led to a significant improvement over the well-known Bayesian models of knowledge tracking, and its results help to reveal a hidden structure in the concepts of skills and can be used to optimize the curriculum [4].

The result from paper [5] was taken as a basis for studying practices and using adaptive learning. In the paper, the authors consider a model of adaptive practice and monitoring. This model is used in a web monitoring system that includes a sophisticated web environment for children to practice arithmetic. Using a new model for responding to an item based on the Elo rating system and an explicit scoring rule, people's ability scores and item difficulty are updated with each item answered, which allows calibrating items on the fly. The evaluation rule takes into account both accuracy and response time. The authors argue that the results obtained after the introduction of the adaptive practice algorithm are: the system selects tasks with an average success probability of 0.75, which makes the tasks difficult, but not too complicated. For ten months, a sample of the authors in the system collected data: 3648 children completed more than 3.5 million arithmetic tasks. Children completed about 33results show the best measurement accuracy, high reliability and reliability, high satisfaction of students, as well as many interesting opportunities for monitoring progress, diagnosing errors and analyzing development.

Using technology to better understand how learning happens has garnered significant attention in recent years, even with a breakdown into specialized areas such as learning analytics and data mining. Learning analytics can be defined as measuring, collecting, analyzing and presenting data about learners and their contexts in order to understand and optimize learning and the environment in which it occurs. Educational data mining involves developing, researching, and applying computerized techniques to discover patterns in large collections of educational data that would otherwise be difficult or impossible to analyze due to the sheer volume of data in which they exist. Educational data mining is more focused on processing large amounts of data, while learning analytics is more focused on the relationship between students and the learning environment.

Common research objectives that have been explored in learning analytics and educational data mining are: modeling student behavior, predicting academic performance, increasing reflection and awareness, predicting dropout rates, improving grades and feedback, improving social interaction in the learning environment, understanding student impact and recommending resources [6, 7]. These goals are achieved using various techniques such as clustering, regression, text mining, social media analysis, statistics, and various visualization techniques. The use of XGBoost and LightGBM have strong properties in applied problems due to the ease of deployment

and not necessarily the presence of big data for training, compared to neural networks of deep learning architectures [?,?].

Despite these opportunities, educators report challenges with advances in the use of technology-based assessment. For example, educators report that they have very large amounts of data from different sources (eg, heterogeneous data) and cannot access the data with enough time to improve learning [8]. In these scenarios, visual analytics tools can help gain insight into student learning paths, the effectiveness of learning materials, and the different approaches students use to accomplish a given task.

Methodology of Data Analysis

Professionals and researchers use information visualization techniques to represent large, complex, heterogeneous data and obtain information from these representations. These ideas are often used to explain phenomena, make decisions, analyze data, and identify patterns in data.

Unlike many computational tools, in which users are not directly involved in data processing, visualization tools include and require human participation. The tool enables analytic data analysis so that users can perform analytical tasks - for example, validate hypotheses, investigate hypothetical situations, categorize and organize data, and identify interesting data features for further study - in the form of a partnership with, not as a complement to, computational processing. Depending on the context, computational processing of visualization can range from simple algorithms and computations to complex data mining and machine learning techniques that can be controlled and directed by users [9].

There are a number of challenges when using visual learning analytics tools in classrooms. First, because social sciences tend to introduce technology at a slower pace compared to technological innovation, it can be difficult to bring human perceptual and cognitive abilities into account using interactive visualizations as interfaces between users and their data, making tasks related to data that are more effective and efficient. Thus, visualization deserves serious consideration as an approach to making sense of complex educational data for educators, students, and administrators.

Therefore, this study has two objectives:

- define the main applications of visualization in educational research;
– to identify gaps and future opportunities for research and creation of visualization tools that can help develop the field of visual learning analytics.

Below you can see some examples of data visualization. The experiments were carried out with a group of 115 first-year undergraduate students from a university in Kazakhstan.

The dataset contains time series of students' results over six sessions of the course lab. There are 6 folders containing student data per session. Each Session folder contains up to 99 CSV files, each dedicated to a specific student log during that session. The number of files in each folder will vary depending on the number of students present in each lesson. Each file contains 13 features. Fig. 2 shows the distribution of the selected 52 students and their grades for laboratory tasks. According to this distribution, we can

say that there are two groups of students, a group that performs the task well and another that may not have mastered the subject and did not complete the task properly.

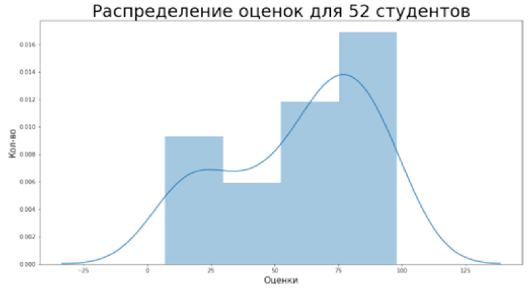

Figure 1. Distribution of grades for students.

Using Fig. 2, you can clearly see the average variation in grades for all students. This graph shows an average score of about 1.5 (with a minimum of 0 and a maximum of 3).

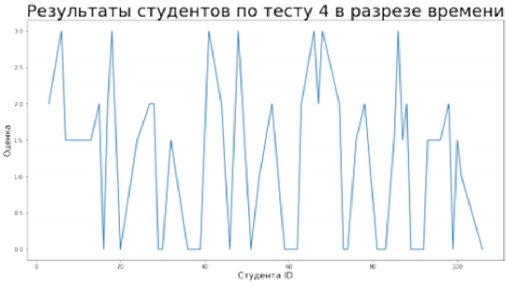

Figure 2. Comparison of all students and their performance

Identifying groups, clusters or patterns in the data is very important to understand how the subject is assimilated, whether it is necessary to improve the delivery of the subject to students. Clustering algorithms (k-means, DBSCAN, Gaussian mixture, etc.) can be used to cluster data. Visualization tools will allow you to visually show such clusters of students and highlight who is doing well in the subject or another group of students who need to spend more time studying the subject Fig. 3.

Fig. 4 shows the clustering of students for test 16.

The distribution of average estimates for our dataset is shown in Fig. 5. The average score for all students is about a grade of 3. This shows that the mastery of the subject is good in this subject.

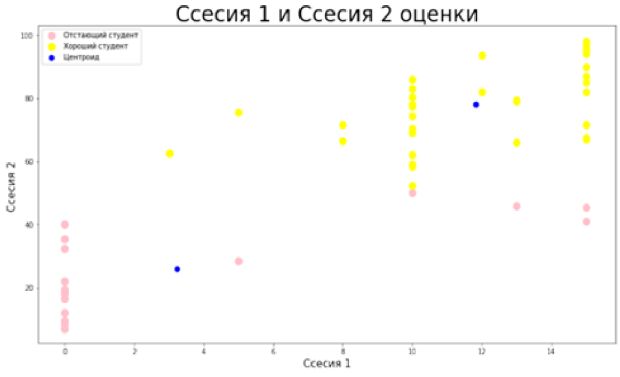

Figure 3. Clustering students by test 16.

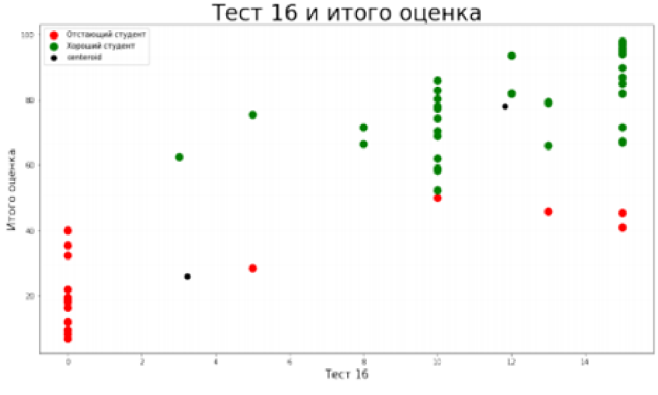

Figure 4. Clustering students by test 16.

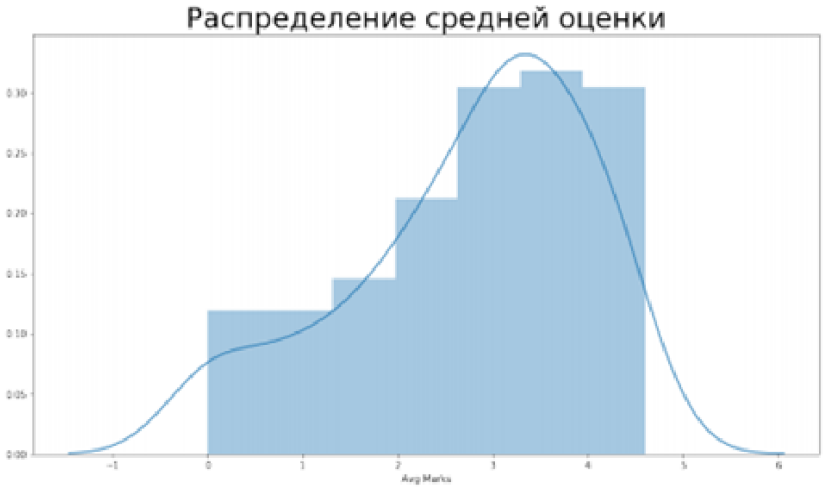

Figure 5. Clustering students by test 16.

Results

Cluster analysis also allows you to markup data and solve the problem of unmarked data or partially marked up. The resulting classes from the clustering algorithms are used as labels, based on these data, regression models were built that predict the average student's grade. The following algorithms were chosen: Linear Regression, Random Forest, Decision Tree, Support Vector Machine. You can see the results of the models in Tab. 1.

Table 1. Result of models by RSME and R2 metrics.

Models	RSME	R2
Linear Regression	6.08e-16	1.0
Random Forest	0.110	0.991
Decision Tree	0.145	0.985
Support Vector Machine	0.131	0.988

Based on Tab. 1, the following conclusions can be drawn:

– The results on the metrics show high accuracy and give rise to hope for good results from the application of machine learning algorithms for this task.

– For a more detailed study of the reasons for such high results, a large sample is required: different subjects, age groups, training levels, etc.

– It is necessary not to allow overfitting of the model, take into account the balancing of the data (take into account the distribution of which data were included in the training and test set).

Comclusion

Combining IRT methods and machine learning algorithms makes it possible to automate the direction of intellectual analysis of educational data. IRT allowsyou to identify patterns of knowledge between students and group students with similar knowledge, while calculations are performed quickly and do not require significant computing power. Machine learning algorithms allow you to accurately assess the readiness of each student for an assignment based on historical data.

This result must be used in smart systems for adaptive learning, this will save the student's time and prepare an adaptive learning plan for each student in automatic mode. In the COVID-19 pandemic lockdown, automation and digitalization technologies are showing their effectiveness and are the lives necessary to provide training remotely.

Acknowledgment

The work was supported by the program-targeted funding projects of the Ministry of Education and Science of Republic of Kazakhstan AP05132648.

References

1. J. S. Brown and R. R. Burton.: Diagnostic models for procedural bugs in basic mathematical skills. Cognitive science, vol. 2, no. 2, 155–192 (1978).
2. M. C. Polson and J. J. Richardson.: Foundations of intelligent tutoring systems. Psychology Press, (2013).
3. A. T. Corbett and J. R. Anderson.: Knowledge tracing: Modeling the acquisition of procedural knowledge. User modeling and user-adapted interaction, vol. 4, no. 4, pp. 253–278, 1994. I, II-B
4. Piech, C., Bassen, J., Huang, J., Ganguli, S., Sahami, M., Guibas, L. J., SohlDickstein, J.: Deep knowledge tracing. In Advances in neural information processing systems. 505-513 (2015).
5. Ritsos, P. D., Roberts, J. C. Towards more visual analytics in learning analytics. In Proceedings of the 5th EuroVis Workshop on Visual Analytics. 61-65 (2014).
6. Vieira, C., Magana, A. J., Boutin, M.: Using pattern recognition techniques to analyze educational data. In Proceedings of Frontiers in Education Conference (FIE), (2017)
7. Merembayev T., Yunussov R. and Amirgaliyev Y.: Machine Learning Algorithms for Classification Geology Data from Well Logging. 2018 14th International Conference on Electronics Computer and Computation (ICECCO). IEEE, 206-212 (2018).
8. Amirgaliyev Y., Shamiluulu S., Merembayev, T. and Yedilkhan D.: Using Machine Learning Algorithm for Diagnosis of Stomach Disorders. International Conference on Mathematical Optimization Theory and Operations Research. Springer, Cham, 343-355 (2019).
9. Keim, D.A., Munzner, T., Rossi, F., Verleysen, M.: Bridging information visualization with machine learning (Dagstuhl Seminar 15101). In Dagstuhl Reports. Vol. 5, No. 3, (2015)

Technology for Creating a User Interface Based on the Developed Adaptive Graphical Editor for XML Records ⋆

Aigul Mukhitova[1,3] [0000−0002−4081−7694], Oleg Zhizhimov [4]

Aigerim Yerimbetova[1,2] [0000−0002−2013−1513], and
Madina Sambetbayeva[1] [0000−0001−9358−1614]

[1] Institute of Information and Computational Technologies CS MES RK,
[2] Kazakh Academy of Transport and Communications named after M. Tynyshpayev,
[3] Al-Farabi Kazakh National University, Almaty, Kazakhstan ,
[4] Institute of Computational Technologies Siberian Branch of the Russian Academy of Sciences (ICT SB RAS) Novosibirsk, Russian Federation
mukhitova.aigul@gmail.com

Abstract The technology of implementing an adaptive graphical editor of XML records for providing access to distributed heterogeneous information resources through graphical user WEB interfaces is Considered. The methodology for creating user interfaces adapted to the structure and functionality of information sources is described. An adaptive graphical WEB interface for editing structured data using client-server applications has been created. The program is a server-side WEB application that provides screen forms for creating and editing XML documents conforming to the selected XSD schema. Screen forms are generated on the server side based on XSD definitions using XSLT technology and are provided to the user as HTML pages. Completed on-screen forms are processed by the server to generate an XML document. When processing XSD by using XSLT, various features of XSD definitions are taken into account, including references and recursion. The program can be used as an independent module for creating and editing data presented in XML format, as well as an embedded module in various server software for heterogeneous information systems.

Keywords: adaptive graphical user and administrative web-interfaces, integration of heterogeneous data, data representation, computer science, active competences, new data analysis methods, XML, XSD, XSLT-transformations, XML-editor.

Introduction

The main task of integrating information resources is to combine them at the physical or virtual level into a single information space to provide users with access to heterogeneous information and the ability to manipulate it. This is done through using

⋆ The researches presented in this paper are supported by Grant funding for scientific and scientific and technical research for 2018-2020 MES RK (No. AP05133550)

specialized adaptive administrative and user graphical web interfaces that can adapt to the structure and functionality of information resources [1].

The development of adaptive user interfaces is the development of client – server applications that would allow transparent (at the protocol and transmission environment level) and easy data exchange between programs that can be located anywhere, be written in any language, and run on any operating system and on any hardware platform.

To simplify the perception of information to users, there are various methods of presenting it. One of the most popular ways of visual representation that allows you to display the structure of information is to write it as an HTML page in the browser. XML and HTML are subsets of SGML, and therefore inherit its basic principles. The structure of an XML document is similar to a normal HTML page. By simple manipulations, information from an XML document can be presented as an HTML page. HTML forms and XML elements are logically equivalent in terms of information content. This makes it possible to automatically convert them via a web browser using a single software tool for any XML data. The generated HTML form, which acts as a data entry form, is essentially an adaptive graphical interface, as it is a simple low-level XML editor based on web programming. With the advent of XML, which brought many convenient features for software system developers, the problem of editing XML files also appeared [2]. There was a need to study the problem that occurs while editing XML data and choosing tools that allow you to make changes to the XML document.

Thus, the task of research and application of adaptive technologies for the development of user and administrative interfaces that provide the ability to manage heterogeneous data (data creation and modification) is urgent.

Russian and foreign scientists have made a great contribution to the research of designing, implementing, and maintaining administrative and user interfaces that support various types of dialog. In view with the above, research aimed at solving the problems of reducing the complexity of designing, prototyping, implementing and maintaining the user interface is relevant. Based on modern achievements in this field, the main paradigms for automating user interface development have been formed.

The purpose of the research was to study and develop methods and software tools for building adaptive administrative and user interfaces that increase the degree of functionality and expand the possibilities of user interaction during the search and edition of heterogeneous information in a distributed information system.

The scientific novelty of the work is to create a set of technical developments and techniques (models and algorithms) that implement a systematic and integrated approach to building adaptive user interfaces.

The theoretical value of the work is to provide a formal description of the developed adaptive model for entering and editing metadata presented in XML format, based on the use of XSD data schema definitions using XSLT technologies and its place in the architecture of a web server application.

The practical value of this work is to develop a server-side Web application that provides on-screen forms for creating and editing XML documents in accordance with the selected XSD schema. Screen forms are generated on the server side and provided to the user as HTML pages. Completed on-screen forms are processed by the server to generate an XML document. This software product can be used as an independent

module for creating and editing data presented in XML format, as well as an embedded module in various server software for heterogeneous.

All the results are confirmed by experiments conducted in accordance with generally accepted standards. The practical significance of results is confirmed by their use in research and production activities of ICT SB RAS.

Description of technology

To simplify the perception of information by users, there are various methods of its presentation. One of the most common methods of visual presentation that allows you to display the structure of information is to write it as an HTML page in a browser. XML and HTML are both subsets of SGML, and therefore inherit its core principles. The structure of an XML document is similar to that of a regular HTML page [3-4]. Through simple manipulations, information from an XML document can be represented as an HTML page. HTML forms and XML elements are logically equivalent in terms of information content. This makes it possible to automatically convert them through a web browser using a single software tool for any XML data. The generated HTML form serving as a data entry form is essentially a simple, low-level, web-based XML editor, and is a responsive GUI [5-7].

The process of converting XML documents from one XML schema to another can be divided into three main parts:

- **Creation of a XML-code** - code generation using the plain text or specialized a XML-code editors. Many databases are equipped with the function of generation a XML-code generation.

- **Creation of style XSL - tables for processing and displaying XML-document.** XSL tables are created by an administrator-programmer.

- **Overlay XSL style sheets.** XSL style sheets are imposed on the XML document according to certain formatting rules, in the result is a document that matches the client's request in the following output formats: HTML, PDF, WML, and XML [4-7].

Client side actions

The last part of the process is transforming XML documents by overlaying XSL stylesheets, usually done on the client side. With this style, the table is loaded only once. Newer browsers understand XML, can plug styles into XML documents, and produce the final document. It works the same way when overlaying a CSS file with an HTML file.

Server side actions

If browsers do not understand full-fledged HTML, and cannot perform xml/xsl transformations themselves, then applying a style to an XML document can be done on the server in two ways:

- manually - compile the collected xml-files and style sheets, and upload the resulting files to the server;

- automatically using a special system (for example, Cocoon), which performs the required transformation of the xml document automatically before giving it to the user. At the same time, at the request of the Acrobat Reader program, the published page will come to the client in PDF format, at the request of a WAP device (Wireless Application

Protocol), the client will receive a WML page (Wireless Markup Language), a regular Web browser will receive an HTML page, a more advanced XHTML client-page.

To manage heterogeneous information in a heterogeneous information system, it became necessary to develop a universal model for constructing an adaptive graphical web interface for entering and editing data. Such interfaces, which are able to adapt to the structure and functionality of information resources, will be adaptive.

The structured XML-format, extracted from various information sources, is the best tool for building adaptive administrative and user WEB-interfaces for data entry and editing. To represent structured information in the XML format itself, there is an XSD data schema description. In terms of XSD [4], rules for the structure of an XML document are formulated that can be processed using standard XSLT tools [7]. Thus, graphical web interfaces built on the basis of XML technologies allow displaying any file structure presented in XML format.

When retrieving a record from a specific information source in a heterogeneous information system and presenting this record in XML format for editing, the main task is to obtain a complete description of the possible structure of the extracted record. The following options are possible [8]:

1) The most standard way is when the root element of the XML record contains definitions of the used namespace, which contains a reference to the used XSD data schema in the form of a URL (the value of the schemaLocation attribute).

2) If the record retrieved for editing XML contains a namespace identifier (URI), but does not contain a link to the used XSD data schema in the form of a URL, then you need to make a request to the information system to provide an XSD by the namespace identifier.

3) If the record retrieved for XML editing does not contain namespace definitions, then a request to the information system is required to provide an XSD by the name of the information resource (database) or to use an XSD that corresponded to the schema requested when generating the data retrieval request.

For all the listed cases of initialization of graphical interfaces, data modification is required:

- Description of the data schema in the form of XML structure in accordance with XSD rules.
- XML structure containing the extracted data for editing (not required to create a new record).
- Description of the styles of forming the elements of the graphical interface (optional).
- Description of the rules for generating elements of the graphical interface in accordance with the rules of the used XSD and the value of the elements of the edited XML record. However, these rules can be XSLT transformation rules applied to XSD.

The principle of operation of the created adaptive XML-records editor in the client-server architecture is as follows:

- on the client side, a ready-made HTML form is provided for entering / editing data. The form will contain all the necessary tools (java scripts) for correct data entry;
- on the server side, the editing form is generated by the XSLT method of transforming the modified XSD structure. First, an empty edit form without data is

generated, which is filled with record data in XML format after the XSLT processor is finished.

For the client part, a ready-made HTML form is provided for entering and (or) editing data. Moreover, this form already contains all the necessary tools (java scripts) for correct data entry, including:

- A script for duplicating elements, the repetition of which is possible in accordance with XSD.
- Script for removing elements, the removal of which is possible in accordance with XSD.
- A script for checking the correctness of data input if the corresponding pattern in the form of a regular expression is present in the XSD.
- Script for hiding-opening any data item in the edit form.

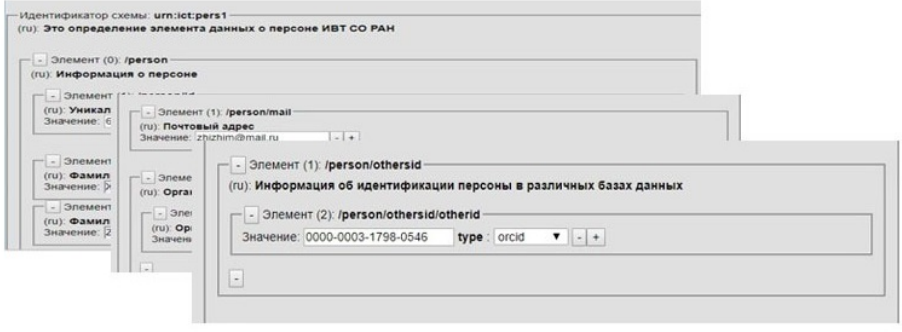

Figure 1. Graphical XML-editor: data entry fields

Conclusion

Thus, the following can be distinguished as the main results obtained in the framework of this work:

- investigated solutions allowing to process XML data;
- selected technologies for building the editor;
- the program framework of the editor has been designed;
- developed an adaptive model for entering and editing information;
- developed a prototype editor for converting XML elements into HTML forms; the main components of the editor are built, which implement the basic principles of the adaptive model for entering and editing XML data.

The developed XML records editor allows you to import any XML data and transform its structure efficiently and easily, while the same processing process will allow you to transform the original data of any structure without any change in the program code.

The created prototype of the described adaptive XML records editor is currently built into the ZooSPACE-W subsystem of the ZooSPACE platform [1,8,9,10]. Work is underway to improve its functionality in terms of expanding the list of supported XSD and JSON elements. When organizing the functioning of client applications and web services, it is necessary to take into account possible problems of interaction of distributed applications caused by uncertainty in the WSDL specifications intended for implementation in different environments. The implementation of the above concepts ensures guaranteed interaction between client and server applications on different platforms when working in heterogeneous environments.

References

1. Mukhitova, A., Zhizhimov, O.L.: Implementation of an adaptive model of input and editing information based on XSLT transformation for heterogeneus data. Open Semantic Technologies for Intelligent Systems, Iss. 3., 173-178, (2019)
2. Zhizhimov, O.L.: Explain Services on ZooSPACE Platform and Adaptive User Interfaces. CEUR Workshop Proceedings, Vol.1536, 30-36, (2015) http://ceur-ws.org/Vol-1536/paper4.pdf.
3. ANSI/NISO Z39.50-2003. Information Retrieval (Z39.50): Application Service Definition and Protocol Speciation. NISO Press, Bethesda, Maryland, U.S.A. Nov 2002. ISSN: 1041-5653. ISBN: 1-880124-55-6.
4. XML Schema Part 0: Primer Second Edition: W3C Recommenda-tion, http://www.w3.org/TR/xmlschema-0, Last accessed 20 Sep 2020
5. XML Schema Part 1: Structures Second Edition: W3C Rec-ommendation, http://www.w3.org/TR/xmlschema-1, Last accessed 20 Sep 2020
6. XML Schema Part 2: Datatypes Second Edition: W3C Rec-ommendation, http://www.w3.org/TR/xmlschema-2, Last accessed 19 Sep 2020
7. XSL Transformations (XSLT) Version 2.0: W3C Recommenda-tion, http://www.w3.org/TR/xslt20, Last accessed 18 Sep 2020
8. Mukhitova, A.A., Zhizhimov, O.L.: Adaptive technologies in the context of designing administrative graphic inter-faces for heterogeneous information systems of inputting and editing data. XVI Russian conference of "The distributed information-computational resources. Science in digital economy"(DICR-2017): Proceedings of XVI All-Russia Conference, Novosibirsk, 142-149, (2017) http://elib.ict.nsc.ru/jspui/bitstream/ICT/1467/20/paper16.pdf
9. Zhizhimov, O.L., Fedotov, A.M., Shokhin, Y.I.: The ZooSPACE platform-access organization to various distributed resources. Digital libraries. The Russian scientific e-magazine, Vol.17, No 2, ISSN 1562-5419, (2014)
10. Mukhitova, A., Zhizhimov, O.L.: Application of XML-technologies in the Construction of Input and Editing Data Model in the Adaptive Administrative Graphical Web Interfaces for Heterogeneous Information Systems. Data Analytics and Management in Data Intensive Domains: XX International Conference DAMDID/RCDL'2018, Moscow: FRC CSC RAS, 157-160, ISBN: 978-5-519-65438-8, (2018).

One Approach to Pattern Recognition Algorithm in Weak Measure Based on the Psychological Theory of JKelly*

Murat K. Nauryzbayev[1,3][0000−0003−4370−6989],
Raxila Z. Tuleushova[2][0000−0002−7574−6355], and
Yernar I. Imangaliyev[1][0000−0001−9760−9709]

[1]National Engineering Academy, Almaty, Kazakhstan
itismurat@yandex.ru

[2]Civil Aviation Academy, Almaty, Kazakhstan
ratu@inbox.ru

[3]Kazakh research inst-itute of livestock and fodder production, Almaty, Kazakhstan

Abstract Pattern recognition in weak measure related to problem in which precise identification of the original image is not required, but it is important to establish the belonging of a given image to a certain class of images. This formulation of the problem was encountered in the development of an algorithm for controlling an active damper of seismic vibrations these acting on a bridge structure. In another case, this problem arose in connection with the problem of determining errors in filling out the database of animal populations on farms.
It was interesting to try to approach the solution of this problem by combining both cases into single formalism, using the representations of the psychological theory of Kelly, developed in the first half of 20th century. By our opinion, the conceptual philosophy embedded in this theory can become a good basis for such formalism. The primary and simple examples that will be discussed in this paper may stimulate interest in the extended interpretation of Kelly's theory in the design and analysis of artificial intelligence systems.

Keywords: Personal construct theory, Pattern recognition in weak measure, Software emulation of the psyche, Statistical description of the image, Artificial intelligence systems, BLUP selection.

Introduction

The definition of "strong measure"refers to ways of comparing two functions and this ways can be expressed in terms of uniform convergence of one function to another. All ways to determine distances between functions different from this definition will be called - "weak measure"which includes for example, convergence in the sense of the mean square.

It is better to express mathematical models of a number of engineering applications in weak measures, since the detail inherent in exact solutions for them is redundant. In calculating the roof strength for resistance to snowfall, the trajectories of falling snowflakes are not calculated, but an integral characteristic is used - daily precipitation.

* Supported by National Engineering Academy

To the based on a weak measure ideologies are also related image recognition algorithms and computer simulation of the psyche. In these cases, processes are activated under external influence - loading an image in the recognition algorithm or an irritant in the emotion simulator. Further, the algorithms build a hierarchy, starting with processing simple primary actions, going through the creation of increasingly complex and ordered data structures to the resulting conclusion. For both cases, situations are characteristic when the input signals may be not equal but lead to the same results.

Kelly's psychological theory of personal constructs [1,2,3] is interesting for its ideology of building a hierarchy of structures of highly fuzzy data. When describing personality psychology, this theory is based on a workable mathematical model, which compares favorably with other theories in psychology. Here, the perception of the surrounding world by a person is based on a system of constructs developed by each individual in the process of expanding his own life experience. The connections between constructs are statistically assessed, and these connections determine the choices and behavior of an individual.

In an extended version of Kelly's idea that the human psyche can be quantitatively described as a formalized set of constructs, the interaction between which is described by mutual correlations, can be useful in simulations of artificial intelligence.

At the same time, the description of the interaction of constructs through probabilistic correlations is not mandatory and, in all likelihood, is used by Kelly due to the dominance in his studies of statistical methods for the experimental identification and assessment of the influence of constructs on human behavior.

It is possible to extend Kelly's representations to objects artificially created in the computer memory in the form of a system of given constructs and given links between them. Then one or more constructs of the system can be connected with the input device. Under external influence on the system input devices the disturbance signal will be associated with part or may be all of the constructs of the system. Since constructs are not initially limited to discrete ranking, such a system will be able to process and display analog signals.

If we impose random modulation on connections between constructs or make connections dependent on previous experience, then the response of the system to the same external influence will be different. This allows in principle to consider such program either as some kind of visualization of the artificial psyche, or simply to consider the resulting system as the simplest implementation of the artificial psyche.

Finally, it will be interesting to try to use the resulting system of constructs as a basis on which to decompose some image. At the same time, there is reason to believe that if another randomly selected image is identified by the system in some measure, this basis will be complete to this measure for the whole class of images.

In this case, the described approach will be useful for pattern recognition in applications in which it is important to determine the belonging of a given image to a certain class of images. In this paper, we will give several such examples.

Kelly's theory

It is necessary to clarify some provisions of Kelly's theory, which will have to rely on below. First, Kelly's theory uses a rational representation of a complex intellectual system in the form of a closed and limited set of constructs and connections between them. This idea has so quite general nature that it's more appropriate to speak of ideology rather than method.

The starting point of Kelly's theory is that the consciousness of each person constantly explores the environment and in the process of research compactly maps the phenomena of the environment interesting to him into constructs. To explain the influence of some constructs on others, our consciousness determines the connections between them, which Kelly calls implicit theories. Thus, each consciousness can be represented as a researcher, mapping elements of the external world into constructs and creating theories to describe the relationships between constructs. That theories or rather their visible manifestation are wanted quantities in the Kelly model.

Kelly's construct itself is a bipolar construction developed by our consciousness that describes the subject's knowledge about surrounding world element in the form of a ranked vector drawn between the extreme manifestations of the concept under study. For example, the construct is ”hot - cold”. At the same time, the concepts of ”hot”or ”cold”are unique for each person, since they are based on individual life experience. For example, a boiling kettle might be the hottest item for a child. An adult may be familiar with the temperature of a hot metal. For many, the coldest temperature is associated with winter, while scientists are familiar with liquid helium. This example shows individual nature of construct ranking.

The system of construct is not static. The human mind is able to analyze correlations between constructs and generate new correlations as a result of inference. Such correlations Kelly called - ”implicit theories.”Taken together, implicit theories and a set of developed constructs determine the psyche and intellect of a person. Kelly determined correlations and constructs in an individual in a series of rather refined tests, using regressions for the desired values. These regressions, together with concepts of constructs and implicit theories, constituted the mathematical formalism of Kelly's theory of personal constructs.

Let's consider the formation of the system's response to external influences in Kelly's theory using an example. Let there be two constructs ”hot - cold”and ”pain - not pain”. These constructs belong to the category of primary ones, since they are associated with direct measurement by the senses, and did not arise as a result of inference. Also, from experience, a correlation is established, asserting that touching a hot kettle is painful, but a cold one does not.

It is essential that the constructs are ranked, i.e. the concept of ”hot”has gradations. A cold kettle just put on the fire may not necessarily be hot. Therefore, the correlation coefficients between the constructs are not strictly equal to 1 and -1, but are found from experience.

The first non-trivial implicit theory arises when an individual realizes that the sensation ”pain”arises not only from hot, but also from a number of other reasons. Consciousness is able to combine these reasons into a new category ”dangerous created by the results of processing statistics of many perturbations acting on one construct

”pain - no pain”. It possible skip two more similar non-principled steps and go straight to the final implicit theory. When the system receives the input signal ”kettle stands on a fire the implicit theory generates a response in the form of the conclusion: ”kettle stands on a fire - definitely not to be handled and if kettle stands on the table is ”probably possible”(Fig. 1).

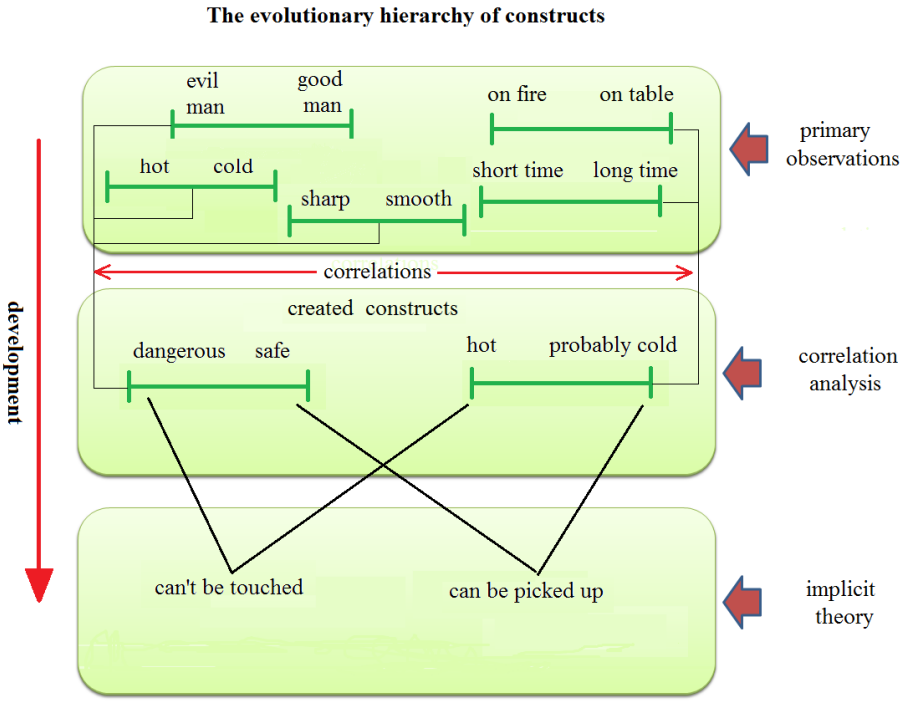

Figure 1. The evolution of primary constructs toward ”implicit theory”.

In contrast to logical constructions based on rules and axioms, here the final reaction of the system arises on the basis of statistical processing of experimental data and is the result of the probabilistic interaction of external influence with a construct created by consciousness itself at the previous stage.

There is a psychologically more vivid example is given [1]. Most people think that a person with a ”warm look”is more kind person than evil. There is a correlation between the constructs ”warm look - cold look”and ”good person - evil person”. As above, the ranking and correlation coefficient of these constructs will be individual for each subject.

We have just looked at an example with the ”hot-pain”correlation. How do you feel now about the slight correction of the correlation ”warm look - kind person”to ”hot look - kind person”. Will these two conclusions be the same for you? Perhaps, during

the reading of the previous paragraphs, the brain managed to create new implicit theories based on the analysis of what was read and thereby predetermined your instantaneous assessment.

In Kelly's theory by means of special tests (repertoire grids), the system of individual constructs and their ranking are first revealed. The second step, based on statistical analysis, determines the correlation coefficients between the constructs. The number of constructs developed by the subject, their ranking and the depth of connections between them depend on the level of intelligence and life experience of the subject.

The starting points of this theory were initially human-oriented and for this reason contained some specific limitations. Due to the generality of the fundamental definitions and principles of Kelly's theory, they can be naturally extended and generalized to the case of society, as well as artificial intelligence, which allows the development of a number of computer formalisms.

Group consciousness

Comparing neural networks and Kelly's set of basic constructs, it is useful to see the analogy with the difference between the thermodynamic description of gas and the description of gas in kinetic theory. Both theories have an overlap area where they give the same results. In this area, the kinetic theory deduces the behavior of the macroscopic volume of matter, based on the movements of individual molecules, in the same way as neural networks use single neurons to form a general image created by the entire network of neurons.

Thermodynamics deals with parameters such as volume, pressure, entropy and temperature, which are applicable to the macroscopic volumes of any substance. Similarly it can be noted that the base of correlated constructs is applicable to any system performing deliberate actions, of course with a loss of accuracy characteristic of macroscopic averaging.

The first logical step is to go from describing an individual person to describing a society formed according to some attribute: ethnicity, age, belonging to a certain consumer group, etc. From the standpoint of Kelly's theory, it is easy to see that a social group as a whole will have its own individual constructs and correlations that identify the group by its behavior.

But then it should be concluded that a social group is equivalent to one single person with intelligence, but at the same time its intelligence is not human, since the reaction of the group is not equal to the algebraic sum of the reactions of its members. Why this happens, perhaps, will explain the corresponding "kinetic theory". Construct theory, like thermodynamics, will draw conclusions, limiting it only to considering the visible parameters and the interactions between them.

After that, we can take the second step and assume that the theory of constructs allows for a formalized "thermodynamic"description of a class of different consciousness, including extraterrestrial intelligence or artificial intelligence, within the accuracy of this technique. The accuracy of the methodology here is determined by the measure in which the belonging of the function to the class is measured.

Direct and inverse problem

The direct task will be to identify the constructs themselves, their ranking and correlations between them.

The next extension of Kelly's theory will be the introduction of the notions of direct and inverse problems in construct theory. The direct task will be to identify the constructs themselves, their ranking and correlations between them. Due to above-mentioned adequacy of the formal description in terms of constructs for an individual and for a group, tasks related to predicting the group's reactions may be interesting for sociologists.

The inverse problem arises when trying to give some "free will"to computer programs. Within the framework of the inverse problem, the initial set of constructs is specified by programmer during design time. The initial correlation coefficients are also set. The influence of constructs on each other has a probabilistic nature, and this interaction is given by random sequences obtained from a random number generator, after which they modulate the correlation coefficients. As a result, it is possible to develop a computer character that will react unpredictably to the same stimuli at different times. Thus, the described extension of Kelly's theory shows a way to create a virtual object with psychical properties.

Let the program define N constructs and let S_i – be one of them. Then for correlations in the general case you can write:

$$\sigma_{ik} = Cor(S_i, S_k).$$

In computer implementations, Kelly's theory can be interpreted quite broadly, since a lot is determined by the programmer's abilities and imagination. In particular, the correlation coefficient is not necessarily equal to the mathematical correlation, but can express any way of describing the relationship between constructs that is convenient for the programmer. Usually this choice is related to the specifics of the program object. Then we understand $Cor(S_i, S_k)$ in this sense.

In the direct problem, constructs are given and correlations are determined. The input signal F acts on ranked constructs of the system. This impact simply changes the meaning of each construct within its ranking. After that, correlations are calculated according to the scheme:

$$F \to (S_0, S_1, S_N) \to |\sigma_{ik}| \tag{1}$$

In the inverse problem, correlations are given and constructs are identified. The input signal changes the correlations by which new values of the constructs are calculated:

$$F \to |\sigma_{ik}| \to (S_0, S_1, , S_N). \tag{2}$$

The solution to the inverse problem is a set of constructs, each of which has a specific meaning. Each set will be called the state of a system of N constructs:

$$H_k(S) = (S_0, S_1, S_N) \tag{3}$$

We will use (1) as a pattern recognition scheme, while (2) is a general illustration of an algorithm for constructing a model of an artificial psyche.

Each state H_k (S) can be programmatically mapped to image visible to the user, for example, a play character generated by the program. To enhance the effect you can add random noise to the influence of external signal. The behavior of a character visible to the user is a sequence of his states that change under the influence of external signals. Due to the presence of random factors, the character's behavior will not repeat exactly when the disturbance is repeated.

Then it is possible to carry out a series of tests with the system, in which the same sequence of signals will be fed to the input. This sequences will create corresponding sequences of system states $-H_k(S)$. Let at the same time:

$$H_k(S) \to H, k \to \infty, \quad H < \infty. \tag{4}$$

This means that there is some statistically dominant state H. Then it can be argued that the play character has a stable psyche in relation to the experienced disturbances. In this case, the state H is the play character's limit cycle.

In relation to play character training, then in this case it is necessary to introduce the target function H(S), which will sets the limit cycle. If condition (4) with respect to a play character is fulfilled, then this means that he has acquired a stable emotional character. If the limit cycle matches the objective function:

$$N = H \tag{5}$$

then this will mean solving the task of learning. In this case, through training, you can achieve the target behavior from the object. If the limit cycle does not exist, then the character will exist as an object with an unstable emotional appearance.

Applied problems

In our case, we will solve the problem of determining the membership of a function given graphically to a certain class of functions. This task will be solved according to the scheme (1). Two cases led to this formulation of the problem.

In one of them, a method of protecting a bridge structure from seismic effects was considered. Let the bridge span be connected to an active damper, in which the force of resistance to an external load (reactive force) can be controlled. The flexural function of the bridge span is measured by sensors in real time. This function is used as a feedback signal driving an active damper.

The bridge structure and the active damper form a feedback oscillating circuit. he control algorithm processes the feedback signal and determines the reactive force mode. Analysis of the mathematical model of the contour showed that various external influences are divided into classes of perturbation functions. Each such class can contain infinitely many modes of various shapes, but any vibration from the class can be suppressed by just one damper mode, common to the entire class.

Technically only a limited number of modes can be implemented in an active damper which must withstand the full range of seismic disturbances. For this reason,

the theoretically established relationship between the classes of perturbed functions and the damping regime allows us to look at the active damping of seismic disturbances as a really feasible process.

It is necessary for this that the control algorithm be able to recognize the belonging of the disturbance function to a certain class. After recognition, the program activates the desired mode, at same time the exact form of the function can be ignored. The independence of the result from the exact form of the function is ensured by the following circumstance.

The mathematical model of the process described above was built in a weak functional measure. Here, a measure refers to a way of measuring the distance between two functions. Equality of functions in a strong measure simply means their coincidence and corresponds to the classical solution of the differential equation of the process. The solution to a weak extent allows not to take into account the degrees of freedom that are redundant for device control and to obtain a result that meets the goal of an engineering application. The question of the measure of distance will appear later in pattern recognizing efforts, since this measure determines the coincidence of the current pattern with the target.

The second need for a fast special recognition algorithm was the problem of identifying incorrect data in the animal database, summarized for a large number of farms (in our case, about 500,000 cows). These errors are critical for the use of BLUP animal indexing. The problem is important because this technique is one of the modern paradigms of genomic selection.

The original data is presented in a table, in which one column contains the dependent data, and the other independent factors. This data can be represented graphically in a space with dimension equal to the number of columns. Knowingly reliable data are selected as a reference, for which a reference data function is constructed. Specifies the weak measure in which the functions will be compared. A check for the difference of each pair of data will correspond to a strong measure here, which in this case will be an excessive requirement. Some errors in indicators that have little effect on the result of factor analysis are neglected within a weak measure.

The pattern recognition in weak measure

It is advisable to start the consideration with an illustration of the algorithm. Figure 2 shows four hand-drawn shapes that was suggested to the program for comparison.

The program recognizes figures a) and b) as the same and rejects options c) and d) due to their structural and geometric differences. In figure c), the lower right branch has a downward concavity, and in figure d), the lower branches do not go out of one node.

The primary constructs here are line segments from their beginning to a branch point or intersection with another line. Image d) is formed from 8 constructs. The decomposition of the image into primary constructs occurs as shown in Fig. 3.

Initially, let's discuss the algorithm's works in general terms. At the first stage, the contour is divided into separate primary constructs according to the contour nodes. At the same time, algorithm make classification of constructs In weak measure, where each construct being assigned the name of the class to which the construct belongs.

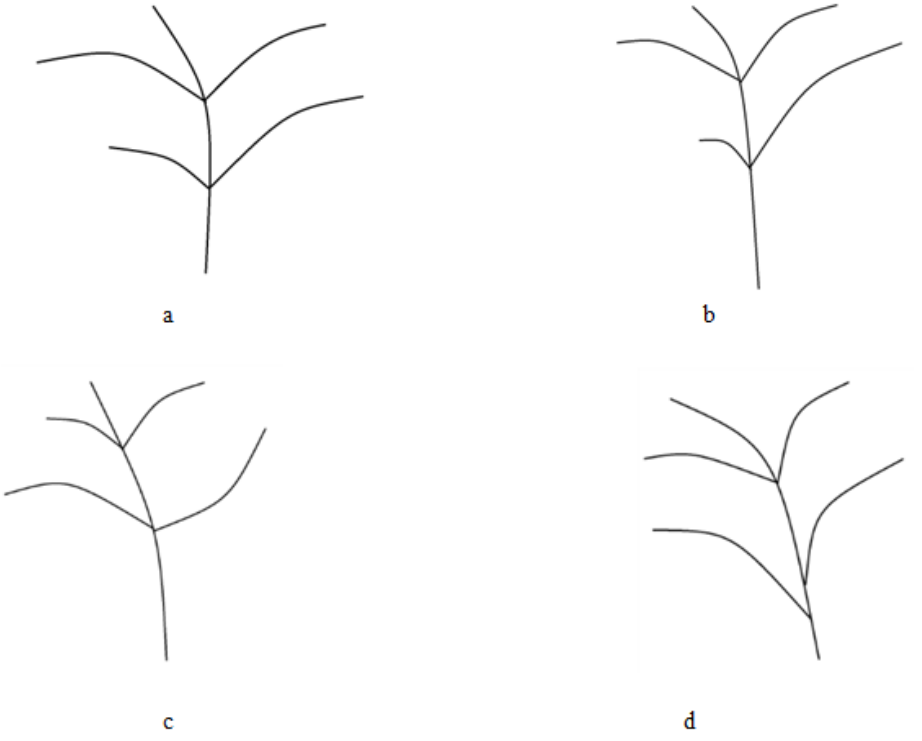

Figure 2. Test images.

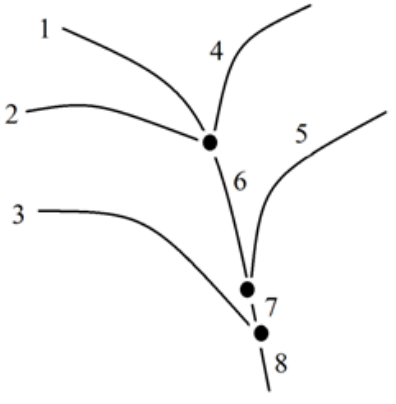

Figure 3. Image decomposition into system of constructs.

In weak measure constructs from the same class are considered the same. Accordingly, the classification of the image in Fig. 3 gives:

branches 1,2,3 belong to class C1; branches 4,5 - class C24; branches 6,7,8 - class C3.

After that, a structural diagram of the image is created (Fig. 4). The match of structural schemes means the coincidence of images. The sampling accuracy is determined by the measure with which the primary constructs are assigned to classes.

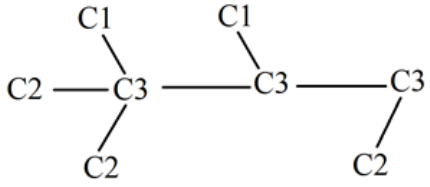

Figure 4. The Structure scheme of the image (Fig. 3) in a weak measure.

If you change the settings in order to strengthen the measure, then the previous structure will look like in Fig 5.

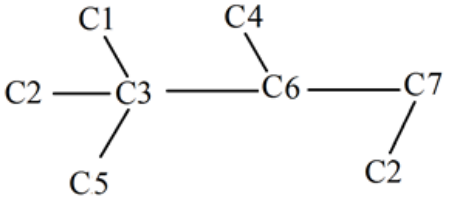

Figure 5. Structure scheme of the image (Fig. 3) in more strongly measure.

The structure of an image decomposed into a basis of constructs in more strongly measure, not match with the structure of the same image in a weak measure. This illustrates the ability of the program to adjust the detail of the image by adjusting the measure. The criterion for selecting a measure is the context of the task or requirement from the application for which the image selection is performed.

The structural diagram (Fig. 4, 5) is equated to a new derived class - CF1, formed by the system and which will play the role of an independent construct in recognizing more complex patterns. For example, the image in Figure 6 represents a composition of 8 primary constructs: C1, C2, C3, C4, C5, C6, C7, C8 and two derivatives: CF2, CF3. This image is far from the usual images, but the figure presented structurally corresponds to the picture of the distribution of experimental data displayed in a certain space.

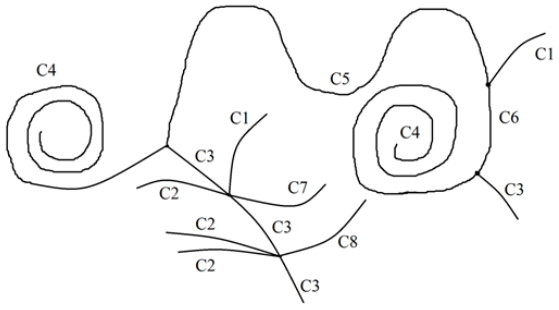

Figure 6. Composition of constructs.

At the final level, its structure is described by the scheme:

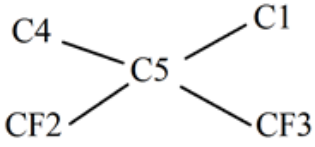

Figure 7. Structure scheme at a high level.

where derived constructs are described by schemes:

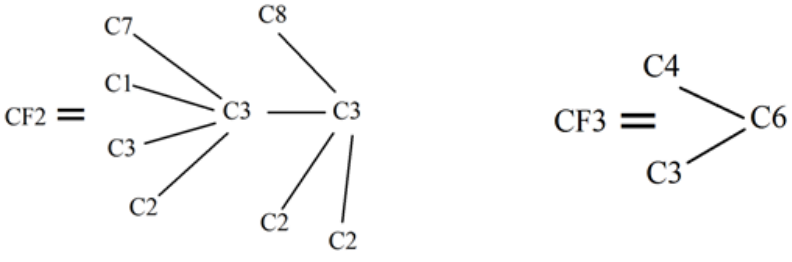

Figure 8. Components of the high-level circuit.

Correlations between constructs are here given by structural schemes, examples of which are given above. The coincidence of schemes means the coincidence of the system of constructs and their correlations in accordance with expression (1). This is

just the simplest way to describe correlation. In these examples, structural correlation determines the topological similarity of the shapes. For a more subtle analysis of geometric correlations, the description of the primary construct includes information about its length in pixels; this information is used in more detailed comparisons (see below).

Thus, the recognition process in this approach is as follows.

1. First, a reference image is set, which is decomposed into constructs and its structural scheme (structural correlation) is created. After that, there is a given system of constructs and correlations between them.
2. The tested figure is decomposed into constructs. If the resulting set of constructs coincides with the reference one, a structural scheme will built. The image will be identified if the structural correlations match. The non-coincidence of the schemes in at least one element will mean that the original images are different.
3. Constructs at one level are combined into one new derivative construct. The order 1 corresponds to the primary construct (the construct created as a result of measurement), then the order of the derived construct created as a result of union previous ones will be equal to the number of unions of the previous constructs into a new one.

The method of constructing structural schemes provides a lot possibility to transform these schemes to set of natural numbers. This means that structural diagrams are easily indexable, that makes it possible to work with large images. In systems with a complex data structure, the program will operate with typical structural diagrams, but on higher-order constructs.

Separation of primary constructs

We will proceed from the fact that the record of the original image stands in a raster, which is processed in any suitable way to highlight the contours of the objects in it. Another way the contours are graphs of functions for which the first operation is not required.

In our tests, the preprocessing of the image is set up so that the outlines of the areas are outlined with lines one pixel thick. This is required to facilitate the work of the algorithm. Pixels that are not area boundaries are filled with zero values.

The contour vectorization is performed as follows. Figure 9a shows a fragment of the pixel grid. Let the pointer be at pixel 0. There are 8 directions for moving the pointer from this place to the adjacent pixel. The directions are numbered in Fig. 9a. Diagonal offsets can be thought of as the sum of the vertical and horizontal offset. For this reason, if the number of pixels is large enough (in practice, more than 4), the contour line can be described by four arrays, in which step-by-step displacements along the main orthogonal axes are written.

The algorithm scans the image matrix line by line from the upper left corner, sequentially traversing all the columns of the matrix. When a non-zero pixel is found this pixel becomes active, its coordinates are written to the scan pointer. Neighboring pixels are scanned clockwise from the direction to the previous active pixel (Figure 9b).

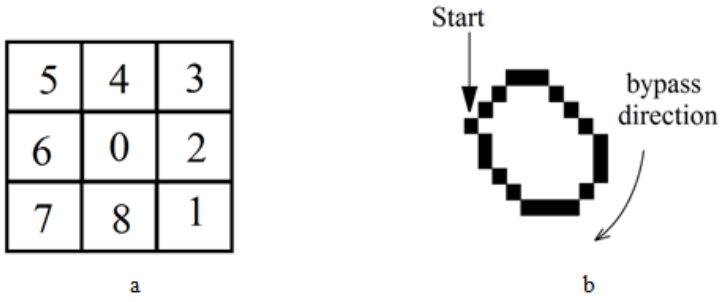

Figure 9. Rules of directions and detours in the algorithm. a - for a pixel, b - for an outline.

When a non-zero neighboring pixel is found, it becomes active, and the movement is written to the corresponding array. After this, the procedure is repeated until the end of the line is reached, or the branching point or intersection of the lines.

Four elementary displacements are recorded in four one-dimensional arrays. The index of the one-dimensional array is the number of the scanned pixel. The array value is 1 when the direction number is equal to the array number and zero in all other cases. For example, for the figure in Fig. 9b, where the pixels are shown as black squares, the beginning of the displacement arrays will be as follows:

Table 1. Writing a contour to arrays of elementary displacements.

Direct number	pixel number													
arrDir2	1	2	3	4	5	6	7	8	9	10	11	12	13	...
arrDir4	1	1	1	1	1	1	1	1	1	1	0	0	0	...
arrDir6	0	0	0	0	0	0	0	0	0	0	0	0	1	...
arrDir8	0	0	0	0	0	0	1	1	1	1	1	1	1	...

Table 1 shows how each line of the image, bounded by nodes or the beginning of a branch, corresponds to four arrays of elementary displacements. To calculate correlations between these arrays, the following rule is set: $Cor(1,1) = 1; \quad Cor(1,0) = Cor(0,1) = 0.5; \quad Cor(0,0) = 0.$

After that, the correlation matrix is calculated:

In the correlation components, straight line segments inclined at different angles to the abscissa axis have the same form and, therefore, are recognized as one construct - an inclined segment (Fig. 10). The same will be the case with curved line segments. This makes the description of the geometric statistics of the figure in Table 2 preferable to the data in Table 1.

Until that time, information about the original image was preserved and all the transformations made are reversible. It is possible to start with Table 2 and build the

Table 2. Correlation matrix.

Corr Between	pixel number													
Cor24	1	2	3	4	5	6	7	8	9	10	11	12	13	...
Cor26	1	1	1	0.5	0.5	0.5	0.5	0.5	0.5	0.5	0	0	0	...
Cor28	0.5	0.5	0.5	0.5	0.5	0.5	0.5	0.5	0.5	0.5	0	0	1	...
Cor46	0.5	0.5	0.5	0	0	0	0	0	0	0	0	0	0.5	...
Cor48	0.5	0.5	0.5	0	0	0	0.5	0.5	0.5	0.5	0.5	0.5	0.5	...
Cor68	0	0	0	0	0	0	0.5	0.5	0.5	0.5	0.5	0.5	0.5	...

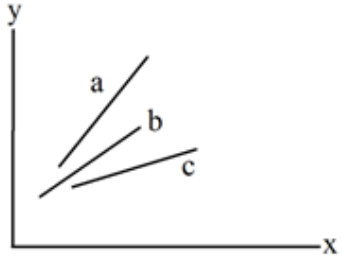

Figure 10. Segments a, b, c in correlation components describe an equivalent object, despite differences in slope and length.

original shape. However, this information is redundant for the problem of recognizing image classes, so will proceed as follows. Let L be the length of the construct in pixels. The construct will to split into N_S equal parts. Then, each of the N_S segments will consist of $p = L/N_S$ The influence of the remainder from division can be neglected for now, relying on its small statistical weight. For each of the N segments of the construct, construct the normalized sum:

$$Cr(i,k) = 1/p \sum_{m=pk}^{p(k+1)} T_{im}, \tag{6}$$

where $T_i m$ – element i-th string m-th column of correlation matrix.

Components of $6 \times N_S$ matrix $-Cr(i,k)$ are equal to the segment average correlation and express the approximate statistical characteristics of the geometric curvature of the segment. These characteristics are normalized to the length of the construct, therefore they can be compared with the same normalized characteristics of other constructs.

According to the methodology (1): $F \rightarrow (S_0, S_1, S_N) \rightarrow |\sigma_{ik}|$, in the process of identification the unknown image F (external influence) is decomposed according to its constructs and for it a correlation matrix is found $Cr'(i,k)$. This matrix is compared with the reference matrix $Cr(i,k)$. The value:

$$d_{ik} = \|Cr(i,k) - Cr'(i,k), \tag{7}$$

used to compare two images. The use of the notation for the norm of a function for a given difference is intended to remind that the measure of comparison of functions here is a metric defined by the programmer. At this stage, two characteristics already appear - N_S and a functional measure that can be used to control the recognition process.

For the above test cases, a simple measure is used:

$$d_ik = \begin{matrix} 0 & if d_{ik} < \varepsilon \\ d_{ik} & if d_{ik} \geq \varepsilon. \end{matrix} \tag{8}$$

The value of ε also determines the course of identification, we established it empirically.

The results of comparison of the reference with several samples can be accumulated in the results matrix:

$$Res(i,k) = Res(i,k) + \begin{matrix} 0 \; if d_{ik} = 0, \\ else 1, \end{matrix} \tag{9}$$

$Res(i,k) \equiv 0$ for first image.

Let the construct be a fragment of a sinusoid. The source images of a sinusoid are drawn by hand, while both the reference and the tested fragments are similar to a sinusoid only in the human mind and will not withstand analytical verification.

We will adjust the program so that the recognition of the sinusoid coincides with the subjective assessments of the person. For this, a quick version of factor analysis is performed, where the factors are the elements $Res(i,k)$.

Having selected one of the images as a reference, the procedure described above with several other figures is carried out. This will result in the accumulation of the matrix $Res(i,k)$. The matrix grows unevenly, some of its components grow with each new test, while others grow quite randomly. Let the maximum number of events accumulated by a factor in a series of Q tests be W:

$$W = \max(Res(i,k)) \leq Q.(12) \tag{10}$$

Let us introduce one more adjustable parameter $\alpha[0,1]$, which sets the confidence interval for accumulated events. If the number of accumulated events:

$$Res(i,k) < \alpha W, \tag{11}$$

then the match for this factor is ignored. As a result, a significant part $(\tilde{Res})(i,k)$, will remains, which participates in the comparison. Let us denote the number of valid elements $(\tilde{Res})(i,k)$, by D.

Now it possible return to the example of recognizing a sinusoid as a single construct. Let the next F-th image be checked against the reference. This reveals coincidences on a subset of elements $(\tilde{Res})(i,k)$. The number of found matches exceeding D will be the final result of the program. The numerical threshold D will also be an adjustable parameter. If, the experimenter (of course, any other context can be used instead of

the experimenter) considers the figure F and the reference are same, then all tunable system parameters will be saved. The resulting set of settings will be used to identify the construct class in the future. Expanding the number of classes of recognizable constructs plays the role of training the system.

It is necessary to pay attention to the following circumstance. The loss of primary information about the image occurred when we split the line of the construct into segments and switched to the segment-average correlations. This is done in order to speed up the operation of the algorithm and make it possible to compare line segments of different lengths and orientations.

After that, the description of the image becomes statistical and there are certain risks that must be taken into account. Figure 11 shows two shapes that the program unexpectedly found to be the same.

Figure 11. Identification failure.

The reason for this is that the statistical contribution of the upper parts of the figures significantly exceeded the contribution of the lower ones. This problem is eliminated by choosing N_S.

Simple kinds of correlations between constructs

The previous section discussed statistical method describe of construct. For this, correlations within the construct were used and these values are not relevant to correlations between constructs. Within the framework of the general ideology, the way of determining correlations between constructs can be set based on the conditions of the problem as it was done above.

Since this approach was developed to obtain high-speed algorithms for real-time damper control, simple methods of calculating correlations take precedence. In fact, in a similar way, it's possible to achieve a sharp increase in the speed of calculations. The

question remains to what extent the introduced simplifications retain the worth of the obtained result.

This can be analyzed in the following example. There is a video surveillance camera installed along the carriageway and recording passing cars. The program performs automatic target acquisition by comparing checksums calculated on two scan lines separated by 20 pixels in the lower half of the frame. Simultaneous change of both amounts is a trigger that starts recording the image in the working memory of the program. The actuation of the trigger plays the role of external disturbance F acting on the system.

In Fig. 12 shows a car captured by a camera in poor visibility conditions (low light and fog). The bad quality of photography here is really due to difficult conditions, not printing disadvantages

Figure 12. Original target image

In accordance with the above, the captured image defines one current state of the construct's system. At the input of the system, the captured frame is a set of pixels of different intensities ordered by columns and rows. According to the condition, the program was supposed to distinguish cars, buses and trucks from each other, as well as determine their speeds. Obviously, one of the target functions will be a subset of pixels corresponding to images of cars.

Shown in Fig. 12. the image is a fragment of a full frame with a size of 1920 x 1080 pixels, in a palette of shades of gray at 8 bits per pixel. After capturing the object, the frame image is rewritten into the program memory in a raster format, taking into account the flip and mirror reflection of the original image in the camera.

To get the maximum speed indicators, this part of the program is written in assembler and uses sparse sampling (see below). The computation time was recorded according to the number of spent processor cycles. The current value of the processor clock counter was determined in a typical way, transferring the code 15, 49 to the processor by bytes and reading the result from the ECX: EAX registers.

The identification of the target contour was carried out using methods of fixing the brightness discontinuities, while various measures were used to determine the discontinuity. For Sony XCG-500 cameras, the use of an integral measure turned out to be optimal, which is determined by the sum of intensities of pixels adjacent to the scanning point normalized with some weight, which helps in conditions of poor visibility. Under normal conditions this is unnecessary and led to time losses.

The target contour image is formed mainly by piecewise smooth curves. This circumstance makes it possible to select scan points not in a row, but across 8 pixels in our case. This technique allows you to increase the speed of program execution in this area by $8^2 = 64$ times, this is called a sparse sample. The result of scanning the original image in Fig. 12 is shown in Fig. 13.

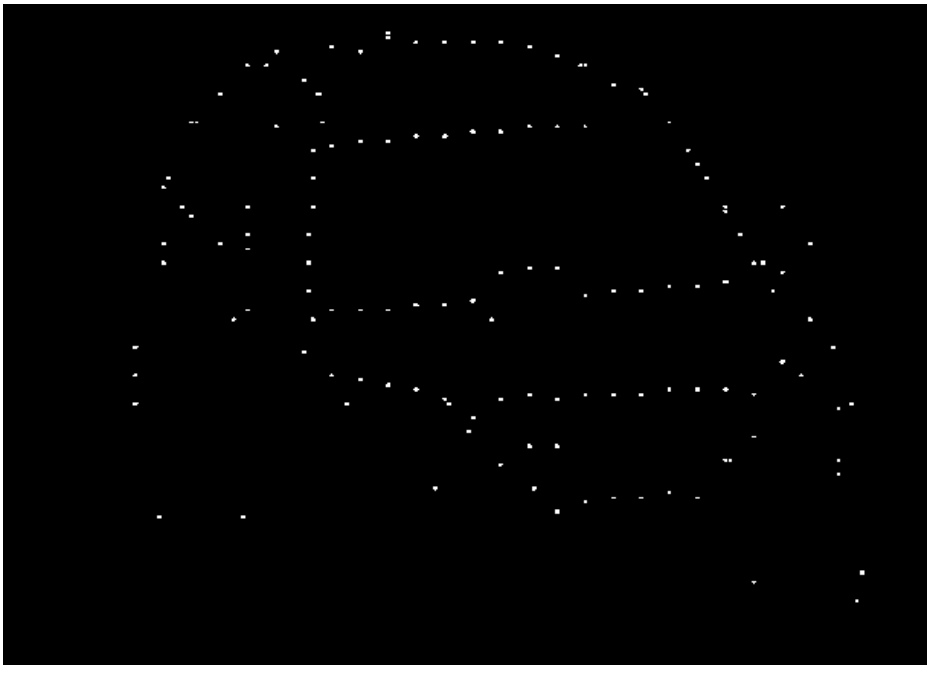

Figure 13. View of the target contour in the sparse sample.

All the operations performed up to this point are quite typical and have no direct relation to the theory of constructs. Let us show how you can identify a vehicle class (car or bus) using the simplest correlations between constructs.

Here we want to show the capabilities of simplified construct and correlation models. The simplest form of the construct is a straight line segment. In this approximation, the image of the target will be decomposed into constructs of only two types.

In the first approximation, the sequences of points in Fig. 13 can be approximated by line segments. If we introduce an orthogonal coordinate system in the figure, then the segments that will have a small deviation from the vertical axis form a system of vertical constructs - h, similarly, segments close to the abscissa axis create horizontal constructs - w, other details are ignored.

To avoid excessive fine-scale detailing, a threshold value for the minimum segment length is entered. In our case, this corresponds to the minimum number of points forming a segment equal to 6 (on the non-sparse original image, this corresponds to a segment with a length of 48 pixels). As a result of the described transformation over the pixel field (Fig. 13), its representation in a system of two types of constructs is obtained (see Fig. 14a).

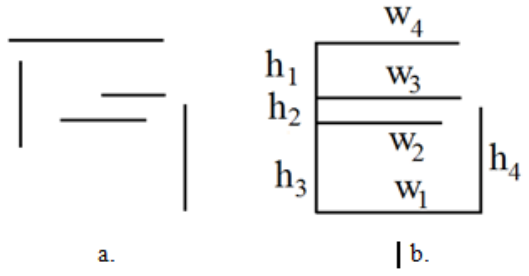

Figure 14. Representations of the original image.

Figure 14a is the result of a direct aproximation to the line segments of points in Figure 13, as described above. In fig. 14b shows the decomposition of these approximations into a system of h-vertical and w-horizontal constructs, that equivalent to the structural schemes used above (Fig. 7). The h_i values are equal to the ratio of the length of the i-th segment in pixels to the maximum vertical size of the area in which the selected segments belong to the same target. Accordingly, w_i are defined in relation to the horizontal dimension.

This area is determined by two consecutive frames, which are also needed to determine the vehicle speed. The details of this process are beyond the scope of this work.

Here important that quite workable correlations can be specified even in such a simplified approach. Let's set:

$$Cor_h(i,k) = h_i/h_k, \qquad Cor_w(i,k) = w_i/w_k, \qquad Cor_{wh}(i,k) = h_i/w_k. \quad (12)$$

The image in Fig. 12 was used as a reference image of a car, based on the fact that when shooting an object in poor visibility conditions, the most characteristic outlines of the car will be highlighted. For the reference car, the coefficients are calculated (14). When loading a new image, the coefficients (14) were calculated using the new data and compared with the previous ones:

$$d_{ik} = \|Cr(i,k) - Cr'(i,k)\|,$$

then there is the accumulation of $Res(i,k)$ on cars of this type, as described in the previous chapter. This technique is characterized by a relatively small sample size for determining the significant part $(\tilde{Res})(i,k)$ in the factor matrix $Res(i,k)$, in our case it was possible to limit ourselves to 15 values of the factors. Target identification is carried out by factor assessment (see above):

$$(\tilde{Res})(i,k) \geq aW, \quad where: W = \max(Res(i,k)), \quad a - adjustable factor.$$

The present description of test of model with simplified constructs and correlation estimates gives about 10% of errors in determining the type of car. A quite large percentage of errors can be explained rather by the fact that the algorithm was not specially modified for this task, than by the influence of simplifications of the constructs and correlations introduced into the model.

At the same time, with an acceptable recognition quality, the algorithm spent about 0.016 s ($4,16 \cdot 10^7$ clock of CPU cycles) per frame on a 2.6 GHz AMD processor on a 1080x1960 frame. During this period, the procedure for forming the contour (Fig. 13) took 13 560 000 cycles or 0.005 s, which is less than 50% of the computation time. The procedure for calculating correlations and comparing them is non-linear and takes almost as long as the selection of contours.

Another case of a simplified model was tested on the data of technological survey of a rail track. The camera was installed on a wheeled carriage bogie and continuously filmed the rail at a rate of 60 frames per second. Capturing one frame corresponds to 0.5m of railway track. The frame size is 400x300 pixels. The specific task was to recognize the rail joint and determine its width. As in the previous case, the computational core of the algorithm is written in assembler, which must be borne in mind when evaluating the speed indicators of the algorithm, since programs in assembler raise this indicator for reasons independent of the algorithm. In fig. 15a shows an image frame, the same frame after preprocessing in Fig. 15b.

Using the approach described above, the sparse sampling method obtains contour images in the form of a system of points (Fig. 15b) $h, w-$ constructs are created. The result of this operation is shown in Fig. 16.

This is enough to measure the dimensions of the joint. In this case jne defect of a simplified model are arising. During initial tests, the algorithm often took the herb captured by frame as a rail joint. In fig. 17 shows a comparison of the structural diagrams of the constructs formed by the plant (fig 17a) and the rail joint (fig 17b). You can see that different objects give the same structural diagram.

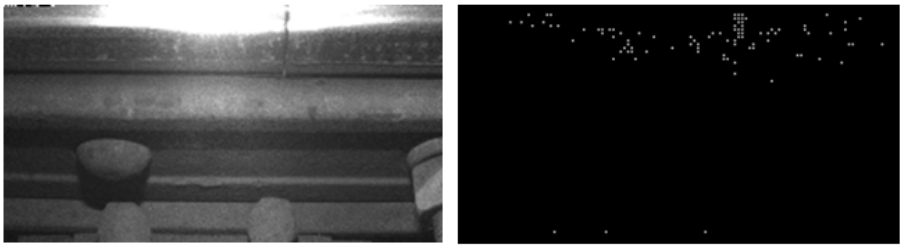

Figure 15. Recognition of rail track joints.

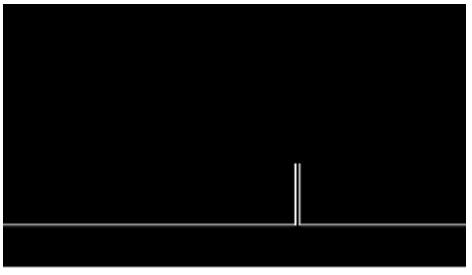

Figure 16. Constructs that describe rail track joints.

This problem can be solved relatively easily, given that the plants are beginning from the ground. Unlike the example above, here the main reason for the failure of the algorithm lies precisely in the simplified formula for calculating the correlation.

The identified shortcomings made the determination of the correlation somewhat more complicated. In the new version, it was taken into account that the plants grow from the ground, and the joints are limited by the rails. After that, false events stopped. In addition, it was nessesary to parry the influence of sun glare on the working surface of the rail.

Once modification accepted, the program received sufficient performance. With a frame size of 400x300 pixels in 256BMP mode, the joints were detected, filtering noise in the form of grass stalks crossing the rail image in the pictures, spending $3.25 \cdot 10^5$ processor cycles per frame or at an exposure 1/1000 about 800 frames per second in video sequence.

Conclusion

Attempts to use elementary graphic templates for pattern recognition have been made since the first works in the field of computer vision. This, for example, is given a place in the early fundamental monographs [7,8]. In these attempts, elementary graphic templates are often associated with graphic primitives such as arc, line, circle, etc. This is facilitated by a certain tendency to perform recognition tasks using a graphics accelerator.

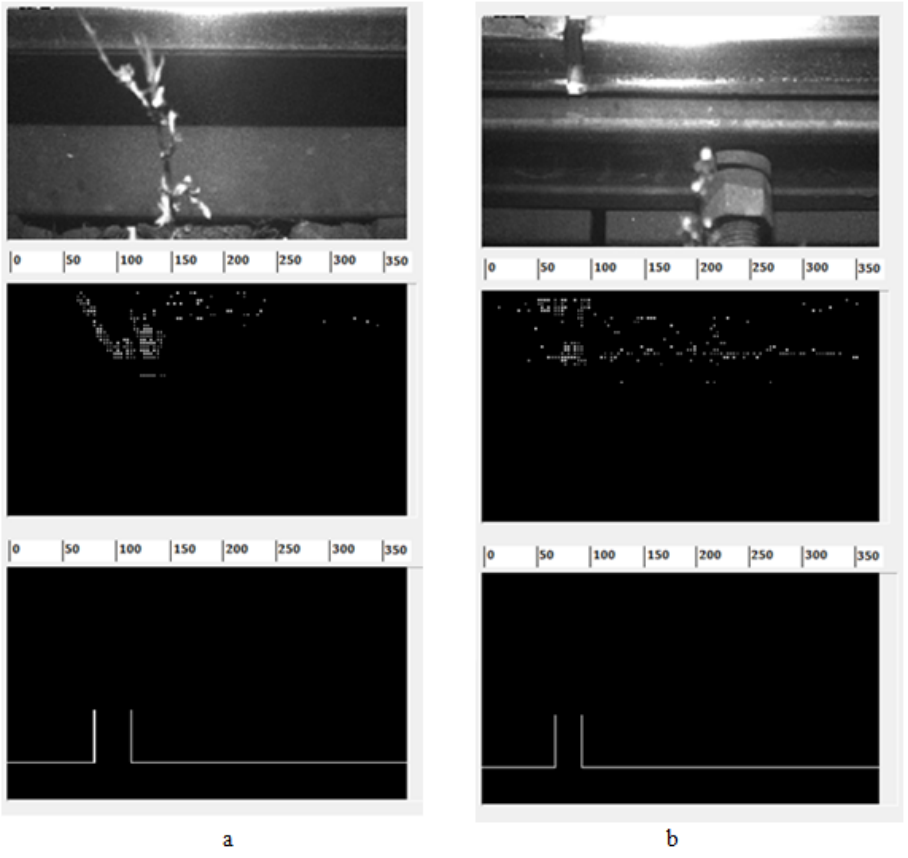

Figure 17. Model failure with insufficiently strong correlation.

An example of another approach based on statistical analysis of contours can be found in [9]. More precisely, this approach is based more on probabilistic concepts, which greatly complicates the practical use of this theory.

The system of constructs linked by correlations has the features of both these approaches, but has its own differences. The construct is not a graphic primitive, but is formed by a line segment of an voluntary shape, bounded at both ends by either branch points, or points of intersection with other lines, or the start and break points of the segment. At the same time, the characteristics of the construct are determined on a statistical basis. Unlike [8], the nature of the statistical model is built taking into account the problems of applied programming. For this purpose the operations was made as simple as possible, minimizing the amount of computation, and the logical part avoids probabilistic interpretations.

From the point of view of the programmer, the construct is a correlation table, a table of custom coefficients and a structural diagram. This data is easily indexed, which

greatly improves the speed of work. The positive side of the algorithm is that learning to recognize one construct occurs on several examples. We have never used a database of more than 15 examples..

However, it should be borne in mind that this algorithm is characterized by a fundamental nonlinearity associated with the combinatorial nature of the calculation of pairwise correlations. In the processing of complex images consisting of many subsystems of nested constructs, this nonlinearity can manifest itself quite radically.

This leads to the current assessment of the field of applicability of this algorithm, as a technique for special applications in science and technology, where it is required to determine the belonging of an unknown function to any known class. On such tasks, the algorithm's weed rates are high enough. In some cases, it can be used for online processing.

Another important aspect of the approach is that the original ideology of Kelly's theory points the way to constructing complex objects from simple ones. This way you can get new classes. Constructs formalized both mathematically and in applied software applications are easy to combine and create new ones. In this case, the control of constructs of different complexity levels occurs according to one algorithmic drawing.

References

1. Fransella, Fay. Bannister, Don.: A Manual for Repertory Grid Technique /Academic Press. London - New York - San Farncisco. 1977.
2. Kelly, G. A.: The psychology of personal constructs: Vol. 1. A theory of personality. London: Routledge, 1991. (Original work published 1955).
3. Kelly, G. A.: The psychology of personal constructs: Vol. 2. Clinical diagnosis and psychotherapy. London: Routledge, 1991. (Original work published 1955).
4. Nauryzbayev M.K., Tuleushova R.ZH. Dempfirovaniye kolebaniy mostovykh konstruktsiy s obratnoy svyaz'yu. ISSN 2073-0071 Aktual'nyye problemy gumanitarnykh i yestestvennykh nauk 6 (89), CH1, str.154 2016g.
5. Nauryzbayev M.K., Tuleushova R.ZH. Opisaniye dinamiki kolebaniyami mostovoy konstruktsii v slaboy mere. ISSN 2073-0071 Aktual'nyye problemy gumanitarnykh i yestestvennykh nauk 6 (89), CH1, str.149 2016g.
6. Nauryzbayev M.K., Tuleushova R.ZH., Sistema monitoringa stabil'nosti konstruktsii mosta po shosse Alash v g. Astana. Mezhdunarodnaya nauchno-prakticheskaya konferentsiya "Aktual'nyye problemy i perspektivy razvitiya stroitel'nykh konstruktsiy: innovatsii, modernizatsiya i energoeffektivnost' v stroitel'stve". Tom II, g. Almaty, 19-20 dekabrya, 2013g.
7. Forsyth David, Computer Vision: A Modern Approach / Pearson, ISBN: 9780273764144, 2012.

Computer Simulation and Calculation of Characteristics of Nonlinear Electronic Devices

Ernazar Nysanov[1] [0000−0002−6053−8262],
Manat Shomanbayeva[1] [0000−0002−2325−9053],
Sevara Kurakbayeva[1] [0000−0001−5463−1930],
Nurlybek Zhumatayev[2] [0000−0001−7840−4425], and
Elmira Musirepova[2] [0000−0002−9349−7057]

[1] M.Auezov South Kazakhstan State University, Shymkent, Kazakhstan,
sevam@mail.ru
[2] SILKWAY International University, Shymkent, Kazakhstan,
nuralmiras@mail.ru

Abstract Modeling and calculating the characteristics of electronic devices using a computer mathematics system is one of the of current interest issues. The scope of the computer mathematics system in computing the characteristics of electronic devices is extensive. Even the earliest versions of a computer math system allowed calculations such as calculating inductance, as well as calculating statistical and dynamic characteristics in a simple electrical circuit. In this article, effective application programs were developed in the Mathcad computer mathematics system for modeling and calculating the characteristics of nonlinear electronic devices. Many linear electronic devices are well studied and have formulas ready to calculate their characteristics. Therefore, we consider modeling and calculating the characteristics of nonlinear electronic devices. The nonlinearity of this system is due to the fact that the dependence of the current of the tunneling diode on voltage is nonlinear. Also in the article, a tunnel diode with positive differential conductivity is considered. It should be noted that the scope of the developed program is immeasurably wider than the simulation of a specific generator circuit on a tunnel diode. The developed application programs can be used in engineering, scientific and technical calculations and laboratory studies of the discipline ”General Physics”.

Keywords: computer mathematics system, electronic device, computer simulation, nonlinear amplifier, tunneling diode, generator, trigger, current-voltage characteristic.

Problem settlement

Let’s consider an example that describes a very simple and interesting device - a tunnel diode generator with a non-linear N-shaped volt-ampere characteristic (VAC). This characteristic is characteristic of devices called “negatrons”. Let the tunnel diode be connected to a constant voltage source E through a series-connected resistor R and inductor L. Let R and L be further selected so that the operating point of the tunnel diode is located on the incident section of its VAC. This circumstance is fundamentally

important, since the differential conductivity of the tunnel diode is then negative. Physically, this means that the tunnel diode gives off energy to the external circuit and self-oscillations are possible in it. If we take into account the capacitance C of the tunnel diode (together with the mounting capacitance and the load capacitance), such a scheme will be described by the following system of nonlinear differential equations [1-3]:

$$\frac{di}{dt} = \frac{E - iR - u}{L}, \qquad \frac{du}{dt} = \frac{i - I(u)}{C};$$

The nonlinearity of this system is due to the fact that in the second equation the current of the tunnel diode $I(u)$ non-linearly depends on the voltage on it and the capacitance. Dependence $I(u)$ is the N-shaped current-voltage characteristic of the tunneling diode. Figure 1 shows the beginning of the program for calculating transients when the considered circuit of the tabulated N-shaped VAC of the tunnel diode in the environment of the Mathcad computer mathematics system [4-8] is included.

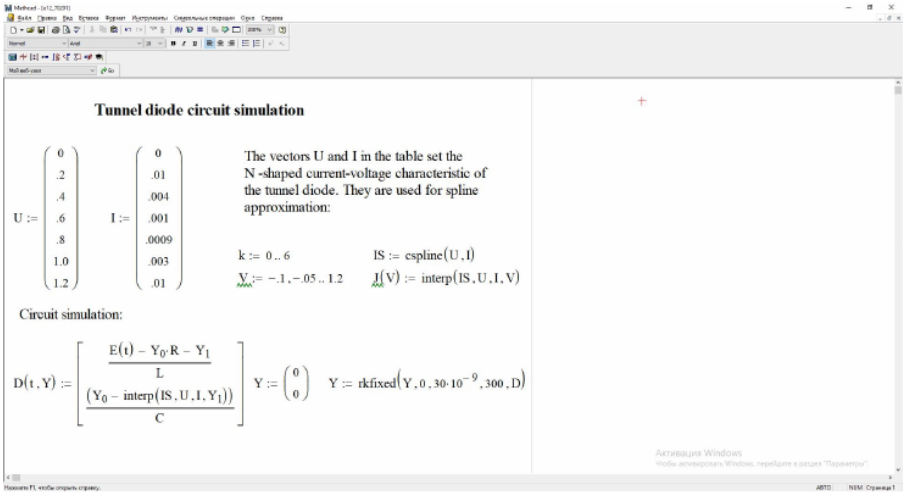

Figure 1. Modeling a generator on a tunnel diode (start of program).

It is defined by its tabular values - elements of the vectors U and I. The N-shaped VAC is obtained by spline interpolation with cubic extrapolation. The solution of the system of differential equations is provided by the Rung-Kutta method with a fixed step using the $Rkfixed$ function.

Problem Solution

Let's start with the case when the operating point of the tunnel diode is set on the falling section of the VAC. In this case, the differential conductivity of the tunneling

diode is negative, and oscillations can occur in the circuit of the RLC circuit. With a sufficiently small amplitude and a sufficiently high quality factor of the circuit, they can be undamped and almost harmonic. The simulation results for this case (Figure 2) are presented in two forms. The first has the form of a phase portrait - the position of each solution point is marked on the graph in the VAC plane. In this case, for each solution point, on one axis of the two-dimensional graph, a variable parameter is delayed, and on the other, derivative parameters (in our case, this is the voltage across the capacitance C and the current flowing through it). For purely harmonic vibrations, the limiting cycle of oscillations in the phase plane should be in the form of an ellipse (or with equal scales of the axes — circles). In the phase plane, a load line is also constructed, which is described by the equation $U(I) = E - I * R$. The VAC and the load line in Figure 2 is plotted in bold lines, and the phase portrait in a thin line. In the phase plane, a load line is also constructed, which is described by the VAC and the load line in Figure 2 is plotted in bold lines, and the phase portrait in a thin line. The load line crosses the VAC at a single point on the falling section of the VAC. The difference between the steady-state phase portrait and the ellipse is small, which indicates, on the one hand, a small effect of nonlinearity, and on the other, the almost harmonic nature of the oscillations. The second form is the time dependence of the voltage on the tunneling diode and the current in the circuit of the capacitor C. These dependencies are close to harmonic ($C = 40pF, L = 15nG$) at the end of a noticeable stage of oscillation establishment, which has the character of damped oscillations (the phase portrait has view of a twisting spiral). The steady-state oscillation cycle is called the limit cycle. It should be noted that the scope of the developed program is immeasurably wider than the simulation of a specific generator circuit on a tunnel diode. In practice, it can be used to simulate the main circuit on any device with an N or Λ-shaped VAC (for example, an inductive relaxer on an avalanche transistor, N and Λ-diodes and transistors, their analogs, etc.). It is enough to set the data of their volt-ampere characteristics and the corresponding initial data. It is worth, for example, to reduce the capacitance C by two to three times, and increase the inductance, as the generator switches to the mode of generation of relaxation oscillations. Oscillations now occur more sharply, the phase portrait begins immediately with a limit cycle, the shape of which is noticeably different from the elliptical one. In this case, the vibrations are of the relaxation type and arise on their own, without any external influence. In practice, after the first cycle of oscillations, their stationary mode is established.

Now we will consider a more interesting case when the load line is located on the ascending part of the VAC with positive conductivity. With constant $E(t)$, this position of the operating point is stable and is not able to cause oscillations in the circuit. But suppose that along with a constant voltage $E = 0.2V$, an alternating voltage with an amplitude of $0.2V$ and a frequency of 100 MHz is supplied to the circuit. This will lead to the movement of the operating point along the VAC, and at some points in time it will begin to fall on the falling section of the VAC, as a result, oscillations may occur. Computer simulation of this case is shown in Figure 3.

This case can be considered from two perspectives. Firstly, it characterizes the operation of the circuit as a nonlinear amplifier. In the steady state, the phase portrait of the oscillations is noticeably different from the ellipse, so that the waveform is sharply

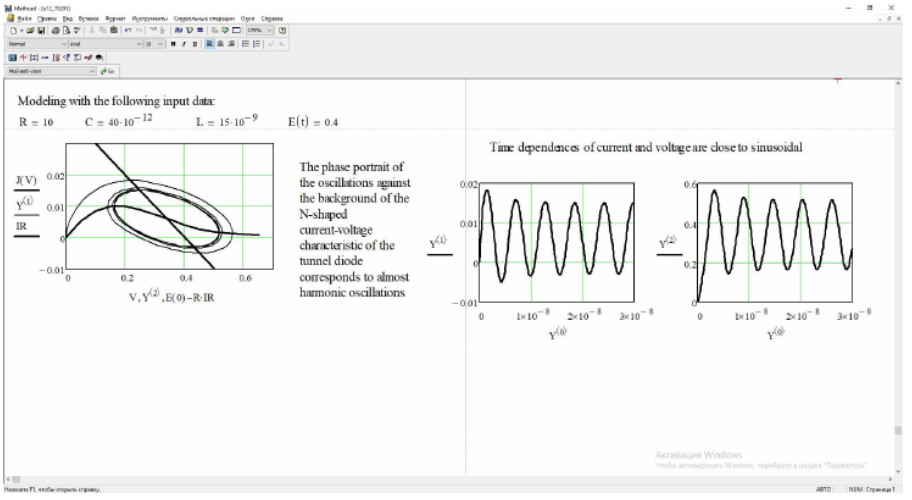

Figure 2. Modeling a generator on a tunnel diode (the case of the generation of almost sinusoidal oscillations).

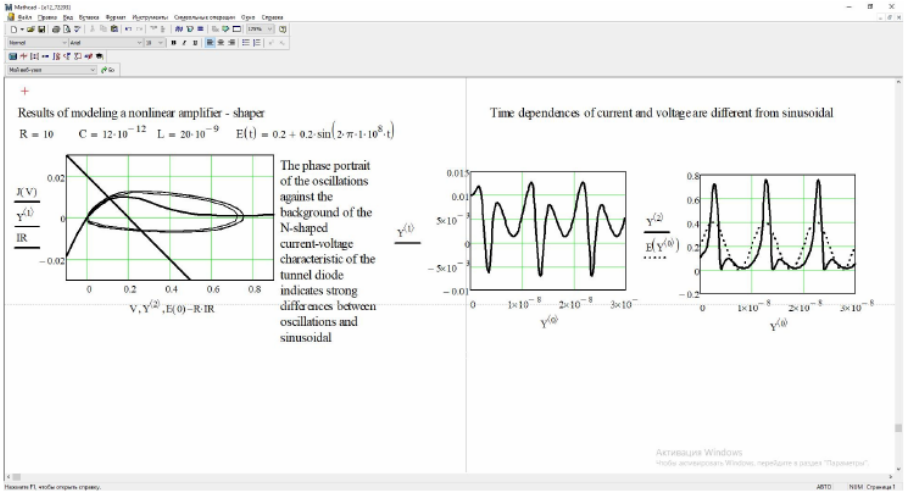

Figure 3. Modeling a nonlinear amplifier on a tunnel diode.

different from the sinusoidal one. Secondly, we can consider the circuit as a waiting relaxation generator, which is triggered by the tops of the sinusoidal input signal.

Consider a simulation in a Mathcad environment of pulse generation by a circuit with a tunneling diode in standby mode (Figure 4). Here, at first, the load line is located on the ascending portion of the VAC with positive differential conductivity, so that the circuit is stable. Then the voltage $E(t)$ is increased by superimposing on the constant component of the pulse. In this case, the load line moves from the initial position (solid line) to the position (dashed line), at which the operating point is on the falling section and loses stability. As is easy to see, in this case, in response to the input (triggering) pulse, the circuit generates one cycle of relaxation oscillations, after which it returns to its original stable state. Of course, at the end of the transients, it can be started again and again.

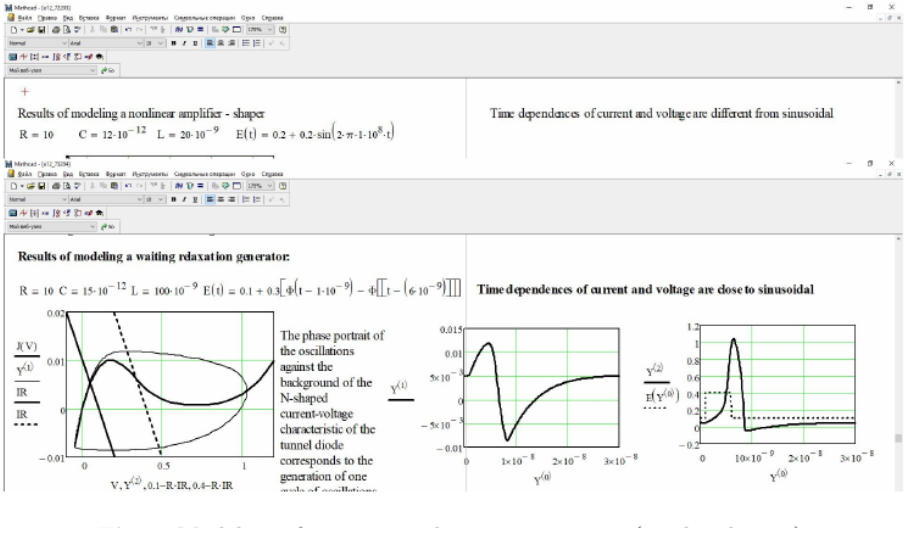

Figure 4. Modeling of a waiting relaxation generator (single vibrator).

Conclusions

At one time, great hopes were pinned on triggers built on tunnel diodes. Their simplicity shocked them - a resistor and a tunneling diode (elements L and C can be considered parasitic). Although these hopes did not materialize (an ordinary trigger turned out to be more stable in operation, and even easier in integrated performance), it is interesting to analyze the operation of our circuit in the trigger mode. Recall that a trigger is a device with two stable equilibrium states into which it passes under the influence of triggering input pulses. For the circuit to operate in trigger mode, it is necessary to select

the supply voltage E and the value of the resistor R so that the load line intersects the VAC at three points. Modeling of this process in the Mathcad environment is shown in Figure 5. Two points in the ascending sections are stable, and the average in the falling section is unstable. All that is needed to switch the trigger is to add a positive pulse to the constant component $E(t)$ to transfer the trigger to a state with a high voltage on the diode or add a negative pulse to transfer to a state with a low voltage on the diode. This is shown in Figure 5. The phase portrait and time dependencies of voltage and current in this case indicate the complexity and specificity of transients and, at the same time, a high degree of their visualization. This is precisely what is characteristic of circuit simulation on special devices, such as tunnel diodes.

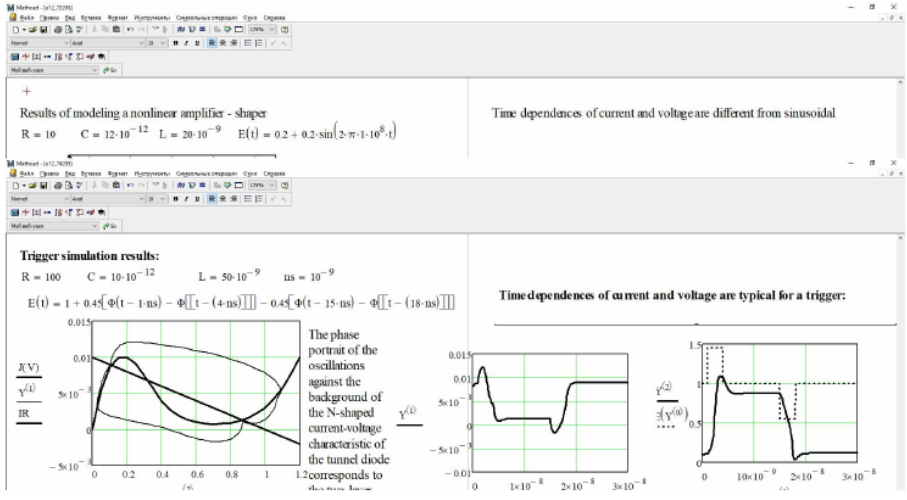

Figure 5. Modeling a trigger on a tunnel diode.

References

1. Nefyodov, V.I. Fundamentals of Radio Electronics. - M.: Higher school, Location (2000)
2. Glushkov, V.A., Nesterenko, A.G., Popov, N.A. Theory of electrical communication. Tutorial. Part 2. Interference immunity. - Ulyanovsk: UVVIUS, Location (2007)
3. Kaganov, V.I. Radio circuits and signals. Computerized Course: Study Guide. - M.: FORUM: INFRA-M, Location (2005)
4. Dyakonov, V. Computer mathematics. Theory and practice. M: Goryachaya liniya - Telecom, Location (2001)
5. Dyakonov, V.P. Encyclopedia of Mathcad 2001i and Mathcad 11. - M .: SOLON-Press, Location (2004)
6. Rakitin, V.I. Mathcad Computing Methods Guide. –M.: Fizmatlit, Location (2005)

7. Makarov, E. Engineering Calculations at Mathcad. Training course. - SPb.: Peter, Location (2005)
8. Brent Maxfield. Engineering with Mathcad: Using Mathcad to Create and Organize your Engineering Calculations. - Butterworth-Heinemann, Location (2006)

Stabilized Finite Element Method for Solving the Saturation Equation in the Two-phase Non-equilibrium Flow Problem

Dinara Omariyeva[1], Nurlan Temirbekov[2], and Muratkan Madiyarov[3]

[1] D. Serikbayev East Kazakhstan Technical University,
Ust-Kamenogorsk, Kazakhstan
dinara_2205@mail.ru
[2] National Engineering Academy of the Republic of Kazakhstan,
Almaty, Kazakhstan
temirbekov@rambler.ru
[3] S. Amanzholov East Kazakhstan University,
Ust-Kamenogorsk, Kazakhstan
madiyarov_mur@mail.ru

Abstract The paper considers a model of two-phase non-equilibrium filtration of immiscible fluids. A stabilized finite element method is proposed for the solution of the problem. The method is demonstrated on a model problem.

Keywords: Non-equilibrium flows in porous media, stabilized finite element method, numerical experiment.

Introduction

The dynamics of filtration flows of a multiphase liquid depends non-linearly on both the structural and mechanical properties of the liquid and the properties of the surrounding skeleton. However, in real reservoir conditions, a significant influence on the filtration process has the property of delayed phase saturation, the study of which led to the emergence of the theory of non-equilibrium filtration. The need to take this phenomenon into account in the development of oil fields is discussed in many works [1,2]. It is necessary to take into account nonequilibrium at all stages of oil field development, since the dependences of the pressure drop on time obtained during laboratory studies of samples of a porous medium for determining the functions of relative phase permeability differ significantly from the theoretical curves calculated in the framework of the classical filtration theory. The effect of nonequilibrium can be significant: the time to establish saturation in the conditions of oil fields is about a year.

There are several approaches to building a non-equilibrium filtration model. The first approach [3] is based on thermodynamic arguments and volume averaging of microscopic equations of conservation of mass and moment. In [3], the concept of dynamic capillary pressure P_c^{dyn} (instantaneous local difference between phase pressures) was introduced, which relates to the static capillary pressure P_c^{stat} (capillary

pressure under quasi-static displacement) by the relation

$$P_c^{\text{dyn}} = P_c^{\text{stat}} - \tau_H\left(s_w\right)\frac{\partial s_w}{\partial t},$$

where p_o and p_w are the phase pressures of oil and water, τ_H is a phenomenological coefficient that takes positive values. During the drainage process, the value $\frac{\partial s_w}{\partial t}$ is negative, so $P_c^{\text{dyn}} > P_c^{\text{stat}}$, which is confirmed by experimental observations [4]. Dynamic capillary pressure has been the subject of many experimental [5] and theoretical [6,7] studies.

The approach proposed by the authors of [3] does not take into account the effects of nonequilibrium on relative phase permeabilities. A more complete model, including the effects of nonequilibrium in both capillary pressure and relative permeability, is proposed by the authors of [8]. With multiphase fluid displacement, an uncountable number of large-scale pore rearrangements occur. The characteristic time of redistribution for the restructuring of stream networks can be significant. As a result, the flow of each phase does not depend only on the current saturation. The approach under consideration is based on the assumption that instantaneous (dynamic) phase permeabilities and capillary pressure depend on static phase permeabilities and capillary pressure in some effective saturation η_w [9]:

$$k_w^{\text{dyn}}\left(s_w\right) = k_w^{\text{stat}}\left(\eta_w\right), \quad k_o^{\text{dyn}}\left(s_w\right) = k_o^{\text{stat}}\left(\eta_w\right), \quad p_c^{\text{dyn}}\left(s_w\right) = p_c^{\text{stat}}\left(\eta_w\right).$$

In this case, the following relation between the true s_w and the effective η_w saturation holds

$$\eta_w - s_w = \tau_B\left(s_w\right)\frac{\partial s_w}{\partial t}.$$

In [2], an original approach is proposed that generalizes the Barenblatt model. The essence of the approach is to consider all flows as non-equilibrium flows, where they differ only in the degree of non-equilibrium.

Generalizations of the nonequilibrium filtration model [8] for the three-phase case are also known. The idea of these generalizations is to introduce a pair of effective saturations of water and gas, which are related to true saturations by means of a local evolution equation. The paper [9] analyzes the influence of non-equilibrium effects on qualitative and quantitative changes in the solution of the three-phase filtration problem. In [10], a mixed finite element method is used for the dynamic capillarity problem.

Formulation of the Problem

Let us consider the problem of two-phase nonequilibrium filtration of incompressible liquids with a generalized nonequilibrium law In a bounded convex domain $\Omega \subset R^2$ with boundary $\Gamma = \Gamma_D \cup \Gamma_N, \Gamma_D \cap \Gamma_N = \emptyset$:

$$\phi\frac{\partial s}{\partial t} + \nabla \cdot \vec{u}_w = q_w\left(p, \eta\right), \tag{1}$$

$$-\phi\frac{\partial s}{\partial t} + \nabla \cdot \vec{u}_o = q_o\left(p, \eta\right), \tag{2}$$

$$\vec{u}_\alpha = -\frac{Kk_\alpha(\eta)}{\mu_\alpha}\nabla p_\alpha, \quad \alpha \in \{w, o\}, \tag{3}$$

$$p_o - p_w = p_c(\eta), \tag{4}$$

$$\tau(x)\frac{\partial s}{\partial t} - \tau(x)\nu(x)\frac{\partial \eta}{\partial t} = \eta - s \tag{5}$$

with initial and boundary conditions

$$s(x, 0) = s_0(x), \tag{6}$$

$$\vec{u}_\alpha \cdot \vec{n} = 0, \qquad x \in \Gamma, \tag{7}$$

where ϕ, K – porosity, absolute permeability of the medium; s, η are respectively, true and effective water saturation; p_α, k_α, μ_α, $\vec{u}_\alpha$ - respectively, pressure, relative phase permeability, viscosity and filtration rate of the phase α; τ is substitution time.

We introduce the total velocity vector $\vec{u} = \vec{u}_w + \vec{u}_o$. Sum the equations (1) and (2) to obtain

$$\nabla \cdot \vec{u} = q(p, \eta),$$

where $q = q_w + q_o$. Using the equations (3), (4), we can express the vector $\vec{u}$ in terms of oil pressure and capillary pressure gradients:

$$\vec{u} = -K\lambda(\eta)(\nabla p_o - f_w(\eta)\nabla p_c(\eta)), \tag{8}$$

where

$$f_w(\eta) = \frac{\lambda_w(\eta)}{\lambda(\eta)}, \quad \lambda_\alpha(\eta) = \frac{k_\alpha(\eta)}{\mu}, \quad \lambda(\eta) = \lambda_w(\eta) + \lambda_o(\eta).$$

Let us introduce a new variable $\pi = \pi(\eta)$, such that

$$\nabla\pi(\eta) = f_w(\eta)\nabla p_c(\eta) \tag{9}$$

which yields

$$\pi(\eta) = \int_0^\eta f_w(\xi)\, p_c'(\xi)\, d\xi.$$

We introduce a new variable, "global pressure" by the formula $p = p_o - \pi$, or

$$p = p_o - \int_0^\eta f_w(\xi)\, p_c'(\xi)\, d\xi.$$

Then (8) is reduced to the form

$$\vec{u} = -K\lambda(\eta)\nabla p. \tag{10}$$

Using (3), (9), one can express $\vec{u}_w$ in terms of $\vec{u}$:

$$\vec{u}_w = f_w(\eta)\vec{u} + K\lambda_o(\eta) f_w(\eta)\frac{dp_c}{d\eta}\nabla\eta. \tag{11}$$

To obtain the equation for water saturation, put (11) in (1) and reduce the equation to the following form:

$$\frac{\partial s}{\partial t}+\frac{df_w}{d\eta}\vec{u}\cdot\nabla\eta+\nabla\cdot\left(K\lambda_o\left(\eta\right)f_w\left(\eta\right)\frac{dp_c}{d\eta}\nabla\eta\right)=q_s\left(p,\eta\right),$$

where $q_s\left(p,\eta\right)=q_w\left(p,\eta\right)-q\left(p,\eta\right)f_w\left(\eta\right)$.

Thus, the original problem (1)-(7) is reduced to the following initial-boundary value problem for determining the vector of the total velocity $\vec{u}$, global pressure p, true s, and effective water saturation η :

$$\nabla\cdot\vec{u}=q\left(p,\eta\right), \tag{12}$$

$$\vec{u}=-K\lambda\left(\eta\right)\nabla p, \tag{13}$$

$$\frac{\partial s}{\partial t}+\frac{df_w}{d\eta}\vec{u}\cdot\nabla\eta+\nabla\cdot\left(K\lambda_o\left(\eta\right)f_w\left(\eta\right)\frac{dp_c}{d\eta}\nabla\eta\right)=q_s\left(p,\eta\right), \tag{14}$$

$$\tau\left(x\right)\frac{\partial s}{\partial t}-\tau\left(x\right)\nu\left(x\right)\frac{\partial\eta}{\partial t}=\eta-s \tag{15}$$

with initial and boundary conditions

$$s\left(x,0\right)=s_0\left(x\right), \tag{16}$$

$$\vec{u}\cdot\vec{n}=0,\qquad x\in\Gamma. \tag{17}$$

Stabilization of the Equation

To solve the equations (12), (13) a mixed finite element method is applied in [11]. Let us focus on solving the equation (14). Let us first consider the stationary case

$$\vec{V}\cdot\nabla T-k\nabla^2T=f,\quad x\in\Omega \tag{18}$$

with the boundary condition

$$T\left(x\right)=g_D,\quad x\in\Gamma. \tag{19}$$

The weak formulation of the problem corresponding to the standard Galerkin method has the form:

$$\left(k\nabla T,\nabla w\right)+\left(\vec{V}\cdot\nabla T,w\right)=\left(f,w\right),\ \ \forall w\in C^\infty\left(\Omega\right). \tag{20}$$

The finite element method then has the form:

$$\left(k\nabla T_h,\nabla w\right)+\left(\vec{V}\cdot\nabla T_h,w\right)=\left(f,w\right),\ \ \forall w\in C^\infty\left(\Omega\right). \tag{21}$$

We seek the solution in the form:

$$T=\sum_{j=1}^{NN}T_jS_j(x,y).$$

According to the Galerkin method, we choose the basis function in the form $w = S_i(x, y)$. Thus, we come to the following system of equations with respect to T_j:

$$\sum_{j=1}^{NN} \left[(\nabla S_j, \nabla S_i) + (\vec{v} \cdot \nabla S_j, S_i) \right] T_j = \sum_{j=1}^{NN} (f, S_i), \quad i = \overline{1, NN}.$$

This yields the system of algebraic equations

$$A \cdot T_j = F \tag{22}$$

with elements

$$A_{i,j} = (\nabla S_j, \nabla S_i) + (\vec{v} \cdot \nabla S_j, S_i), \quad F_i = (f, S_i).$$

It is known [12,13,14] that the application of the classical Galerkin method to calculate saturation using the widely used IMPES method in the vicinity of the gap leads to non-physical oscillations. One of the ways to overcome such oscillations is the counterflow finite element method SUPG [15]. Here we will consider a method for constructing high-order convergence schemes for convection-diffusion equations that are resistant to the appearance of numerical oscillations. The method is known as the Streamline Upwinding Petrov-Galerkin method (SUPG). It was proposed by Brooks and Hughes and later earned the attention of many researchers. The SUPG method is well suited for discretization of equations with convective terms by the finite element method. The essence of this method is to add an additional artificial viscosity, depending on the number of Peclet. In [16], three stabilization parameters are proposed.

According to the counterflow finite element method, we modify the elements of the stiffness matrix $A_{i,j}$ as follows:

$$A_{i,j}^{SUPG} = A_{i,j} + \sum_K \tau_K^{SUPG} \int_K \left(\vec{V} \cdot \nabla S_j, \nabla S_i \right), \tag{23}$$

where

$$\tau_K^{SUPG} = \begin{cases} \dfrac{h_K}{2\left|\vec{V}_K\right|} \; when \; Pe_K \geq 1, \\ \dfrac{h_K^2}{12k} \quad when \; Pe_K < 1, \end{cases}$$

where $Pe_K = \dfrac{\left|\vec{V}_k\right| h_K}{6k}$, h_K is diameter of the triangle K.

To check the correctness of this method, the following model problem is considered. In $\Omega = [0, 1]^2$ consider the problem (18), (19) with the parameters $\vec{V} = \left(\frac{\sqrt{2}}{2}, -\frac{\sqrt{2}}{2}\right)$, $k = 10^{-4}$, $f = 0$, $g_D = \begin{cases} 1, \; y = 0 \; or \; x \leq 0.8, \\ 0, \; otherwise. \end{cases}$. Choosing the coefficient k in this form makes the problem with a predominance of convection.

This problem has a gap along the gap line $y = -0.8 + x$, including at the point $(0,\ 0.8)$ on the boundary of the area. During computational experiments, it was found

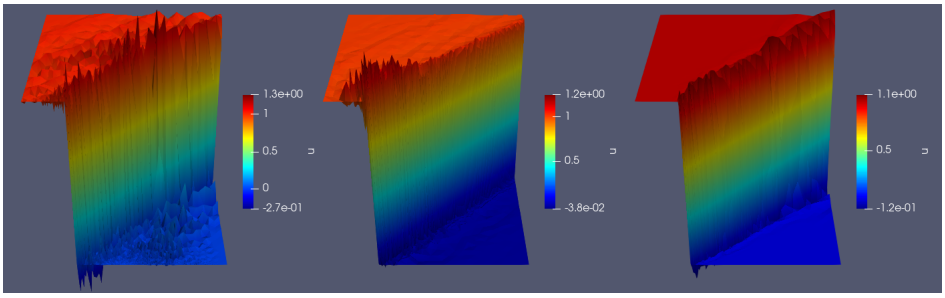

Figure 1. Solution of the model problem obtained without stabilization

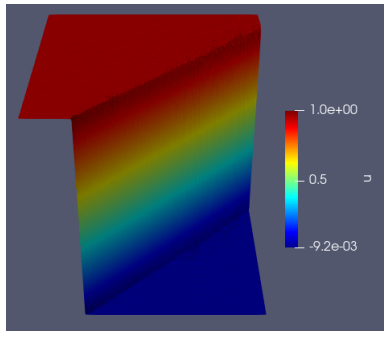

Figure 2. Solution of the model problem obtained with stabilization

that stabilization significantly improves and smoothes the solution on a regular grid (without thickening). To suppress the oscillations, it was necessary to thicken the grid along the break line and near the break at the border. Figure 1 shows the solution obtained without stabilization on different meshes with different level of thickness. Figure 2 shows the solution obtained with stabilization.

Now we apply this method to the problem (12)-(17). The following test parameters where considered: $K = 1.0$, $\varphi = 1.0$, $\mu_w = 1.0$, $\mu_o = 1.0$, $s_0 = 0.0$, $k_w(s) = s$, $k_w(s) = 1 - s$, $\Delta_t = 0.0025$. It is assumed that the injection well is located in the lower-left corner of the design area. Figure 3 shows the water saturation distribution at $t = 100\tau, 250\tau, 500\tau$.

Acknowledgments

This work was supported by the Ministry of education and Science of the Republic of Kazakhstan (grant No. AP08053189).

References

1. Faizulin T. Mathematical modeling of relaxation phenomena during the flow of an inhomogeneous liquid in porous media: thesis. - Ufa, 2007.

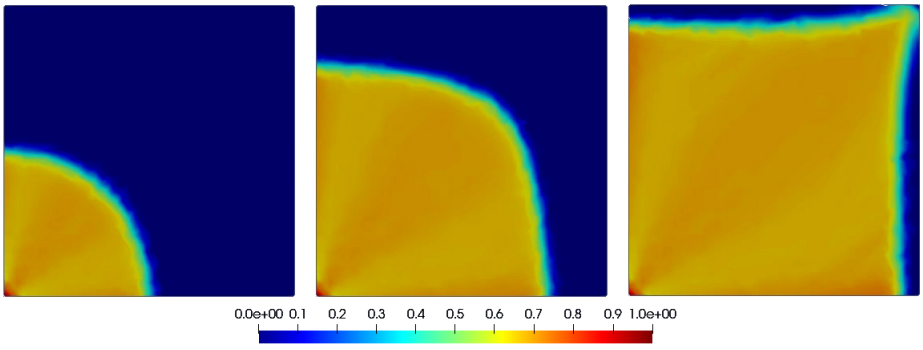

Figure 3. Distribution of water saturation s at $t = 100\tau$ (left); $t = 250\tau$ (center); $t = 500\tau$ (right)

2. Ermagambetov T. K. Solvability and numerical study of a model of nonequilibrium filtration of a two phase incompressible fluid with a generalized nonequilibrium law: thesis. - Almaty, 2010.
3. Hassanizadeh S.M., Graw W.G. Toward an Improved Description of the Physics of Two-Phase Flow // Advances in Water Resources. - 1993. - Vol. 16, No. 1. - pp. 53–67.
4. Hassanizadeh S.M., Celia M.A., Dahle H.K. Dynamic Effects in the Capillary Pressure-Saturation Relationship and Its Impact on Unsaturated Flow // Vadose Zone Journal. - 2002. - Vol. 1, No. 1. - pp. 38–57.
5. O'Carroll D.M., Phelan T.J., Abriola L.M. Exploring Dynamic Effects in Capillary Pressure in Multistep Outflow Experiments // Water Resour Res. - 2005. - Vol. 41, No. 11. - p. W11419.
6. Cuesta C., Duijn C.J. van, Hulshof J. Infiltration in Porous Media with Dynamic Capillary Pressure: Travelling Waves // Eur J Appl Math. - 2000. - Vol. 11. - pp. 381–397.
7. DiCarlo D.A., Juanes R., LaForce T., Witelski T.P. Nonmonotonic Travelling Wave Solutions of Infiltration in Porous Media // Water Resour Res. - 2008. - Vol. 44. - p. W02406.
8. Barenblatt G.I. Filtration of Two Nonmixing Fluids in a Homogeneous Porous Medium // Mechanics of Gas and Fluids. - 1971. - Vol. 5, No. 8. - pp. 57–64.
9. Juanes R. Nonequilibrium Effects in Models of Three-Phase Flow in Porous Media // Advances in Water Resources. - 2008. - Vol. 31. - pp. 661–673.
10. Cao X., Mitra K. Error Estimates for a Mixed Finite Element Discretization of a Two-Phase Porous Media Flow Model with Dynamic Capillarity // Journal of Computational and Applied Mathematics. - 2019. - Vol. 353. - pp. 164–178.
11. Baigereyev D. R., Temirbekov N. M. Omarieva D. A. Construction of an iterative method for solving nonlinear equation of elliptic type on the basis of the mixed finite element method // Bulletin of KazNU. Series mathematics, mechanics, computer science. - 2020. - Vol. 106, No. 2. - pp. 104–120.
12. Juanes R. A Variational Multiscale Finite Element Method for Multiphase Flow in Porous Media // Finite Elements in Analysis and Design. - 2005. - Vol. 41. - pp. 763–777.
13. Helmig R., Huber R. Comparison of Galerkin-Type Discretization Techniques for Two-Phase Flow in Heterogeneous Porous Media // Advances in Water Resources. - 1998. - Vol. 21, No. 8. - pp. 697–711.
14. Ivanov M., Kremer I., Laevsky Yu. On one counterflow scheme for solving the filtration problem / / Siberian electronic mathematical news. - 2019. - Vol. 16. - pp. 757–776.

15. Hughes T. A Simple Scheme for Developing Upwind Finite Elements // International Journal of Numerical Methods. - 1978. - Vol. 12. - pp. 1359–1365.
16. Asensio M., Russo A. Stabilized Finite Elements with Matlab. - 2002.

Creating A Trajectory with Kinematic and Dynamic Smoothness

N. M. Temirbekov[1], B. O. Bostanov[2,4], E. S. Temirbekov[3,4], A. A. Adamov[2]

[1] National Engineering Academy of the Republic of Kazakhstan
[2] Eurasian National University named after L. N. Gumilev
[3] Al-Farabi Kazakh National University
[4] IMES named after academician U. A. Dzholdasbekov

Abstract The article considers the problem of forming a smooth combined trajectory of the robot's movement and determining the position of the connection points that provide kinematic and dynamic smoothness conditions. When the trajectory is paired in the form of arcs of curves, there are irregularities at the junction in the form of a break and a jump in the radii of curvature.
You can plan a combined robot trajectory to search for a conflict-free movement by using the insert transition section method. To eliminate undesirable jumps when creating a trajectory, various methods and ways are used, such as stroke, spline, various interpolations and approximations. There are also specially developed smoothing special curves such as the majorant curve, clotoid, elastic line, lemniscata and velocity curve.
All these methods and ways used for planning and smoothing curved robot paths are less accurate and approximate. To ensure kinematic and dynamic smoothness conditions, we use the method of inserting a transition section between arcs, the model of which is a second-order curve (conic).
An original method has been developed for the analytical determination of the type and shape of a conic transition area that continuously matches the smoothness of the second order. Mathematical relations are determined that express the conditions for connecting the trajectory arcs without a jump in the radii of curvature at the places of docking. By setting the starting point of the connection and using the mathematical condition of smoothness of the connection, you can determine the final point of the connection. To determine the end point, a slidecrank mechanism has been developed, the coulisse of which slides along a given high-order curve. The developed method allows us to form complex technical forms and create new models of a combined robot trajectory of continuous curvature from arcs of high-order curves with a conical transition section.

Keywords: conic, kink, smoothness of the trajectory, transition curve, curvature jump, and docking point.

Introduction

One of the key tasks of mobile robotics is to find a route for traffic and optimize it. When moving in a work area, the robot must constantly evaluate the surrounding environment,

determine its position and the position of objects surrounding it.
In the course of robot control, the task of synthesizing the trajectory of the robot's transition from a certain initial state to a target state by changing coordinates in space is relevant, i.e., the task of planning the robot's trajectory.
In [1-3], the approach to trajectory planning based on graph theory, spline inertia, and the advantages of piecewise linear approximation and the method of repulsive swarming of particles are highlighted. Planning of the obstacle avoidance trajectory based on a genetic algorithm, generation method and trajectory correction are presented in [4-7], and algorithms for solving the inverse kinematics problem of a redundant manipulator in a confined medium are also considered. In [8-12], methods of planning the robot's trajectory based on the methods of potential fields, copying and learning the natural optimization of human hand movement, an analytical approach using Jacobi matrices, Bezier curves, etc. were studied.One of the key tasks of mobile robotics is to find a route for traffic and optimize it. When moving in a work area, the robot must constantly evaluate the surrounding environment, determine its position and the position of objects surrounding it. In the course of robot control, the task of synthesizing the trajectory of the robot's transition from a certain initial state to a target state by changing coordinates in space is relevant, i.e., the task of planning the robot's trajectory.
In [1-3], the approach to trajectory planning based on graph theory, spline inertia, and the advantages of piecewise linear approximation and the method of repulsive swarming of particles are highlighted. Planning of the obstacle avoidance trajectory based on a genetic algorithm, generation method and trajectory correction are presented in [4-7], and algorithms for solving the inverse kinematics problem of a redundant manipulator in a confined medium are also considered. In [8-12], methods of planning the robot's trajectory based on the methods of potential fields, copying and learning the natural optimization of human hand movement, an analytical approach using Jacobi matrices, Bezier curves, etc. were studied.
Previously, shop vehicles were trolleys that moved along rails. They have now been replaced by robocars – mobile robots of various types and for various tasks, and the rails laid along the shop floor have been replaced by a web of trajectory guides drawn on the floor. Since the real environment in which the robotics located usually contains various obstacles, it is necessary to avoid them, and often the guiding trajectory is a composite and can have a combined form. Various restrictions can be imposed on the actual route, for example: some sections of the route may be off-limits, and some may only be reached after passing through others.
In addition to restrictions on the route, certain requirements can also be imposed on the trajectory itself.
The paper considers the trajectory problem - the problem of moving the robot along a horizontal plane along a prescribed trajectory, set in a physical and mathematical form. Earlier [13], trajectories consisting only of spherical arcs were considered. In the presented paper, the combined trajectory with the final interface point is a curve of a higher (fourth) order. At the smoothing interface points, a kinematic smoothness condition must be provided, a condition under which the directions and velocity values must coincide. Similarly, the transition conic eliminates the impact effect at the docking point, thereby achieving a dynamic smoothness condition. The method of inserting a

conical transition section between the arcs of curves above the second order makes it possible to create new combined robot paths with continuous curvature.

Problem statement.

Let's consider the robot's movement along a complex trajectory made up of arcs of curves $F(x, y) = 0$ and $G(x, y) = 0$. There are two most important aspects of the problem that this research paper is devoted to.
First, S there is no common tangent at the docking point (Fig. 1A). The junction point is a break point, which has the property that the branches of the arcs into which this point divides the robot's initial trajectory have different tangents at this point.

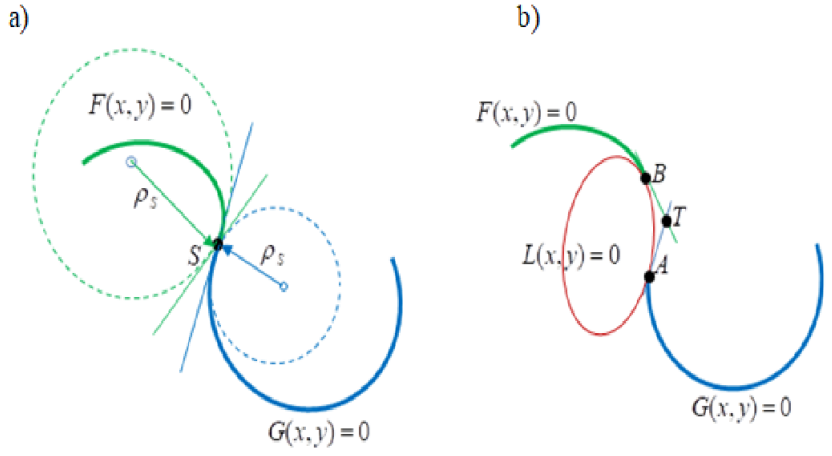

Figure1.a) jumps in speed and acceleration, b) insertion of a transition cone.

This means that the robot's speed changes with a jump when it passes through a breakpoint. The robot's speed before the break point will be one, and then another, so that at the break point itself, the speed has an abruption.
In practice, it is required that the docking a process is a smooth.
Secondly, there is also a normal acceleration abruption at the docking point, since at this point the connecting curves have different radii of curvature. Undesired shock effects occur.
To exclude these two types of jumps when the robot moves along the formed trajectory [14], a method of inserting the transition section is proposed. The mathematical model of the transition area is a second-order curve (conic) (Fig. 1b).
The desired transition section $L(x, y) = 0$ in the form of a conical arc must meet the following conditions:

a) the arc must pass through the docking points A and B . The point taken on the arc $G(x, y) = 0$ is called the starting point. The second point B taken on the arc $F(x, y) = 0$ is called the finish point.
b) the connecting and connecting arcs must have common tangents AT and BT at these points, respectively.
c) the connecting and connecting arcs must have radii of curvature at these points respectively.
In practice, conditions a) and b) are called smoothness of the first order, and the fulfillment of all three conditions simultaneously is called smoothness of the second order or smoothness .

Conditions that ensure that the robot moves without jumping.

Studying the properties of conics, previously unknown reference properties were found [13-15] , which relate the radius of curvature to the elements of the conic itself.

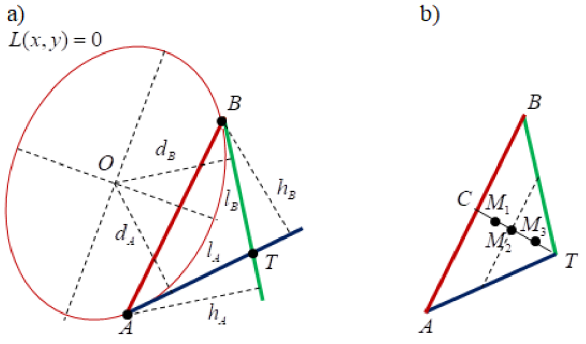

Figure2.a) reference triangle, b) the discriminant of engineering.

Let's introduce a dimensionless coefficient $\eta = \sqrt[3]{\frac{\rho_A}{\rho_B}}$, which is an indicator of curvature.
The following statement is true (Fig. 2A).
If we have two points A and B an ellipse with radii of curvature ρ_A and ρ_B, then the ratio between the corresponding elements of the reference triangle ΔATB made up of tangents AT ,BT and the chord AB is equal to the curvature index η

$$\frac{l_A}{l_b} = \frac{d_B}{d_A} = \frac{h_A}{h_B}$$

The elements of the reference triangle are: $l_A = AT$, $l_B = BT$ tangent lengths, d_A, d_B distance from the center of the ellipse to the tangents, h_A , h_B distance from the

starting and finishing points to the tangents.
In practice, the more convenient way to set a conic is the engineering way of setting it – it is to set it with two tangents, points of contact on them, and an engineering discriminant. The engineering discriminant is a special coefficient. This coefficient is the ratio of the segment CM that is cut off at the median from the base of the median to the value of this median CT (figure 2b):

$$f = \frac{CM}{CT}$$

By the coefficient f , you can determine which type of cone this curve belongs to: $f < 0.5$ - ellipse (pointM_1), parabola (dotM_2),$f > 0.5$ hyperbole (dotM_3). The radius of curvature at a point is determined by the formula

$$\rho_A = \frac{2f^2}{(1-f)} \frac{l_A^2}{h_g}$$

The Laiming equation for the transition conic.

We can find an equation of a conic section that has two given tangents at two points and passes through a third point using the Laiming equation [13-16].

$$(1-\lambda)L_{A\tau}L_{B\tau} - \lambda L_{AB}^2 = 0$$

where $L_{A\tau}$- the tangent equation AT, $L_{B\tau}$ - the tangent equation BT , L_{AB} - the chord equation (Fig. 2b).
a) the case of a smooth connection. This parameter λ is defined by setting some arbitrary point $M(x_M, y_M)$

$$\lambda = \frac{L_{A\tau}(x_M, y_M)L_{B\tau}(x_M, y_M)}{L_{A\tau}(x_M, y_M)L_{B\tau}(x_M, y_M) - L_{AB}^2(x_M, y_M)}$$

b) the case of smooth connections.
The coordinates of the point $M(x_M, y_M)$ are found using the engineering discriminant ratio

$$f = \frac{1}{1 + \sqrt{\frac{2l^2}{h\rho}}}$$

Illustrations and variants.

Let's consider the robot trajectory, which is combined from arcs of curves of the second and fourth orders

$$G(x, y) = (x - 9.61812)^2 + (y + 7.0905)^2 - 36 = 0$$

and the Bernoulli lemniscate

$$F(x, y) = [x^2 + (y-7)^2]^2 - 2a^2[x^2 - (y-7)^2] = 0,$$

$a = 5$.
And select some arbitrary starting point $A(4.8621; -3.5157)$ on the arc of the second-order curve $G(x, y) = 0$.
a)**smooth connection.** Let us assume that we need to connect the curve $F(x, y) = 0$ at a point $B(6; 9)$. We have a reference triangle with sides (Fig. 4):

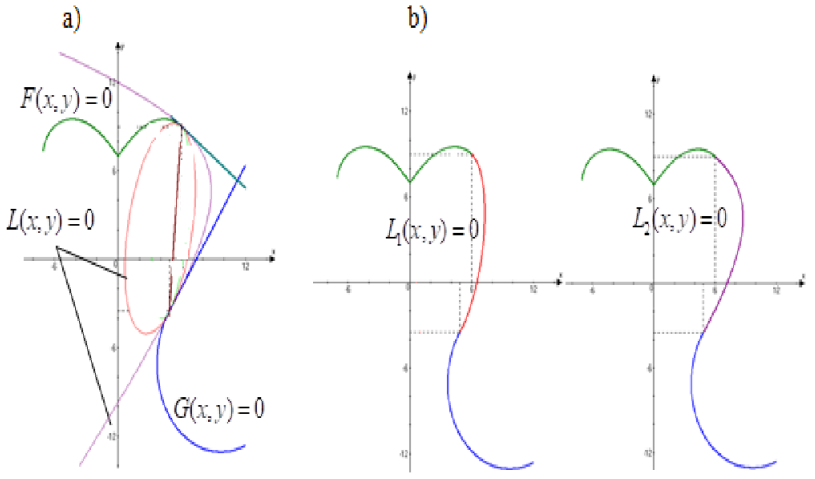

Figure4. a) the Laiming Equation and b) smooth conic variants.

$$L_{A\tau} = 1.383x - y - 10.2399 = 0, L_{B\tau} = -0.6923x - y + 13.1538 = 0$$

$$L_{AB} = 10.9989x - y - 56.9932 = 0$$

Transition conic equations in the form of the Laiming equation

$$L_1(x, y) = 5.0435x^2 + 1.14y^2 - 1.8251xy - 36.1414x + 2.6397y + 20.98 = 0, \lambda = 0.05$$

-ellipse

$$L_2(x, y) = (1 + \lambda)(1.383x - y - 10.23399)(-0.6923x - y + 13.1538) +$$

$$\lambda(10.9989x - y - 56.9932)^2 = 0, \lambda = 0.0055$$

-hyperbole

Checking the smoothness condition of the connection. Radius of curvature of the lemniscata

$$\rho_B = \frac{2a^2}{3r_B} = \frac{50}{3 * 6 * 3246} = 2.635$$

Curvature index

$$\eta = \sqrt[3]{\frac{\rho_A}{\rho_B}} = \sqrt[3]{\frac{6}{2.635}} = 1.316$$

We'll find $\frac{l_A}{l_B} = \frac{10.94}{6.4126} = 1.7$ it . This condition is not met. This means that there is not a single conic that ensures smooth docking. All transition conics create only smooth interfaces.

C) smooth connection.

Using the model of the swing mechanism and solving the system of equations, we will find the angular coefficient $k = tg\gamma = -1.9155$ and then performing all the mathematical calculations, we will find the finish point $B(6.8; 8.1)$. Starting point $A(4.8621; -3.5157)$.

Radius of curvature of the lemniscata

$$\rho_B = \frac{2a^2}{3r_B} = 2.4195$$

Curvature index

$$\eta = \sqrt[3]{\frac{\rho_A}{\rho_B}} = \sqrt[3]{\frac{6}{2.4195}} = 1.35$$

The reference triangle (Fig.5a)

$$L_{A\tau} = 1.383x - y - 10.2399 = 0, L_{A\tau} = -1.9155x - y + 21.1258 = 0$$

$$L_{AB} = 5.9939x - y - 32.6589 = 0$$

Find the ratio of tangent lengths

$$\frac{l_A}{l_B} = \frac{7.93}{5.86} = 1.35$$

Engineering discriminant (Fig. 2b):

$$f = \frac{1}{1 + \sqrt{\frac{2l^2}{h\rho}}} = \frac{1}{1 + \sqrt{\frac{2*7.93^2}{5.2357*6}}} = 0.07, \sigma = \frac{f}{1-f} = 0.075$$

$$x_M = \frac{x_C + \sigma x_T}{1 + \sigma} = 6.0876$$

$$y_M = \frac{y_C + \sigma y_T}{1 + \sigma} = 2.335,$$

$\lambda = 0.9298$. As a result, we obtain the transition conic equation in the form of the Laiming equation

$$L(x, y) = 28.2928x^2 - 10.1189xy + 2.8596y^2 - 269.7894x + 39.7249y + 574.2621 = 0$$

The resulting equation is an ellipse and the arc of this conical curve provides a smooth transition from one section to another of the robot's trajectory. On (Fig.5b) a mirror version of the robot's trajectory is presented.

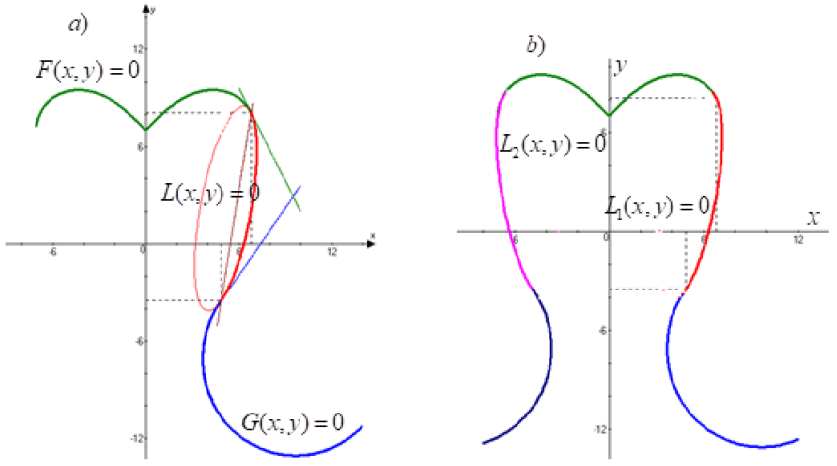

Figure5. a) smooth transition conic and b) mirror version.

Conclusion

The proposed algorithm for creating an unstressed trajectory allows us to obtain new technical forms of the combined robot trajectory, which provide kinematic and dynamic smoothness. The work was performed with the support of fellowship financing of scientific-technical programs and projects of the Committee of science of Ministry of Education and Science of the Republic of Kazakhstan, grant AP05135609.

References

1. Pogorelov, A. D. an Overview of scheduling algorithms trajectory of manipulators // Youth scientific and technical Bulletin. 2016. №8. Pp. 2-2. Boldyrev V. I. Method of piecewise-linear approximation for solving optimal control problems // Differential equations and control processes. 2004. No. 1, Pp. 28-123
2. Lin H.I. A fast and unified method to find a minimum-jerk robot joint trajectory using particle swart optimization // Journal of Intelligent and Robotic Systems: Theory and Applications. 2014. Vol. 75. №3-4. P.379-392.
3. Qi R., Zhou W., Wang T. An obstacle avoidance trajectory planning scheme for space manipulators based on genetic algorithm // Jiqiren / Robot. 2014. Vol. 36. № 3. P.263-270.
4. Howard T., Pivtoraiko M., Knepper R.A., Kelly A. Model-predictive motion planning // IEEE Robotics and Automation Magazine. 2014. Vol.21. №1. P. 64-73
5. Liu W ., Chen D., Zhang L. Trajectory generation and adjustment method for robot manipulators in human-robot collaboration // Jiqiren/Robot. 2016. Vol.38. №4. P. 504-5120
6. Chen Y.J., Ju M. Y., Hwang K.S. A virtual torque-based approach to kinematic control of redundant manipulators // IEEE Transactions on Industrial Electronics. 2017. Vol. 64. № 2. P.1728-1736.
7. Kazakov K. A., Semenov V. A. Review of modern traffic planning methods. Trudy ISP RAS, 2016, vol. 28, no. 1 (in Russian).4. Pp. 241-293.

8. Alekh V., Rahul E.S., Bhavani R. R. Comparative study of the potential field and sampling algorithms for the manipulator obstacle avoidance // International Journal of Control Theory and Applications. 2016.№ 9. P.71-78
9. Ren Z. W., Zhu Q. G., Xiong R. Trajectory planning of 7-DOF humanoid manipulator under rapid and continuous reaction and obstacle avoidance environment // Zidonghua Xuebao/Acta Automatica Sinica. 2015. Vol.41. № 6. P.1131-1144.
10. Pham C.D.,Coutinho F., Lizarrable F., Hsu L., From P.J. An analytical approach to operational space control of robotic manipulators with kinematic constrains // IFAC Proceedings Volumes (IFAC-PapersOnlie).2014. № 19. P. 8509-8515.
11. Simba K., Uchiyama N., Aldibaja M., Sano S. Vision-based smooyh obstacle avoidance motion trajectory generation for autonomous mobile robots using Bezier curves // Proceedings of the Institution of Mechanical Engineers, Part C: Journal of Mechanical Engineering Science. 2017. Vol.231. № 3. P. 541-554.
12. E. S.Temirbekov, B. O.Bostanov. Analytical definition плавof the plan transitions of contours of clothing details. Proceedings of higher educationaleinstitutions. Technology of the textile industry No. 5 (365), Ivanovo, 2016. 160-165.
13. Bayandy O. Bostanov, Erbol S. Temirbekov, Dauren T. Matin. The Model of a Transition Region with Smoothness Conditions of the Second Order. AIP Conference Proceedings 1997, 020038 (2018); doi: 10.1063/1.5049032.
14. Temirbekov, E.S. , Bostanov, B.O. , Dudkin, M.V. , Kaimov, S.T. , Kaimov, A.T. Combined trajectory of continuous curvature (2019) Mechanisms and Machine Science, 2019., 68, pp . 12-19.
15. Fox A. et al. Computational geometry. Application: TRANS. Moscow: Mir publ., 1982, 304p.

Содержание